Fluorinated Flavins and the Rational Design of their Luminescence Properties

INAUGURAL-DISSERTATION
zur Erlangung des Doktorgrades
der Mathematisch-Naturwissenschaftlichen Fakultät
der Heinrich-Heine-Universität Düsseldorf

vorgelegt von

Mira Kristin Kubitz

aus Düsseldorf

Düsseldorf, Oktober 2023

Aus dem Institut für Organische Chemie und Makromolekulare Chemie
der Heinrich-Heine-Universität Düsseldorf

Gedruckt mit der Genehmigung der
Mathematisch-Naturwissenschaftlichen Fakultät der
Heinrich-Heine-Universität Düsseldorf

Berichterstatter:
1. Prof. Dr. Constantin Czekelius
2. Prof. Dr. Peter Gilch

Tag der mündlichen Prüfung: 24.01.2024

Ich versichere an Eides Statt, dass die Dissertation von mir selbständig und ohne unzulässige fremde Hilfe unter Beachtung der „Grundsätze zur Sicherung guter wissenschaftlicher Praxis an der Heinrich-Heine-Universität Düsseldorf“ erstellt worden ist. Die Dissertation wurde in dieser oder vergleichbarer Form noch keinem anderen Prüfungsgremium vorgelegt und es wurde noch kein erfolgloser Promotionsversuch unternommen.

Düsseldorf, 11. Oktober 2023

Mira Kristin Kubitz

Danksagung

Hiermit möchte ich meinen tiefen Dank und meine Anerkennung an eine Vielzahl von Personen und Institutionen ausdrücken, deren Beitrag zur erfolgreichen Realisierung dieser Dissertation von unschätzbarem Wert war.

Mein aufrichtiger Dank gilt in erster Linie Prof. Constantin Czekelius für seine großzügige Ermöglichung dieser Dissertation, seine Unterstützung und sein Vertrauen in meine Fähigkeiten. Unsere fachlichen Diskussionen und seine kontinuierliche Supervision haben mein Verständnis für das Fachgebiet vertieft und meine Motivation stets aufs Neue gestärkt. Besonders weiß ich sein jederzeit offenes Ohr und seine ansteckende Begeisterung für die Chemie zu schätzen.

Ebenso danke ich Prof. Peter Gilch für die Erstellung des Zweitgutachtens und seine freundliche Unterstützung und Beratung in jeglichen photophysikalischen Fragestellungen, die im Rahmen dieser Arbeit auftraten.

Die Deutsche Forschungsgemeinschaft (DFG) verdient Anerkennung für die finanzielle Unterstützung dieser Dissertation und die Förderung des Graduiertenkollegs 2482 - ModISC. Besonders hervorzuheben sind die vom Graduiertenkolleg ModISC geschaffenen idealen Rahmenbedingungen für die Bildung von neuen Kooperationen. Eine große Anerkennung geht hierbei an Prof. Thomas J. J. Müller und Prof. Peter Gilch als Sprecher, Dr. Martina Holz als administrative Koordinatorin und den PhD Sprecher*innen Dr. Fabian Dinkelbach, Simon Hédé, Dr. Julia Wiefermann, Lena Halbrügge, Jeremy Kaminski, Tobias Böhmer, Monika Flörke, Simon Metz und Annette Vollrath für ihre exzellente Organisationsarbeit. Ein Dank gebührt ebenfalls allen PIs für die interessanten Vorlesungen im Rahmen unserer regelmäßigen Seminare, welche mein Verständnis für die Thematik erweitert haben. Ebenfalls möchte ich den herausragenden Zusammenhalt unter den Doktoranden hervorheben, der

für mich eine äußerst bereichernde Erfahrung war. Die gemeinsamen Abende an der Kegelbahn werden mir in guter Erinnerung bleiben.

Besonderer Dank gilt zusätzlich unseren Kooperationspartnern Prof. Peter Gilch, Prof. Claus A. M. Seidel, Prof. Christel M. Marian, Dr. Martin Kleinschmidt, Dr. Ralf Kühnemuth, Dr. Mario Bracker, Wiebke Haselbach und Dragana Sretenović für die äußerst produktive Zusammenarbeit und die gemeinsame Erstellung von Publikationen.

Ich danke dem CeMSA@HHU (Center for Molecular and Structural Analytics an der Heinrich Heine Universität) für die Aufnahme der massenspektrometrischen und NMR-spektroskopischen Daten sowie Philipp Schmeinck und Leonard Karl für die Durchführung und Auswertung von kristallographischen Messungen.

Dennis Nürenberg möchte ich für seine engagierte Mitarbeit während seiner Bachelorarbeit und später als wissenschaftliche Hilfskraft danken. Unsere Diskussionen boten häufig das Fundament für neue Ideen bei schwierigen Problemstellungen. Außerdem danke ich ihm für seine hohe Frustrationstoleranz wenn die Chemie mal wieder nicht so wollte wie wir wollten.

Ein herzlicher Dank gebührt Sabine Houben für ihre tatkräftige Unterstützung im Labor, die cleveren Tricks und Kniffe hinsichtlich der Laborarbeit und die interessanten Gespräche. Außerdem möchte ich ihr dafür danken, dass sie mir stets einen reibungslosen Arbeitsablauf ermöglicht und sich den kleinen und großen Problemen am Institut gewidmet hat.

Dr. Stefan Beutner, Heidi Webers, Dagmar Riedl, Dagmar Koschel und Ute Köhler verdienen eine große Anerkennung für die reibungslose Organisation jeglicher Praktikums- und Betreuungsdienste.

Für die ausführliche Korrektur dieser Arbeit und die stets geduldige Unterstützung und Beratung in stilistischen und technischen Fragestellungen, möchte ich meinem Partner Frank Dumont einen großen Dank aussprechen. Ebenfalls gebührt Nick Yu und Christian Wulkesch für die fachliche und sprachliche Korrektur dieser Arbeit besondere Anerkennung.

Ein großer Dank gilt meinem Laborpartner Christian Wulkesch, der mit seinem Humor stets eine angenehme Atmosphäre innerhalb und außerhalb des Labor geschaffen hat. Er hätte seine Aufgabe als "Party-Manager"nicht besser ausfüllen kön-

nen und es war mir eine große Freude mit ihm gemeinsam unser Labor mit Leben zu füllen und unsere Freitags-Playlist weiter zu entwickeln. Ich danke ihm ebenfalls für sein stets offenes Ohr, sowohl bei wissenschaftlichen als auch bei privaten Problemen.

Dem gesamten Arbeitskreis in all seinen Konstellationen danke ich für die tolle Arbeitsatmosphäre, die Hilfsbereitschaft bei (technischen) Problemen, die vielen wissenschaftlichen Diskussion und besonders natürlich für die witzigen gemeinsamen Mittagspausen, die Billard Spiele, die zahlreichen BBQs und Freitag-Abende. Mir wird die Zeit mit euch unvergesslich bleiben.

Mein größter Dank gilt selbstverständlich meiner Familie und meinem Partner, die mir dieses Studium und die Promotion erst ermöglicht haben. Ich bin ihnen zutiefst dankbar für ihren Rat und ihre tatkräftige Unterstützung, für die Ablenkung und Freude, ihre Zuneigung und Zuversicht, die sie mir stets entgegenbrachten.

Zuletzt, aber keinesfalls weniger wichtig, möchte ich meinen Freunden danken. Ihre Begleitung und Aufmunterung, unsere gemeinsamen Zeiten des Albernsein und der tiefgehenden Gespräche haben mir stets den nötigen Rückhalt gegeben und diese Reise unvergesslich gemacht.

Abstract

Inspired by promising quantum chemical predictions, a methylisoalloxazine (MIA) difluorinated in 7- and 8-position was synthesized and its photophysical properties were investigated in collaboration with the groups of P. Gilch and C.A.M. Seidel. The results, together with details of two other flavin derivatives, 9-F-MIA and a riboflavin derivative difluorinated in 7- and 8-position, have been published in: *ChemPhotoChem* 2023, *7*, e202200334. The experimental data were in excellent agreement with the quantum chemical predictions, showing an increased fluorescence quantum yield of 0.42 for 7,8-dF-MIA compared to non-fluorinated MIA with 0.22.

Another theoretical study (*ChemPhotoChem* 2022, e202200040) revealed flavin derivatives with major structural changes at the pteridine moiety as promising candidates for a potential shift of the emission maximum and an increased triplet quantum yield, respectively. Based on this, the synthesis of a 1-deazalumiflavin fluorinated in 1-position was developed, allowing the investigation of its photophysical properties. The synthesis was based on the common synthetic pathway to 1-deazaflavin derivatives combined with a late-stage electrophilic fluorination. In addition, the synthesis of flavin derivatives trifluoromethylated in 2- and 4-position, respectively, was investigated *via* several synthetic approaches.

Zusammenfassung

Inspiriert durch vielversprechende quantenchemische Vorhersagen wurde ein in 7- und 8-Position zweifach fluoriertes Methylisoalloxazin (7,8-dF-MIA) synthetisiert und seine photophysikalischen Eigenschaften in Kooperation mit den Gruppen von P. Gilch und C.A.M. Seidel untersucht. Die Ergebnisse wurden zusammen mit Details zu zwei weiteren Flavin-Derivaten, 9-F-MIA und einem in 7- und 8-Position difluorierten Riboflavin-Derivat, in der folgenden Publikation veröffentlicht: *ChemPhotoChem* 2023, *7*, e202200334. In hervorragender Übereinstimmung mit den quantenchemischen Vorhersagen konnte für das 7,8-dF-MIA eine experimentelle Fluoreszenzquantenausbeute von 0.42 bestimmt werden, was eine deutliche Verbesserung gegenüber dem unfluorierten MIA mit 0.22 darstellt.

Eine weitere quantenchemische Untersuchung von Flavinen mit starken strukturellen Modifikationen des Pteridinrings (*ChemPhotoChem* 2022, e202200040) ergab vielversprechende Kandidaten mit einer potentiellen Farbänderung der Emission bzw. einer potentiell erhöhten Triplettquantenausbeute. Basierend auf diesen Ergebnissen wurde die Synthese eines in 1-Position fluorierten 1-Deazalumiflavins entwickelt, wodurch die spektroskopische Untersuchung seiner photophysikalischen Eigenschaften ermöglicht wird. Die Synthese basiert auf den üblichen Syntheserouten zu 1-Deazaflavinderivaten und schließt mit einer späten Funktionalisierung mittels elektrophiler Fluorierung ab. Darüber hinaus wurde die Synthese von in 2- bzw. 4-Position trifluormethylierten Flavinderivaten über verschiedene synthetische Ansätze untersucht.

Inhaltsverzeichnis

List of Abbreviations

APCI	Atmospheric pressure chemical ionization
ASAP	Atmospheric Solids Analysis Probe
a.u.	Arbitrary unit
BLUF	Blue-light sensor using FAD
CMF	Carboxymethylflavin
CRY	Cryptochromes
Cys	Cysteine
DABCO	1,4-Diazabicyclo[2.2.2]octan
ddeMe	Didemethyl
DIPA	Diisopropylamine
DMAP	4-(Dimethylamino)pyridine
DMF	*N*,*N*-Dimethylformamide
DMSO	Dimethylsulfoxide
ESI	Electrospray ionization
eq	Equivalent(s)
FAD	Flavin adenine dinucleotide

FbFPs	Flavin-binding fluorescent proteins
FC	Flash chromatography
FMF	Formylmethylflavin
FMN	Flavin mononucleotide
FQY	Fluorescence quantum yield
GFP	Green fluorescent protein
HPLC	High performance liquid chromatography
HRMS	High resolution mass spectrometry
Hz	Hertz
IC	Internal conversion
IR	Infrared spectroscopy
ISC	Intersystem crossing
J	Coupling constant
LC	Lumichrome
LF	Lumiflavin
LOV	Light-oxygen-voltage
MIA	Methylisoalloxazine
M.Pt.	Melting point
NFSI	*N*-Fluorobenzenesulfonimide
NIR	Near-infrared
NMR	Nuclear magnetic resonance
NOESY	Nuclear overhauser enhancement spectroscopy

NP	Neopentyl
ppm	Parts per million
RIA	Ribitylisoalloxazine
RF	Riboflavin
r.t.	room temperature
sat.	Saturated
TFA	Trifluoroacetic acid
TFE	Trifluoroethanol
THF	Tetrahydrofuran
TLC	Thin-layer chromatography
TMS	Trimethylsilyl

Preface

Parts of this work have been published in international scientific journals. The first part 'Part I: Xylene Ring Derivatization of Flavins' presents the synthetic results of the following publication together with a brief summary on the spectroscopic results:

- *Increasing the Fluorescence Quantum Yield and Lifetime of the Flavin Chromophore by Rational Design*

  M. K. Kubitz, W. Haselbach, D. Sretenović, M. Bracker, M. Kleinschmidt, R. Kühnemuth, C. A. M. Seidel, P. Gilch, and C. Czekelius.

  ChemPhotoChem **2023**, *7*, e202200334.

  Own contribution: All experimental investigations with respect to synthetic preparation, purification, characterization and analysis of methylisoalloxazine derivatives fluorinated in 9-position and difluorinated in 7- and 8-position as well as of the riboflavin derivative difluorinated in 7- and 8-position. The steady state spectroscopic measurements of both methylisoalloxazine derivatives were performed together with W. Haselbach. The first concept of the manuscript and the writing of the parts Introduction, Synthesis and Conclusion including creating of the synthesis schemes. The written parts were corrected and supplemented with further details by all other authors.

The second and the third part of this work 'Part II: 1-F-Lumiflavin - Aiming at a shift of emission' and 'Part II: Trifluoromethylated Deoxolumiflavins - Aiming at an Increased Triplet Quantum Yield' are based on quantum chemical calculations of the following publication, from which selected results are explained and used in the argumentation:

- *Computer-Aided Design of Fluorinated Flavin Derivatives by Modulation of Intersystem Crossing and Fluorescence*

  M. Bracker, M. K. Kubitz, C. Czekelius, C. M. Marian, and M. Kleinschmidt.

  ChemPhotoChem **2022**, e202200040.

  Own contribution: Discussion and assessment of synthetic feasibility of described methylisoalloxazines. Proofreading of the written manuscript.

Furthermore, some experimental investigations of the second and the third part of this work 'Part II: 1-F-Lumiflavin - Aiming at a shift of emission' and 'Part II: Trifluoromethylated Deoxolumiflavins - Aiming at an Increased Triplet Quantum Yield' were supported by D. Nürenberg as part of his bachelor thesis and as undergraduate assistant.

- *Preparation and Fluorination of Lumiflavin Derivatives*

  D. Nürenberg

  Bachelor Thesis, Heinrich-Heine-Universität Düsseldorf, 2021.

  Own contribution: Supervision of the experimental work and assistance in the interpretation of the results.

1 Introduction

Flavins, a class of yellow redox-active chromophores, play an important role in enzymatic processes of living organisms.[1] All flavin derivatives are derived from riboflavin, commonly known as vitamin B2.[1] However, the majority of the naturally occuring riboflavins are bounded to enzymes, mainly as flavin mononucleotide (FMN) and flavin adenine dinucleotide (FAD). Figure 1.1 shows the structures of riboflavin, FMN as well as FAD. Intrinsically, these riboflavin derivatives consist of a dimethylisoalloxazine core, a ribityl side chain at 10-position and other essential components. For instance, on the basis of the dimethylisoalloxazine backbone with the ribityl side chain, FMN has a 5'-phosphoryl group installed, while FAD is extended with adenosine monophosphate.[2]

With their ability to undergo both one- and two-electron transfer processes, flavins are unique in nature.[1] Since they are additionally versatile regarding substrate scope and variable in terms of redox potentials, they are involved in numerous essential reactions in metabolism. In general, three redox states are accessible: oxidized, semiquinone and hydroquinone. For each state, acid-base equilibria with specific pKa values provide three different protonation states. The pKa values given in Scheme 1.1 refer to free flavins in solution, since a protein environment can significantly change its redox properties and pKa values.[1–5]

In addition to their redox-activity, flavins are known for their pivotal role as absorbing chromophores in light-sensing processes of bacteria and plants.[7] For instance, the light-oxygen-voltage (LOV) domain is one of the three major flavin photosensor classes.[8] This blue-light sensing photoreceptor binds FMN noncovalently and plays a role in the light-induced regulation of protein activities.[8,9] As a domain of phototropin it is involved in various biological processes such as the regulation of the circadian rhythm, phototropism, and chloroplast movement.[9–11] The excitation

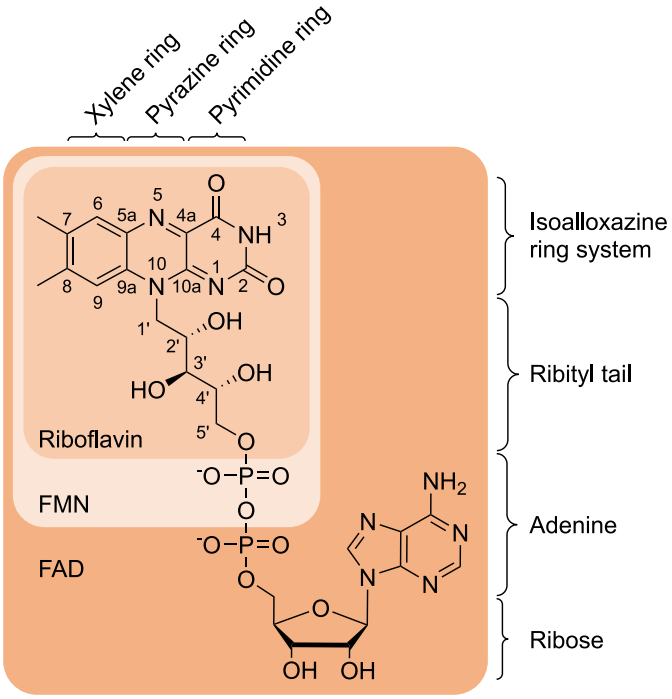

Figure 1.1 Structures of riboflavin, FMN and FAD. The isoalloxazine ring as the catalytic core system consists of a xylene, pyrazine and pyrimidine ring. Riboflavin has a ribityl chain at N10, while FMN additionally exhibits a 5'-phosphoryl group and FAD is further extended with adenosine monophosphate. The term nucleotide in FMN and FAD may be considered inaccurate due to the absence of a glycosidic linkage between the ribityl chain and N10 of the isoalloxazine core.[1–3]

of the flavin chromophore, followed by intersystem crossing (ISC) as well as the formation of a covalent bond between a nearby cysteine and C4 of the isoalloxazine ring is initiated by blue light. The whole process takes place on a microsecond time scale (Scheme 1.2).[9–12]

The remaining two major flavin photosensor classes are designated as blue-light sensor using FAD (BLUF) proteins and cryptochromes (CRYs).[8] Different from LOV domains, both BLUF proteins and CRYs possess FAD as a cofactor. They support functions like sensory transduction in processes like the circadian timekeeping, or as photomagnetoreceptors in insects, migratory birds and fish.[8,9,11–15] Upon blue-light excitation, BLUF proteins undergo hydrogen bond network rearrangements, in contrast to CRYs where redox reactions occur as a response.[11,16]

Overall, photoexcitation triggers a series of conformational changes in flavin-binding photosensors, starting from the chromophore and transmitting through the

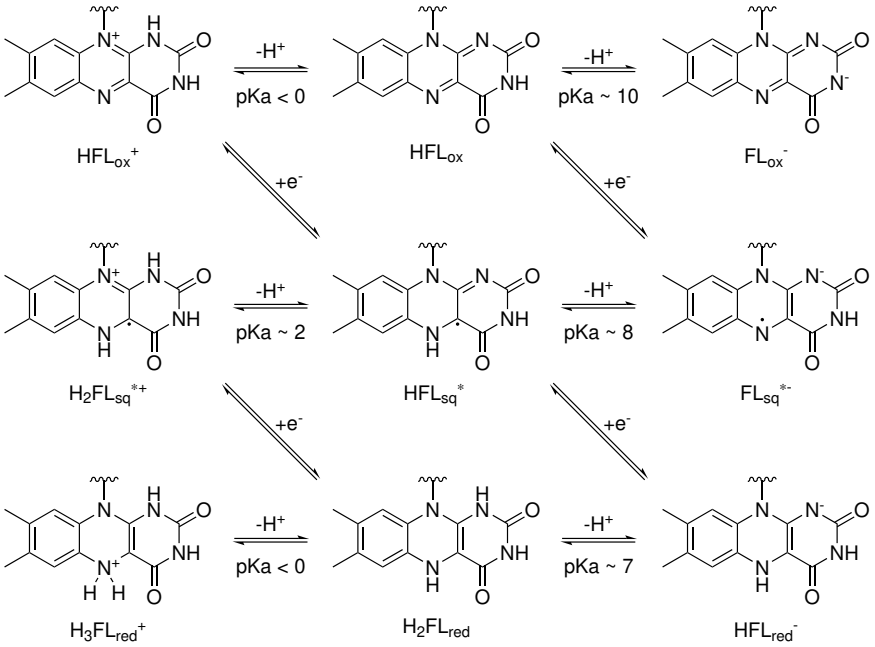

Scheme 1.1 One- and two-electron redox processes as well as acid-base equilibrium of free flavin in oxidized state (FL_{ox}), semiquinone (FL_{sq}) and hydroquinone (FL_{red}) in solution.[6]

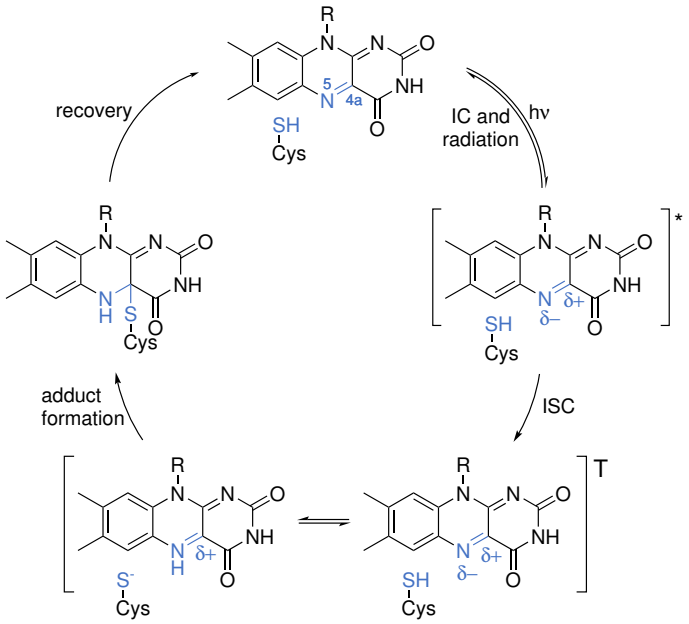

Scheme 1.2 Proposed LOV domain photocycle. Before photoexcitation, the LOV domain binds to FMN non-covalently. Upon photoexcitation and non-radiative relaxation *via* ISC, the triplet state is stabilized by deprotonation of a nearby cysteine of the LOV domain, followed by formation of a cysteinyl-FMN adduct. These structural changes can completely recover in darkness.[10,12]

microenvironment, eventually reaching the surface of the photosensory domain. On the whole, these conformational changes affects the protein-protein interaction network, thus leading to the biological response.[11]

In addition to their role in light sensing, flavin-binding fluorescent proteins (FbFPs) were discovered to be useful for placing cellular processes under light control (optogenetics) and as fluorescent tags.[11] Another prominent candidate for this purpose is the green fluorescent protein (GFP), that has been discovered in the early 1960s by Osamu Shimomura.[17] Nowadays it is highly relevant in cell biology for *in vivo* and *in vitro* analysis of protein localization, interaction, expression and movement.[18,19]

Although GFP is widely applicable, it has some limitations that require an alternative. For instance, it shows dimmed or no fluorescence in low-oxygen environments.[18–23] It is quite bulky with 240 amino acids, which has been reported to potentially hinder the functionality of the protein due to steric constraints.[13,21–23] In addition, it is pH sensitive and exhibits slow fluorescence maturation (10-40 minutes for half maximal fluorescence recovery), which hinders real-time imaging of gene expression dynamics or viral infection and localization tracking.[7,13,21–24] For these purposes, FbFPs are a good alternative as their fluorescence has been shown to be oxygen independent.[18,20–23] They are quite small with 110-118 amino acids and show rapid fluorescence maturation with <3 min.[7,13,21–24] In addition, they allow for a wide operational pH range (pH 4-11) and are additionally stable at temperatures up to 60 °C.[7,23]

For the application as a fluorescent tag, LOV already fulfills the basic requirements as the contained flavin chromophore shows emission with a maximum at around $\lambda_{em,max}$ = 535 nm and an excitation maximum at around $\lambda_{ex,max}$ = 450 nm.[7] Also, fluorescence quantum yields (FQYs) of LOV domains of up to Φ_{fl} = 0.39 allow this application.[11] However, their photocycle upon excitation, involving a FMN-cystein bond formation, is responsible for the fluorescence loss of FMN.[7] Therefore, the structure of the LOV domain was altered by mutations to replace the responsible cysteine with alanine or serine, successfully avoiding any covalent bond formation.[11] The mutation resulted in a hypsochromic shift of the fluorescence emission ($\lambda_{em,max}$ = 495 nm), but the excitation maximum was unaffected.[7]

Certainly, FbFPs are not free of drawbacks and limitations. For instance, their FQY is significantly lower (Φ_{fl} = 0.2 - 0.4) compared to that of GFP (Φ_{fl} = 0.6).[21] Also, while a wide range of GFP variants with fluorescence emission colors over the whole visible spectrum exists, FbFPs are typically green fluorescent depending on the flavin chromophore.[19] Additionally, in some cases cellular growth rate was reduced due to overexpression of FbFPs and the associated metabolic stress.[7] Summarizing, improvements concerning photostability, brightness and cellular expression need to be addressed by further engineering.[7]

In literature, several modulations of LOV-based FbFPs with improved properties such as brightness and photostability have been reported.[21] For instance, new LOV variants have been engineered by Christie *et al.*, revealing one with enhanced fluorescence, named iLOV.[24] Furthermore, iLOV has been found to be more suitable for repeated laser scanning as it proves to be spontaneously recoverable, in contrast to GFP, which photobleaches irreversibly at high light intensities.[24] Another LOV variant called phiLOV showes a strongly increased photostability but at the expense of a reduced FQY.[21] Overall, numerous genetically distinct LOVs are available, with improved properties such as pH tolerance, thermal stability, brightness and photostability, respectively. However, there is still a need of further improvements.[21] To achieve considerable changes like a variation of color, LOV domain mutations might be insufficient, as only small shifts of emission ($\sim$10 nm) have been reported, caused by changes in hydrogen bonding.[21,25,26]

An approach for brightness improvements and emission wavelength shift could be the replacement of the flavin chromophore by novel synthetic flavin derivatives. In the literature survey, several derivatives have been reported, often featuring alkyl- or halogenyl-functional groups at the xylene moiety. Due to its minor role regarding protein interaction, a relatively large flexibility exists for functionalization in 6-, 7-, 8- and 9-position.[27]

Several flavin derivatives have been reported to exchange the FMN in LOV such as naturally occuring roseoflavin, riboflavin and FAD.[28–31] An exchange with synthetic flavins has been for instance reported by Mansurova *et al.* with 8-isopropylriboflavin (8-*i*Pr-riboflavin) and 7,8-didemethylriboflavin (7,8-ddeMe-riboflavin) (Figure 1.2).[29] Even the increased steric constraints generated with 8-isopropylriboflavin

was proven to be acceptable and showed the naturally occurring photocycle including spontaneous thermal recovery.[29] Moreover, an enhancement of FQY with incorporation into LOV from Φ_{fl} = 0.27 to 0.40 was observed for 8-isopropylriboflavin, confirming the combination of chemically designed novel flavin derivatives with LOV domains could be promising with respect to its fluorescence labeling property.[29]

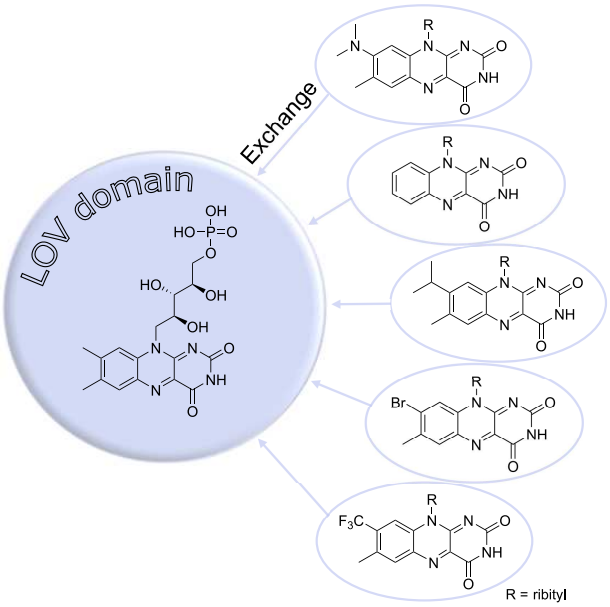

Figure 1.2 Schematic illustration of riboflavin derivatives which have been successfully used for an exchange of the naturally incorporated FMN (left) within LOV domains. The riboflavin derivatives are roseoflavin, 7,8-ddeMe-riboflavin, 8-*i*Pr-riboflavin, 8-Br-riboflavin and 8-CF_3-riboflavin (right side, from top to bottom).[29,31,32]

Another research work done by Gärtner *et al.* reported the photophysical properties of 8-CF_3- and 8-Br-riboflavins in solution and their embedment into the LOV domain (Figure 1.2).[32] In solution, 8-Br-riboflavin showed a considerably promoted triplet quantum yield of Φ_T = 0.97 compared to riboflavin with Φ_T = 0.60, which could be particular important for singlet oxygen generation in the context of photodynamic therapy as well as photoredox catalysis in organic syntheses.[22] The high triplet quantum yield could be attributed to the heavy atom effect and the associated prominent spin-orbit coupling.[32,33] Derivatization with a trifluoromethyl functionality attached at 8-position, resulted in a strongly increased FQY of Φ_{fl} = 0.70 compared to riboflavin with Φ_{fl} = 0.27. In both cases, embedding into the LOV domain was successful and the typical photocycle upon blue light excitation was observed. However, both chromophore-protein adducts are limited by their instability compared

to the adducts with naturally occurring flavin and alkyl-modified flavins such as 8-*i*Pr-riboflavin.[29,32]

Gilch, Czekelius *et al.* reported the synthesis of three different monofluorinated methylisoalloxazines (MIAs) with fluorine substituents in 6-, 7- or 8-position.[34] With this substitution pattern, they demonstrated a significant impact on the photophysical properties depending on the position of substitution, including both, hypsochromic (8-F-MIA) and bathochromic (6-F- and 7-F-MIA) shifts of transition up to 500 cm^{-1}.[34] Furthermore, triplet quantum yields and FQYs are affected, giving for instance a 50% increase of FQYs in the case of 7-F-MIA compared to non-fluorinated MIA (from Φ_{fl} = 0.22 to 0.33). These findings open up new perspectives for fluorescence labeling applications.[34]

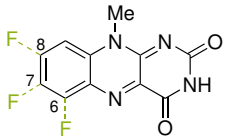

Figure 1.3 Structure of monofluorinated MIAs with fluorine substituents in 6-, 7- or 8-position, synthesized and characterized by Gilch, Czekelius and coworkers.[34] Bonds to fluorine atoms are dashed to represent different options of monofluorinated MIAs.

Kleinschmidt and coworkers reported the reproduction of the results by quantum chemical calculations.[35] Furthermore, they offered an explanation for the influence of fluorine substituents in 6- to 9-position on the photophysical properties of MIAs.[35] In vacuum, ISC from the first singlet state S_1 of $\pi\pi^*$ character to the second triplet state T_2 of $n\pi^*$ character is accessible and fast since it is El-Sayed-allowed. In aqueous medium, conversely, T_2 is strongly destabilized making this ISC channel no longer accessible. Instead, the third triplet state T_3 of $\pi\pi^*$ character will undergo a dramatically redshift all the way down below T_2 and even slightly below S_1. Herein, ISC to this state is El-Sayed-forbidden, but becomes accessible *via* vibronic spin-orbit coupling. Last but not the least, the first triplet state T_1 is of $\pi\pi^*$ character and separated from S_1 by 0.5 eV. This large energy level separation in combination with the El-Sayed rule, determining this transition as forbidden, will eventually lead to small vibronic rate constants for ISC to this triplet state.[35–38]

Depending on the position of fluorination, all the aforementioned states are shifted differently. For instance, fluorination in 6-position lowers the T_3 state

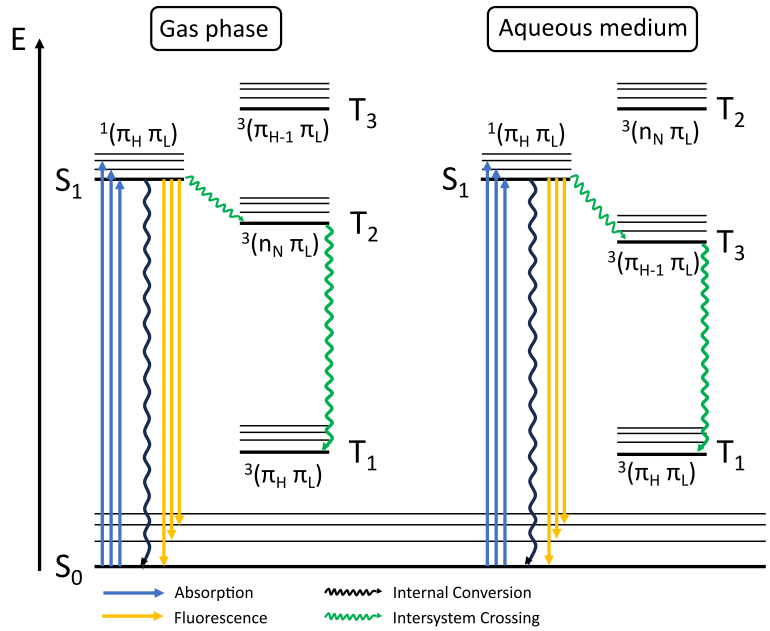

Figure 1.4 Schematic visualization of singlet and triplet states of MIAs in the gas phase and aqueous medium.[35] In the gas phase, non-radiative deactivation *via* ISC is fast due to the El-Sayed-allowed, accessible T_2 state of $n\pi^*$ character. In aqueous medium, this state is strongly destabilized while the T_3 state of $\pi\pi^*$ character becomes thermodynamically available by vibronic spin-orbit coupling.[35–38]

energy.[35] A fluorine substituent in 8-position causes a blue shift of all $\pi\pi^*$ state energies and fluorination at 9-position has a similar effect as fluorination at 6-position.[35] For 7-F-MIA, the high FQY obtained in the experiment was confirmed by quantum chemical calculations.[34,35] Explanations are based on a slight blue shift of the T_3 state, which brings S_1 and T_3 into close proximity. Even small modifications of this gap have a strong influence on the calculated ISC rate constants, providing a new perspective for further optimization of the MIA substitution pattern.[35] If it would be possible to influence the S_1/T_3-gap so that T_3 is shifted above S_1, ISC rate constants would be decreased while enhancing the FQY.[35,36]

2 | Motivation

For application in optical imaging, limitations of FbFPs such as the low FQY or rather the brightness (Φ_{fl} x 1^{st} ε_{max}) need to be addressed.[36,39] So far, only limited effects have been achieved by protein mutations. Therefore, an alternative strategy would be to replace the naturally incorporated flavin chromophore with new synthetic flavin derivatives. Especially, modification with substitutents exerting a strong electronic effect on the photophysical properties of the chromophore are promising.

For this purpose, fluorine substituents are particularly beneficial, as they exert a strong electon-withdrawing effect.[36,40,41] With their small size, the steric impact on the protein binding would be low, avoiding a negative impact on the biological activity of the targeting protein.[41,42] The synthesis of xylene ring mono- and polyfluorinated flavin derivatives, with the aim to increase the FQY for application in optical imaging, has been desribed in the first part of this dissertation.

For the selection of a suitable xylene-ring substitution pattern, a quantum chemical study by Kleinschmidt *et al.* was consulted, which focused on the effects of xylene ring fluorination on the singlet and triplet states of MIAs.[35] As aforementioned (Section 1), the results from calculations revealed the S_1/T_3-gap as responsible for the high FQY of 7-F-MIA (see also Figure 1.4).[34,35] Therefore, further modifications of this gap towards smaller values or even a shift of T_3 above S_1 would be a reasonable starting point to achieve high FQYs.[35] In their study, Kleinschmidt and coworkers found a method to easily predict the effects caused by polyfluorination relative to the properties of non-fluorinated MIA.[35] By simply summarizing the effects caused by monofluorination, they observed the shifts induced by polyfluorination and calculated them for all possible xylene ring substitution patterns.[35] These results were screened for flavin derivatives with a significant impact on the S_1/T_3-gap giving one promising derivative, 7,8-dF-MIA.

With difluorination in 7- and 8-position, the first singlet state S_1 is slightly upshifted by 0.01 eV compared to non-fluorinated MIA.[35] The third triplet state T_3 on the other hand, mainly responsible for non-radiative deactivation *via* ISC, is blueshifted by 0.15 eV.[35] Since the S_1/T_3-gap is intrinsically not far apart, this unnegligible blueshift could potentially lead to a T_3-shift above the S_1 state, thus decreasing the ISC rate constant to this triplet state (Figure 2.1).

Therefore, the synthesis of the difluorinated MIA, 7,8-dF-MIA, was investigated in this work. For completeness as well as validation of quantum chemical postulations, investigations were made to synthesize 9-F-MIA as well, a monofluorinated MIA which has not been reported in the past. Both derivatives were characterized with respect to their photophysical properties.[36] As an initial approach towards incorporation into proteins, the synthesis of 7,8-dF-riboflavin (7,8-dF-RIA) was additionally investigated.

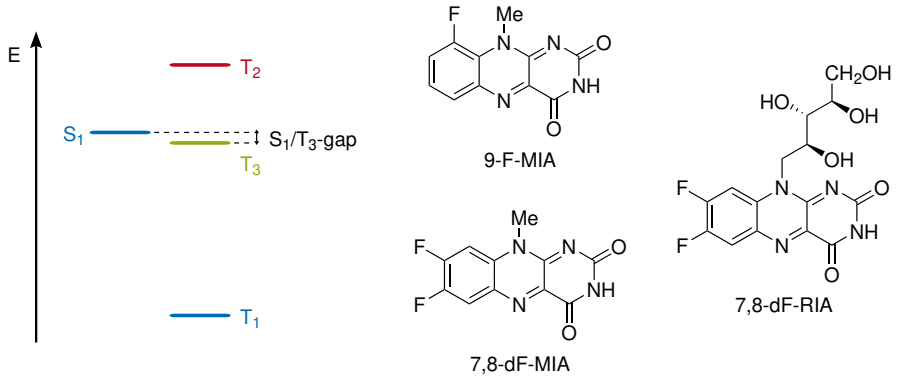

Figure 2.1 Schematic visualization of the S_1/T_3-gap whose small value was made responsible for the high FQY of 7-F-MIA.[34,35] The structure of 7,8-dF-MIA is shown on the right, whose fluorination pattern exerts a strong impact on this gap according to quantum chemical predictions.[35] 7,8-dF-RIA as the difluorinated riboflavin analogue is an initial approach towards a potential protein incorporation.

In the spirit of altering the emission wavelength of FbFPs for optical imaging, considerable modifications to the flavin chromophore are required. In collaboration with Kleinschmidt *et al.*, new flavin derivatives with fluorine substituents at the pteridine moiety of the isoalloxazine core were discussed.[38] Their photophysical properties investigated by quantum chemical calculations, mainly performed by Dr. M. Bracker, have been reported.[38] For this purpose, the quantum chemical method already ap-

plied in the past was complemented with further high-level calculation methods.[35,38] The synthesis of flavin derivatives fluorinated at the pyrimidine ring with the target to significantly shift the emission maximum for multicolor optical imaging, has been described in the second part of this dissertation.

Convincing flavin derivatives include 1-fluoro-1-deaza-MIA (1-F-MIA) and 2-difluoromethylidene-2-deoxo-MIA (2-CF_2-MIA), as their S_1 states are suggested to be highly stabilized according to quantum chemical calculations.[38] This stabilization leads to a deactivation of the ISC channel to the T_3 state and to a striking shift in their emission maxima towards the red to near-infrared (NIR) region.[38] Specifically, Kleinschmidt and coworkers indicated emission maxima at 844 nm for 2-CF_2-MIA and 765 nm for 1-F-MIA. However, nonradiative deactivation could be a potential competitor for fluorescence as declared by the energy gap law.[38,43] These considerations are confirmed by high level quantum chemical calculations, whose results predicted them to be the dominating deactivation process for both derivatives.[38] Nevertheless, to validate these quantum chemical calculations, the synthesis of 1-fluoro-1-deazalumiflavin (1-F-lumiflavin) was investigated in this work.

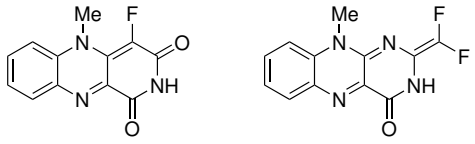

Figure 2.2 Structures of 1-F-MIA and 2-CF_2-MIA as promising flavin derivatives with shifted emission maxima. For both derivatives, the emission maxima are projected to shift towards the red to NIR-region.[38]

Kleinschmidt *et al.* also reported flavin derivatives with considerable modifications at the pyrimidine moiety which were expected to enhance ISC.[38] These derivatives could be promising as potential triplet sensitizer for singlet oxygen generation in terms of photodynamic therapy or for photocatalytic applications.[13,21,44–49] In the third part of this dissertation, synthetic investigations of flavin derivatives with considerable modifications at the pyrimidine ring have been described, which potentially lead to favored ISC as deactivation process.

Two promising flavin derivatives were highlighted by Kleinschmidt and coworkers, namely 2-trifluoromethyl-2-deoxo-MIA (2-CF_3-MIA) and 4-trifluoromethyl-4-

deoxo-MIA (4-CF_3-MIA).[38] For both derivatives, the second triplet state T_2 of $n\pi^*$ character is expected to be strongly stabilized, even in polar solvents. This stabilization is pronounced enough to enable the fast El-Sayed-allowed transition from S_1 to T_2, thus quenching fluorescence reliably. Herein, the synthesis of both derivatives was investigated in this work.

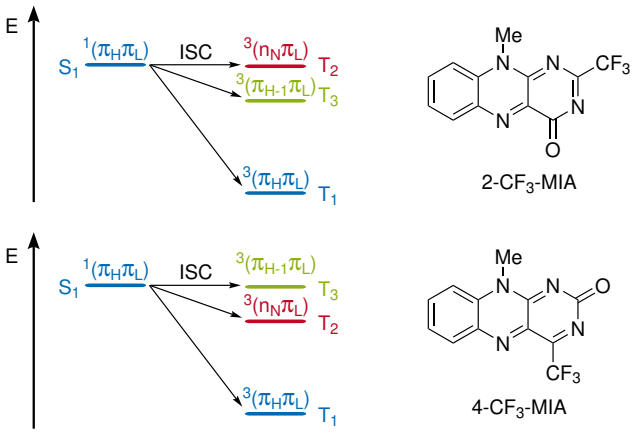

Figure 2.3 Schematic representation illustrating the impact of trifluoromethyl groups introduced at 2- or 4-position, respectively, on the singlet and triplet states of MIAs. These considerable structural modifications lead to remarkable stabilization of the second triplet state T_2 which is of $n\pi^*$ character, facilitating an efficient El-Sayed-allowed ISC channel. Notably, this stabilization is more pronounced when the trifluoromethyl group was attached at 4-position.[38]

3 | Part I: Xylene Ring Derivatization of Flavins

3.1 Literature Overview of Flavins Derivatized at the Xylene Ring

Up to the present, several flavins with different functionalizations on the xylene ring motif have been reported in the literature such as 8-CF_3-, 8-Br-, 8-*i*Pr-riboflavin, 7,8-didemethylriboflavin and roseoflavin.[30,32,50] Often, the synthetic pathways begin with the corresponding functionalized (amino-/nitro-) anilines and alloxan monohydrate as the building blocks.[34,50,51] After functionalization of the aniline with a ribityl side chain, it is coupled with alloxane monohydrate in the presence of boric acid. The utilization of boric acid in the context of this condensation was first described by Kuhn *et al.* in 1935.[52] This procedure is perfectly adaptable to MIAs, which bear a methyl group at 10-position instead of a ribityl group.[53] This was demonstrated by Gilch, Czekelius and coworkers with the synthesis and spectroscopic characterization of 6-, 7- and 8-F-MIAs (**4**).[34] They reported a synthetic route which begins with the methylation of commercially available fluorinated nitroanilines (**1**), followed by reduction of the *N*-methyl-nitroanilines (**2**). The herein formed 1,2-diaminobenzene derivatives serve as fundamental building blocks for the subsequent condensation with alloxan monohydrate (**3**) according to the Kuhn condensation.[34,52]

The one-pot procedure used for *N*-methylation of nitroanilines **1** was initially reported by Brown and Rizzo and is particularly advantageous due to its concise preparation.[54] Both, trifluoroacetamide protection and phase-transfer conditions,

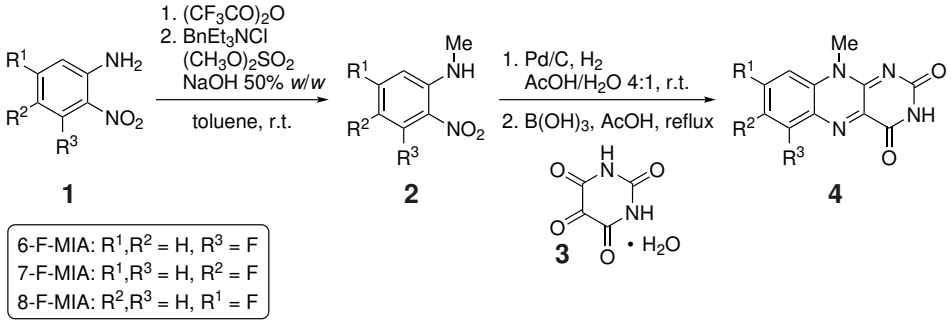

Scheme 3.1 Synthetic route to 6-, 7- and 8-F-MIAs reported by Gilch, Czekelius and coworkers which begins with the methylation of the corresponding fluorinated nitroanilines. The final condensation with alloxan monohydrate in the presence of boric acid was derived from the method described by Kuhn *et al.* in 1935.[34,52]

effectively prevent the amine from multiple methylation.[54] This outcome is explained by the enhanced acidity of the amide, which enabled *N*-alkylation within biphasic conditions. Once the protecting group is hydrolyzed, the *N*-alkylation of the free amine will considerably be slow down.[54] A disadvantage of this procedure is the moderate yield. This limitation is hardly improvable due to the fact that the hydrolysis of the protecting group and methylation of the amide are competitive with each other.

3.2 Synthesis of 9-F-MIA: Corroborating Quantum Chemical Calculations for the Rational Design of Novel Flavins

Recently, it was shown that monofluorination at 6-, 7- or 8-position, respectively, induces shifts of transition which influences the FQYs of MIAs depending on their substitution pattern.[34] These experimental results were subsequently reproduced quantum chemically and besides, predictions were made regarding 9-F-MIA, a monofluorinated flavin derivative whose optical properties have not been reported in the past.[35]

All computational results are based on MIAs as simplified structures, as a high number of atoms lead to strongly increased quantum chemical computation times and resources.[35] To allow a comparison with these theoretically investigated flavin derivatives, it would be advantageous to rely on similar structural motifs, when experimentally investigating fluorinated flavin derivatives. Therefore, Gilch, Czekelius and coworkers also used MIAs as model compounds, which are derivatized with a methyl group at 10-position instead of a ribityl group.[34,35] Consequently, this structural motif was also chosen for the 9-F-flavin derivative.

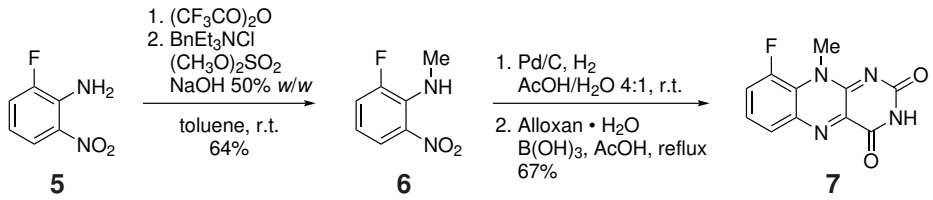

Scheme 3.2 Synthesis route to 9-F-MIA (**7**) beginning with fluorinated nitroaniline **5** according to the typical procedure by Kuhn *et al. via* reduction of the *N*-alkylated nitroaniline followed by coupling with alloxane monohydrate in the presence of boric acid.[52] The *N*-methylation was performed using the one-pot procedure reported by Brown and Rizzo.[54]

According to the most commonly used synthetic approach reported by Kuhn *et al.*, the synthesis of 9-F-MIA begins with the corresponding commercially available fluorinated nitroaniline **5**.[34,52] On the basis of the aforementioned one-pot procedure by Brown and Rizzo, methylated nitroaniline **6** was obtained.[54] As described in Section 3.1, the observed moderate yield of 64% is primarily attributed to the

competing hydrolysis of both amides, methylated and non-methylated, leading to either product formation or starting material recovery. Nevertheless, the particular simplicity of preparation, reaction rate and straightforward purification rational the reason behind application of this method despite the low yield.

The reduction of methyl-nitroaniline **6** was performed by heterogeneous catalysis with palladium and hydrogen. The resulting 1,2-diaminobenzene derivative is highly air-sensitive so that it is advisable to avoid air-contact until condensation with alloxan monohydrate (**3**), necessitating the omission of an intermediary work-up procedure. Instead of a typical work-up procedure, the 1,2-diaminobenzene derivative was directly filtered through a syringe filter into a degassed mixture of alloxane and boric acid in acetic acid. The utilization of a syringe filter is feasible for the purpose of palladium catalyst removal when handling small quantities, as it contributes to generate particularly little decomposition products. For larger scales, filtration through a Büchner funnel under a continuous stream of nitrogen is more practical, taking the higher amount of decomposition products into account.

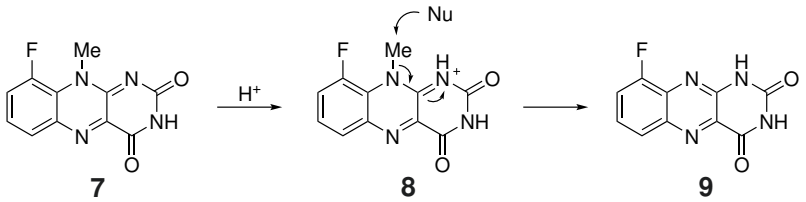

Scheme 3.3 Mechanism of the alloxazine by-product formation, occuring during heating of MIAs in the presence of acids.[34] The mechanism is illustrated using the example of 9-F-MIA (**7**), resulting in 9-F-alloxazine (**9**). Depending on the substitution pattern at the xylene ring, the rate of this formation varies significantly from either exceptionally rapid to only barely noticeable.

Following the condensation with alloxan monohydrate, the poorly soluble 9-F-MIA (**7**) precipitated promptly from the reaction mixture with a satisfying purity. As spectroscopic analyses of photophysical properties require a particularly high degree of purification, many attempts were made to achieve further purification. The limited solubility hamper the application of conventional methods such as flash chromatography (FC) or HPLC. Nevertheless, recrystallization appears to hold promise, though the number of viable solvents is limited. Purification protocols reported in the literature often involve solvents such as acetic acid or formic acid. However, the

propensity of MIAs to form alloxazine by-products upon heating with traces of acid hinders the utilization of such organic acids for recrystallization (Scheme 3.3). In this context, trifluoroethanol (TFE) was employed as a proper alternative based on its polarity without being acidic or nucleophilic. After recrystallization from TFE, 9-F-MIA (**7**) was obtained in high purity, allowing the study of its optical properties.

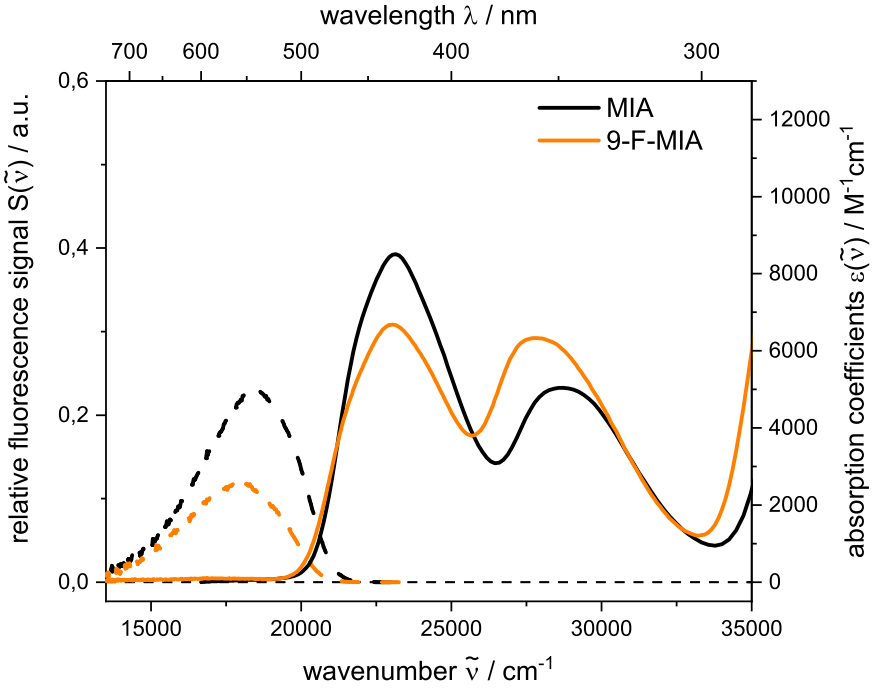

Figure 3.1 Absorption and fluorescence emission spectrum of 9-F-MIA (**7**) in water compared to the corresponding spectrum of non-fluorinated MIA in water. The fluorescence emission spectra are normalized to their FQY and were obtained by tuning the excitation to 420 nm. This graph was created in collaboration with W. Haselbach.[36]

The theoretical study by Kleinschmidt and coworkers suggested a similarity of the photophysical properties of 9-F-MIA (**7**) with the ones of 6-F-MIA.[34,35] In collaboration with W. Haselbach, the photophysical properties of 9-F-MIA were investigated.[36] In Figure 3.1 its absorption and emission spectra are shown, together with the spectra of non-fluorinated MIA for comparison. The absorption spectrum of 9-F-MIA (**7**) shows two strong bands that are only slightly shifted with respect to the bands of MIA. Similar shifts have been reported for 6-F-MIA by Gilch, Czekelius and coworkers.[34] The emission spectrum is scaled according to the FQY that was determined relative to coumarin 153 in ethanol (Φ_{fl} = 0.544[55]), visualizing its decrease to Φ_{fl} = 0.12 with fluorination in 9-position compared to non-fluorinated

MIA with Φ_{fl} = 0.22 and matching the FQY of 6-F-MIA with Φ_{fl} = 0.12 that has been previously reported by Gilch, Czekelius and coworkers.[34,36] Impressively, the experimental results are in line with the theoretical prediction.[35] A detailed discussion of the photophysical properties of 9-F-MIA (**7**) can be found in Ref. [36], Chapter 10.

3.3 Synthesis of 7,8-dF-MIA: A Compound Exhibiting Favorable Attributes for Fluorescence Labeling Purposes

By summarizing the impact of monofluorination on singlet and triplet states, the shifts resulting from multiple fluorination can be determined.[35] Since monofluorination in 7-position induces a proximity between the first singlet state S_1 and the third triplet state T_3, polyfluorinated MIAs were screened for an optimized substitution pattern with respect to a more pronounced blueshift of the T_3 state.[35] The 7,8-dF-MIA, fluorinated at both 7- and 8-position, was found to show a significant destabilization of the T_3 state.[35] Noticeably, this particular fluorination pattern could plausibly prompt the T_3 state even surpass the S_1 state, which makes the fluorescence more favorable.[35] This potentially increased brightness of this flavin derivative renders it particular promising for optical imaging.

As aforementioned, to allow comparability between experimental results and theoretical suggestions, it is advantageous to employ MIA as a simplified structure for the 7,8-dF-flavin derivative. The synthetic route to 7,8-dF-MIA (**14**) begins with the corresponding difluorinated nitroaniline **10** (Scheme 3.4). When the practical and facile one-pot procedure by Brown and Rizzo was applied on nitroaniline **10** for its methylation, a strong tendency towards the formation of side-products was observed, including unknown monofluorinated products.[54] Probably, upon addition of sodium hydroxide, the fluorine substituent in *para*-position to the nitro functionality was substituted by the nucleophile.

An alternative way to introduce a methyl-substitutent in *N*-position of nitroaniline **10** is in a multi-step manner *via* Boc-protection, similar to the procedure described by Xie and Liao *et al.* in Ref. [56] for the methylation of a monofluorinated nitroaniline. The procedure used for Boc-protection involved 4-(dimethylamino)-pyridine (DMAP) as catalyst and triethylamine (NEt_3) as base and was initially reported by Wojciechowski and Hudson.[57] The combination of both additives, DMAP and NEt_3, enables Boc-protection of amines exhibiting a low nucleophilicity and leads to a bis-*N*-Boc-protected intermediate.[56,57] Subsequently, one of the Boc-

protecting groups was removed reliably under acidic conditions. To avoid the risk of a nucleophilic aromatic substitution, sodium hydride as a non-nucleophilic base was utilized for the subsequent methylation cooperating with methyl *p*-toluenesulfonate.[56] Eventually, the Boc-protecting group is removed under acidic conditions.[56]

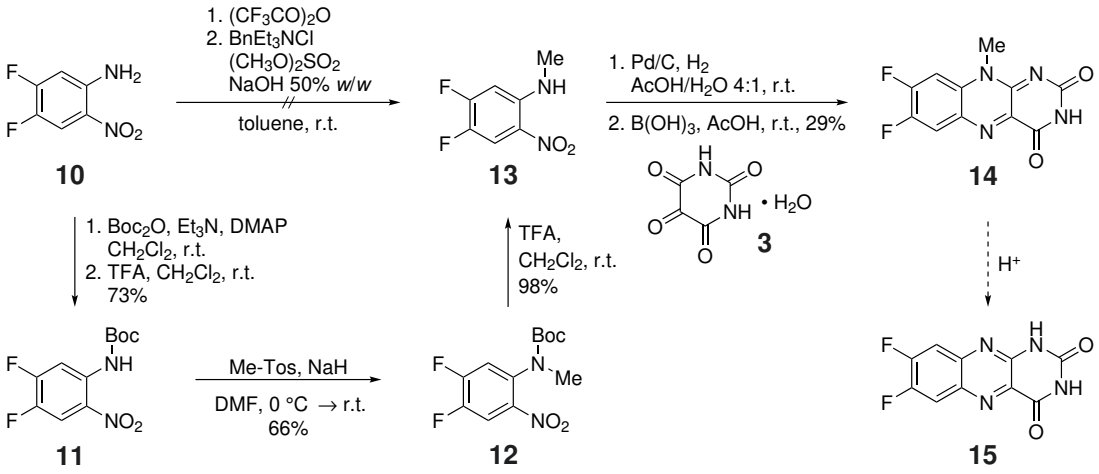

Scheme 3.4 Synthesis route to 7,8-dF-MIA (**14**) begins with difluorinated nitroaniline **10**. The one-pot procedure by Brown and Rizzo[54] proved to be unrealistic for methylation, as it led to unexpected nucleophilic aromatic substitution. Therefore, nitroaniline **10** was methylated over three steps *via* Boc-protection. This route, involving bis-Boc-protection and partial deprotection, have been already implemented by Xie and Liao *et al.* for the methylation of a nitroaniline monofluorinated in *para*-position to the nitro functionality.[56] The reaction conditions for the final condensation with alloxan monohydrate (**3**) were derived from the procedure reported by Kuhn and coworkers.[34,52] However, the tendency of 7,8-dF-MIA (**14**) to form alloxazine by-product **15** necessitated some adaptation to these conditions.

The methylated nitroaniline **13** was reduced by hetergeneous catalytic reduction, followed by condensation of the resulting 1,2-diaminobenzene derivative with alloxan monohydrate (**3**) as described before. Application of the condensation procedure demonstrated in the synthetic route to 9-F-MIA (**7**, Section 3.2), led in the synthesis route to 7,8-dF-MIA (**14**) to a mixture with many different side-products including alloxazine **15**. Several attempts to purify this mixture *via* recrystallization and FC were unsuccessful. The increased solubility of 7,8-dF-MIA (**14**) affected by difluorination enabled the utilization of purification procedures such as FC. However, due to various side-products in high amounts, the desired product could merely be isolated in low yield with minor impurity. In the context of recrystallizations, the

slight increase in solubility led to only minimal precipitation.

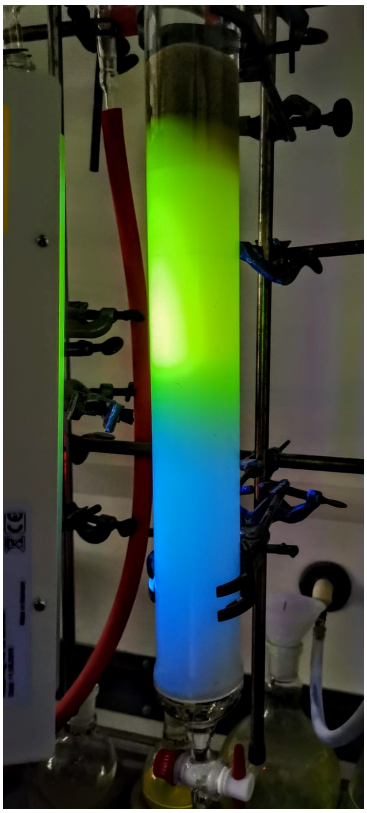

Figure 3.2 Fluorescing 7,8-dF-MIA (**14**) during FC.

Therefore, an optimization of the reaction conditions was indispensable. The avoidance of exposing 7,8-dF-MIA (**14**) to any heat, especially in the presence of acids, turned out to be an essential factor and suppressed the formation of alloxazine by-product **15** significantly. Specifically, the condensation was conducted at room temperature, astonishingly achieving full conversion within one hour. While the unsoluble 9-F-MIA (**7**) promptly precipitated from the reaction mixture as soon as it was formed, the increased solubility promoted by difluorination prevented spontaneous precipitation of 7,8-dF-MIA (**14**). Therefore, the solvent of the reaction mixture was reduced in volume under high vacuum conditions at ambient temperatures to a few milliliters, thus inducing precipitation. The raw material consisted of a mixture of the main product **14** with alloxazine **15** and an unknown mono-fluorinated side-product in a ratio of 1.0 : 0.4 : 0.2, which was determined from its NMR-spectra. The relatively high purity of the raw product made purification *via* FC feasible, using TFE as solvent for column loading (see experimental for further details). By applying this procedure, 7,8-dF-MIA was obtained in a high purity allowing the study of its optical properties.

Quantum chemical calculations for 7,8-dF-MIA (**14**) revealed an increase in FQY facilitated by the pronounced destabilization of the T_3 state potentially beyond the S_1 state. In collaboration with W. Haselbach, the experimental photophysical properties of this MIA derivative were investigated. In Figure 3.4 the absorption and emission spectrum of 7,8-dF-MIA (**14**) are shown, together with the spectra of non-fluorinated MIA for comparison. The absorption spectrum of 7,8-dF-MIA (**14**) shows two strong bands that are only

Figure 3.3 Fluorescing 7,8-dF-MIA (**14**) in water.

slightly shifted with respect to the bands of MIA. The emission spectrum is scaled according to the FQY that was determined relative to coumarin 153 in ethanol (Φ_{fl} = 0.544[55]), visualizing the increased FQY to Φ_{fl} = 0.42 with difluorination in 7- and 8-position compared to non-fluorinated MIA with Φ_{fl} = 0.22.[36] Again, the experimental results are in line with the theoretical assumptions.[35] A detailed discussion of the photophysical properties of 7,8-dF-MIA (**14**) can be found in Ref. [36], Chapter 10.

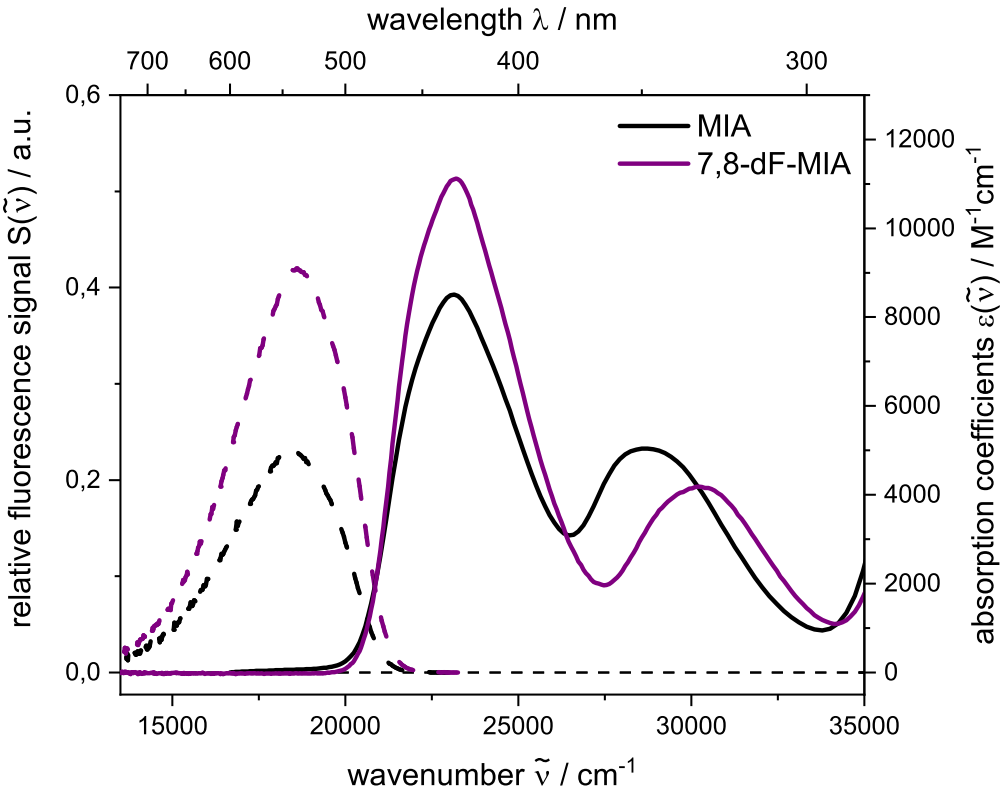

Figure 3.4 Absorption and fluorescence emission spectrum of 7,8-dF-MIA in water in comparison with the spectrum of non-fluorinated MIA in water. The fluorescence spectra are normalized on the basis of their FQY. This graph was created in collaboration with W. Haselbach.[36]

Within optimization tests of the condensation, reaction conditions reported by Hasford and Rizzo were tested including the utilization of methanol as solvent for the reduction of nitroaniline **13**.[58] By applying this method, a side-product was obtained in small amounts with one fluorine substituent and one methoxy functionality. Presumably, 7-fluoro-8-methoxy-MIA (8-MeO-MIA, **17**) has been formed, considering the activated *para*-position to the nitro functionality with respect to nucleophilic

aromatic substitution. Since this flavin-derivative has not been reported in literature, further investigations regarding its characterization could be desirable. Alternatively, the synthesis of 8-MeO-MIA (**17**) according to the typical synthetic procedure would begin with the corresponding functionalized nitroaniline **16**, which is commercially available but extravagant.[34,52,59] Optimization of the reaction conditions and purification of the product has not been pursued, as this work was focused on other fluorinated flavin derivatives.

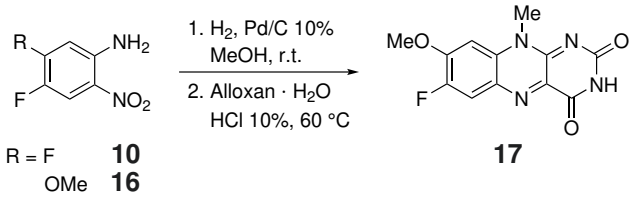

Scheme 3.5 Schematic illustration of the synthetic route of 8-MeO-MIA (**17**) beginning with difluorinated nitroaniline **10**, which was obtained by following the procedure described by Hasford and Rizzo.[58] The same product can likely be obtained beginning with the suitably functionalized nitroaniline **16**, following either the method by Hasford and Rizzo or the commonly used procedure by Kuhn and coworkers.[34,52,58]

3.4 Synthesis of 7,8-dF-RIA: An Initial Approach Towards Protein Incorporation

For the application of FbFPs in optical imaging, a further improvement of their brightness is necessary.[36,39] Due to the increased FQY of 7,8-dF-MIA with Φ_{fl} = 0.42 in comparison with the FQY of non-fluorinated MIA with Φ_{fl} = 0.22, a flavin derivative difluorinated in 7- and 8-position could be a convincible candidate for a chromophore exchange in FbFPs. Especially advantageous would be the combination with appropriate protein mutations, which have an additional effect on the FQY.[21,24] As an initial approach towards protein incorporation, the synthesis of 7,8-dF-RIA was investigated.

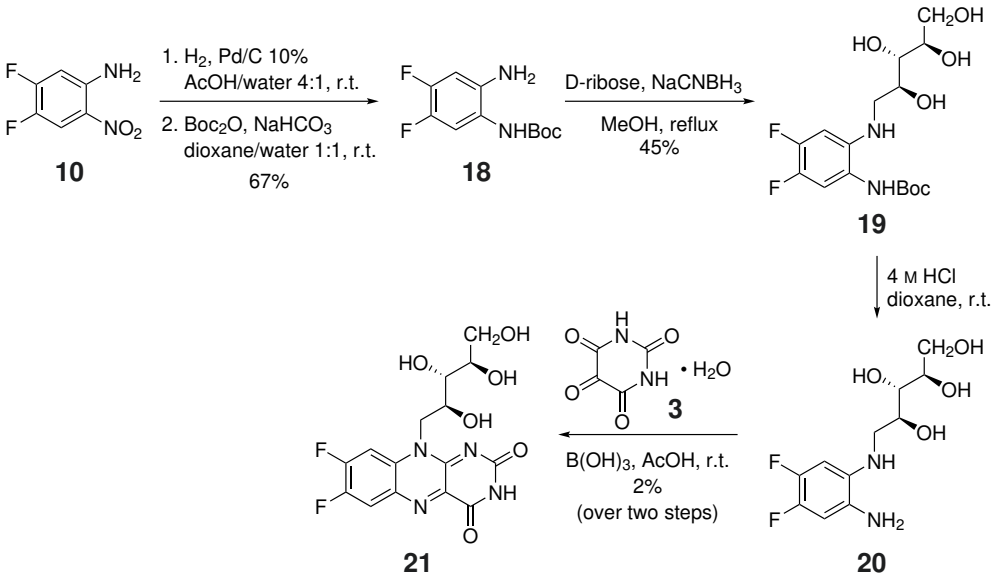

Scheme 3.6 Schematic illustration of the synthetic route to 7,8-dF-RIA (**21**) beginning with difluorinated nitroaniline **10** derived from the procedures described by Gärtner *et al.*[50] By initial reduction of the nitro group, the risk of fluorine substitution was minimized significantly. Since the free 1,2-diaminobenzene derivative was highly air sensitive, the Boc-protection of one amine functionality *in situ* was proven necessary (**18**). After ribityl installation and Boc-deprotection, the free ribityl-1,2-diaminobenzene **20** and the 7,8-dF-RIA (**21**), subsequently obtained from condensation with alloxan monohydrate (**3**), required careful handling.[36,52]

The synthetic route to 7,8-dF-RIA (**21**) shown in Scheme 3.6 was inspired by the synthetic route to 7,8-didemethylriboflavin reported by Gärtner and coworkers.[50,52]

Additionally, the procedures described by Carlson and Kiessling were consulted for comparison.[60] To minimize the risk of a nucleophilic aromatic substitution (see Section 3.3), the reduction of the nitro functionality was selected to initiate the synthesis. An amine functionality was then Boc-protected to prevent the 1,2-diaminobenzene **18** from decomposition upon contact with air. The subsequent reductive amination was conducted with D-ribose and sodium cyanoborohydride, which is a mild reducing agent and is typically used for the reduction of imines.[61] Since it was difficult to achieve a complete conversion to **19**, the reductive amination can be designated as the bottle neck reaction regarding yield. For instance, after refluxing for three days with two equivalents of both, D-ribose and sodium cyanoborohydride, 59% Boc-protected 1,2-diaminobenzene **18** was recovered. To improve the yield, it was tested to add excess equivalents of both reagents successively over several days. However, this method led to nonignorable side-product formation and a decrease in yield. Conversely, while the excess equivalents of both reagents were added at the beginning, a moderate yield of 45% could be afforded.

After Boc-deprotection and coupling with alloxan monohydrate, 7,8-dF-RIA (**21**) required precautious procedures due to its sensitivity to light and heat. These chemical properties are comparable to the particular light sensitivity of riboflavin (RF) reported in the literature.[62–64] Upon illumination, the ribityl chain is known to be photooxidized to deliver a broad spectrum of photoproducts, including formylmethylflavin (FMF), carboxymethylflavin (CMF), lumiflavin (LF) and lumichrome (LC).[62–64] Consequently, all purification procedures necessitated careful operation in the dark. Additionally, the heat sensitivity, which was already reported for 7,8-dF-MIA (**14**, see 3.3), required conduction of all procedures at ambient temperatures (see Experimental for details).

On account of the detailed discussion of the photophysical properties of 7,8-dF-RIA (**21**) in Ref. [36], Chapter 10, only selected details will be mentioned in this context. One vital observation was the decrease of FQY by installation of a ribityl side chain at 10-position instead of a methyl substituent. Specifically, a FQY of $\Phi_{fl} = 0.27$ was obtained for 7,8-dF-RIA (**21**) which is significantly lower than the one of 7,8-dF-MIA (**14**) with $\Phi_{fl} = 0.42$.[36] Spectroscopic analyses in deuterated water as solvent, performed by D. Sretenović, demonstrated the strong influence of water quenching on the FQY.[36]

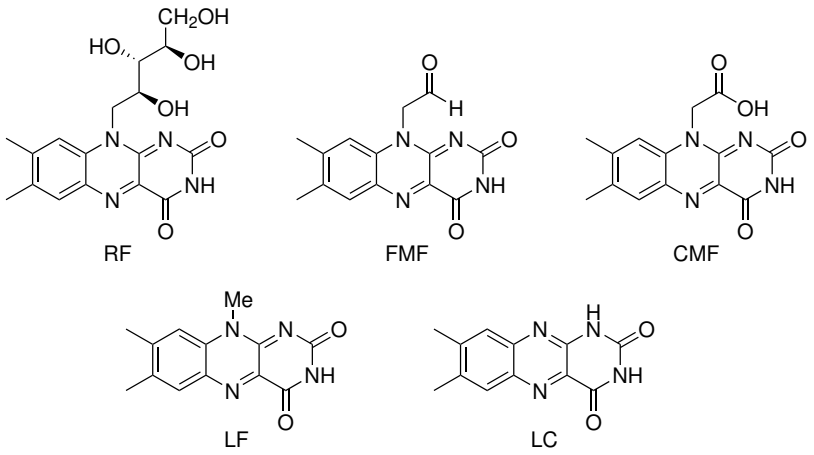

Figure 3.5 Structures of photoproducts, which are formed when riboflavin is illuminated with light. Besides several unknown products, formylmethylflavin (FMF), carboxymethylflavin (CMF), lumiflavin (LF) and lumichrome (LC) are formed.[62–64]

The synthesis of all flavin derivatives with fluorine substituents at the xylene ring facilitated the evaluation of the accuracy of quantum chemical predictions for the purpose of rational design of new flavin derivatives. Overall, an excellent agreement between computational predictions and experimental results was observed. With a rational chemical estimation, novel flavin derivatives can be designed and their photophysical properties predicted by quantum chemical calculations. Consequently, this method is a powerful implement for application purposes such as optical imaging, singlet oxygen generation (photodynamic therapy) or photocatalytic applications.[36]

4 Part II: 1-F-Lumiflavin - Targeting a Shift of Emission

For applications such as optical imaging, the utilization of fluorescent proteins of different emission wavelengths is advantageous because it allows the comparison of multiple protein fates or gene expression levels.[65] In contrast to GFP, which offers colors over the entire range of the visible spectrum, the emission color of FbFP is limited to the emission of the flavin chromophore, which is in the green region. Therefore, the modification FbFPs with the target to shift the emission wavelength is still a subject of research.

Only limited effects achieved by protein mutations have been reported in the literature with respect to an altered emission color. For instance, shifts of up to 10 nm have been reported which were caused by changes in hydrogen bonding.[21,25,26] Consequently, replacing the flavin-chromophore with new synthetic derivatives would be an alternative strategy.[21,25,26] In order to screen for suitable flavin derivatives, the quantum chemical method described in Chapter 3 can be utilized as a powerful tool. This has been initiated by Kleinschmidt and coworkers, who investigated the photophysical properties of flavins derivatized at the pyrazine- or pyrimidine-ring, yielding several hits with potentially shifted emission maxima.[38] For instance, the structures of 1-F-MIA and 2-CF_2-MIA are shown in Figure 4.1, whose emission maxima were predicted to shift to 765 nm and 844 nm, respectively, giving emission colors in the red to NIR region.[38] These wavelengths are particularly advantageous for optical imaging because they are less absorbed by living tissue, thus enabling deep tissue imaging.[38,66,67] Additionally, photoexcitation is possible under mild conditions with green light, which is less harmful for living tissues.[38]

Notably, a substantial limitation of both derivatives is their potentially reduced

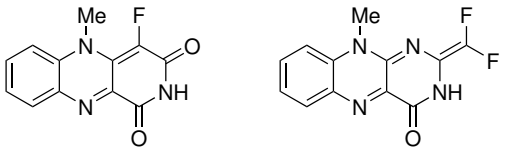

Figure 4.1 Structures of 1-F-MIA and 2-CF_2-MIA which were part of the screening by Kleinschmidt *et al.* of flavin derivatives modified at the pyrazine- or pyrimidine-ring. Both MIAs were predicted to show strong shifts of emission from the green to the red to NIR region.[38]

FQY, caused by high nonradiative transition rates due to the strong stabilization of their singlet states S_1.[38,43] This behavior is literature known and is called the energy gap law.[38,43] It was also confirmed by high-level quantum chemical calculations, which identified internal conversion (IC) as a pronounced non-radiative deactivation process for both derivatives.[38] Possibly, the characteristics of 1-F-MIA and 2-CF_2-MIA are comparable to those of the non-fluorinated 1-deazaflavin derivative, which has been investigated in several studies.[68–70] Specifically, its fluorescence has been reported to be observable on a picosecond time scale with an emission maximum at about 700 nm and a FQY well below one.[68–70] However, the predictions by Kleinschmidt and coworkers regarding the shifts of emission caused by these considerable structural changes in 1- and 2-position hold promise for multicolor optical imaging.[38] In addition, the synthesis and characterization of the two featured flavin derivatives would facilitate the experimental evaluation of the high-level quantum chemical calculations, introduced by Kleinschmidt *et al.* for the prediction of IC rate constants.[38]

4.1 Literature Overview of 1-Deazaflavin Derivatives

The study by Kleinschmidt and coworker revealed two flavin derivatives, 1-F-MIA and 2-CF_2-MIA (Figure 4.1), with promising photophysical characteristics.[38] To evaluate these theoretical predictions, synthetic investigations are required for experimental characterization. For both derivatives, no synthetic approach existed in the literature, but several approaches to a possible precursor, 1-deazariboflavin, have been reported.[50,60,71,72] Since the calculated emission maxima of both derivatives are in the red to NIR region, the focus was set on the synthesis of a 1-F-flavin derivative and the synthesis of the 2-CF_2-flavin derivative was not further investigated.[38]

The first synthetic approach to 1-deazariboflavin (**25**) was reported by Rogers *et al.* in 1977.[71] This route became the most commonly used route to 1-deazaflavin derivatives and begins with ribityl-1,2-diaminobenzene **22**. The two main steps are 1) The coupling of 1,2-diaminobenzene **22** with bromooxoglutarate **23** followed by spontaneous air oxidation giving **24** and 2) The ring closure with ammonia (Scheme 4.1).[71]

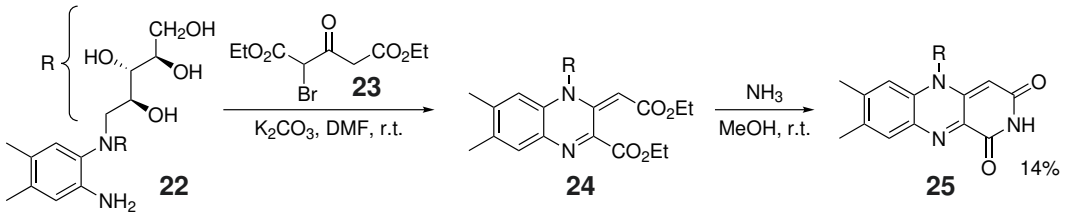

Scheme 4.1 Synthetic approach to 1-deazariboflavin (**25**) reported by Rogers *et al.* in 1977.[71] Two main steps can be emphasized: 1) The pyrazine ring formation by coupling with bromooxoglutarate **23** and 2) The final ring closure with ammonia.

Due to its difficulty and poor reproducibility, the synthesis of 1-deazariboflavin remained largely unmodified until 2004, when Carlson and Kiessling published optimized protocols for the synthesis of ribitylated 1,2-diaminobenzene **22** and for the coupling with bromooxoglutarate **23**.[60] They mono-Boc-protected the commercially available 1,2-diaminobenzene **26**, followed by reductive amination to introduce the ribityl side chain.[60] Finally, the Boc-protecting group was removed using conventional procedures.[60] By utilization of the more soluble cesium carbonate in the subsequent coupling with bromooxoglutarate **23**, they significantly improved the yield of the quinoxaline intermediate **24** from 20% to 55%.[60,71] After cyclization with ammo-

nia, the 1-deazariboflavin was obtained with an overall yield of 11%. This approach was reproduced by Gärtner *et al.* in 2008 with a total yield of 21%.[50]

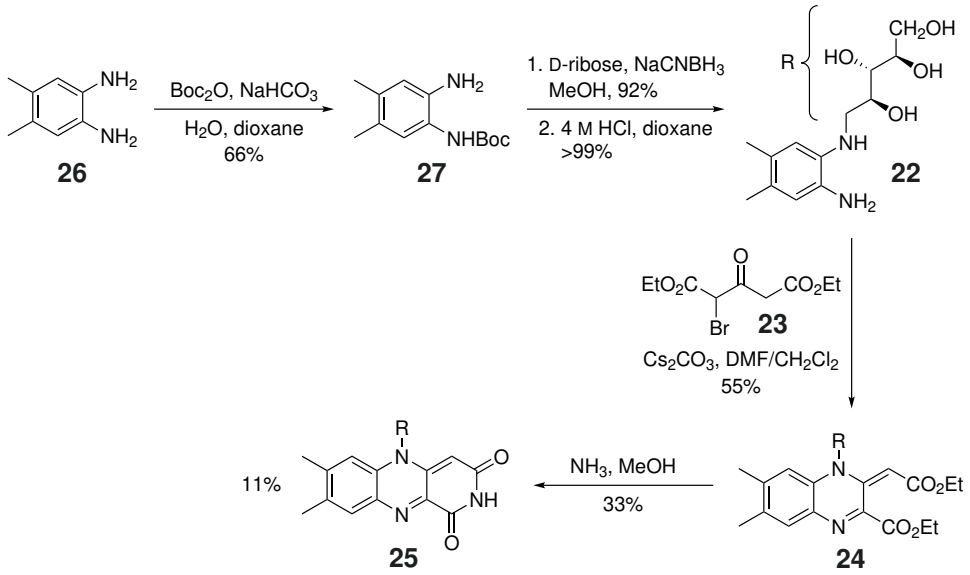

Scheme 4.2 Synthetic approach to 1-deazariboflavin (**25**) reported by Carlson and Kiessling.[60] They demonstrated an optimized protocol for the synthesis of ribitylated 1,2-diaminobenzene **22** and for the coupling with quinoxaline **24**, resulting in an improved yield of 55%.[60] A similar approach was reported by Gärtner *et al.* with an overall yield of 21%.[50]

In 2015, Richter *et al.* published optimized protocols for each step of the common synthetic route shown in Scheme 4.2 and reported an impressive overall yield of 61%.[72] They achieved improved yields primarily for three steps: 1) The Boc-protection of 1,2-diaminobenzene **26** (66% $\rightarrow$ 92%), 2) The coupling of ribityl-1,2-diaminobenzene **22** with bromooxoglutarate **23** (55% $\rightarrow$ 77%), and 3) The final ring closure with ammonia (33% $\rightarrow$ 92%).[72] The protocol for the Boc-protection of 1,2-diaminobenzene **26** is similar to that reported by Carlson and Kiessling.[60,72] For the coupling of ribityl-1,2-diaminobenzene **22** with bromooxoglutarate **23**, they screened numerous solvent systems and were able to reproduce the yield of 55% reported by Carlson and Kiessling.[60,72] In addition, by using a mixture of dry methanol and dichloromethane, they were able to increase the yield to 77%, arguing for a better miscibility and a sensitivity of the reaction to moisture.[72] The subsequent cyclization was conducted in a stoppered flask with a saturated solution of ammonia in methanol, which was freshly prepared at -78 °C.[72] However, no purification procedure of the crude product was reported within this work.[72]

4.2 Synthesis of 1-F-Lumiflavin: A Flavin Derivative with a Predicted Modified Emission Color

To enable comparability with recently published fluorinated flavin derivatives and theoretical suggestions, a simplified structure for the 1-F-flavin derivative was envisioned.[34–38] However, the poor solubility observed for 9-F-MIA (**7**) and 7,8-dF-MIA (**14**) proved problematic in terms of purification. Instead, lumiflavin (Figure 3.5) as a simplified structural motif holds promise, since the methyl-substituents in 7- and 8-positions contribute to the solubility, while exerting only a negligible effect on the photophysical properties of the flavin. Consequently, the structural motif investigated was 1-F-lumiflavin (**33**), whose synthetic approach is depicted in Scheme 4.3.

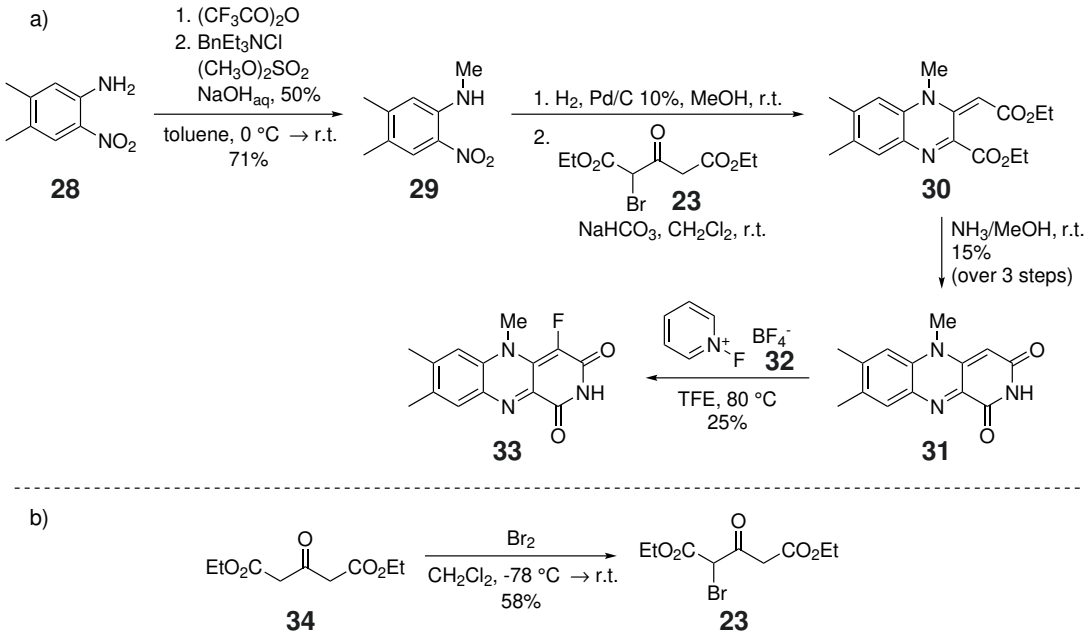

Scheme 4.3 a) Synthesis route to 1-F-lumiflavin (**33**) beginning with nitroaniline **28**. The first part is adapted from the typical synthetic route of MIAs with one-pot methylation and heterogeneous catalytic reduction *in situ*.[34,36,52,54,58] The following two steps, involving condensation with bromooxoglutarate **23** and ring closure with ammonia, are inspired by the synthetic routes discussed in Section 4.1.[50,60,71,72] 1-F-Lumiflavin (**33**) was finally obtained *via* late-stage electrophilic fluorination with a *N*-F-pyridinium salt.[73] b) Formation of bromooxoglutarate **23** by conversion of oxoglutarate **34** with bromine.[72]

The synthetic approach to 1-F-lumiflavin (**33**) begins with methylation of nitroaniline **28** by applying the one-pot procedure by Brown and Rizzo.[34,36,54] Subse-

quently, the nitro functionality was reduced with hydrogen by heterogeneous catalysis to form a 1,2-diaminobenzene derivative.[34,36,53] Due to stability issues, the 1,2-diaminobenzene derivative was coupled *in situ* with bromooxoglutarate **23** (see Section 3.2 for more details on stability issues).

The bromooxoglutarate **23** utilized for the formation of quinoxaline **30** was freshly prepared following a procedure by Richter *et al.*[72] In general, a mixture of product and starting material was formed with a highly variable ratio of product to starting material ranging from 50 : 50 to 77 : 23 (obtained from raw NMR-spectra), without significant variation in the experimental procedures. Purification of the mixtures *via* FC was attempted, however with little success, as only a slight improvement of the product/starting material ratio to 88 : 12 was achieved. Remarkably, despite its alleged instability, the product mixtures appeared to be stable at -40 °C for months.[60,72] Also, the formation of multiply brominated products as reported in the literature was not observed.[72]

Figure 4.2 Product mixture obtained from the coupling to quinoxaline **30**.

Due to the unsuccessful purification of bromooxoglutarate **23**, the product/starting material mixture was consequently used for coupling with the 1,2-diaminobenzene derivative to form quinoxaline **30**. First attempts using reaction conditions derived by Richter *et al.* (cesium carbonate, MeOH/CH_2Cl_2) produced a wide range of different compounds.[72] This mixture appeared impossible to purify, thus impeding the identification of the desired product (Figure 4.2).

Assuming that bromooxoglutarate **23**, which is reported in the literature to be quite unstable, may decomposes prior to condensation reaction, its stability was assessed within different environments.[60,72] The assessment was conducted in CH_2Cl_2 solution at room temper-

ature under TLC monitoring. With the addition of cesium carbonate, bromooxoglutarate **23** was completely consumed within half an hour, presumably forming a deprotonated species followed by intramolecular substitution of the bromine substituent. When sodium bicarbonate was added instead, this effect was less pronounced.

When the reaction conditions were adapted by utilization of sodium bicarbonate as base, considerable product formation was observed. Since it was still accompanied by the formation of various by-products, a determination of the yield of quinoxaline **30** proved difficult. This was only possible by accepting high losses caused by poor separation on FC, resulting in a yield of 16%. Instead, for rough estimation and comparison of reaction conditions, weight percentages of roughly separated product fractions were calculated, giving yields of 30 – 50 w% for test batches and 64 w% for large scale.

For yield optimization, the reaction conditions reported by Carlson and Kiessling, Rokita *et al.* and Gärtner *et al.* were additionally tested, involving cesium carbonate as base in a DMF/CH_2Cl_2 solvent system.[50,60,74] For this purpose, the reduction of nitroaniline **29** required an additional solvent exchange step. Therefore, the 1,2-diaminobenzene derivative was precipitated as hydrochloride to avoid decomposition, resulting in a very stable product **35** (Scheme 4.4).[75] For condensation with bromooxoglutarate **23**, it was redissolved directly in the DMF/CH_2Cl_2 solvent mixture. By applying this procedure, a yield of 63 w% was already obtained for a small-scale reaction, which promises even higher yields for upscaled batches. Further adaptations, such as replacing the base with sodium bicarbonate, could exert additional positive effects on yields due to less decomposition of bromooxoglutarate **23**.

In Table 4.1, the reaction conditions tested for the formation of quinoxaline **30** are listed with their yields in weight percent obtained from roughly separated product fractions. Applying the conditions reported by Richter *et al.* (No. 1, Table 4.1), no product formation was observed.[72] Possibly, the deprotonation of bromooxoglutarate **23** with subsequent intramolecular nucleophilic substitution of the bromine was faster than coupling with the 1,2-diaminobenzene derivative. When sodium bicarbonate was utilized as a base, product formation was observed and gave yields of 30 – 50 w%

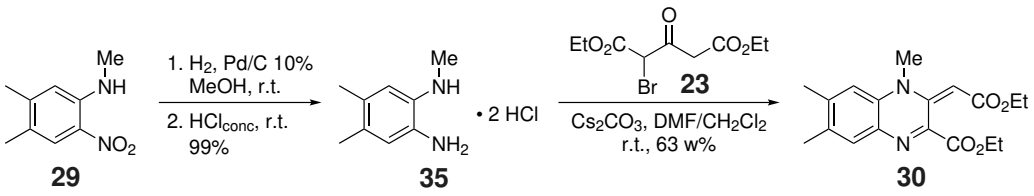

Scheme 4.4 Scheme of quinoxaline **30** formation beginning with nitroaniline which was reduced and precipitated as hydrochloride *in situ*.[75] 1,2-Diaminobenzene hydrochloride **35** was then dissolved for the condensation reaction with bromooxoglutarate **23** giving a yield of 63 w%.[50,60,74]

(No. 2, Table 4.1). Finally, the reaction conditions repeatedly reported in the literature (No. 3, Table 4.1) gave the best yield within this study, which could be promising for upscaling.[50,60,74]

Table 4.1 Overview of small-scale syntheses of quinoxaline **30** using different reaction conditions.[50,60,72,74] Yields are given in weight percent and are obtained by rough purification of the poorly purifiable raw material. All yields refer to nitroaniline **29** regardless whether an intermediate work-up was performed.

No.	Starting material for condensation	Solvent system	Base	Yield [w%] based on nitroaniline **29**
1	**29**	MeOH/ CH_2Cl_2	Cs_2CO_3	n.d.
2	**29**	MeOH/ CH_2Cl_2	$NaHCO_3$	30-50
3	**35**	DMF/ CH_2Cl_2	Cs_2CO_3	63

In general, a mixture of *E*-/*Z*-isomers of quinoxaline **30** was visible in the NMR spectra with a ratio of 1.00 : 0.70 in chloroform-*d*. The ratio is not expected to affect the subsequent 1-deazalumiflavin (**31**) formation, as a zwitterionic resonance structure is conceivable, as shown in Scheme 4.5.[50]

For the subsequent ring closure with ammonia (Scheme 4.3), the reaction conditions proposed by Richter *et al.* included condensation of ammonia at -78 °C and warming to room temperature in a closed reaction vessel.[72] By applying this method with a pressure tube, low yields of about 7% were obtained. In contrast, cyclization

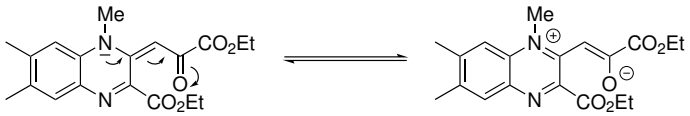

30 **36**

Scheme 4.5 Resonance structure of quinoxaline **30** with formation of zwitterionic quinoxaline **36**. Due to the loss of rotation barrier, the yield of 1-F-lumiflavin (**33**) is independent of the *E*-/*Z*-isomer value.[50]

using a solution of ammonia in methanol, previously prepared by simply purging ammonia through methanol until the volume stopped increasing, gave moderate yields of 15%.[50] The poorly soluble product precipitated promptly from the reaction mixture, allowing isolation *via* filtration and washing with several solvents such as EtOAc and CH_2Cl_2, so that the raw material was already in a sufficient degree of purification for yield calculation.

For spectroscopic purposes, a particularly high purity is mandatory. Hence, various purification methods were tested, including FC and recrystallization.[1] Chromatographic purification of flavin derivatives is often challenging due to their usually low solubility. Therefore, it is advantageous to completely dissolve the flavin and distribute it over a large surface area by adding silica gel prior to solvent evaporation. The "loaded" silica gel obtained in this way can be applied to a column analogous to Celite™ diatomaceous earth. Depending on the solubility of the flavin derivative being treated, up to a hundred times the amount may be required to ensure good solubility on FC. Therefore, this method is only applicable for small amounts and moderate solubilities, as otherwise the column size and solvent volume quickly reach impractical dimensions. The same applies to the dissolution of the flavin prior to silica gel loading. Any solvent or solvent mixture can be used as long as it is easily removable. However, if the solubility of the flavin is too low or a large amount needs to be purified, other purification methods should be considered to avoid wasting solvents.

For 1-deazalumiflavin (**31**), a sixfold amount of silica gel was sufficient to obtain good solubility on FC. Only the poor separation impeded a successful purification, thus relying instead on recrystallization methods. In his bachelor thesis, D. Nürenberg tested solvent mixtures such as formic acid/ acetic acid/ water and formic acid/ water, but struggled with low precipitation rates.[76] Therefore, after the suc-

1. Some tests were performed by D. Nürenberg as part of his bachelor thesis[76].

cessful employment of TFE as a potent recrystallization solvent for the purification of 9-F-MIA (**7**) (see Section 3.2 for further details), it was also successfully applied to the purification of 1-deazalumiflavin (**31**). For its recrystallization, two options are possible, both leading to a very pure product. One is to cool the solution of 1-deazalumiflavin (**31**) in TFE extremely slowly and allow recrystallization at low temperatures over a long period of time (for further details, see Experimental Section 7.3.5). This time-consuming procedure is then rewarded by the formation of needles of 1-deazalumiflavin (**31**), which are probably suitable for analysis in X-ray crystallography. A much faster procedure is to induce precipitation of **31** from TFE by layering with EtOAc (for further details, see Experimental Section 7.3.5), a method suitable enough to quickly remove small amounts of impurities.

Since efficient purification methods were developed for 1-deazalumiflavin (**31**), it could be considered omitting the rough purification of quinoxaline **30** and accept a lower degree of purity of crude 1-deazalumiflavin (**31**). These suggestions resulted from the comparison of the yield of quinoxaline **30** and 1-deazalumiflavin (**31**) with respect to nitroaniline **29**, which are in the same range at about 16%. Since quinoxaline **30** additionally appears to decompose slowly during FC, this procedure may need to be addressed to optimize the overall yield.

Figure 4.3 Needles formed by slow recrystallization of 1-deazalumiflavin from TFE.

For the late-stage functionalization of 1-deazalumiflavin (**31**) in 1-position (Scheme 4.6), an electrophilic fluorination was conducted. For this type of reaction, several reagents exhibiting a positively polarized fluorine source have been developed and are nowadays commercially available.[77–79] Their development in the 1980s was driven by the need for safe and easy to handle electrophilic fluorinating agent, as the formerly used elemental fluorine is highly toxic and requires special handling techniques.[77–79] The most common utilized N–F reagents provide a high stability that allow for easy and less hazardous handling, while maintaining sufficient reactivity for fluorination under mild conditions.[77–79] They can be either neutral compounds or quaternary ammonium salts with non-

nucleophilic anions as counter ions, that can exert an additional effect on the reactivity of the salt.[77–80]

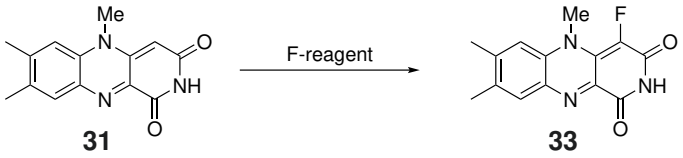

31 **33**

Scheme 4.6 Late-stage functionalization of 1-deazalumiflavin (**31**) with formation of 1-F-lumiflavin (**33**).

For instance, Takeuchi *et al.* reported the utilization of Selectfluor™ (**40**), a DABCO derivative with two quaternary ammonium centers and probably the most popular N–F reagent, for the synthesis of 3-fluorooxoindoles (**39**) from indoles (**37**).[81,82] For this purpose, two equivalents of Selectfluor™ (**40**) are necessary, as the initially introduced fluorine substituent is attacked by water to form an oxoindole **38**, which is finally fluorinated.[81]

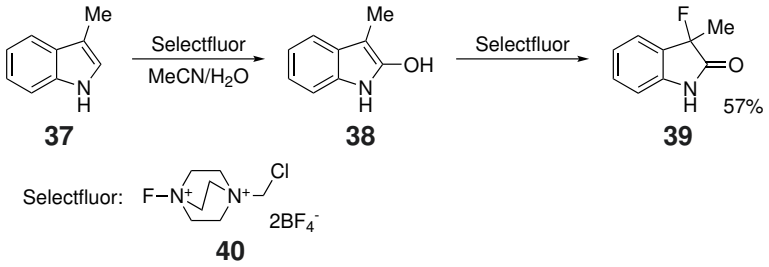

37 **38** **39**

40

Scheme 4.7 Scheme of the formation of fluorooxoindoles **39** from indoles **37** *via* double fluorination with Selectfluor™ (**40**) reported by Takeuchi *et al.*[81]

This example illustrates the degree of activation required for fluorination with N–F reagents. Typically, the functionalization of highly nucleophilic structural motifs such as enols, enamines and carbanions, for instance deprotonated malonates or Grignards, has been demonstrated.[77–79] However, recent studies have revealed several fluorination reagents that allow functionalization also in aromatic positions.[77–79] This large variety of available N–F reagents with different reactivities and selectivities allows precise fine-tuning of reactions. Therefore, several studies have focused on a ranking for quantitative or qualitative classification. A comprehensive summary was provided by Rozatian and Hodgson in 2020.[78–80]

A qualitative ranking of *N*-fluoropyridinium salts was reported by Umemoto

et al., who compared the reaction conditions required to obtain a high conversion of fluorination.[80] The results correlated with the electron withdrawing or donating character and position of the substituents on the pyridine. Consequently, the "fluorination power" decreased with the introduction of electron donating substituents such as methyl groups with respect to the unsubstituted *N*-fluoropyridinium salt. In contrast, electron withdrawing substituents such as Cl- and CO_2Me groups increased the reactivity, especially when located at 2-, 4- and/or 6-position, together with an increasing number of those substituents.[80]

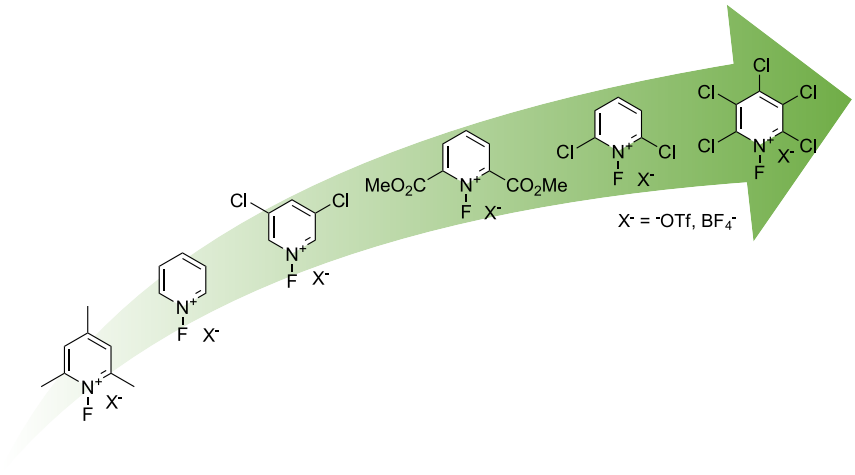

Figure 4.4 Relative representation of "fluorination power" of *N*-fluoropyridinium salts found by Umemoto *et al.* and summarized by Rozatian and Hodgson.[79,80] The "fluorination power" correlates with the character and position of the substituents at the pyridine ring.

Mayr *et al.* published in 2018 a quantitative ranking of five different fluorination reagents, derived from kinetic studies of reactions with carbanions and enamines.[78,79] Interestingly, the fluorination reagents considered in this study differed strongly, as in addition to *N*-fluoropyridinium salts, Selectfluor™ and *N*-fluorobenzenesulfonimide (NFSI) have been investigated. According to their results, Selectfluor™ is the reagent with the highest reactivity, closely followed by 2,6-dichlorosubstituted *N*-fluoropyridinium salt. The reactivity of NFSI can be classified in the middle range and both unsubstituted as well as 2,4,6-trimethylated pyridinium salts are rather less reactive reagents.[78] Similar results were obtained in a kinetic study by Hodgson *et al.* in 2018 by fluorination of 1,3-dicarbonyl compounds.[83] They generated a reactivity ranking of nine different N–F fluorinating agents with respect to Selectfluor™.[79,83] The structures are illustrated in Figure 4.5

and ordered on a relative reactivity scale.

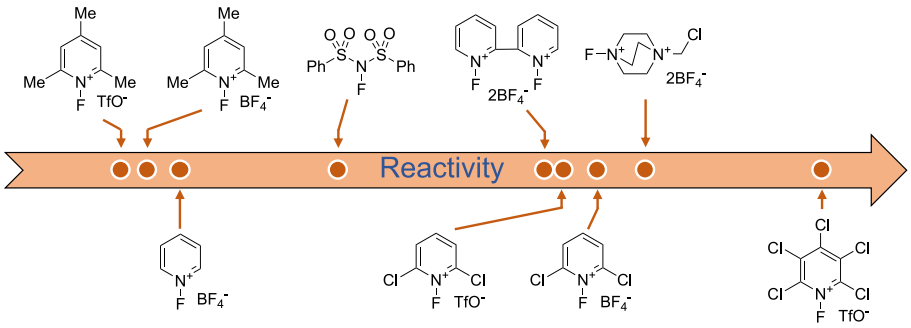

Figure 4.5 Ranking of the reactivity of various fluorinating agents with respect to Selectfluor™ as reported by Hodgson *et al.* and similarly reported by Mayr and coworkers. First row, from left to right: 2,4,6-Trimethyl-*N*-fluoropyridinium salts, NFSI, Synfluor™ and Selectfluor™. Second row, from left to right: Unsubstituted *N*-fluoropyridinium salt, 2,6-dichloro-*N*-fluoropyridinium salts and fully substituted chloro-*N*-fluoropyridinium salt.[78,79,83]

Initially, electrophilic fluorination of 1-deazalumiflavin (**31**) was tested with Selectfluor™ (Scheme 4.8).[81] It soon became apparent that solvent and solubility will be limiting factors, as large amounts of the starting material remained unaffected in the solid state. Moreover, the slightly increased solubility with introduction of a fluorine atom in 1-position led to the risk of consumption of 1-F-lumiflavin (**33**) if the reaction conditions were too harsh. This resulted in the formation of side-products which made product identification difficult as they exhibited product-like signals in their NMR spectra (Figure 4.6).

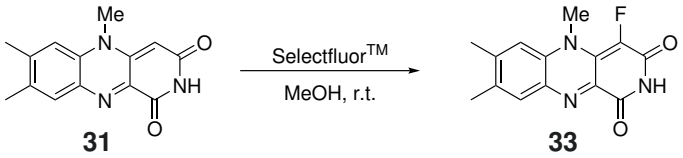

31 **33**

Scheme 4.8 Initial electrophilic fluorination tests of 1-deazalumiflavin (**31**) with Selectfluor™ with side-product formation, which exhibited product-like signals in their NMR spectra.[81]

Overall, the electrophilic fluorination of 1-deazalumiflavin (**31**) required optimization of the reaction conditions. A considerable difficulty was the partially contrary solubility and stability of both Selectfluor™ and 1-deazalumiflavin (**31**). For instance, Selectfluor™ is fairly soluble in acetonitrile, cold water and dilute hydro-

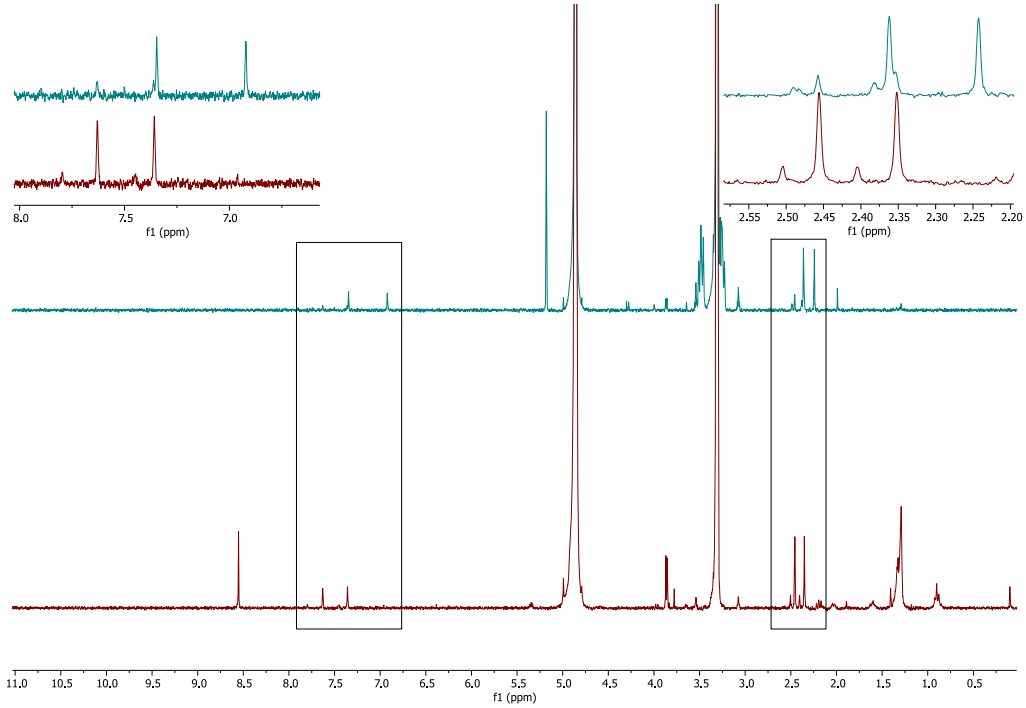

Figure 4.6 ^{1}H-NMR spectrum of the product obtained from fluorination reaction with Selectfluor^{TM} in methanol at room temperature (green) compared to the ^{1}H-NMR spectrum of 1-F-lumiflavin (**33**) (red). For better comparison, both aromatic proton signals and the signals of both methyl groups have been expanded to illustrate that the shifted signal set can be misinterpreted as that of 1-F-lumiflavin (**33**).

chloric acid, but poorly soluble in lower alkanols and acetone, which can be improved by the addition of small amounts of water or organic acids.[82] It decomposes rapidly in solvents such as DMF, DMSO and dilute sodium hydroxide.[82] In contrast, 1-deazalumiflavin (**31**) shows moderate solubility in DMSO, but is hardly soluble in acetonitrile, cold water and lower alkanols except TFE where moderate solubility is observed. A good solubility is obtained in dilute acids, which is one of the few overlaps with the solubility of Selectfluor^{TM}, but is accompanied by the risk of decomposition of 1-F-lumiflavin (**33**) with increasing temperature.

Several solvents and solvent systems were screened, including methanol, formic acid, TFE, MeOH/TFA/water, formic acid/water, formic acid/MeCN, formic acid/water/$CHCl_3$ and TFE/water/$CHCl_3$, to some extent performed by D. Nürenberg as part of his bachelor thesis.[76] In all cases, product formation was observed when one equivalent of fluorinating agent was used, sometimes accompanied by the formation of various side-products. The results were not quantitatively evaluated, since

the purification of 1-F-lumiflavin again proved to be difficult, a typical phenomenon in the synthesis of flavins already described for 9-F-MIA (Section 3.2), 7,8-dF-MIA (Section 3.3), 7,8-dF-RIA (Section 3.4) and 1-deazalumiflavin (current Section). Therefore, the products from the reactions in different solvents were qualitatively evaluated with respect to product and side-product formation as well as practicality with respect to product isolation.

Figure 4.7 Color change of 1-deazalumiflavin (**31**, left) upon fluorination in 1-position to form 1-F-lumiflavin (**33**, right).

Electrophilic fluorination in TFE, formic acid/water/$CHCl_3$, TFE/water/$CHCl_3$ or MeOH/TFA/water gave 1-F-1-deazalumiflavin (**33**) as the main product. Fluorination in other solvents and solvent systems resulted in the formation of side-product in equal or predominant amounts (see Experimental Section 7.3.6 for further details). A remaining challenge was the large amount of 1-deazalumiflavin (**31**) which remained untouched, leading to only little product formation, e.g. 7-12 mg of product **33** was obtained from 20-100 mg of 1-deazalumiflavin (**31**). Higher equivalents of Selectfluor^{TM} resulted in increased side-product formation with consumption of 1-F-lumiflavin (**33**). However, to complete the conversion it proved necessary to fluorinate with superstoichiometric quantities of fluorinating agents. Since the consumption of 1-F-lumiflavin (**33**) had to be avoided at the same time, several fluorinating agents were selected for fluorination tests, based on the rankings by Mayr *et al.* and Hodgson *et al.*[78,79,83] These reagents exhibited reactivities across the entire Hodgson reactivity scale (Figure 4.5) and are depicted in Scheme 4.9.

With utilization of each fluorinating agent shown in Scheme 4.9, the formation of 1-F-lumiflavin (**33**) was observed at room temperature, except for the two

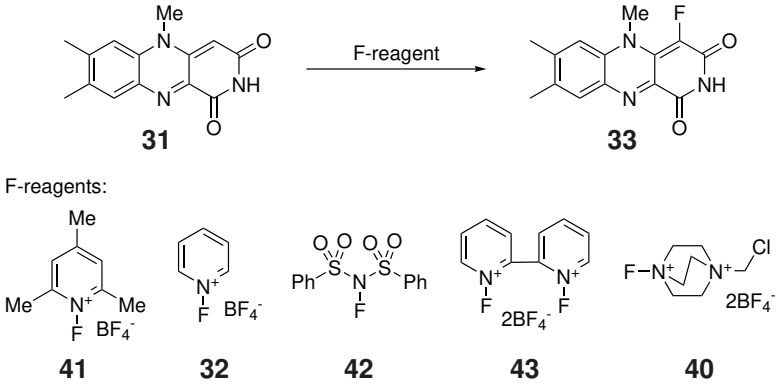

Scheme 4.9 Electrophilic fluorination of 1-deazalumiflavin (**31**) to form 1-F-lumiflavin (**33**). For this reaction type, a wide variety of fluorinating agents are commercially available, allowing precise fine-tuning of the required reaction conditions. The selected fluorinating agents exhibited reactivities across the entire reactivity scale created by Hodgson *et al.* and are ordered by increasing reactivity from left to right.[78,79,83]

N-pyridinium salts, **41** and **32**, which required elevated temperatures of 90 °C and 80 °C, respectively (see Experimental Section 7.3.6 for further details). All fluorinating agents were tested in TFE, as it provided sufficient solubility and allowed heating without decomposition of the flavins. The resulting raw NMR spectra from these tests were then evaluated qualitatively. In contrast to the results obtained from fluorination with Selectfluor™, the use of all other reagents resulted in exclusive formation of 1-F-lumiflavin (**33**). It is still unclear whether this is due to the lower reactivity of the fluorinating agents or a phenomenon related to the structure of Selectfluor™. However, by increasing the amounts of fluorinating agent, an increase in side-product formation and consumption of 1-F-lumiflavin (**33**) was observed for all reagents regardless of their reactivity. Therefore, the N–F reagent that gave the purest raw NMR spectrum, the unsubstituted *N*-pyridinium salt **32**, was selected for large scale synthesis and the incomplete conversion was taken into account.

For the purification of 1-F-lumiflavin (**33**), methods such as HPLC, FC and recrystallization were tested. Interestingly, the use of HPLC increased the level of impurities in the sample, suggesting a water sensitivity of 1-F-lumiflavin (**33**), especially with slight heating as required for the removal of acetonitrile *via* rotary evaporation. Therefore, solvent removal was performed analogously to the procedure described for 7,8-dF-MIA and 7,8-dF-RIA in Sections 3.3 and 3.4 under high vacuum at ambient temperature followed by lyophilization. By applying this method,

pure **33** was obtained in small amounts (5.5 mg from four HPLC runs). However, since a larger amount of material is required for extensive spectroscopic characterization, a combination of FC and recrystallization was additionally tested. Sole purification *via* FC did not provide a sufficient degree of purification, but at least separation from 1-deazalumiflavin (**31**) starting material was achieved. The increased solubility caused by the introduction of a fluorine atom in 1-position facilitated column loading dissolved in TFE, a procedure already described for 7,8-dF-MIA (**14**) in Section 3.3. Finally, successive recrystallizations from TFE and DMSO gave 1-F-lumiflavin (**33**) in a high degree of purification (see Experimental for further details). For structure validation, the crystal structure of 1-F-lumiflavin (**33**) was measured by P. Schmeinck and L. Karl. This unambiguous evidence for the formation of the desired 1-F-lumiflavin (**33**) together with the high degree of purification allows its spectroscopic characterization.

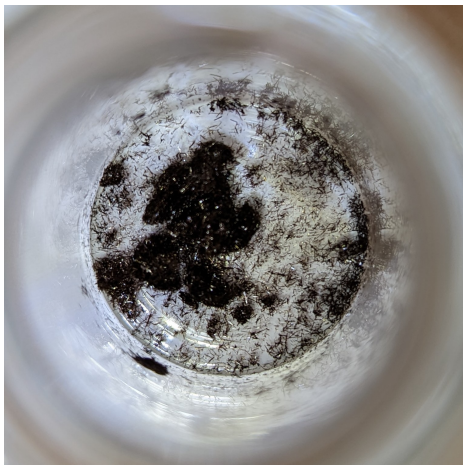

Figure 4.8 Needles formed by slow recrystallization of 1-F-lumiflavin from DMSO.

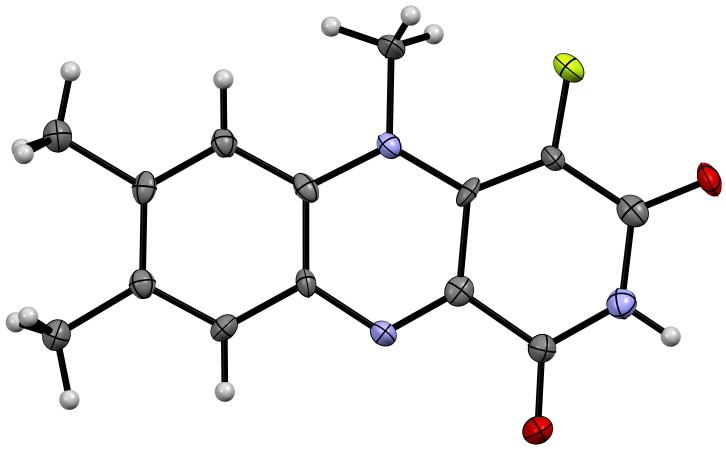

Figure 4.9 Molecular structure (thermal ellipsoid plot) of 1-F-lumiflavin (**33**) measured by P. Schmeinck. Structure solution was done in collaboration with L. Karl. Incorporated DMSO was omitted for clarity. Thermal displacement ellipsoids are drawn at the 50% probability level.

5 | Part III: Trifluoromethylated Deoxolumiflavins - Targeting an Increased Triplet Quantum Yield

The recent screening of flavins derivatized at the pyrazine- or pyrimidine-ring by Kleinschmidt and coworkers revealed two more flavin derivatives with promising calculated characteristics.[38] Instead of the typical carbonyl functionality in 2- and 4-positions they exhibit a trifluoromethyl functionality, respectively, and are therefore referred to as 2-CF_3- and 4-CF_3-MIA (Figure 5.1). This functional exchange results in an additional double bond at the pyrimidine ring and removal of the hydrogen atom in 3-position. These considerable structural changes enable rapid El-Sayed-allowed ISC due to a strong stabilization of the second triplet states of $n\pi^*$ character, which are typically inaccessible in aqueous medium.[38] This effect is predicted to reliably exceed fluorescence and is expected to be more pronounced with a trifluoromethyl functionality in 4-position than in 2-position.[38]

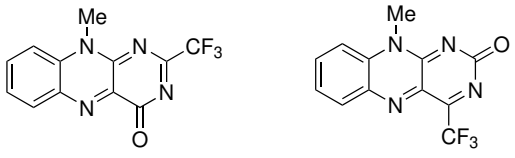

Figure 5.1 Structures of 2-CF_3- and 4-CF_3-MIAs reported by Kleinschmidt and coworkers which exhibit considerable structural changes resulting in promising calculated properties, a possible increased triplet quantum yield.[38]

Increased triplet quantum yields offer great potential for singlet oxygen generation in the context of photodynamic therapy.[21] For instance, LOV-based FbFPs have

been reported to be highly phototoxic proteins that generate sufficient amounts of singlet oxygen. For this purpose, it would be beneficial if the triplet quantum yield of the incorporated flavin would be increased.[21,47–49,84] In addition to medicinal applications, flavins with high triplet quantum yields could be used as photosensitizers for chemical purposes.[85] Several substrates have been successfully photooxidized by flavin derivatives, rendering them as green and versatile organocatalysts.[85,86] Clearly, some limitations such as their poor photostability require further investigations.[85]

5.1 Synthetic Pathways to Flavins Beyond the Kuhn Synthesis

Besides the common flavin synthesis by Kuhn *et al.* *via* coupling of 1,2-diaminobenzene derivatives with alloxan monohydrate, several synthetic strategies have been reported in the literature.[52,87–91] For instance, the so-called Tishler condensation (Scheme 5.1) is a classical synthetic route first published in 1947 and was developed due to availability difficulties of alloxan monohydrate and stability issues with the 1,2-diaminobenzene derivative.[88] Therefore, the Tishler condensation is based on the coupling of barbituric acid (**47**) with *o*-aminoazo-compounds (**46**).[88,90,91]

o-Aminoazo compounds **46** are commonly obtained *via* azo-coupling of suitably functionalized anilines (**44**) with *para*-substituted anilines (**45**) that are diazotized *in situ*. The coupling can be challenging due to the formation of three potential isomers: 2-azobenzene **46**, 6-azobenzene **49** and triazene **50**.[88,90] The ratio of the azo-isomers to triazene **50** can be influenced to some extent by adjusting the reaction conditions, as their formation is strongly pH dependent.[92] Very low pH values suppress any coupling, since protonation of amine **44** impedes activation of the benzene by the positive mesomeric effect (+M-effect) of the amine.[92] In contrast, neutral or very weakly acidic solutions favor coupling with the free amine, which represents the position of highest electron density, thus leading to triazene **50** formation.[92] Consequently, the pH must be adjusted individually to enhance the formation of the desired 2-azoaniline (**46**), which was for instance demonstrated by Erlenmeyer *et al.*, who reported the exclusive formation of 2-azobenzene (**46**, R=Me) in 85% formic acid.[90]

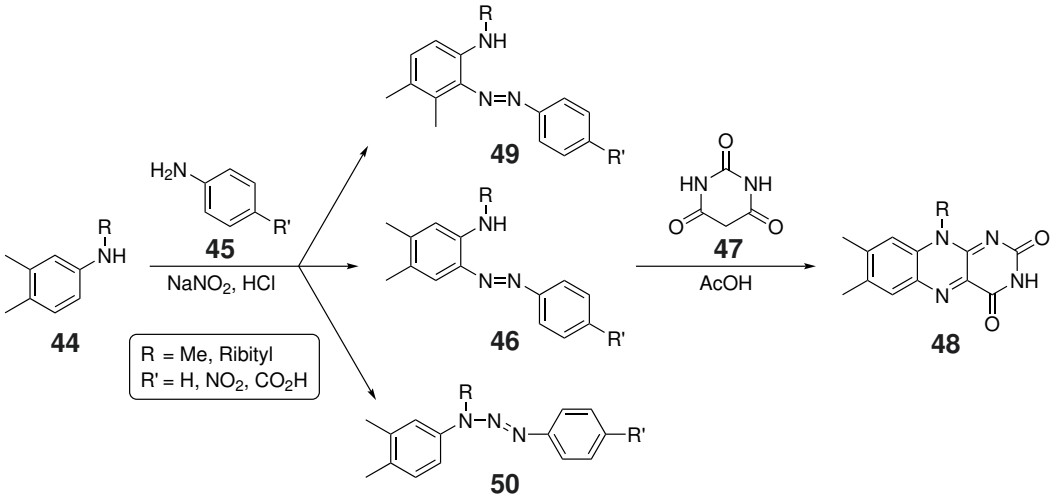

Scheme 5.1 Scheme of Tishler condensation as an alternative synthetic approach to flavin derivatives. Functionalized aniline **44** is coupled with a *para*-substituted aniline **45** to form an azobenzene (**46**), which is then reacted with barbituric acid (**47**). The azo-coupling can occur in three positions with formation of different isomers: 2-Azobenzene **46**, 6-azobenzene **49** and triazene **50**.[88,90,91]

Another synthetic approach to flavins has been reported by Erlenmeyer *et al.* in 1959 which is based on the coupling of anilines **51** with violuric acid derivatives (**52a** – **52e**).[89] By application of this method they demonstrated the synthesis of various roseoflavins derivatized in 2- and/or 4-position, such as thio- and imino-flavins (**53a** – **53e**).[89] For this purpose, they prepared the corresponding violuric acid building blocks (**52a** – **52e**) from suitably functionalized barbituric acid derivatives *via* nitrosation.[89]

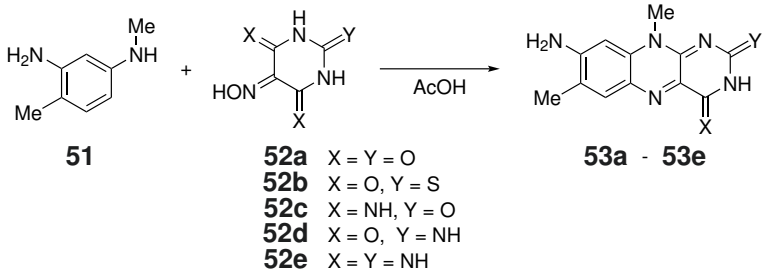

Scheme 5.2 Synthetic approach by Erlenmeyer *et al.*, who obtained roseoflavin derivatives functionalized in 2- and/or 4-position (**53a** – **53e**) *via* condensation with violuric acid derivatives **52a** – **52e**.[89]

In 1972, Yoneda *et al.* developed a synthetic approach to flavin derivatives *via*

the formation of isoalloxazine-*N*-oxides (**56**, Scheme 5.3).[93] They coupled 6-chlorouracil (**54**) with functionalized anilines **44** and closed the pyrazine ring using sodium nitrite to form the isoalloxazine-*N*-oxides **56** and **57**.[93] By subsequent deoxygenation, riboflavin (**48**), lumiflavin (**48**) and other flavin derivatives (**58** - **60**) were accessible.[93] In 1976, they extended the cyclization method with a protocol utilizing sodium nitrate.[94]

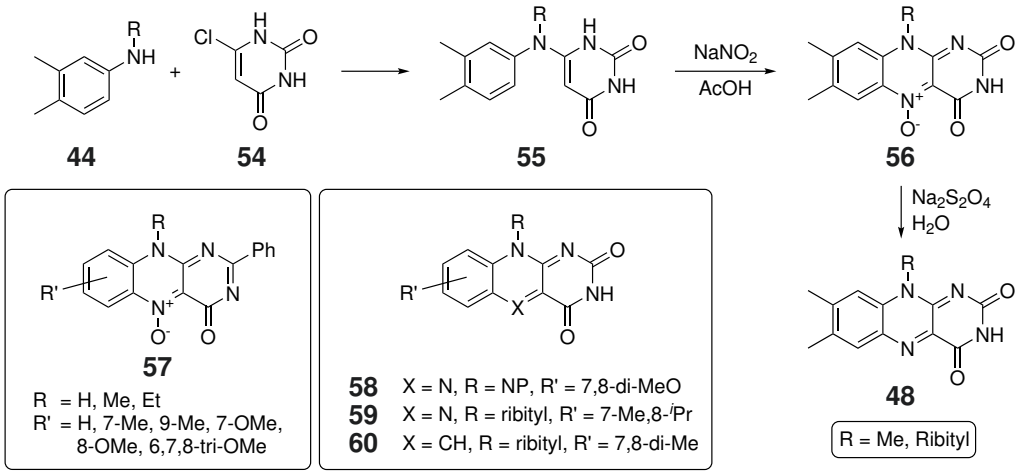

Scheme 5.3 Synthetic procedure published by Yoneda *et al.* in 1972, in which aniline **44** is coupled with 6-chlorouracil (**54**) and the pyrazine ring is subsequently closed by sodium nitrite.[93] By utilization of a similar route, the syntheses of 2-phenylflavin *N*-oxides **57**, di-MeO- (**58**) and *i*Pr-flavin derivatives (**59**) as well as 5-deazariboflavin (**60**) have been reported.[50,60,95–97] This illustration does not show all published compounds, for more details see references cited above.

This synthetic approach has been successfully applied to several flavin derivatives, such as 2-phenylflavin-*N*-oxides (**57**), 7,8-di-MeO-isobutylflavin (**58**), 8-*i*Pr-riboflavin (**59**) and 5-deazariboflavin (**60**) (Scheme 5.3).[50,60,95–97] Often, difficulties regarding the coupling with 6-chlorouracil (**54**) were reported, such as low yields or isolation problems.[50,60,97] Therefore, several modifications of this step are available in the literature.[50,60,98] For instance, Carlson and Kiessling as well as Gärtner *et al.* reported a catalytic effect of malononitrile.[50,60,98] In addition, Gärtner *et al.* observed a positive effect, when freshly prepared 6-chlorouracil (**54**) was used and the coupling was conducted under well maintained dry conditions.[50]

Typically, 6-chlorouracil (**54**) was obtained from the partial hydrolysis of 2,4,6-trichloropyrimidine (**62**) with sodium hydroxide. Instead of initially preparing

6-chlorouracil (**54**), aniline **61** can be coupled directly with 2,4,6-trichloropyrimidine to form tertiary amine **63**, as demonstrated by both Gärtner *et al.* and Fenner and Hochhuth.[32,99] In Scheme 5.4, this approach is exemplified by the synthesis of 8-Br- and 8-CF_3-riboflavins reported by Gärtner and coworkers.[32] The protection and deprotection steps of the ribityl side chain reported in the original procedure were omitted within this context for clarity.[32] Following the formation of tertiary amine **63**, the remaining chloro-substituents at the pyrimidine ring were hydrolyzed in two steps *via* introduction of benzyloxy-functions, giving **64**. Eventually, reductive deprotection yielded the hydrolyzed derivative **65**.[50,99] Notably, a disadvantage of this approach occurs when coupling is performed with trichloropyrimidine **62** instead of 6-chlorouracil (**54**), as the formation of two possible isomers has been reported, thus affecting the overall yield.[50,99]

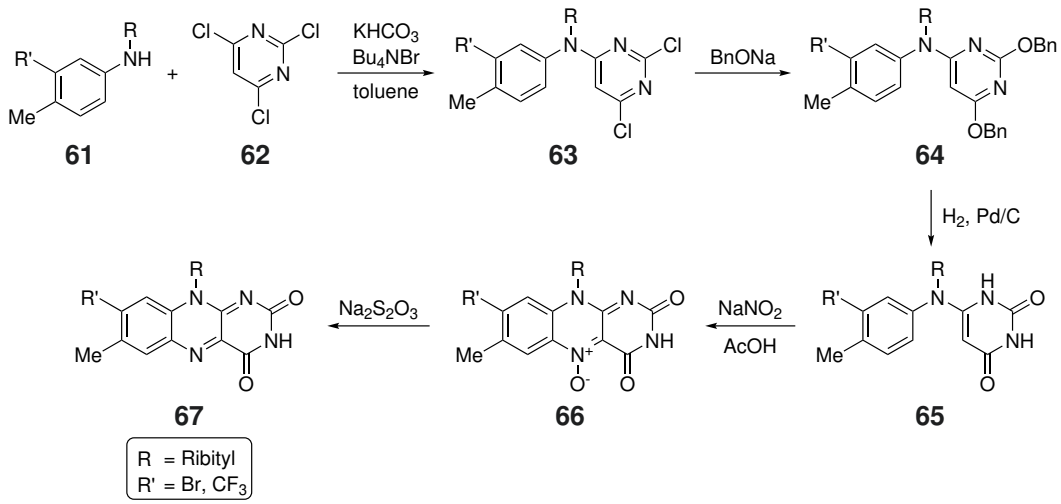

Scheme 5.4 Synthesis of 8-Br- and 8-CF_3-riboflavins reported by Gärtner *et al. via* coupling of aniline **61** with 2,4,6-trichloropyrimidine (**62**) and ring closure with sodium nitrite.[32] The protection and deprotection steps of the ribityl side chain were omitted for better clarity. For further details see Ref. [32].

Yoneda *et al.* reported another approach to flavins in 1976 *via* heating of aminouracils **68** with excess of nitrosobenzene. The resulting flavin derivatives **69** alkylated in 10-position were formed already after 20 min (Scheme 5.5).[94] In 1979, the range of products accessible by this approach was complemented by the synthesis of 10-aryl-3-methylisoalloxazines by Yoneda *et al.* and in 2013 by the synthesis of isoalloxazines non-functionalized in 3-position by Cibulka *et al.*[86,100]

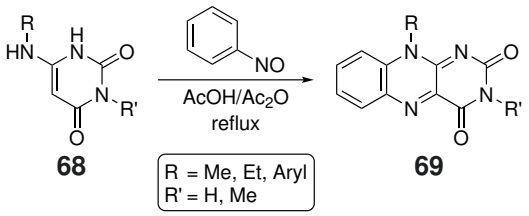

Scheme 5.5 Synthetic approach to flavin derivatives **69** *via* heating of aminouracil derivatives **68** with nitrosobenzene.[86,94,100]

5.2 Investigations on the Synthesis of Trifluoromethylated Deoxolumiflavins: Flavin Derivatives with Predicted Enhanced Triplet Quantum Yields

To ensure comparability with previously reported flavin derivatives and suggestions from quantum chemical calculations, lumiflavins were considered as simplified structures for the trifluoromethylated flavin derivatives. These considerations are based on several advantages already discussed in Sections 3.2, 3.3 and 4.2. In addition, the synthesis of trifluoromethylated lumiflavin derivatives substituted with a neopentyl group in 10-position was investigated. The introduction of a neopentyl group results in two improvements: 1) A better stability with respect to alloxazine formation (for further details regarding alloxazine formation, see Section 3.2) and 2) An improved solubility, which facilitates purification.

For the synthesis of 2-trifluoromethyl-2-deoxolumiflavin (**75**, 2-CF_3-lumiflavin) and 4-trifluoromethyl-4-deoxolumiflavin (**79**, 4-CF_3-lumiflavin) and their neopentyl-analogs, 2-CF_3-neopentylflavin (**76**, 2-CF_3-NP-flavin) and 4-CF_3-neopentylflavin (**80**, 4-CF_3-NP-flavin), similar methods were investigated. Therefore, the syntheses will be discussed collectively in the following section. Within this work, the investigation of three different approaches will be discussed: 1) *via* Kuhn-condensation, 2) *via* Tishler-condensation and 3) *via* *N*-oxide formation.[32,52,88,99]

The synthetic approach *via* Kuhn condensation required suitably trifluoromethylated alloxan derivatives **72** and **78** (Scheme 5.6). Their syntheses were investigated beginning with the corresponding barbituric acid derivatives **71** and **77**, respectively, following the protocol for the oxidation of barbituric acid with chromium oxide to alloxan monohydrate.[52,101] The oxidation products were then used for the following coupling with suitably functionalized 1,2-diaminobenzene derivatives, according to the condensation protocol by Kuhn *et al.* in the presence of boric acid.[52] Heterogeneous catalytic reduction of nitroaniline **29** gave *N*-methyl-1,2-diaminobenzene **70**. *N*-Neopentyl-1,2-diaminobenzene **74** was prepared *via* reductive amination with initial amide formation of nitroaniline **28** with pivaloyl chloride, followed by reduc-

tion with borane dimethylsulfide to form neopentylnitroaniline **73**.[102,103] Eventually, the nitro functionality was reduced by heterogeneous catalysis for the final Kuhn coupling.[34,52]

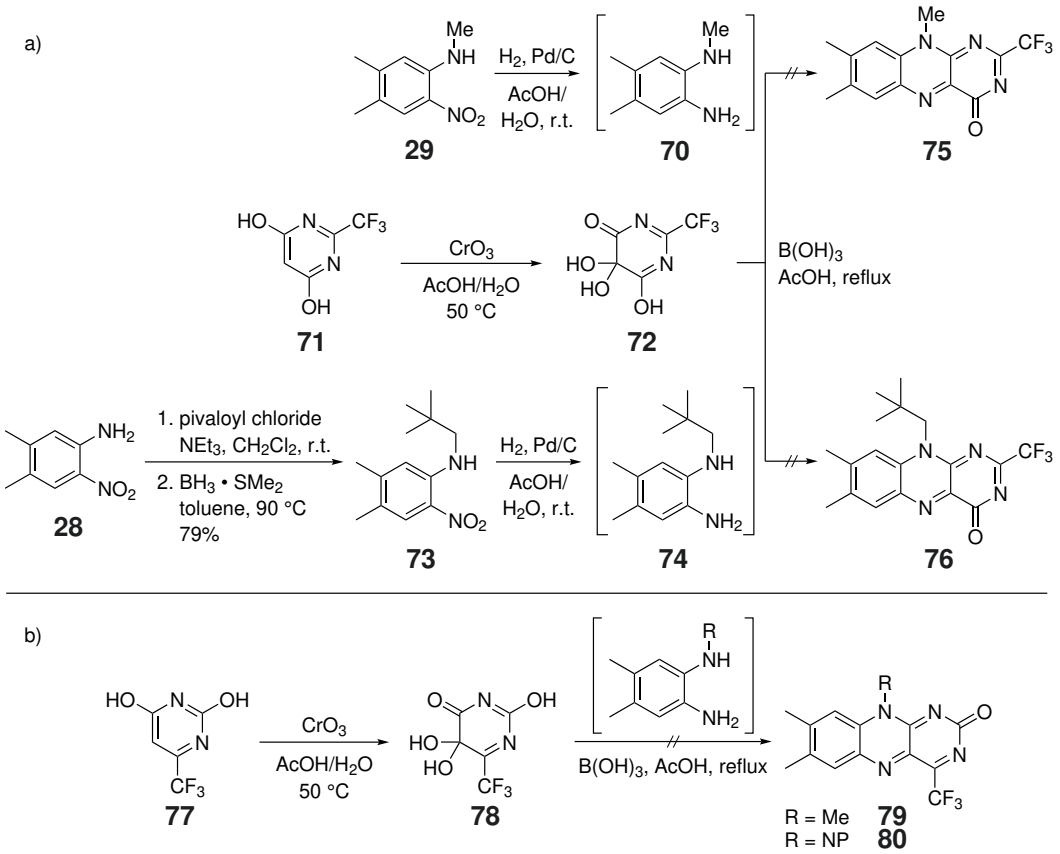

Scheme 5.6 a) Synthetic approach to 2-CF_3-lumiflavin (**75**) and 2-CF_3-NP-flavin (**76**) analogous to the Kuhn condensation.[52,101] It is based on the oxidation of trifluoromethylated dihydroxypyrimidine **71**, followed by coupling with 1,2-diaminobenzenes **70** and **74**, respectively. The coupling resulted in an unidentified product mixture. b) Similarly, the synthesis of 4-CF_3-lumiflavin (**79**) and 4-CF_3-NP-flavin (**80**) was investigated. The formation of 4-CF_3-flavin derivatives **79** and **80** was hardly achieved in any of the coupling experiments performed.

When 1,2-diaminobenzenes (**70** and **74**) were coupled with the material observed from the oxidation of barbituric acid derivative **71**, various products were obtained, some of which were colorful and/or fluorescent. This mixture of products was pre-purified *via* FC and the fractions obtained were analyzed *via* mass spectrometry. However, the masses of the desired flavin derivatives **75** and **76**, respectively, could not be measured. Consequently, this route was not further investigated as the large

amount of side products proved to be detrimental with respect to reasonable yields of the desired products. When the 4-CF_3-flavin precursor **78** was coupled with 1,2-diaminobenzenes **70** and **74**, respectively, hardly any product formation was observed. So, this synthetic approach was also not investigated further.[1]

The synthetic approach *via* Tishler-condensation (Scheme 5.1) required an azo-compound (**85**), that is coupled with barbituric acid derivative **71** to form 2-CF_3-lumiflavin (**75**). To synthesize azo-compound **85**, dimethylaniline **81** was initially methylated in a three-step manner *via* Boc-protection. The thus functionalized *N*-methylaniline **82** was then utilized for azo-coupling studies.[88] However, triazene side-product **84** was formed exclusively under the usual buffered conditions. When the pH was adjusted with dilute hydrochloric acid, which was expected to reduce the amount of neutral amine in the solution, triazene **84** was still the main product and the desired 2-azo-compound **85** was obtained in very small amounts (Scheme 5.7). Therefore, the following coupling with barbituric acid derivative **71** could not be examined in this context.

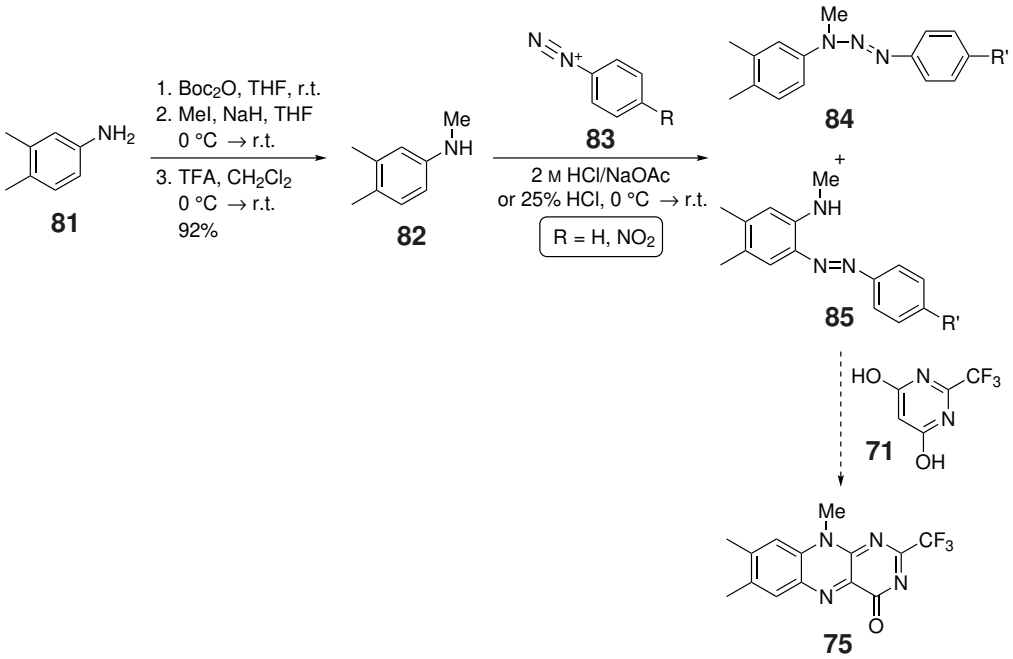

Scheme 5.7 Investigations on the synthesis of azo-compound **85** *via* typical azo-coupling procedures. In general, the formation of triazene **84** was predominant and azo-compound **85** was formed only in small amounts, thus hampering investigations with respect to the subsequent coupling with barbituric acid derivative **71**.

1. The procedures were performed in parts by D. Nürenberg under my instruction.

As an alternative synthetic approach to a suitable azo-compound, a method published by Parquette *et al.* was tested as shown in Scheme 5.8. It is based on the coupling of a nitroso group with an aromatic amine to form an azo functionality.[104] Analogous to the synthetic route reported by Parquette *et al.*, methylated nitroaniline **29** was initially protected as acetamide to give **86**.[104] The nitro group was then converted to a nitroso functionality *via* a reduction-oxidation sequence. Subsequently, the azo-formation was performed with *m*-nitroaniline analogous to Parquette *et al.*[104–106] Acetamide deprotection under basic conditions led to the formation of the product in small amounts. Since purification *via* FC provided no sufficient purity, a yield calculation and full characterization of the product was impossible. Further purification attempts were omitted due to the small amount of material available. Since NMR spectroscopic analysis revealed a signal set, indicating the possible formation of azo-compound **89**, the mixture was used for cyclization tests with barbituric acid derivatives **71** and **77**, respectively. The cyclization was initiated with various acids, including organic acids such as acetic acid or trifluoroacetic acid and inorganic Lewis acids such as $ZnCl_2$, $Yb(Tf)_3$ or $Sc(Tf)_3$, respectively. However, conversion to trifluoromethylated flavin derivatives **75** and **79** was hardly achieved under any of the conditions tested, indicating that this route is unsuitable for this purpose.

Since both previously discussed synthetic approaches to trifluoromethylated flavin derivatives were unsuccessful, a third synthetic approach *via* *N*-oxide formation was investigated. In this context, two routes are possible: 1) Following the route published by Yoneda *et al.* by utilization of a trifluoromethylated 6-chlorouracil derivative and 2) analogous to the procedures by Gärtner *et al.* and Fenner and Hochhuth using a trifluoromethylated dichloropyrimidine derivative.[32,93,99] Since the second option was developed due to the problematic coupling of anilines to 6-chlorouracils, the focus was on the route to 2-CF_3-lumiflavin (**75**) *via* coupling with a trifluoromethylated dichloropyrimidine derivative **90**.[32,50,60,97,99,107] The synthetic preparation of this compound has already been described in the literature, which begins with commercially available trifluoromethylated dihydroxypyrimidine **71**.[108] Accordingly, chlorination of dihydroxypyrimidine **71** with phosphorus oxychloride was the first step in the synthetic route towards 2-CF_3-lumiflavin (**75**) shown in Scheme 5.9. Subsequent coupling with functionalized aniline **82** gave tertiary

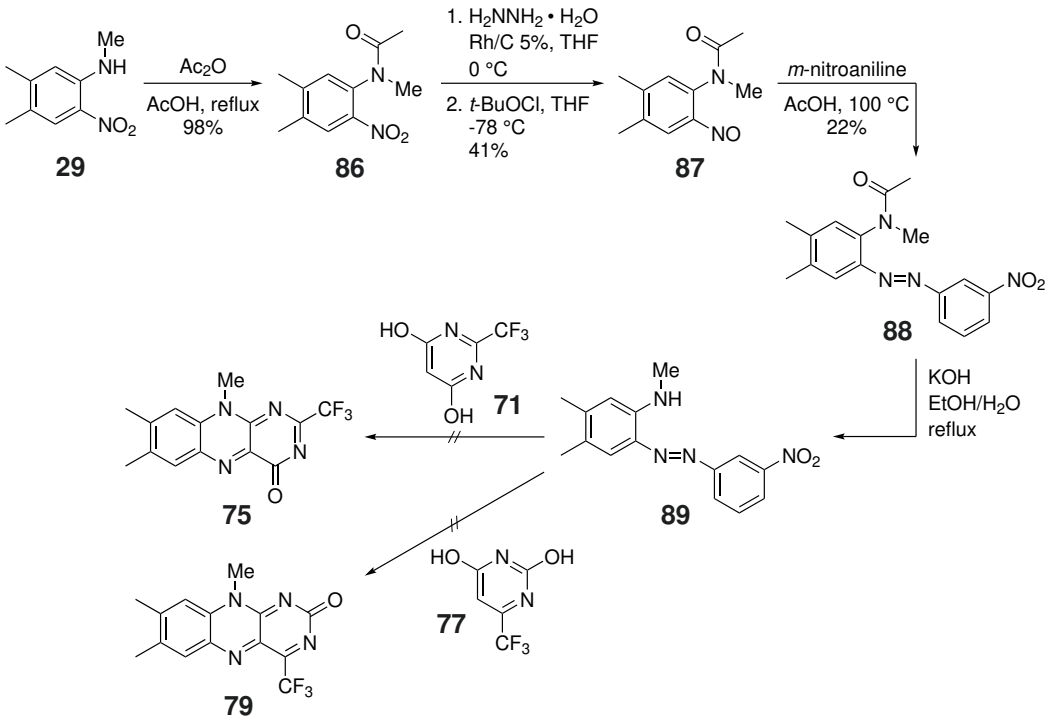

Scheme 5.8 Synthetic approach to 2-CF_3-lumiflavin (**75**) and 4-CF_3-lumiflavin (**79**) *via* coupling with 2-azo-aniline **89**, obtained by applying a protocol by Parquette *et al.*[104] In the final cyclization tests hardly any conversion was observed, indicating that this approach is unsuitable for the synthesis of trifluoromethylated flavin derivatives **75** and **79**.

amine **91** after only a few hours at room temperature, possibly promoted by the effect of the electron-withdrawing trifluoromethyl group.[1] In addition, the methyl substituent in *N*-position of aniline **82** exerts significantly lower steric hindrance than the common ribityl substituent at anilines utilized in the literature.[32,50,60,97,99,107]

The substitution of the chloro substituent was achieved *via* a straightforward protecting group strategy demonstrated by Gärtner *et al.* and Fenner and Hochhuth.[32,99] Therefore, a benzyloxide functionality was introduced first, followed by heterogeneous catalytic reductive deprotection. The subsequent ring closure to *N*-oxide **94** was tested with sodium nitrite, giving an orange product already at ambient temperature. After deoxygenation with sodium dithionite, the raw material was analyzed *via* mass spectrometry, which revealed the mass of 2-CF_3-lumiflavin (**75**), indicating that it might have been formed. However, it could only be isolated in very small amounts and at low purity, which prevented its full characterization. Specifically, from 200 mg

1. The procedures were performed in parts by D. Nürenberg under my instruction.

of tertiary amine **93**, only 11 mg of potential product was obtained in low purity and most of amine **93** was recovered from the reaction mixture. All attempts to complete the conversion, such as gentle heating to 50 °C, remained unsuccessful, as they resulted in mixtures of unknown compounds that were difficult to purify. After deoxygenation trial of this mixture, the desired product **75** could not be identified, suggesting that *N*-oxide **94** might be unstable at higher temperatures in acetic acid (see alloxazin formation in Section 3.2).[1]

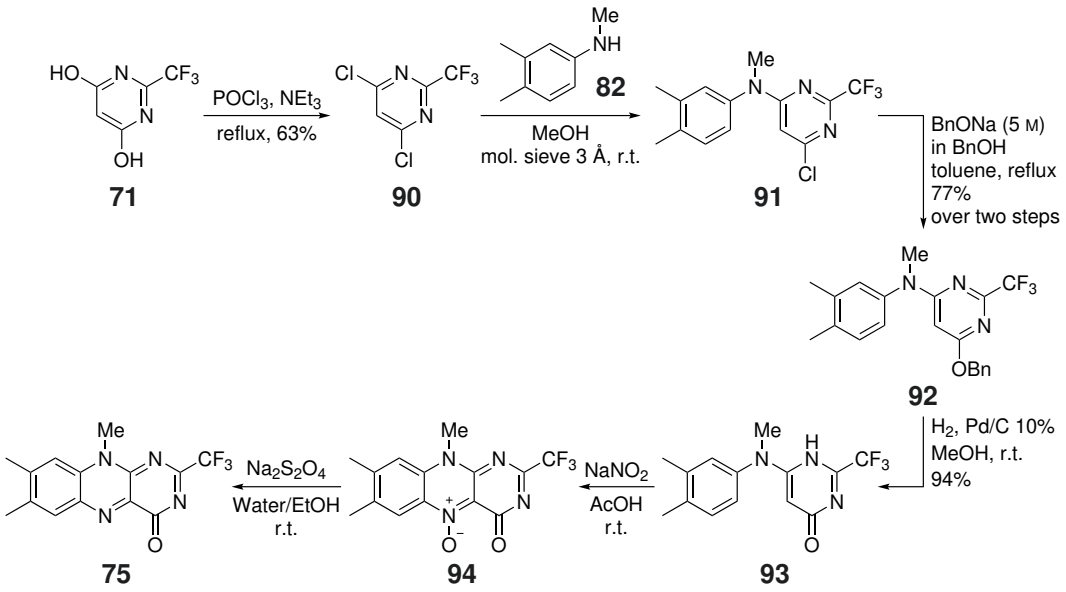

Scheme 5.9 Synthetic approach to 2-CF_3-lumiflavin analogous to the procedures described by Gärtner *et al.* and Fenner and Hochhuth.[32,99] It was based on the formation of tertiary amine **93** *via* protecting group strategy, followed by *N*-oxide formation and subsequent deoxygenation.

Due to the stability problems observed in context of the *N*-oxide formation to 2-CF_3-*N*-oxide (**94**), the synthesis of 2-CF_3-NP-flavin (**76**), an alternative trifluoromethylated deoxoflavin derivative, was additionally investigated. This structural motif provides two essential advantages: 1) A higher resistance against alloxazine formation and 2) A better solubility facilitating purification.

The synthetic approach to 2-CF_3-NP-flavin is shown in Scheme 5.10 and was planned analogous to the route described above (Scheme 5.9). For this approach, a suitably functionalized aniline **95** was required, which was prepared *via* reductive amination. For this purpose, an amide was formed by coupling with pivaloyl chloride that was subsequently reduced with borane dimethylsulfide.[102,103] The cou-

pling of NP-aniline **95** with dichloropyrimidine **90** gave **96** in good yields. However, the increased steric hindrance significantly reduced the reaction rate of this coupling, thus necessitating heating over a long period of 12 days. For this purpose, TFE was utilized as solvent instead of methanol as it allowed slightly higher temperatures. All attempts to increase the coupling rate, such as the addition of sodium bicarbonate derived from the protocol by Gärtner *et al.* and Fenner and Hochhuth, or the addition of malononitrile as reported by Gärtner *et al.* and Carlson and Kiessling, led either to the consumption of dichloropyrimidine **90** and remaining NP-aniline **95** or to the formation of side-products.[32,50,60,98,99]

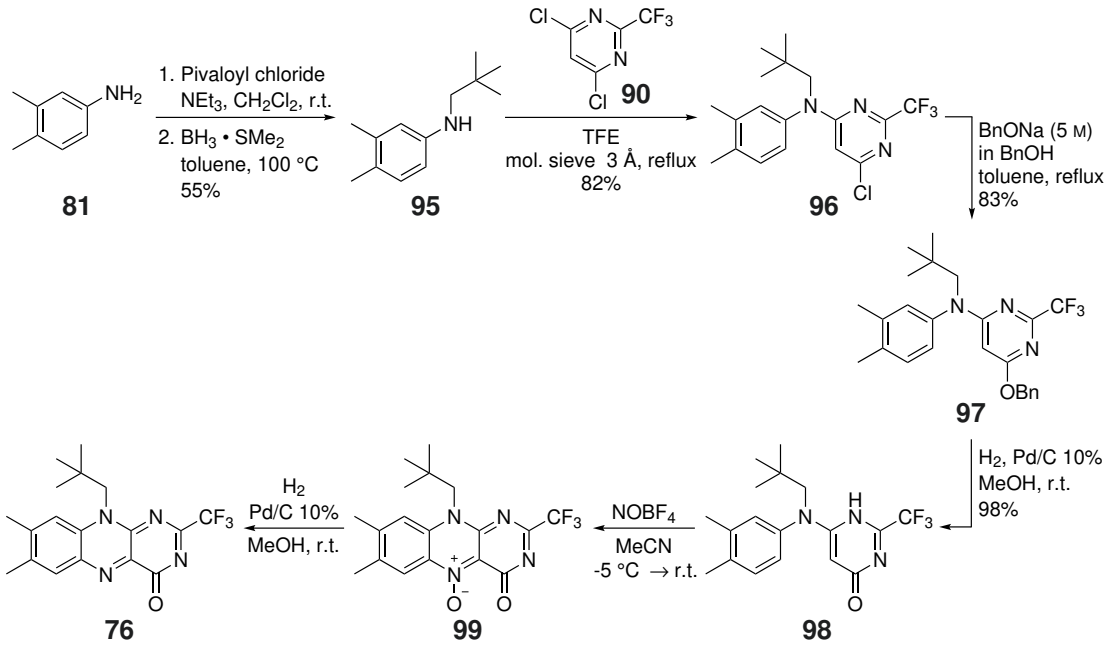

Scheme 5.10 Synthetic approach to 2-CF_3-NP-flavin (**76**) *via* protecting group strategy and *N*-oxide formation.[32,99,109] Cyclization with nitrosyl tetrafluoroborate yielded exclusively *N*-oxide **99**. However, the low purity of the raw material prevented a yield calculation. For the subsequent deoxygenation to 2-CF_3-NP-flavin (**76**), the reaction conditions are given, with which the mass of 2-CF_3-NP-flavin (**76**) was observed when the product was analyzed by mass spectrometry. Until now, pure material was hardly obtained mainly due to stability reasons.

The substitution of the chloro substituent was again achieved by applying the straightforward protecting group strategy *via* introduction of a benzyloxy functionality and subsequent heterogenous catalytic reductive deprotection. The tertiary amine **98** obtained by this sequence was utilized for cyclization tests to *N*-oxide **99**

with subsequent deoxygenation to 2-CF_3-NP-flavin (**76**). However, using the conventional cyclization method with sodium nitrite, even at high temperatures, complete conversion was hardly achieved.[32,50,53,94,99] In addition, significant side product formation upon heating hampered the identification of *N*-oxide **99** and increased the difficulty of the following deoxygenation due to low yields and problematic purification. Instead, an alternative cyclization protocol by utilization of nitrosyl tetrafluoroborate was developed that required strict oxygen and water-free conditions.[109] Using this protocol, *N*-oxide **99** was formed without residual starting material and with only little side-product formation. However, the low purity of the raw material hampered any yield calculation and purification was omitted due to stability reasons.

Typically, the deoxygenation of *N*-oxides to flavins is performed with reagents such as sodium dithionite or sodium thiosulfate as demonstrated by Gärtner *et al.*, Averill *et al.* and Yoneda *et al.*[32,50,53,94] However, the conversion of *N*-oxide **99** with sodium dithionite formed an extremely delicate product that decomposed rapidly in contact with solvents such as TFE and methanol. In degassed deuterated DMSO (Figure 5.2), three signals were visible in the aromatic region and one at ∼12 ppm. This signal and an additional one at ∼7 ppm (Figure 5.2, marked in red) disappeared after addition of deuterated water. The structure could not be elucidated unambiguously, but a structural motif as shown in Figure 5.2 would fit to the obtained signal set and a mass obtained by mass spectrometry of the raw material. When deoxygenation was performed by heterogeneous catalytic reduction, the mass of the desired 2-CF_3-NP-flavin (**76**) was detected by mass spectrometry, indicating that the desired product was formed. However, its rapid decomposition rendered purification very challenging, so 2-CF_3-NP-flavin (**76**) was not yet unambiguously identified.

The synthetic approach by Gärtner *et al.* and Fenner and Hochhuth *via* protecting group strategy and *N*-oxide formation was also tested for the synthesis of flavin derivatives with a trifluoromethyl group in 4-position.[32,99] Similar to the synthetic investigations described for 2-CF_3-flavin derivatives, a lumiflavin as a minimal structural motif was first investigated for the 4-CF_3-flavin derivative. For this purpose, trifluoromethylated dihydroxypyrimidine **77** was chlorinated analogous to the method described above (Scheme 5.11).[108] In contrast to dichloropyrimidine **90** utilized for the synthesis of 2-CF_3-flavin derivatives, the corresponding dichloropyrimidine **100** used for the synthesis of 4-CF_3-flavin derivatives exhibited no C_2 axis,

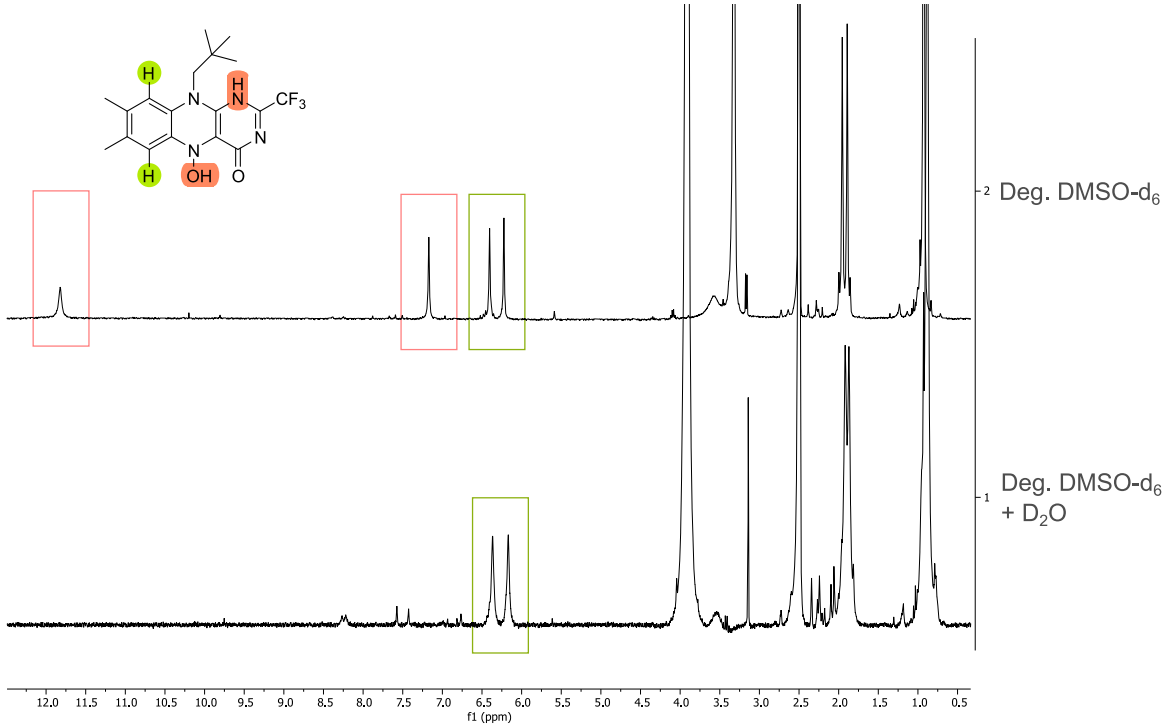

Figure 5.2 Comparison of NMR-spectra of the raw material from deoxygenation of *N*-oxide **99** with sodium dithionite in degassed DMSO-d_6 and degassed DMSO-d_6 with deuterated water. Based on the behavior upon addition of deuterated water and a mass obtained from mass spectrometry of the raw material, the structural motif shown is proposed.

thus enabling the formation of two coupling products, namely **101** and **102**. In the literature, this phenomenon has already been reported by Fenner and Hochhuth when 2,4,6-trichloropyrimidine (**62**) was utilized for this purpose.[99] However, when dichloropyrimidine **100** was coupled with suitably functionalized aniline **82**, exclusively one product was formed after only a few hours at room temperature. Analysis by NOESY-experiments showed a spatial proximity between the aromatic protons and the C*H* of the pyrimidine ring. Together with a similarity to the NOESY results of tertiary amine **91** formed in the synthesis of 2-CF_3-lumiflavin (**75**), it was suggested that the desired product **101** was formed. This suggestion was finally unambiguously validated *via* X-ray crystallography (Figure 5.3).[1]

The substitution of the chloro substituents was again achieved by applying the protecting group strategy shown above.[32,99] The introduction of the benzyloxy functionality was straightforward, but the purification of the product **103** proved chal-

1. The experiments were performed in parts by D. Nürenberg under my instruction.

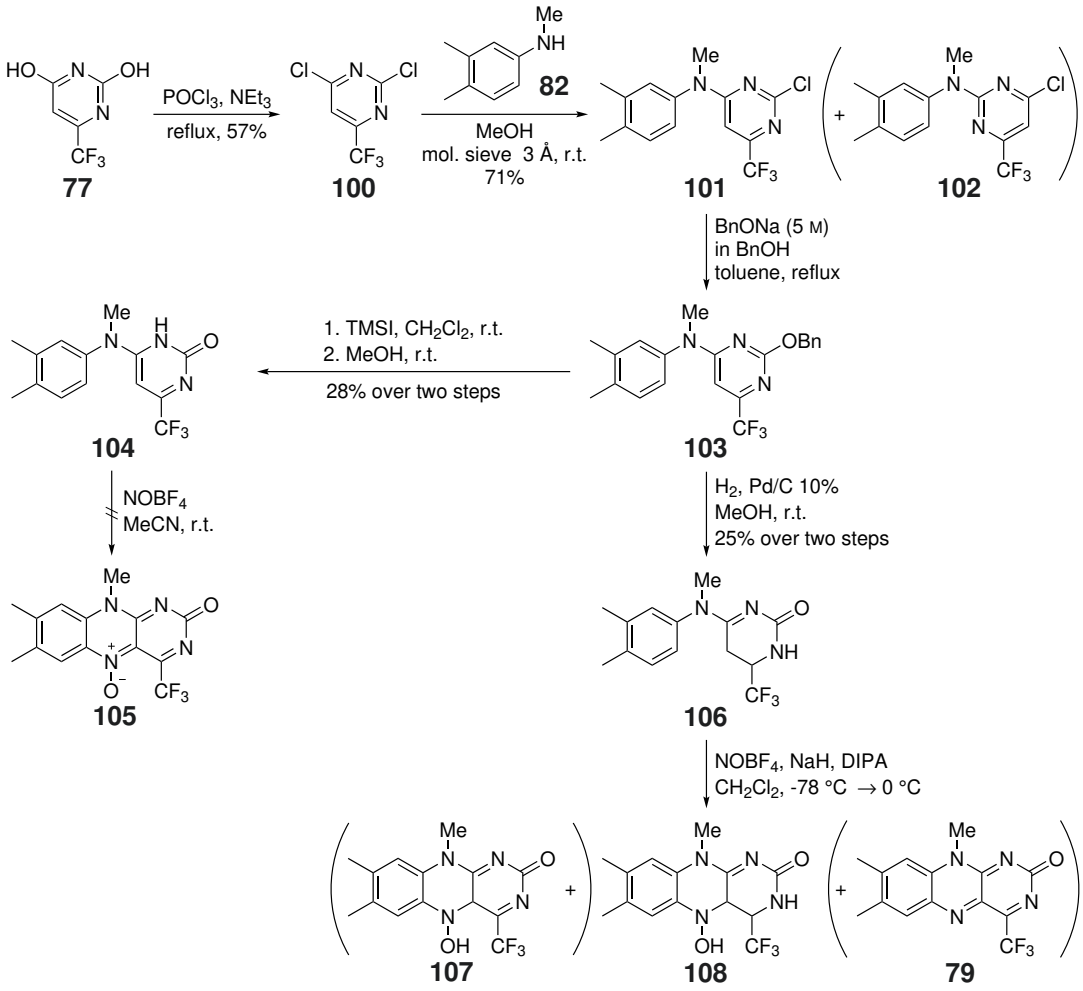

Scheme 5.11 Synthetic approach to 4-CF_3-lumiflavin (**79**) *via* protecting group strategy and *N*-oxide formation.[32,99,109] When dichloropyrimidine **100** was coupled with aniline **82**, the formation of two isomers was possible. However, NMR experiments indicated that only chlorinated amine **101** was formed. The purification of benzyloxy-derivative **103** proved challenging, forcing the utilization of poorly purified material in the subsequent synthetic step. When deprotection was performed by heterogeneous hydrogenation, reduction of a double bond at the pyrimidine ring was observed, forming dihydropyrimidine **106**. Therefore, deprotection was performed *via* silyl-ether formation.[110,111] The cyclization of flavin precursor **104** with nitrosyl tetrafluoroborate showed no conversion. Instead, an attempt to deprotonate dihydropyrimidine **106** followed by ring closure with nitrosyl tetrafluoroborate gave a mass two protons lower than expected for **108**, suggesting the formation of **107** or a related compound. In addition, a mass of the desired 4-CF_3-lumiflavin (**79**) was detected.

lenging, forcing the use of a poorly purified material for the subsequent synthetic step. The use of typical heterogeneous catalytic reductive deprotection conditions resulted in an additional reduction of a double bond at the pyrimidine ring, giving dihydropyrimidine derivative **106** (Figure 5.3). Therefore, a method by Schinazi *et al.* was used, which was already successfully applied by S. A. Malaczynski for the synthesis of an 8-bromoflavin derivative within his master thesis.[110,111] It is based on the formation of a silyl-ether and subsequent hydrolysis with methanol.[110,111] By applying this method, the desired product **104** was obtained after only a few hours at room temperature.[1]

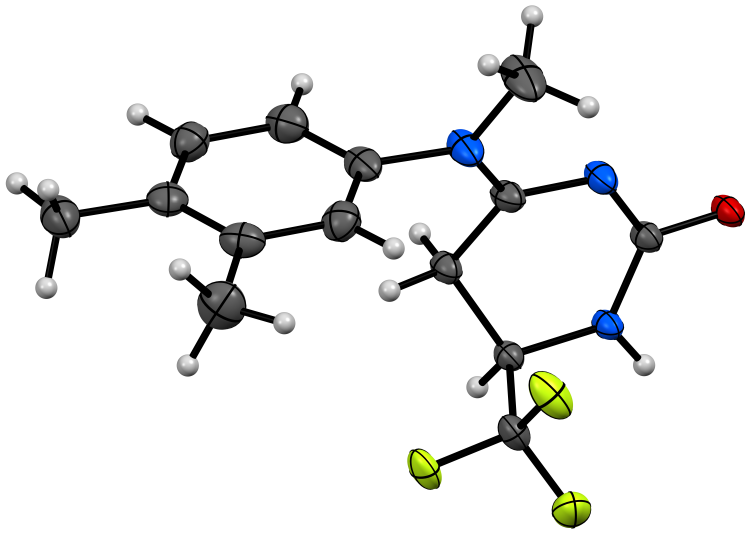

Figure 5.3 Molecular structure (thermal ellipsoid plot) of dihydropyrimidine **106** measured by P. Schmeinck. Cocrystallized reduced dihydroxypyrimidine **77** was omitted for clarity. Thermal displacement ellipsoids are drawn at the 50% probability level.

For the cyclization of flavin precursor **104**, the protocol developed for the synthesis of 2-CF_3-NP-*N*-oxide (**99**), which is based on the utilization of nitrosyl tetrafluoroborate under strict oxygen- and water-free conditions, was applied. However, in the context of *N*-oxide **105** synthesis, hardly any product formation was observed after several days at -5 °C, room temperature and finally at 50 °C. Only some new spots were detected on TLC, but without any indication of 4-CF_3-*N*-oxide (**105**) formation, suggesting a too low nucleophilicity in vicinal position to the trifluoromethyl group. Instead, dihydropyrimidine derivative **106** could be advantageous, since it could be

1. The experiments were performed in parts by D. Nürenberg under my instruction.

deprotonated causing an increased nucleophilicity. Consequently, its deprotonation was attempted using a combination of sodium hydride and diisopropylamine at low temperatures, followed by the addition of nitrosyl tetrafluoroborate. Already at 0 °C, a yellow fluorescent spot was observed on TLC, giving a mass spectrometry result that was two protons lower than expected for **108**, but which was consistent with a suspected product such as **107**. In addition, a mass matching the desired 4-CF_3-lumiflavin (**79**) was detected. However, due to purification problems the structures have not yet been unambiguously identified.

In addition, the synthesis of 4-CF_3-NP-flavin (**80**) was investigated in order to prevent purification problems caused by alloxazine formation (see Section 3.2 for further details of alloxazine formation). The investigated synthetic route is shown in Scheme 5.12.

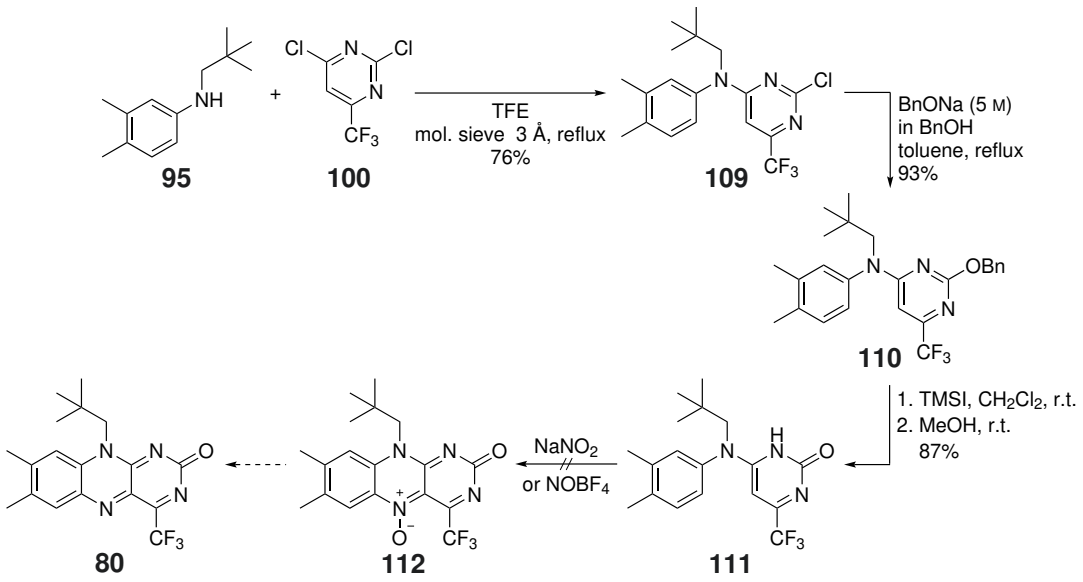

Scheme 5.12 Synthetic approach to 4-CF_3-NP-flavin (**80**) *via* modified protecting group strategy and *N*-oxide formation.[32,99,109–111] After a straightforward synthesis of flavin precursor **111**, its cyclization remained unsuccessful using both sodium nitrite in acetic acid and nitrosyl tetrafluoroborate, respectively, suggesting a low nucleophilicity in *ortho*-position to the trifluoromethyl group.

The route begins with NP-aniline **95** that was utilized for coupling with dichloropyrimidine **100**, forming only one of two possible isomers. Structure elucidation was achieved *via* X-ray crystallography in collaboration with P. Schmeinck, presenting the desired isomer **109** (Figure 5.4).

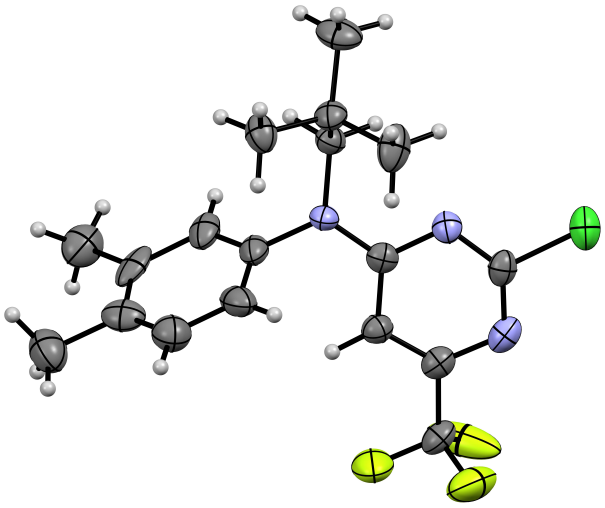

Figure 5.4 Molecular structure (thermal ellipsoid plot) of tertiary amine **109** measured by P. Schmeinck. Thermal displacement ellipsoids are drawn at the 50% probability level.

The substitution of the chloro substituent was again achieved by applying the adapted protecting group strategy *via* introduction of a benzyloxy functionality and subsequent deprotection *via* silyl-ether formation. By conducting this multi-step procedure, flavin precursor **111** was obtained.[32,99,110,111] However, cyclization to *N*-oxide **112** was again unsuccessful, as already described within the discussion of the synthetic investigation to 4-CF_3-lumiflavin (**79**). Specifically, no conversion was observed with either sodium nitrite in acetic acid or nitrosyl tetrafluoroborate, suggesting that the nucleophilic attack at the nitrosyl cation is typically initiated from the pyrimidine ring. Replacing the keto functionality with a trifluoromethyl group in vicinal position seems to reduce its nucleophilicity and increases the steric shielding, resulting in chemical inertness for this type of reaction. Instead, the synthetic approach discussed for the synthesis of 4-CF_3-lumiflavin (**79**) *via* partial reduction of the pyrimidine ring and subsequent deprotonation followed by addition of nitrosyl tetrafluoroborate could be a promising alternative.

6 | Conclusion and Outlook

Fluorinated flavin derivatives have been extensively investigated with three different goals: 1) Increasing the FQY to overcome brightness limitations of FbFPs for application in optical imaging, 2) Shifting the emission maximum to achieve a varied emission color and enable multicolor optical imaging using FbFPs and 3) Increasing the triplet quantum yield for application in photodynamic therapy or as photosensitizers for chemical purposes. In general, the selection of suitable flavin derivatives was carried out in close collaboration with theoretical chemists, in particular Dr. M. Bracker, who developed a method to reliably predict the photophysical properties of new flavin derivatives by quantum chemical calculations.[35,38] The results of these calculations were found to be in excellent agreement with previously reported experimental photophysical properties of monofluorinated MIAs published by Gilch, Czekelius and coworkers.[34]

The structural changes applied on the isoalloxazine core of flavin derivatives investigated in this work differ strongly with the desired goal (Figure 6.1). For instance, multiple fluorination at the xylene ring, specifically in 7- and 8-position, was predicted to increase the FQY due to a destabilizing effect on the third triplet state T_3, which is mainly responsible for non-radiative deactivation *via* ISC in aqueous solution.[35] In contrast to the xylene ring functionalization, considerable modifications of the pyrimidine ring were predicted to exert strong electronic effects, resulting in either a shifted emission maximum or an increased triplet quantum yield (Figure 6.1).[38] For instance, the emission maximum of 1-F-lumiflavin is predicted to shift to the red to NIR region, since its first singlet state S_1 is suggested to be strongly stabilized. In contrast, the replacement of the keto-functionalities in 2- and 4-positions by trifluoromethyl functionalities, respectively, is predicted to increase the triplet quantum yield due to activating of an El-Sayed allowed ISC channel to the

second triplet state T_2 of $n\pi^*$ character.[38]

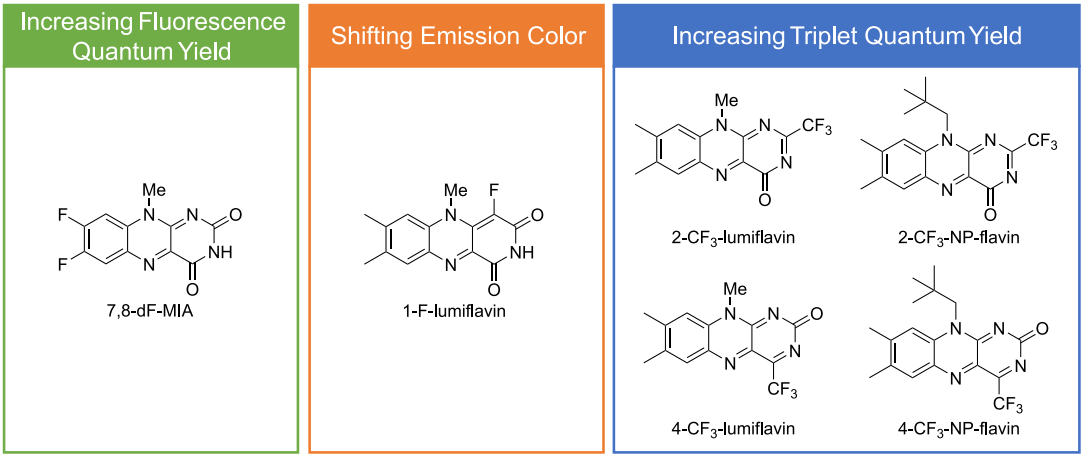

Figure 6.1 Fluorinated flavin derivatives synthesized and investigated in this work. 7,8-dF-MIA was synthesized with the goal to increase the FQY and was published together with two other flavin derivatives in Ref. [36]. The synthesis of 1-F-lumiflavin was developed, which allows the investigation of its photophysical properties. Finally, several synthetic approaches to trifluoromethylated flavin derivatives 2-CF_3-lumiflavin, 2-CF_3-NP-flavin, 4-CF_3-lumiflavin and 4-CF_3-NP-flavin were investigated. Although a promising approach was developed, hardly any product has been unambiguously proven, so further investigations are required in this context.

To evaluate the accordance of quantum chemical suggestions by Kleinschmidt and coworkers with experimental results, two xylene ring functionalized fluorinated flavin derivatives were synthesized: 7,8-dF-MIA (**14**) and 9-F-MIA (**7**).[35] Both derivatives were synthetically accessible *via* the common synthetic approach by Kuhn *et al.* with individually tailored procedures for *N*-alkylation (Scheme 6.1).[34,52] The synthesis of both flavin derivatives has been published in Ref. [36] together with their extensively studied photophysical properties, mainly determined by W. Haselbach and D. Sretenović. Indeed, the experimental results were in excellent agreement with the quantum chemical predictions, giving for instance an increased FQY of $\Phi_{fl} = 0.42$ for the difluorinated MIA compared to the non-fluorinated MIA with $\Phi_{fl} = 0.22$.[35,36] As an initial approach towards protein incorporation, the synthesis of 7,8-dF-RIA (**21**) was additionally published in Ref.[36] (Scheme 6.1). This derivative was synthetically accessible *via* functionalization of a difluorinated 1,2-diaminobenzene derivative with subsequent Kuhn condensation, a synthetic approach to riboflavin derivatives derived from Gärtner *et al.*[50,52]

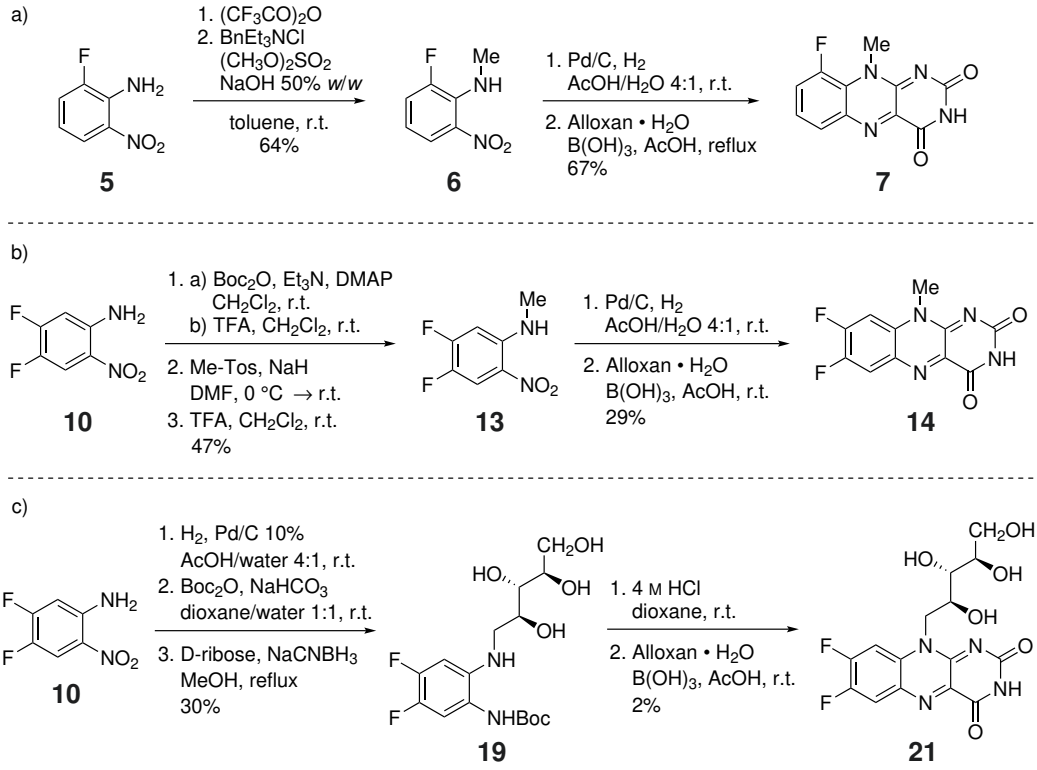

Scheme 6.1 Synthetic routes to a) 9-F-MIA (**7**), b) 7,8-dF-MIA (**14**) and c) 7,8-dF-RIA (**21**) as published in Ref. [36]. All shown flavin derivatives were synthetically accessible by application of the Kuhn procedure to suitably functionalized 1,2-diaminobenzene derivatives, which were *N*-alkylated by individually tailored procedures.[34,50,52]

In addition to xylene ring functionalization, flavin derivatives exhibiting considerable structural changes at the pteridine moiety of the isoalloxazine core were discussed and investigated by quantum chemical calculations, mainly performed by Dr. M. Bracker, resulting in the publication Ref. [38]. Based on the promising results predicting a shift of the emission maximum into the red to NIR region, the synthesis of 1-F-lumiflavin (**33**) was developed. It proved to be synthetically accessible by preparation of the 1-deazaisoalloxazine core following reported protocols for the corresponding deazariboflavin and subsequent late-stage electrophilic fluorination.[50,60,71,72,78–81,83] To optimize the overall yield of this route, the purification of quinoxaline **30** could be omitted, as its purification *via* FC seemed to be accompanied by product decomposition. This would lead to a less pure raw material of 1-deazalumiflavin (**31**), which could be subjected to the optimized purification protocol. Another focus of optimization could be the synthesis of bromooxoglutarate **23**, since a mixture of product and starting material was always obtained. This

value could possibly be positively influenced with superstoichiometric quantities of bromine. Eventually, since the optimized purification protocol for 1-F-lumiflavin (**33**) yielded spectroscopically pure material, allowing its structure to be confirmed by X-ray crystallography, its photophysical properties can be examined by spectroscopic methods.

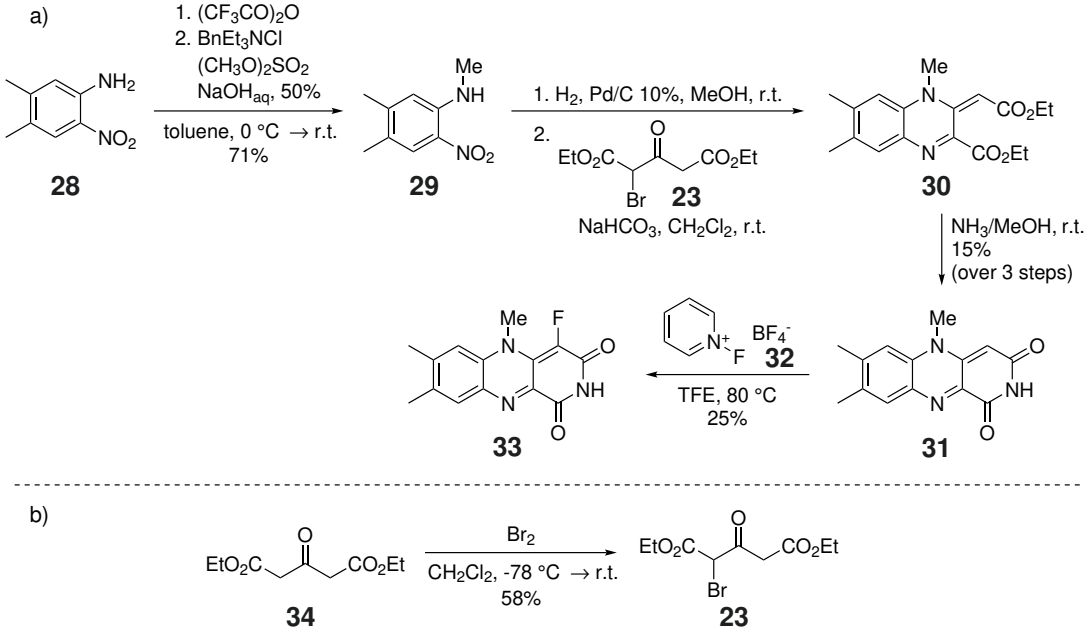

Scheme 6.2 a) Synthesis route to 1-F-lumiflavin (**33**) *via* formation of the 1-deaza-isoalloxazine core and subsequent late-stage electrophilic fluorination.[50,60,71,72] b) Formation of bromooxoglutarate **23** by conversion of oxoglutarate **34** with bromine.

The quantum chemical study by Kleinschmidt and coworkers of pteridine functionalizations additionally revealed trifluoromethylated deoxo-flavin derivatives that were predicted to exhibit enhanced triplet quantum yields.[38] Therefore, the synthesis of 2-CF_3-flavin (**75** and **76**) and 4-CF_3-flavin derivatives (**79** and **80**) was investigated *via* several synthetic approaches. The most promising approach *via* protecting group strategy and *N*-oxide formation is shown in Scheme 6.3 and is an approach towards 2-CF_3-NP-flavin (**76**).[32,99,109] Typically, the synthesis of MIAs or lumiflavins has been pursued as simplified structures of flavins, as it has the advantage of direct comparability with recently published flavin derivatives and with the derivatives investigated by quantum chemical calculations.[34–36,38] But due to numerous challenges in the synthesis of flavin derivatives with trifluoromethyl groups in 2-position, it proved advantageous to eliminate the risk of alloxazine formation and improve solubility by

replacing the methyl group in 10-position with a neopentyl group. Although the mass of the desired 2-CF_3-NP-flavin (**76**) was found by mass spectrometry, stability and purification problems prevented to provide unambiguous evidence for its formation so far.

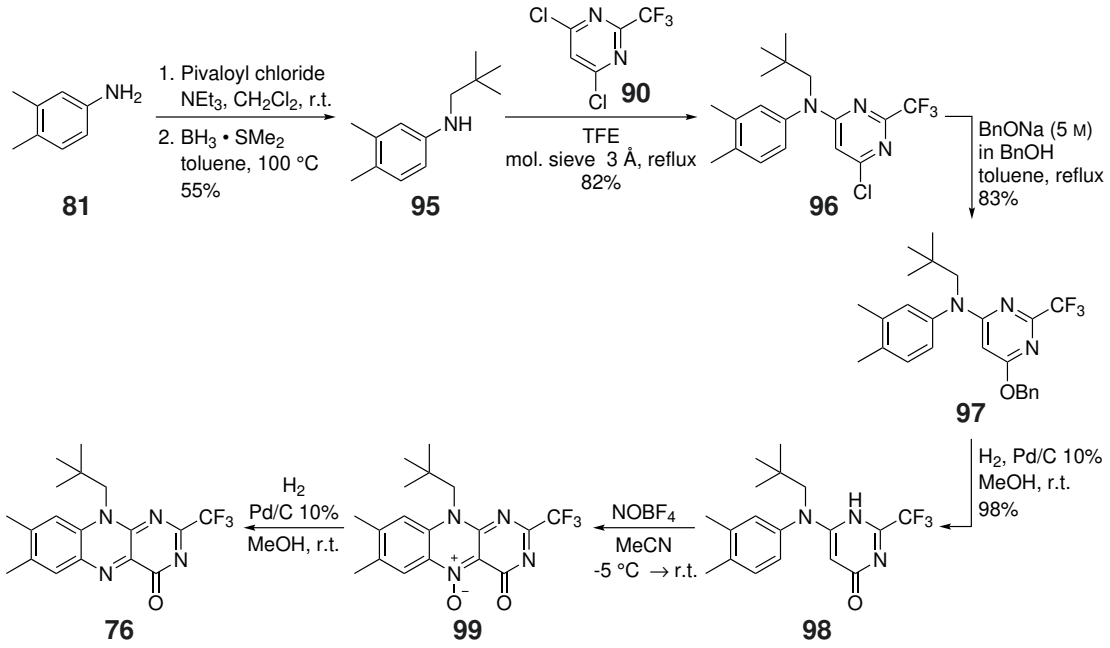

Scheme 6.3 Synthetic approach to 2-CF_3-NP-flavin (**76**) *via* protecting group strategy and *N*-oxide formation.[32,99,109] *N*-oxide **99** was formed by cyclization with sodium tetrafluoroborate, however yield calculation was hampered due to the low purity the raw material and stability problems. The formation of 2-CF_3-NP-flavin (**76**) have not yet been unambiguously proven.

For the synthesis of a flavin derivative with a trifluoromethyl group in 4-position, the most promising approach is shown in Scheme 6.4 and was tested for the synthesis of 4-CF_3-lumiflavin (**79**).[32,99,109–111] Due to the decreased nucleophilicity in vicinal position of the trifluoromethyl group at the pyrimidine ring, the cyclization towards a flavin derivative required activation. This was attempted by deprotonation of dihydropyrimidine **106**, followed by cyclization with nitrosyl tetrafluoroborate, yielding a product that most likely matches hydroxylamine **108**. However, its structure could not be unambiguously clarified so far.

Both trifluoromethylated flavin derivatives require further investigation with respect to their synthesis. Although the right mass was found by mass spectrometry for both derivatives, 2-CF_3-NP-flavin (**76**) and 4-CF_3-lumiflavin (**79**), their formation

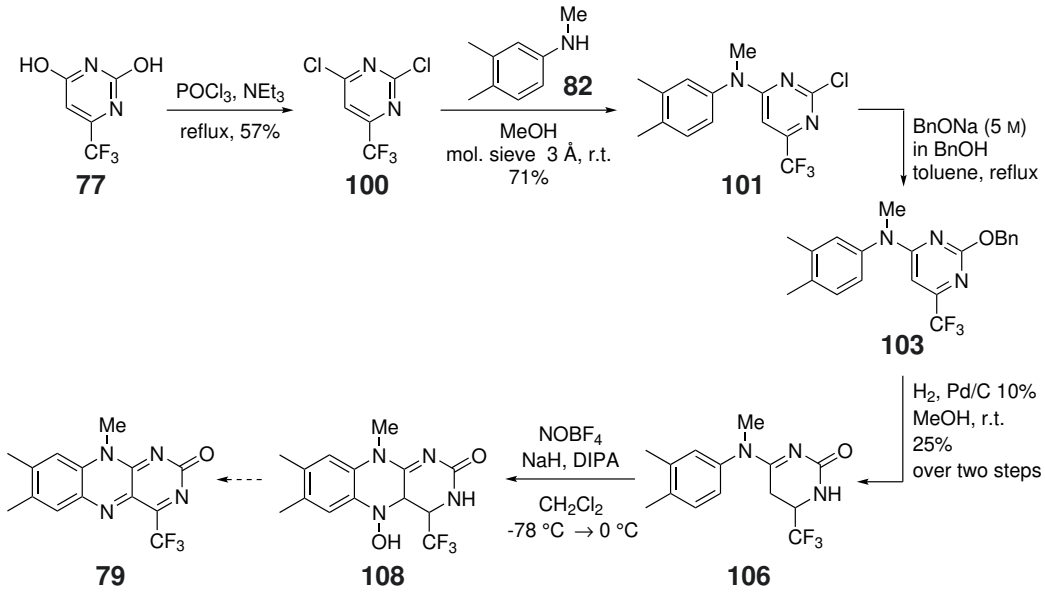

Scheme 6.4 Most promising synthetic approach to a 4-CF_3-flavin derivative *via* protecting group strategy with reduction of a double bond at the pyrimidine ring, followed by cyclization activated by deprotonation. However, the cyclization product shown (**108**) has not been unambiguously evidenced. The same applies to the formation of 4-CF_3-lumiflavin (**79**).

could not be unambiguously proven so far. In particular, their rapid decomposition and challenging purification were limiting factors within this context. For the synthesis of 2-CF_3-NP-flavin (**76**), especially the final deoxygenation of 2-CF_3-*N*-oxide (**99**) and the purification procedure require optimization. For the synthesis of a flavin derivative trifluoromethylated in 4-position, a promising modification would be to apply the deprotonation approach to the synthesis of 4-CF_3-NP-flavin (**80**), as it is characterized by an increased resistance to alloxazine formation and a better solubility, facilitating purification.

7 | Experimental Section

7.1 General

In all experiments chemicals by the companies Merck, Acros, Fluka, Sigma Aldrich, TCI, Fluorochem, J&K, Euristop, Apollo Scientific, Carbolution and BLDPharm were used and if necessary purified by recrystallisation or distillation before use. The solvents *n*-hexane, ethyl acetate, dichloromethane and acetone for work-up and purification were purchased in technical purity and distilled before use by a rotary evaporator Rotavapor R-210 by Büchi and diaphragm pumps by vacuubrand. All other solvents as well as those used for syntheses were purchased in analytical purity, dried over molecular sieve if necessary and used without further purification. Dry solvents like dichloromethane, acetonitrile, toluene and diethylether were taken from a solvent drying system MBraun MB SPS-800.

Air-sensitive reactions were carried out under exclusion of oxygen and water on a combined vacuum-nitrogen line using conventional Schlenk techniques. Glass appliances were dried in a compartment dryer overnight at 120 °C and additionally heated under high vacuum with a heat gun by Meterk. High vacuum was generated by a rotary vane oil pump by vacuubrand. Nitrogen was dried by molecular sieve (3 Å) and orange gel before use and nitrogen flow was checked by a bubble counter. Liquids were transferred by syringe through a septum and solids were added to the reaction flask in nitrogen countercurrent. If necessary, reaction mixtures or solvents were degassed by purging with nitrogen or by freeze-pump-thaw.

For stirring a PTFE-coated stirring bar and magnetic stirrers with heating plates by Ika RCT or Heidolph MR were used, equipped with a thermometer and a silicone oil bath. Room temperature reactions were considered within a range of 18-30 °C. An ice

water bath and an acetone dry ice bath were used to generate temperatures of 0 °C and -78 °C. The rotary evaporator Rotavapor R 210 of the company Büchi and a diaphragm pump of the company vacuubrand were used to remove solvents *in vacuo*.

Chromatography

Thin layer chromatography was performed on Alugram© XTRA SIL G/UV_{254} standard silica aluminum plates by Macherey-Nagel to check the progress of reactions and flash chromatographies. The spots were detected by means of UV light (254 nm) and if necessary by staining with a potassium permanganate solution of the composition 3.0 g $KMnO_4$, 20 g K_2CO_3, 5.0 ml 5% NaOH and 300 ml H_2O followed by developing with a heat gun by Meterk. For flash chromatography silica gel 60M by Macherey-Nagel was used. Flash chromatography was either performed manually with nitrogen pressure or by using a MPLC system by Büchi including a Control unit C-620, a Fraction collector C 660, a UV Photometer C-640 and Pump Modules C-605. Reversed Phase HPLC was performed using the following devices: Knauer HPLC Pump 64, Merck-Hitachi L-6250 Intelligent Pump, Knauer Dynamic Mixing Chamber, Knauer Automatic HPLC Valve, Latek HMV-P, Knauer Variable Wavelength Monitor, Merck-Hitachi L-4000 UV Detector, Erma Degasser ERC-3510, Waters Fraction Collector II, Lichrospher© 100 RP-18 (5 μm) Sorbent Lot No. HX391811 Hibar© RT 250-25, Knauer Eurospher 100-C18 (5 μm), 4.0 MMID. For data processing, the software Clarity was used.

Analytics

For mass spectrometry a Bruker Daltonic UHR-QTOF maXis 4G (HRMS) or an Advion expression CMS (APCI) with an Advion plate express or an ASAP was used. Mass spectra were recorded from samples in solution (acetone, methanol) or in solid state on TLC plates or *via* ASAP.

For IR-spectroscopy a Jasco FT/IR-6200 spectrometer was used. Infrared spectra were recorded from samples as a film on a sodium chloride single crystal or on a diamond plate. For evaluation, the absorption band intensity was designated with the following abbreviations: very strong = vs, strong = s, medium = m and weak = w.

Melting points were measured on a Büchi B-540 melting point apparatus and are uncorrected. For mass spectra (HRMS) a Bruker Daltonics UHR-QTOF Maxis 4G spectrometer was used.

For NMR spectroscopy chloroform-*d*, methanol-d_4 and dimethylsulfoxide-d_6 were used. The standardization of NMR spectra was performed using the following solvent residual proton signals[112]:

Chloroform-*d*:	^{1}H-NMR	δ = 7.26 ppm.
	^{13}C-NMR	δ = 77.16 ppm.
Methanol-d_4:	^{1}H-NMR	δ = 3.31 ppm.
	^{13}C-NMR	δ = 49.00 ppm.
Dimethylsulfoxide-d_6:	^{1}H-NMR	δ = 2.50 ppm.
	^{13}C-NMR	δ = 39.52 ppm.

For evaluation, the NMR-signal multiplicity was abbreviated as follows: singlet = s, doublet = d, triplet = t, quartet = q and multiplet = m and combinations of these. Coupling constants *J* are given in Hertz (Hz) and chemical shifts δ in ppm. The following devices were used for recording of NMR-spectra:

NMR-Spectroscopy	^{1}H-NMR	Bruker Avance III – 300, 300 MHz
		Bruker Avance III – 600, 600 MHz
	^{13}C-NMR	Bruker Avance III – 300, 75 MHz
		Bruker Avance III – 600, 151 MHz
	^{19}F-NMR	Bruker Avance III - 300, 282 MHz
		Bruker Avance III - 600, 565 MHz

NMR spectra were visualized with MestReNova Version 14.2.0 by Mestrelab Research S.L. and schemes were drawn with ChemDraw 20.1.1.125 by PerkinElmer Informatics.

7.2 Synthesis of 8-MeO-MIA (17)

7.2.1 7-Fluoro-8-methoxy-10-methylbenzo[*g*]pteridine-2,4(3*H*,10*H*)-dione (17)

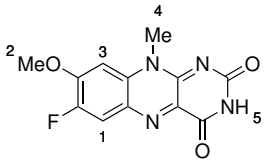

The reaction was done by adapting the method by Hasford and Rizzo[58]: Difluorinated nitroaniline **10** (81.5 mg, 433 μmol) was dissolved in MeOH (2.20 mL) and Pd/C (10%, 7.6 mg, 7.1 μmol, 0.02 eq) was added. The mixture was degassed by purging with N_2 for 30 min before it was set under H_2 atmosphere and stirred vigorously overnight. HCl (10%, 8.30 mL) was degassed by purging with N_2 for 45 min followed by addition of 1,2-diaminobenzene through a syringe filter. Alloxan monohydrate (**3**) was added and the mixture was stirred at 60 °C overnight. The precipitate was filtered off yielding the product as a green powder (33.8 mg, 122 μmol, 28%).

^{1}H-NMR (600 MHz, DMSO-d_6) δ 11.31 (s, 1H, H-5), 8.06 (d, J = 11.0 Hz, 1H, H-1), 7.44 (d, J = 7.8 Hz, 1H, H-3), 4.15 (s, 3H, H-4), 4.02 (s, 3H, H-2) ppm.

^{19}F{^{1}H}-NMR (565 MHz, DMSO-d_6) δ -134.76 ppm.

MS (APCI): m/z = 277.0 [M+H$^+$] (calculated: 277.0).

7.3 Synthesis of 1-F-Lumiflavin (33)

Scheme 7.1 shows an overview of the synthetic route to 1-F-lumiflavin (**33**) beginning with nitroaniline **28**.

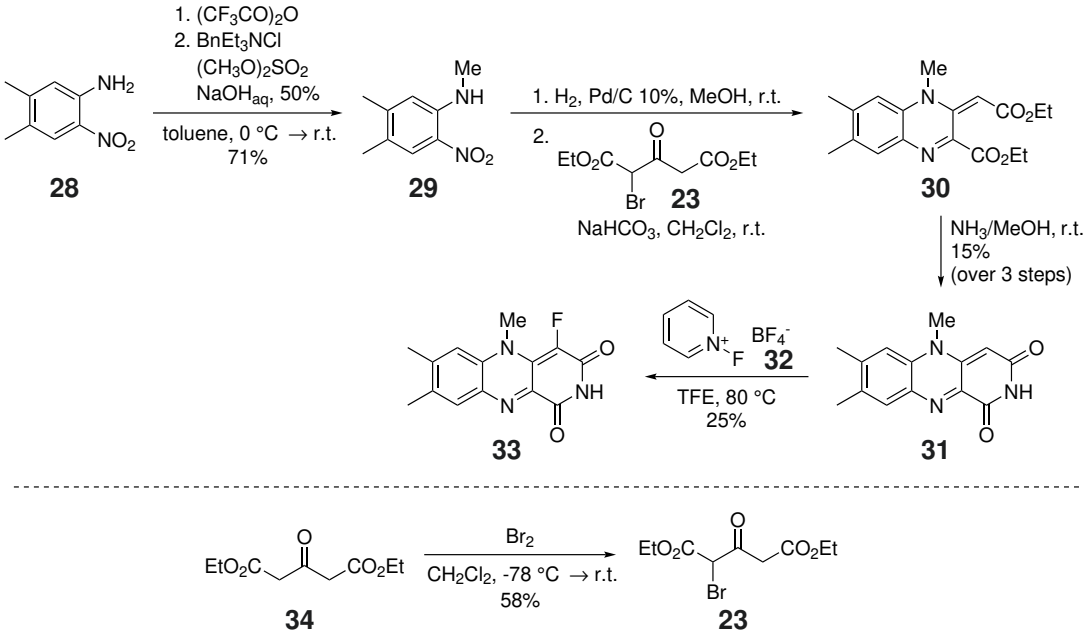

Scheme 7.1 Overview of the synthetic route to 1-F-1-deazalumiflavin (**33**).

7.3.1 *N*,4,5-Trimethyl-2-nitroaniline (29)

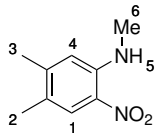

The reaction was done analogous to the method by Brown and Rizzo[54]: 4,5-Dimethyl-2-nitroaniline (**28**) (8.06 g, 48.5 mmol) was suspended in toluene (97.0 mL) and the mixture was cooled to 0 °C. Trifluoroacetic anhydride (13.0 mL, 19.6 g, 93.5 mmol, 1.9 eq) was added and the mixture was stirred for 30 min at r.t. before successive addition of benzyltriethylammonium chloride (9.16 g, 40.2 mmol, 0.8 eq), dimethyl sulfate (5.80 mL, 7.73 g, 61.3 mmol, 1.3 eq) and NaOH (50% *w*/*w*, 48.0 mL). The mixture was stirred at r.t. for 1 h before sat. NH_4Cl-solution (150 mL) and CH_2Cl_2 (150 mL)

were added. The layers were separated and the aqueous layer extracted with CH_2Cl_2 (3 x 150 mL). The combined organic layers were dried over Na_2SO_4, filtered and the solvent was removed *in vacuo*. After purification *via* FC (*n*-hexane/CH_2Cl_2 7:3 – 3:7), the product was isolated as an orange-red powder (6.18 g, 34.3 mmol, 71%). The spectroscopic data are in agreement with the literature[113].

$\mathbf{R_f}$(*n*-hexane/EtOAc 7:3): 0.70.

^{1}H-NMR (300 MHz, chloroform-*d*) δ 7.93 (s, 2H, H-1,5), 6.61 (s, 1H, H-4), 3.00 (d, J = 5.1 Hz, 3H, H-6), 2.28 (s, 3H, H-3), 2.18 (s, 3H, H-2) ppm.

7.3.2 *N*^{1},4,5-Trimethylbenzene-1,2-diaminium chloride (35)

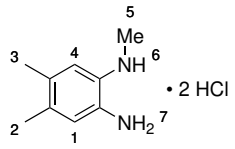

The reaction was done by adapting the method by Gilch, Czekelius *et al.*[34] and Averill *et al.*[53] for reduction of the nitro group, with the work-up procedure by Skibo *et al.*[75]: A solution of nitroaniline **29** (1.03 g, 5.71 mmol) in MeOH (95.0 mL) was degassed by purging with N_2 for 1 h. Then, Pd/C (10%, 85.5 mg, 80.3 μmol, 0.01 eq) was added. The mixture was set under H_2 atmosphere and stirred at r.t. for 2 h, before it was filtered through a syringe filter. Conc. HCl (3 mL) was added and the solvent was removed *in vacuo* to yield the product as colorless crystals (1.27 g, 5.66 mmol, 99%).

$\mathbf{R_f}$(*n*-hexane/EtOAc 7:3): 0.47.

^{1}H-NMR (600 MHz, chloroform-*d*) δ 7.28 (s, 1H, H-1/4), 7.21 (s, 1H, H-1/4), 3.08 (s, 3H, H-5), 2.32 (s, 3H, H-2/3), 2.31 (s, 3H, H-2/3) ppm.

^{13}C{^{1}H}-NMR (151 MHz, chloroform-*d*) δ 139.45, 139.35, 130.37, 126.20, 124.61, 124.43, 36.87, 19.36, 19.29 ppm.

IR (Film): $\tilde{\nu}$ [cm^{-1}] 3345 (m), 3228 (w), 2920 (m), 2693 (m), 2467 (m), 2361 (m), 1636 (m), 1594 (m), 1513 (s), 1459 (m), 1294 (w), 1277 (w), 1141 (w).

HRMS (ESI): m/z = 149.1071 [M+H$^+$] (calculated: 149.1073).

M.Pt.: 190.7 – 192.2 °C.

7.3.3 Diethyl 2-bromo-3-oxopentanedioate (23)

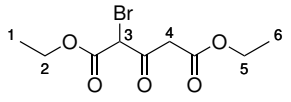

The reaction was done following a method by Richter *et al.*[72]: Diethyl 3-oxoglutarate **34** (30.0 mL, 33.4 g, 165 mmol) was dissolved in CH_2Cl_2 (460 mL) and the mixture was cooled to -78 °C before Br_2 (8.38 mL, 26.1 g, 164 mmol, 1.0 eq) was added dropwise. After 45 min, the cooling bath was removed and the mixture was stirred at r.t. for 45 min. Sat. $NaHCO_3$-solution (320 mL) and sat. Na_2SO_3-solution (100 mL) were added and the phases were separated. The aqueous phase was extracted with CH_2Cl_2 (3 x 200 mL). The combined organic layers were washed with brine (100 mL), dried over $MgSO_4$ and filtered. The solvent was removed *in vacuo* to yield the raw product as a light-brown oil in a mixture with the starting material (42.8 g, 63% product, 37% starting material) which was utilized for the next synthetic step without further purification (calculated yield: 27.0 g, 96.1 mmol, 58%). The spectroscopic data are in agreement with the literature.[72]

$\mathbf{R}_f$(*n*-hexane/EtOAc 8:2): 0.31.

^{1}H-NMR (300 MHz, chloroform-*d*) δ 5.02 (s, 1H, H-3), 4.24 (m, 9H, H-2,5 + starting material), 3.87 (d, J = 16.4 Hz, 1H, H-4), 3.76 (d, J = 16.4 Hz, 1H, H-4), 1.29 (m, 13H, H-1,6 + starting material) ppm.

7.3.4 Ethyl-3-(2-ethoxy-2-oxoethylidene)-4,6,7-trimethyl-3,4-dihydroquinoxaline-2-carboxylate (30)

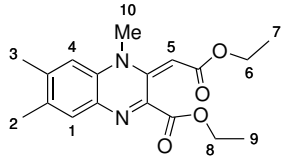

The reaction was done by adapting the method by Richter *et al.*[72]: *N*-Methylnitroaniline **29** (12.0 g, 66.6 mmol) was suspended in MeOH (200 mL) and the mixture was

degassed by purging with N_2 for 30 min. Then, Pd/C (10%, 960 mg, 902 μmol, 0.01 eq) was added, followed by setting the mixture under H_2 atmosphere and vigorous stirring at r.t. overnight. Bromooxoglutarate **23** (42.8 g) was dissolved in CH_2Cl_2 (200 mL) and degassed by purging with N_2 for 30 min. Then, $NaHCO_3$ (5.59 g, 66.5 mmol, 1.0 eq) was added followed by addition of reduced aniline **29** in MeOH which was filtered directly through a syringe filter into the reaction mixture. It was stirred at r.t. overnight before filtration of the reaction mixture, followed by evaporation of the solvent *in vacuo*. After purification *via* FC (*n*-hexane/EtOAc 9:1 – 7:3), the pre-purified product was isolated as a red oil and was utilized for the next synthetic step without further purification (7.65 g, 64 w% with respect to nitroaniline **29**).

$\mathbf{R_f}$ (*n*-hexane/EtOAc 7:3): 0.50.

^{1}H-NMR (300 MHz, chloroform-*d*) δ 7.42 (s, 1H, H-1), 7.16 (s, 1H, H-4), 4.31 (q, J = 7.2 Hz, 2H, H-6/8), 4.18 – 4.02 (m, 3H, H 6/8+EtOAc), 3.42 (s, 3H, H-10), 2.39 (s, 3H, H-3), 2.29 (s, 3H, H-2), 1.36 (t, J = 7.2 Hz, 3H, H-7/9), 1.32 – 1.19 (m, 5H, H-7/9+EtOAc) ppm.

Instruction for coupling with 1,2-diaminobenzene hydrochloride 35:

The reaction was done by adapting the method by Carlson and Kiessling[60]: Bromooxoglutarate **23** (2.65 g) raw material was dissolved in DMF (38.0 mL) and CH_2Cl_2 (44.0 mL) followed by addition of 1,2-diaminobenzene hydrochloride **35** (1.00 g, 4.47 mmol). Cs_2CO_3 (2.82 g, 8.67 mmol, 1.9 eq) was added and the mixture was stirred at r.t. overnight before it was filtered. Water (70 mL) was added to the filtrate and the phases were separated after extraction. The aqueous phase was extracted with EtOAc (3 x 30 mL) and the combined organic phases were dried over $MgSO_4$, filtered and the solvent was removed *in vacuo*. The residue, still containing DMF, was diluted with EtOAc (30 mL) and washed with water (5 x 20 mL). After removal of the solvent *in vacuo* and purification *via* FC (*n*-hexane/EtOAc 85:15 - 6:4), the pre-purified product was isolated as a red oil (511 mg, 61 w% with respect to nitroaniline **29**).

7.3.5 5,7,8-Trimethylpyrido[3,4-*b*]quinoxaline-1,3(2*H*,5*H*)-dione (31)

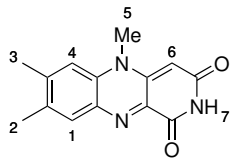

The reaction was done by adapting the method by Richter *et al.*[72]: MeOH was purged with NH_3 under gentle cooling in a water bath until the volume stopped increasing. Pre-purified quinoxaline **30** (7.65 g) was dissolved in NH_3/MeOH-solution (700 mL) and the flask was stoppered with a balloon as pressure compensation. The mixture was stirred at r.t. overnight before addition of NH_3/MeOH (7 M, 700 mL) and stirring at r.t. for one more night. The precipitate was filtered off and washed with EtOAc until the filtrate appeared colorless. Subsequently, it was dried *in vacuo* to give the raw product as a deep-purple powder in a high purity already sufficient for yield calculation (2.51 g, 9.83 mmol, 15% with respect to nitroaniline **29**, Section 7.3.4, over three steps, deep purple powder). A fraction of the raw material (486 mg) was submitted to the optimized purification protocol (see below) yielding material of high purity grade that was sufficient for spectroscopic purposes (324 mg). The yield of this product was calculated accordingly over three steps with regard to nitroaniline **29** as starting material (1.67 g, 6.54 mmol, 10% deep-purple powder).

R_f ($CHCl_3$/MeOH 95:5): 0.20.

^{1}H-NMR (300 MHz, DMSO-d_6) δ 11.16 (s, 1H, H-7), 7.63 (s, 1H, H-1), 7.51 (s, 1H, H-4), 5.32 (s, 1H, H-6), 3.51 (s, 3H, H-5), 2.40 (s, 3H, H-3), 2.30 (s, 3H, H-2) ppm.

IR (Film): $\tilde{\nu}$ [cm^{-1}] 3078 (w), 2799 (w), 1690 (m), 1618 (s), 1578 (s), 1560 (s), 1518 (m), 1460 (m), 1412 (w), 1319 (m), 1256 (s), 1198 (w), 1013 (w).

HRMS (ESI): m/z = 256.1082 [M+H^+] (calculated: 256.1081).

M.Pt.: >300 °C.

Optimized purification protocol:

Raw product (486 mg) was dissolved by heating in 200 mL TFE followed by hot filtration. The filtrate was cooled and 200 mL EtOAc was layered on top. The precipitate

was filtered off and dried in high vacuum at 80 °C yielding 328 mg product with 13w% TFE incorporated.

7.3.6 4-Fluoro-5,7,8-trimethylpyrido[3,4-*b*]quinoxaline-1,3(2*H*,5*H*)-dione (33)

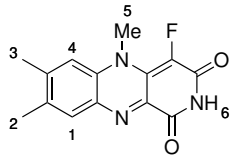

The reaction was done by adapting the method by Umemoto *et al.*[73]: 1-Deaza-lumiflavin (**31**, 519 mg, 2.03 mmol) was suspended in TFE (215 mL) and heated to 100 °C. Before addition of *N*-F-pyridinium salt **32** (459 mg, 2.48 mmol, 1.2 eq) the heat was lowered to 80 °C. The mixture was stirred for 5.5 h before removal of the solvent. After purification *via* FCs and recrystallizations (for details see optimized purification protocol), the product was isolated as a dark purple powder (140 mg, 511 μmol, 25%).

R$_f$ ($CHCl_3$/MeOH 95:5): 0.33.

^{1}H-NMR (300 MHz, DMSO-d_6) δ 11.62 (s, 1H, H-6), 7.55 (s, 1H, H-1), 7.36 (s, 1H, H-4), 3.71 (d, J = 4.8 Hz, 3H, H-5), 2.38 (s, 3H, H-3), 2.28 (s, 3H, H-4) ppm.

^{19}F{^{1}H}-NMR (282 MHz, DMSO-d_6) δ -167.91 ppm.

IR (Film): $\tilde{\nu}$ [cm-1] 2995 (w), 1707 (m), 1639 (m), 1581 (m), 1519 (m), 1470 (m), 1404 (m), 1377 (m), 1302 (m), 1267 (m), 1184 (m), 1169 (m), 1136 (m), 1032 (m).

HRMS (ESI): m/z = 274.0988 [M+H$^+$] (calculated: 274.0986).

M.Pt.: Sublimation >250 °C, no visible decomposition up to 300 °C.

Optimized purification protocol for photophysical measurements:

The raw material was pre-purified via FC (applied in TFE, $CHCl_3$/MeOH 98:2 – 95:5) to give 128 mg “FC-pure” product and a mixed fraction that was collected separately. The mixed fractions were purified *via* five successive FCs ($CHCl_3$/MeOH 99:1 - 95:5) yielding another 79.2 mg "FC-pure" product. “FC-pure” product obtained from first FC (128 mg) was recrystallized from 10 mL TFE, filtered hot and chilled

at r.t. overnight and at 0 °C over 3 d. Filtration gave 67.0 mg pure product, which was considered for yield calculation. "FC-pure" product obtained from FCs 2 - 5 and residues from earlier recrystallizations were separately recrystallized from DMSO giving 39.0 mg and 33.5 mg pure product, respectively, which were also considered for yield calculation. To obtain spectroscopically pure product, the product obtained from recrystallization from TFE (67.0 mg) was again recrystallized from TFE (5 mL) and from DMSO (3 mL, 100 °C bath-T), respectively, to yield 39.9 mg spectroscopically pure product as dark purple needles.

Crystallization protocol for X-ray crystallography:

1-F-Lumiflavin (**33**) (approx. 5 mg) was dissolved in a NMR-tube in DMSO-d_6 (0.6 mL) by heating with a heat gun. Cooling to r.t. formed needles which were subjected to X-ray crystallography.

Test batches with different fluorination agents:

Table 7.1 Test batches of electrophilic fluorination of 1-deazalumiflavin (**31**) with the selected fluorinating agents: Selectfluor™ (**40**), NFSI (**42**), Synfluor™ (**43**), *N*-fluoropyridinium tetrafluoroborate (**32**) and *N*-fluoro-2,4,6-trimethylpyridinium tetrafluoroborate (**41**). The qualitative evaluation was based on the appearance of 1-F-lumiflavin (**33**) signals in the NMR-spectra.

No.	Reagent	Eq	Solvent	Temperature	Time	Product Formation?
1	**40**	2.0	MeOH	reflux	48 h	no
2	**40**	1.0	MeOH	r.t.	0.5 h	no
3	**40**	1.0	MeOH	r.t.	4 h	no
4	**40**	1.0	MeOH	r.t.	24 h	yes
5[1]	**40**	1.0	MeOH/TFA/H_2O	r.t.	4 h	yes
6[1]	**40**	1.0	MeOH/TFA/H_2O	r.t.	24 h	yes
7[1]	**40**	1.0	formic acid	r.t.	24 h	yes
8[1]	**40**	1.0	formic acid	r.t.	24 h	yes
9[1]	**40**	1.0	formic acid/H_2O	r.t.	24 h	yes
10[1]	**40**	1.0	formic acid/MeCN	r.t.	24 h	yes
11	**40**	1.0	formic acid/H_2O/$CHCl_3$	r.t.	4 h	yes
12	**40**	1.0	formic acid/H_2O/$CHCl_3$	r.t.	24 h	yes
13	**40**	1.0	TFE/H_2O/$CHCl_3$	r.t.	4 h	yes
14	**40**	1.0	TFE	r.t.	4 h	yes
15	**42**	6.0	TFE	r.t.	6 h	no
16	**42**	1.0	TFE	60 °C	3 h	yes
17	**43**	0.5	TFE	r.t.	7 d	yes
18	**43**	0.5	TFE	r.t.	24 h	yes
19	**43**	1.5	TFE	r.t.	3 d	no
20	**32**	1.0	TFE	80 °C	24 h	yes
21	**32**	1.0	TFE	80 °C	24 h	yes
22	**32**	9.0	TFE	80 °C	24 h	yes
23	**41**	3.0	TFE	90 °C	3 d	yes

[1] Procedures were performed by D. Nürenberg.[76]

7.4 Investigated Synthesis of 2-CF_3-Lumiflavin (75)

Scheme 7.2 shows the most promising synthetic approach to 2-CF_3-lumiflavin (**75**).[1]

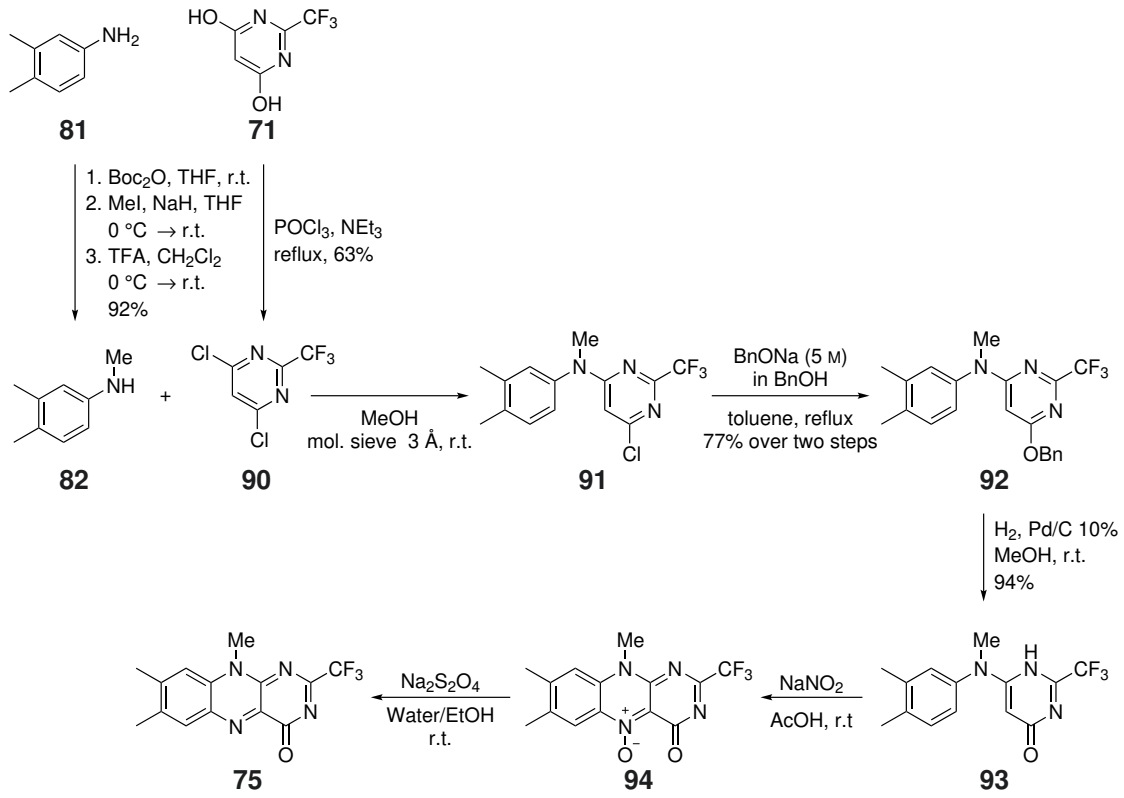

Scheme 7.2 Most promising synthetic approach to 2-CF_3-lumiflavin (**75**) *via* protecting group strategy and *N*-oxide formation.[32,99]

The synthetic procedures for the most promising synthetic approach *via* *N*-oxide formation are described initially, followed by the procedures for the synthetic approaches *via* Kuhn condensation and *via* Tishler condensation. For the schemes of the latter two synthetic approaches see Scheme 5.6, Scheme 5.7 and Scheme 5.8.

1. Parts of the procedures were performed by D. Nürenberg under my instruction.

7.4.1 *tert*-Butyl(3,4-dimethylphenyl)carbamate (113)

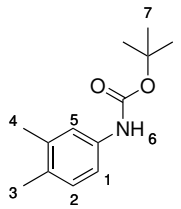

The reaction was done by adaption of a protocol by Lavrard and Popowycz[114]: Aniline **81** (3.09 g, 25.5 mmol) was dissolved in THF (25.0 mL), followed by Boc_2O (6.00 mL, 5.70 g, 26.1 mmol, 1.0 eq) addition. The mixture was stirred at r.t for 3.5 h before removal of the solvent *in vacuo* yielding the product as a white powder, which was subjected to the next synthetic step without purification.

$\mathbf{R}_f$(*n*-hexane/EtOAc 7:3): 0.76.

^{1}H-NMR (300 MHz, chloroform-*d*) δ 7.19 (s, 1H, H-1/2/5), 7.03 (d, J = 1.4 Hz, 2H, H-1/2/5), 6.36 (s, 1H, H-6), 2.23 (s, 3H, H-3/4), 2.20 (s, 3H, H-4/4), 1.51 (s, 9H, H-7) ppm.

7.4.2 *tert*-Butyl(3,4-dimethylphenyl)(methyl)carbamate (114)

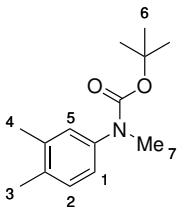

The reaction was done following a synthesis instruction by Guan *et al.*[115]: Boc-protected aniline **113** was dissolved in THF (20.0 mL) and the mixture was cooled to 0 °C before NaH (60% dispersion in mineral oil, 1.23 g, 30.7 mmol, 1.2 eq) was added. Then, MeI (1.90 mL, 4.33 g, 30.5 mmol, 1.2 eq) was added and the mixture was stirred for 5 more minutes at 0 °C and at r.t. overnight. Finally, ice was added slowly followed by addition of water (30 mL). The aqueous phase was extracted with CH_2Cl_2 (3 x 30 mL) and the combined organic layers were washed with brine (30 mL), dried over Na_2SO_4 and filtered. After removal of the solvent *in vacuo*, the product

was isolated as a bright yellow oil (6.45 g) and was used for the next synthetic step without purification.

$\mathbf{R_f}$(*n*-pentane/Et_2O): 0.53.

^{1}H-NMR (300 MHz, chloroform-*d*) δ 7.07 (d, *J* = 8.0 Hz, 1H, H-1/2/5), 7.01 (d, *J* = 2.3 Hz, 1H, H-1/2/5), 6.95 (dd, *J* = 8.0, 2.4 Hz, 1H, H-1/2/5), 3.23 (s, 3H, H-7), 2.24 (s, 3H, H-3/4), 2.23 (s, 3H, H-3/4), 1.45 (s, 9H, H-6) ppm.

7.4.3 *N*,3,4-Trimethylaniline (82)

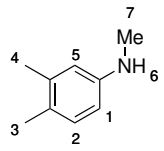

The reaction was done analogous to the method by Han *et al.*[116]: Boc-protected *N*-methylaniline **114** (6.45 g) was dissolved in CH_2Cl_2 (16.0 mL) and the mixture was cooled to 0 °C. TFA (7.00 mL, 10.4 g, 91.4 mmol, 3.6 eq) was added over 10 min and the mixture was stirred at 0 °C for 10 more minutes and then at r.t. for 4 h. Sat. $NaHCO_3$-solution (60 mL) and CH_2Cl_2 (30 mL) were added slowly. The phases were separated and the aqueous phase was extracted with CH_2Cl_2 (2 x 30 mL). The combined organic layers were dried over Na_2SO_4, filtered and the solvent was removed *in vacuo*. The residue was again dissolved in CH_2Cl_2 (8.00 mL) and the mixture cooled to 0 °C. TFA (3.80 mL, 5.66 g, 49.6 mmol, 1.6 eq) was added slowly and the mixture was stirred at 0 °C for 5 more minutes and then at r.t. overnight. Then, the mixture was again cooled to 0 °C and TFA (2.00 mL, 2.98 g, 26.1 mmol, 1.0 eq) was added before stirring at r.t. for 4.5 h. Sat. $NaHCO_3$-solution (60.0 mL) and CH_2Cl_2 (60.0 mL) were added, the phases were separated, and the aqueous phase was extracted with CH_2Cl_2 (2 x 30 mL). The combined organic layers were dried over Na_2SO_4, filtered and the solvent was removed *in vacuo*. After purification *via* FC (*n*-hexane/EtOAc 99:1 – 95:5), the product was isolated as a bright yellow oil (3.17 g, 23.5 mmol, 92% with respect to aniline **81**).

$\mathbf{R_f}$(*n*-hexane/EtOAc 7:3): 0.67.

^{1}H-NMR (300 MHz, chloroform-*d*) δ 6.96 (d, *J* = 8.0 Hz, 1H, H-2), 6.43 (m, 2H, H-1,5), 3.51 (s, 1H, H-6), 2.82 (s, 3H, H-7), 2.22 (s, 3H, H-4), 2.17 (s, 3H, H-3) ppm.

^{13}C{^{1}H}-NMR (75 MHz, chloroform-*d*) δ 147.72, 137.31, 130.34, 125.34, 114.42, 110.02, 31.20, 20.14, 18.78 ppm.

IR (Film): $\tilde{\nu}$ [cm^{-1}] 3406 (br-m), 2920 (m), 2878 (m), 2808 (w), 1617 (s), 1513 (vs), 1446 (m), 1320 (s), 1262 (m).

HRMS (ESI): m/z = 136.1121 [M+H^{+}] (calculated: 136.1121).

7.4.4 4,6-Dichloro-2-(trifluoromethyl)pyrimidine (90)

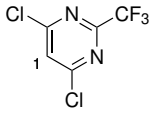

The reaction was done analogous to the method by Madding *et al.*[108]: pyrimidine **71** (2.02 g, 11.2 mmol) was suspended in $POCl_3$ (5.00 mL, 8.23 g, 53.6 mmol, 4.8 eq) and NEt_3 (3.10 mL, 2.25 g, 22.2 mmol, 2.0 eq) was added over 10 min. The mixture was heated to 130 °C for 3 h and after cooling to r.t. it was poured onto an ice/water mixture (80.0 g) in one batch. The aqueous phase was extracted with CH_2Cl_2 (3 x 30 mL) and the combined organic layers were dried over $MgSO_4$, filtered and the solvent was removed *in vacuo*. After purification *via* distillation under reduced pressure (approx. 50 mbar), the product was isolated as a colorless liquid (1.52 mg, 7.01 mmol, 63%).

R$_f$ (CH_2Cl_2/MeOH 95:5): 0.93.

^{1}H-NMR (300 MHz, methanol-d_4) δ 8.06 (s, 1H, H-1) ppm.

^{13}C{^{1}H}-NMR (75 MHz, methanol-d_4) δ 164.61, 157.51 (q, J = 38.8 Hz), 125.91, 119.84 (q, J = 275.1 Hz) ppm.

^{19}F{^{1}H}-NMR (282 MHz, methanol-d_4) δ -72.31 ppm.

IR (Film): $\tilde{\nu}$ [cm^{-1}] 3115 (w), 2358 (w), 1549 (vs), 1418 (m), 1389 (m), 1269 (m), 1232 (m), 1169 (m), 1110 (w).

7.4.5 6-Chloro-*N*-(3,4-dimethylphenyl)-*N*-methyl-2-(trifluoromethyl)pyrimidin-4-amine (91)

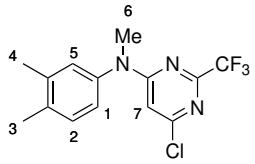

This reaction was done by adapting the method by Gärtner *et al.*[32]: Aniline **82** (902 mg, 6.67 mmol) and dichloropyrimidine **90** (1.52 g, 7.01 mmol, 1.1 eq) were dissolved in MeOH (60.0 mL). Molecular sieve (3 Å) was added and the mixture was stirred at r.t. overnight before filtration and removal of the solvent *in vacuo* to yield the product as a beige powder in a good purity (2.46 g), which was utilized for the next synthetic step without purification.

$\mathbf{R}_f$ (*n*-hexane/EtOAC 95:5): 0.45.

^{1}H-NMR (300 MHz, chloroform-*d*) δ 7.26 (d, J = 7.9 Hz, 1H, H-2), 7.02 – 6.90 (m, 2H, H-1,5), 6.28 (s, 1H, H-7), 3.50 (s, 3H, H-6), 2.32 (s, 3H, H-3/4), 2.31 (s, 3H, H-3/4) ppm.

^{13}C{^{1}H}-NMR (151 MHz, chloroform-*d*) δ 163.77, 159.47, 156.39 (q, J = 36.7 Hz), 140.51, 139.48, 137.32, 131.76, 127.56, 123.85, 120.12 (q, J = 275.49 Hz), 104.78, 38.74, 20.02, 19.59 ppm.

^{19}F{^{1}H}-NMR (282 MHz, chloroform-*d*) δ -71.32 ppm.

IR (Film): $\tilde{\nu}$ [cm^{-1}] 2926 (w), 1575 (vs), 1508 (m), 1408 (m), 1385 (m), 1199 (s), 1172 (m), 1148 (m), 999 (w).

HRMS (ESI): m/z = 316.0828 [M+H$^+$] (calculated: 316.0823).

M.Pt.: 84.6 – 86.6 °C.

7.4.6 6-(Benzyloxy)-*N*-(3,4-dimethylphenyl)-*N*-methyl-2-(trifluoromethyl)pyrimidin-4-amine (92)

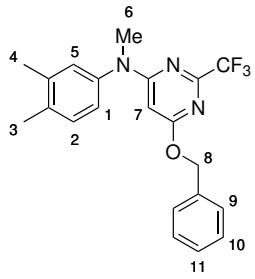

This reaction was done by adapting the method by Gärtner *et al.*[32]. BnONa was prepared following a method by Leonelli, Piancatelli and coworkers[117]: To a cooled flask (0 °C) containing NaH (60% dispersion in mineral oil, 1.56 g, 39.0 mmol, 5.9 eq) was added BnOH (7.75 mL, 8.10 mg, 74.9 mmol, 11 eq). Then, the ice-bath was removed and the mixture was stirred at r.t. for 30 min. Toluene (80.0 mL) was added, followed by addition of tertiary amine **91** (2.46 g) and the mixture was heated to reflux for 3 h. After cooling to r.t., it was filtered over silica and the solvent was removed *in vacuo*. After purification *via* FC (*n*-hexane/EtOAc 98:2 – 95:5), the product was isolated as a colorless oil (2.00 g, 5.17 mmol, 77% over two steps).

$\mathbf{R}_f$ (*n*-hexane/EtOAC 95:5): 0.54.

^{1}H-NMR (300 MHz, chloroform-*d*) δ 7.42 – 7.28 (m, 5H, H-9,10,11), 7.19 (d, J = 7.9 Hz, 1H, H-2), 7.00 – 6.88 (m, 2H, H-1,5), 5.64 (s, 1H, H-7), 5.32 (s, 2H, H-8), 3.47 (s, 3H, H-6), 2.28 (s, 3H, H-3/4), 2.26 (s, 3H, H-3/4) ppm.

^{13}C{^{1}H}-NMR (151 MHz, chloroform-*d*) δ 169.79, 164.88, 155.50 (q, J = 35.8 Hz), 141.79, 138.86, 136.48, 136.25, 131.37, 128.70, 128.60, 128.31, 127.94, 124.19, 119.73 (q, J = 276.0 Hz), 88.48, 68.50, 38.30, 19.97, 19.50 ppm.

^{19}F{^{1}H}-NMR (282 MHz, chloroform-*d*) δ -71.39 ppm.

IR (Film): $\tilde{\nu}$ [cm^{-1}] 3032 (w), 2945 (w), 1597 (vs), 1506 (m), 1426 (m), 1318 (m), 1287 (m), 1237 (m), 1195 (s), 1144 (s).

HRMS (ESI): m/z = 388.1636 [M+H$^+$] (calculated: 388.1631).

7.4.7 6-((3,4-Dimethylphenyl)(methyl)amino)-2-(trifluoromethyl)pyrimidin-4(1*H*)-one (93)

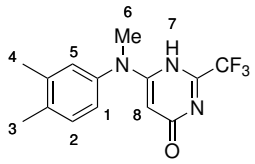

This reaction was done by adapting the method by Gärtner *et al.*[32]: To a mixture of benzyloxy derivative **92** (2.00 g, 5.17 mmol) in MeOH (30.0 mL) was added Pd/C (10%, 275 mg, 258 μmol, 0.05 eq). The mixture was set under H_2 atmosphere and stirred at r.t. for 1.5 h. After filtration, the solvent was removed *in vacuo* to yield the product as a white powder (1.45 g, 4.88 mmol, 94%).

$\mathbf{R_f}$ (CH_2Cl_2/MeOH 97:3): 0.32.

^{1}H-NMR (300 MHz, chloroform-*d*) δ 7.21 (d, J = 7.9 Hz, 1H, H-2), 7.05 – 6.89 (m, 2H, H-1,5), 5.53 (s, 1H, H-8), 3.47 (s, 3H, H-6), 2.29 (s, 3H, H-3/4), 2.28 (s, 3H, H-3/4) ppm.

^{13}C{^{1}H}-NMR (75 MHz, chloroform-*d*) δ 168.49, 164.31, 153.76 – 151.73 (m), 141.35, 138.92, 136.55, 131.39, 127.82, 124.06, 118.89 (q, J = 276.5 Hz), 88.02, 38.43 (d, J = 2.4 Hz), 19.98, 19.52 ppm.

^{19}F{^{1}H}-NMR (282 MHz, chloroform-*d*) δ -71.12 ppm.

IR (Film): $\tilde{\nu}$ [cm^{-1}] 3023 (w), 2949 (w), 2661 (w), 2551 (w), 1624 (s), 1556 (m), 1516 (m), 1435 (w), 1397 (w), 1358 (w), 1197 (vs), 1173 (w), 1139 (s).

HRMS (ESI): m/z = 298.1166 [M+H$^+$] (calculated: 298.1162).

M.Pt.: 203.4 – 205.2 °C.

7.4.8 7,8,10-Trimethyl-4-oxo-2-(trifluoromethyl)-4,10-dihydrobenzo[*g*]pteridine-5-oxide (94)

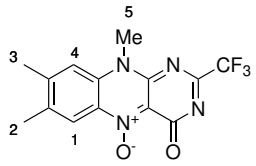

This reaction was done by adapting the method by Gärtner *et al.*[32]: Flavin precursor **93** (205 mg, 688 μmol) was dissolved in AcOH (3.40 mL) and $NaNO_2$ (237 mg, 3.43 mmol, 5.0 eq) was added in the dark. The mixture was stirred at r.t. for 3 h before addition of water (2.80 mL). Stirring was continued for 2.5 h before the solvent was removed *in vacuo* at ambient temperature. The residue was used for the next synthetic step without purification.

7.4.9 7,8,10-Trimethyl-2-(trifluoromethyl)benzo[*g*]pteridine-4(10*H*)-one (75)

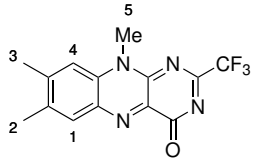

This reaction was done by adapting the method by Gärtner *et al.*[32]: 2-CF_3-*N*-oxide (**94**) raw material was suspended in EtOH (24.0 mL) and $Na_2S_2O_4$ (212 mg, 1.04 mmol, 1.5 eq), dissolved in water (24.0 mL), was added in small portions. The mixture was stirred at r.t. for 1.5 h before removal of the solvent *in vacuo* at ambient temperature to a rest amount of 5 mL, forcing precipitation. The precipitate was filtered off, washed with water and dried in a desiccator overnight. The raw material was subjected to FC (CH_2Cl_2/MeOH 98:2 - 95:5) to achieve separation from remaining starting material. Thereby, a product mixture (11.2 mg) was obtained, showing ^{1}H-NMR signals which would match the desired product.

^{1}H-NMR (300 MHz, DMSO-d_6) δ 7.64 (s, 1H, H-1), 7.40 (s, 1H, H-4), 3.64 (s, 3H, H-5), 2.40 (s, 3H, H-3), 2.30 (s, 3H, H-4) ppm.

$^{19}F\{^1H\}$-NMR (282 MHz, DMSO-d_6) δ -85.09 ppm.

HRMS (ESI): m/z = 309.0963 [M+H^+] (calculated: 309.0958),
341.1225 [M+MeOH+H^+] (calculated: 341.1220).

Procedure B: *via* Kuhn condensation:

The reaction was done by adapting a method by Gilch, Czekelius and coworkers[34] and Averill *et al.*[53]: Nitroaniline **29** (224 mg, 1.24 mmol) was suspended in water (1.5 mL) and AcOH (6.1 mL) and the suspension was degassed by purging with N_2 for 30 min. Pd/C (10%, 18.8 mg, 17.7 μmol, 0.01 eq) was added, the flask was set under H_2 atmosphere and stirring was continued at r.t. overnight. CF_3-alloxan derivative **72** was dissolved in AcOH (15.5 mL) followed by addition of $B(OH)_3$ (487 mg, 7.87 mmol, 6.3 eq). This mixture was degassed by purging with N_2 for 30 min followed by addition of 1,2-diaminobenzene **70** *via* syringe filter. It was stirred at r.t. for 1.5 h, at 70 °C for 1.5 h and at reflux for 1.5 h before several work-up and purification procedures were tested. No desired product could be obtained.

Procedure C: *via* Tishler condensation:

The reaction was done by adapting a method by Neti and Poulter[91], Folkers *et al.*[118] and Tishler *et al.*[88]:

General procedure: Azo-compound **89** was suspended in the particular solvent and catalyst was added. The conversion of the reaction was monitored *via* TLC.

Table 7.2 Synthetic attempts to 2-CF_3-lumiflavin (**75**) *via* Tishler condensation. With all tested reaction conditions no conversion could be observed.

No.	Solvent	Catalyst	Temperature	Time
1	n-BuOH	AcOH	120 °C	3.5 h
2	n-BuOH	TFA	r.t. – 150 °C	3 d
3	DMF	$ZnCl_2$	r.t. – 150 °C	3 d
4	DMF	$Yb(Tf)_3$	r.t. – 150 °C	2 d
5	DMF	$Sc(Tf)_3$	r.t. – 150 °C	2 d
6	THF	$ZnCl_2$	r.t. – 75 °C	6 h
7	THF	$Yb(Tf)_3$	r.t. – 75 °C	6 h

7.4.10 5,5,5-Trihydroxy-2-(trifluoromethyl)pyrimidin-4(5*H*)-one (72)

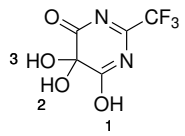

The reaction was done by adapting a synthesis instruction by Holmgren and Wenner[101]: CF_3-Dihydroxypyrimidine **71** (30.0 mg, 167 μmol) was added to a solution of CrO_3 (25.2 mg, 252 μmol, 1.5 eq) in AcOH (500 μL) and water (50 μL). The mixture was stirred at 80 °C for two days before cooling to 5-10 °C and addition of H_2SO_3 (1.0 mL). The solvent was removed *in vacuo* and the raw material was directly uitlized for the next synthetic step.

^{1}H-NMR (300 MHz, methanol-d_4) no signals visible.

^{19}F{^{1}H}-NMR (282 MHz, methanol-d_4) δ -77.56 ppm.

7.4.11 *N*,4,5-Trimethyl-2-((nitro-)phenyldiazenyl)aniline (85)

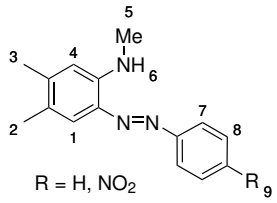

General instruction with buffered conditions:

The instruction was adapted from a method by Neti and Poulter[91], Folkers *et al.*[118] and Tishler *et al.*[88]: Aniline or 4-nitroaniline, respectively, was dissolved/ suspended in water and conc. HCl and cooled to 0 °C. $NaNO_2$ was added in small portions, keeping the temperature at 0 °C. The mixture was stirred for 30 min at 0 °C before it was added to a mixture of Methyl-aniline **82** and NaOAc in water and conc. HCl followed by stirring for 3 h at 0 °C. The ice bath was removed and at 15 °C was added NaOAc dissolved in water, to adjust the pH to approximately 4 inducing precipitation. The precipitate was filtered off and dried *in vacuo*.

Azo-coupling with aniline:

Aniline (390 mL, 399 mg, 4.28 mmol, 1.0 eq) in water (3.40 mL) and conc. HCl (1.50 mL); $NaNO_2$ (297 mg, 4.30 mmol, 1.0 eq); Methyl-aniline **82** (581 mg, 4.30 mmol) and NaOAc (1.45 g, 17.7 mmol, 4.1 eq) in water (8.00 mL) and conc. HCl (1.50 mL); NaOAc (727 mg, 8.86 mmol, 2.1 eq) in water (5.50 mL). The precipitate was filtered off to give triazene side-product **84** (739 mg).

Azo-coupling with p-nitroaniline:

p-Nitroaniline (595 mg, 4.31 mmol, 1.0 eq) in water (3.40 mL) and conc. HCl (1.50 mL); $NaNO_2$ (295 mg, 4.27 mmol, 1.0 eq); Me-aniline **82** (583 mg, 4.31 mmol) and NaOAc (1.46 mg, 17.8 mmol, 4.1 eq) in water (8.00 mL) and conc. HCl (1.50 mL); NaOAc (731 mg, 8.91 mmol, 2.1 eq) in water (5.00 mL). Purification *via* FC (*n*-hexane/EtOAc 99:1 - 92:8) gave triazene side-product **84** (955 mg).

Instruction with a 25% HCl solution:

The reaction was done by adapting a method by Becker *et al.*[92]: Aniline (350 mL, 358 mg, 3.84 mmol, 1.0 eq) was dissolved in HCl (25%, 1.00 mL) and the solution was cooled to 0 °C. $NaNO_2$ (262 mg, 3.80 mmol, 1.00 eq) dissolved in water (1.50 mL) was added slowly, keeping the temperature below 5 °C. Methyl-aniline **82** was dissolved in HCl (1 M, 3.80 mL), cooled to 0 °C and added slowly to diazotized aniline. The mixture was slowly warmed to r.t. and stirred overnight before addition of sat. Na_2CO_3-solution to pH 9 and adjusting with HCl (1 M) to pH 7 - 8. CH_2Cl_2 (10 mL) was added and the phases were separated. The aqueous phase was extracted with CH_2Cl_2 (3 x 10 mL) and the organic phase was dried over Na_2SO_4, filtered and the solvent was evaporated *in vacuo*. After purification *via* FC (pentane), the product was isolated as a yellow oil in a purity not sufficient for yield calculation (8.1 mg).

^{1}H-NMR (300 MHz, methanol-d_4) δ 7.83 – 7.73 (m, 2H, H-7), 7.58 – 7.42 (m, 3H, H-8,9), 7.11 (d, J = 8.6 Hz, 1H, H-1), 6.59 (d, J = 8.6 Hz, 1H, H-4), 2.93 (s, 3H, H-5), 2.61 (s, 3H, H-3), 2.25 (s, 3H, H-2) ppm.

7.4.12 *N*-(4,5-Dimethyl-2-nitrophenyl)acetamide (115)

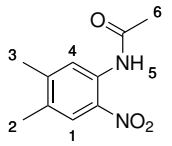

The reaction was done by adapting a method by Parquette *et al.*[104]: Nitroaniline **28** (2.22 g, 13.3 mmol) was suspended in AcOH (8.00 mL) and Ac_2O (1.40 mL, 1.51 g, 14.8 mmol, 1.1 eq) was added before stirring at reflux for 3 h. Then, water (45 mL) and $CHCl_3$ (10 mL) were added and the phases were separated. The aqueous phase was extracted with $CHCl_3$ (3 x 10 mL) and the combined organic phases were dried over Na_2SO_4, filtered and the solvent was removed *in vacuo*. After purification *via* FC (*n*-hexane/EtOAc 9:1 – 8:2), the product was isolated as yellow needles (2.61 g, 12.5 mmol, 94%). The spectroscopic data agree with the literature.[119]

$\mathbf{R_f}$ (*n*-hexane/EtOAC 8:2): 0.41.

^{1}H-NMR (300 MHz, $CDCl_3$) δ 10.27 (brs, 1H, H-5), 8.52 (s, 1H, H-1), 7.95 (s, 1H, H-4), 2.33 (s, 3H, H-3), 2.26 (s, 3H, H-2), 2.26 (s, 3H, H-6) ppm.

7.4.13 *N*-(4,5-Dimethyl-2-nitrophenyl)-*N*-methylacetamide (86)

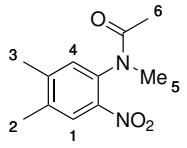

The reaction was done by adapting a method by Parquette *et al.*[104]: *N*-methyl-nitroaniline **29** (3.00 g, 16.7 mmol) was suspended in AcOH (8.50 mL). Ac_2O (1.70 mL, 1.84 g, 18.0 mmol, 1.1 eq) was added and the mixture was refluxed for 2.5 h and stirred at r.t. overnight. Additional Ac_2O (1.00 mL, 1.10 mg, 10.6 mmol, 0.6 eq) was added and refluxing was continued for 2 h, followed by addition of AcOH (5.00 mL) and Ac_2O (1.00 mL, 1.10 g, 10.6 mmol, 0.6 eq). Heating was continued for 3 h before quenching with water (55 mL) and extraction with $CHCl_3$ (3 x 30 mL). The combined organic phases were washed with water (30 mL), dried over Na_2SO_4, filtered and the

solvent was removed *in vacuo*. After purification *via* FC (*n*-hexane/EtOAc 1:1), the product was isolated as a yellow powder (3.64 g, 16.4 mmol, 98%).

$\mathbf{R}_f$ (*n*-hexane/EtOAC 1:1): 0.27.

^{1}H-NMR (300 MHz, chloroform-*d*) δ 7.82 (d, J = 3.1 Hz, 1H, H-4,4' (2 rotamers)), 7.08 (d, J = 17.4 Hz, 1H, H-1,1'), 3.37 (s, 0.5H, H-5'), 3.18 (s, 2.5H, H-5), 2.42 – 2.28 (m, 6H, H-2,2',3,3'), 2.23 (s, 0.5H, H-6'), 1.80 (s, 2.5H, H-6) ppm.

^{13}C{^{1}H}-NMR (75 MHz, chloroform-*d*) δ 171.43, 170.12, 144.99, 144.52, 143.86, 143.67, 138.82, 137.34, 135.36, 135.10, 131.61, 130.57, 126.52, 126.26, 39.35, 36.71, 22.04, 20.57, 19.98, 19.53, 19.41 ppm.

IR (Film): $\tilde{\nu}$ [cm^{-1}] 2925 (w), 1670 (s), 1611 (w), 1572 (w), 1522 (s), 1401 (w), 1372 (m), 1343 (s), 1302 (w), 1146 (w), 1030 (w).

HRMS (ESI): m/z = 223.1082 [M+H$^+$] (calculated: 223.1077).

M.Pt.: 87.7 – 90.2 °C.

7.4.14 *N*-(4,5-Dimethyl-2-nitrosophenyl)-*N*-methylacetamide (87)

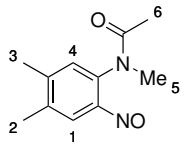

The reaction was done by adapting a method by Parquette *et al.*[104]: Methylacetamide **86** (4.22 g, 19.0 mmol) was dissolved in THF (20 mL) and Rh/C (5%, 140 mg, 68 μmol, 0.004 eq) was added. The mixture was cooled to 0 °C and hydrazine monohydrate (1.01 mL, 1.05 g, 20.9 mmol, 1.1 eq) was added over 3 h. Then, the mixture was filtered through celite and silica gel, followed by removal of the solvent *in vacuo*. The residue was dissolved in THF (900 mL) and cooled to -78 °C before addition of *t*-BuOCl (2.36 mL, 2.27 g, 20.9 mmol, 1.1 eq) in one portion, followed by stirring for 30 min in the dark. The solvent was evaporated *in vacuo* and purification of the residue *via* FC (*n*-hexane/EtOAc 1:1 – 3:7) yielded the product as yellow crystals whose full characterization was omitted due to instability (1.62 g, 19.0 mmol, 41%).

$\mathbf{R}_f$ (*n*-hexane/EtOAC 1:1): 0.27.

^{1}H-NMR (300 MHz, chloroform-*d*) δ 7.32 (s, 1H, H-4), 6.16 (s, 1H, H-1), 3.56 (s, 3H, H-5), 2.36 (s, 3H, H-3), 2.27 (s, 3H, H-2), 1.92 (brs, 3H, H-6) ppm.

7.4.15 *N*-(4,5-Dimethyl-2-((3-nitrophenyl)diazenyl)phenyl)-*N*-methylacetamide (88)

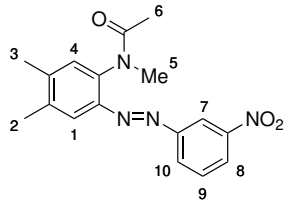

The reaction was done by adapting a method by Parquette *et al.*[104]: Nitroso-derivative **87** (1.57 g, 7.60 mmol) was dissolved in AcOH (62 mL), followed by addition of 3-nitroaniline (1.16 g, 8.36 mmol, 1.1 eq). The mixture was stirred at 100 °C for 2.5 h before it was diluted with $CHCl_3$ (150 mL) and extracted with water (5 x 100 mL). The organic phase was dried over Na_2SO_4, filtered and the solvent was removed *in vacuo*. After purification *via* FC (*n*-hexane/EtOAc 1:1 – 4:6), the product was isolated as an orange powder (550 mg, 1.69 mmol, 22%).

R_f (*n*-hexane/EtOAC 1:1): 0.26.

^{1}H-NMR (300 MHz, chloroform-*d*) δ 8.75 (t, J = 2.1 Hz, 1H, H-7), 8.33 (ddd, J = 8.2, 2.3, 1.1 Hz, 1H, H-8), 8.11 (dt, J = 8.2, 1.3 Hz, 1H, H-10), 7.72 – 7.61 (m, 2H, H-9,4), 7.19 (s, 1H, H-1), 3.32 (s, 3H, H-5), 2.38 (s, 3H, H-2/3), 2.37 (s, 3H, H-2/3) 1.82 (s, 3H, H-6) ppm.

^{13}C{^{1}H}-NMR (75 MHz, chloroform-*d*) δ 171.29, 153.14, 149.13, 145.87, 143.67, 141.76, 138.01, 130.26, 129.99, 125.85, 125.46, 120.64, 117.98, 38.12, 22.71, 20.23, 19.78 ppm.

IR (Film): $\tilde{\nu}$ [cm^{-1}] 2923 (w), 1663 (s), 1604 (m), 1530 (s), 1493 (m), 1447 (m), 1401 (m), 1352 (s), 1309 (m), 1146 (w).

HRMS (ESI): m/z = 327.1452 [M+H$^+$] (calculated: 327.1452).

M.Pt.: 163.6 – 167.0 °C.

7.4.16 *N*,4,5-Trimethyl-2-((3-nitrophenyl)diazenyl)aniline (89)

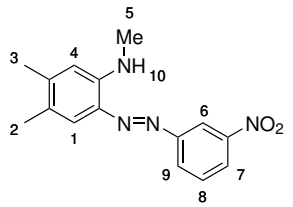

The reaction was done by adapting a method by Parquette *et al.*[104]: Protected Azo-compound **88** (480 mg, 1.47 mmol) was suspended in EtOH (10 mL) and water (10 mL), followed by addition of KOH (1.65 g, 29.4 mmol, 20 eq). The mixture was refluxed for 2.5 h before EtOH was evaporated and the residue was diluted with water (10 mL). The product was extracted with $CHCl_3$ (3 x 24 mL) and the combined organic phases were dried over Na_2SO_4, filtered and the solvent was removed *in vacuo*. The raw material was subjected to FC (*n*-hexane/EtOAc 95:5 – 8:2) yielding a moderately pure red powder that showed ^{1}H-NMR signals which indicated the formation of the desired product (48.2 mg).

$\mathbf{R}_f$ (*n*-hexane/EtOAc 9:1): 0.47.

^{1}H-NMR (300 MHz, chloroform-*d*) δ 8.87 (s, 1H, H-10), 8.60 (t, J = 2.1 Hz, 1H, H-6), 8.18 (ddd, J = 8.2, 2.3, 1.1 Hz, 1H, H-7), 8.10 (ddd, J = 7.9, 1.9, 1.0 Hz, 1H, H-9), 7.68 – 7.56 (m, 2H, H-1,8), 6.60 (s, 1H, H-4), 3.02 (d, J = 5.2 Hz, 3H, H-5), 2.33 (s, 3H, H-3), 2.26 (s, 3H, H-2) ppm.

7.5 Investigated Synthesis of 2-CF_3-NP-Flavin (76)

Scheme 7.3 shows the most promising synthetic approach to 2-CF_3-NP-flavin (**76**).

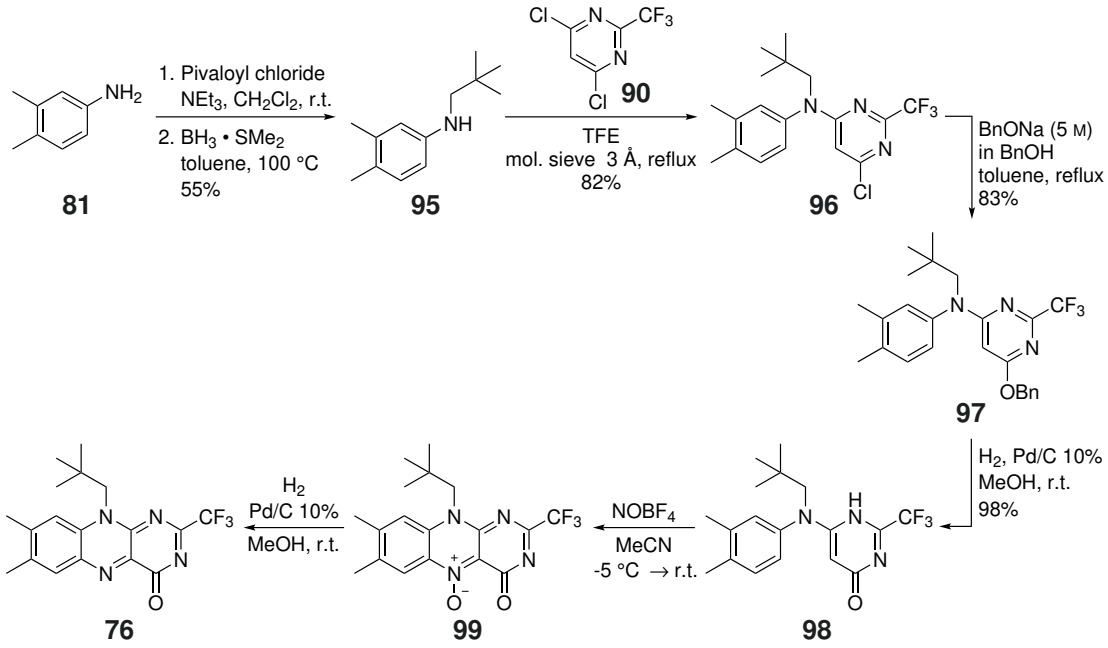

Scheme 7.3 Most promising synthetic approach to 2-CF_3-NP-flavin (**76**) *via* protecting group strategy and *N*-oxide formation.

The synthetic procedures for the most promising synthetic approach *via* *N*-oxide formation are described initially, followed by the procedures for the synthetic approach *via* Kuhn condensation. For an overview of the synthetic approaches *via* Kuhn condensation see Scheme 5.6.

7.5.1 *N*-(3,4-Dimethylphenyl)pivalamide (116)

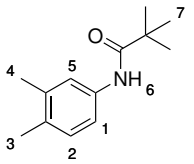

The reaction was done following the method by Mei and Lu [102]: To dimethylaniline **81** (5.01 g, 41.3 mmol) dissolved in CH_2Cl_2 (140 mL) was added NEt_3 (8.50 mL, 6.17 g, 61.0 mmol, 1.5 eq) and the mixture was cooled to 0 °C before pivaloyl chloride (6.00 mL, 5.87 g, 48.7 mmol, 1.2 eq) was added dropwise. The mixture was stirred for 30 min at 0 °C and for 1.5 h at r.t. before NH_4Cl-solution (150 mL) was added. The pH was adjusted to pH 1 using 5 M HCl (5 mL) and the aqueous phase was extracted with CH_2Cl_2 (3 x 70 mL). The combined organic layers were dried over Na_2SO_4, filtered and the solvent was removed *in vacuo* yielding the product as a white powder which was utilized without purification in the next synthetic step (9.40 g). The spectroscopic data are in agreement with the literature.[102]

$\mathbf{R}_f$(*n*-hexane/EtOAc): 0.48.

^{1}H-NMR (300 MHz, chloroform-*d*) δ 7.36 (d, J = 2.3 Hz, 1H, H-2), 7.27 – 7.17 (m, 2H, H-1,6), 7.06 (d, J = 8.1 Hz, 1H, H-5), 2.24 (s, 3H, H-3), 2.21 (s, 3H, H-4), 1.30 (s, 9H, H-7) ppm.

7.5.2 3,4-Dimethyl-*N*-neopentylaniline (95)

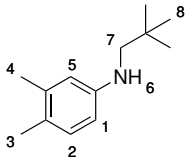

The reaction was done by adjusting a method by Ötvös and Kappe[103]: Pivalamide **116** (9.40 g) was suspended in toluene (140 mL) and cooled to 0 °C. $BH_3{\cdot}SMe_2$ (4.40 mL, 5.66 g, 74.5 mmol, 1.8 eq) was added dropwise and the mixture was stirred for 15 min at 0 °C followed by heating to reflux. After 3.5 h additional $BH_3{\cdot}SMe_2$ (2.00 mL, 2.57 g, 33.9 mmol, 0.8 eq) was added and refluxing was continued

for 2 h. Then, 10% Na_2CO_3 (50 mL) was added slowly and the mixture was stirred at r.t. overnight. The phases were separated and the aqueous phase was extracted with toluene (3 x 40 mL). The combined organic phases were dried over Na_2SO_4, filtered and the solvent was removed *in vacuo*. After purification *via* FC (*n*-hexane/EtOAc 98:2 – 96:4), the product was isolated as a light purple oil (4.36 g, 22.8 mmol, 55% over two steps).

$\mathbf{R_f}$ (*n*-hexane/EtOAc 9:1): 0.70.

^{1}H-NMR (300 MHz, chloroform-*d*) δ 6.96 (d, J = 8.0 Hz, 1H, H-2), 6.53 – 6.40 (m, 2H, H-5,1), 3.51 – 3.45 (brs, 1H, H-6), 2.91 (s, 2H, H-7), 2.23 (s, 3H, H-4), 2.19 (s, 3H, H-3), 1.02 (s, 9H, H-8) ppm.

^{13}C{^{1}H}-NMR (75 MHz, Chloroform-d) δ 147.47, 137.32, 130.36, 124.96, 114.67, 110.16, 56.38, 31.94, 27.80, 20.17, 18.77 ppm.

IR (Film): $\tilde{\nu}$ [cm^{-1}] 3415 (w), 2953 (s), 2865 (m), 1619 (s), 1583 (w), 1513 (s), 1477 (m), 1364 (w), 1321 (m), 1257 (m), 1216 (w), 1173 (w), 1126 (w).

HRMS (ESI): m/z = 192.1749 [M+H$^+$] (calculated: 192.1747).

7.5.3 6-Chloro-*N*-(3,4-dimethylphenyl)-*N*-neopentyl-2-(trifluoromethyl)pyrimidin-4-amine (96)

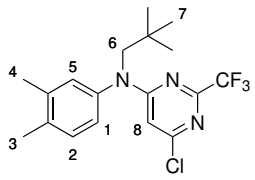

The reaction was done by adapting the method by Gärtner *et al.*[32]: Neopentylaniline **95** (1.00 g, 5.25 mmol) and dichloropyrimidine **90** (800 μL, 1.27 g, 5.84 mmol, 1.1 eq) were dissolved in TFE (50.0 mL) with molecular sieve (3 Å) and the mixture was refluxed for 12 days. Then, celite (9 g) was added, the solvent was removed *in vacuo* and the residue was purified *via* FC (*n*-hexane/EtOAc 8:2). After additional purification *via* recrystallization from *n*-hexane/EtOAc 95:5, the product was isolated as a beige powder (1.60 g, 4.31 mmol, 82%).

$\mathbf{R_f}$ (*n*-hexane/EtOAc 9:1): 0.66.

^{1}H-NMR (300 MHz, chloroform-*d*) δ 7.23 (d, J = 7.8 Hz, 1H, H-2), 7.04 – 6.93 (m, 2H, H-1,5), 6.27 (s, 1H, H-8), 3.96 (s, 2H, H-6), 2.31 (s, 3H, H-4), 2.30 (s, 3H, H-3), 0.90 (s, 9H, H-7) ppm.

^{13}C{^{1}H}-NMR (75 MHz, chloroform-*d*) δ 164.85, 159.61, 155.94 (q, J = 37.0 Hz), 140.80, 139.18, 136.91, 131.46, 128.41, 124.96, 117.38 (q, J = 276.1 Hz), 104.57 (d, J = 2.6 Hz), 61.46, 34.48, 28.61, 20.09, 19.60 ppm.

^{19}F{^{1}H}-NMR (282 MHz, chloroform-*d*) δ -71.41 ppm.

IR (Film): $\tilde{\nu}$ [cm^{-1}] 2953 (w), 2871 (w), 2358 (w), 1577 (vs), 1523 (m), 1503 (m), 1397 (w), 1324 (w), 1190 (s), 1148 (s), 1119 (m), 1083 (w).

HRMS (ESI): m/z = 372.1452 [M+H^{+}] (calculated: 372.1449).

M.Pt.: 125.1 – 126.8 °C.

7.5.4 6-(Benzyloxy)-*N*-(3,4-dimethylphenyl)-*N*-neopentyl-2-(trifluoromethyl)pyrimidin-4-amine (97)

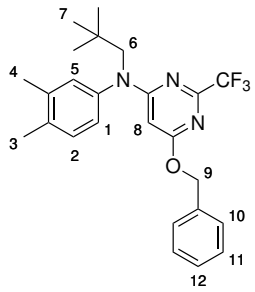

The reaction was done by adapting the method by Gärtner *et al.*[32]. BnONa was prepared following a method by Leonelli, Piancatelli and coworkers[117]: To NaH (60% dispersion in mineral oil, 553 mg, 13.8 mmol, 5.0 eq) cooled in an ice bath was added benzyl alcohol (2.80 mL, 2.93 g, 27.1 mmol, 9.8 eq). The ice bath was removed and the mixture was stirred vigorously for 30 min. Toluene (15 mL) was added followed by tertiary amine **96** (1.03 g, 2.76 mmol) dissolved in 15 mL toluene. The mixture was refluxed for 2 h before it was filtered over celite and the solvent was removed *in vacuo*. After purification *via* FC (*n*-hexane/EtOAc 98:2) followed by recrystallization from *n*-hexane/EtOAc 95:5 (3 mL) and several recrystallizations of the respective filtrates from *n*-hexane/EtOAc 99:1, the product was isolated as a colorless powder (1.02 g,

2.29 mmol, 83%).

R_f (*n*-hexane/EtOAc 95:5): 0.67.

^{1}H-NMR (300 MHz, chloroform-*d*) δ 7.45 – 7.28 (m, 5H, H-10 – H-12), 7.17 (d, J = 7.8 Hz, 1H, H-2), 7.03 – 6.91 (m, 2H, H-1,5), 5.61 (s, 1H, H-8), 5.32 (s, 2H, H-9), 3.95 (s, 2H, H-6), 2.28 (s, 3H, H-4), 2.27 (s, 3H, H-3), 0.90 (s, 9H, H-7) ppm.

^{13}C{^{1}H}-NMR (75 MHz, chloroform-*d*) δ 169.87, 165.92, 154.96 (q, J = 36.0 Hz), 142.13, 138.60, 136.45, 135.90, 131.12, 129.01, 128.79, 128.61, 128.33, 125.42, 119.76 (q, J = 275.7 Hz), 88.26, 68.48, 60.98, 34.44, 28.63, 20.04, 19.51 ppm.

^{19}F{^{1}H}-NMR (282 MHz, chloroform-*d*) δ -71.46 ppm.

IR (Film): $\tilde{\nu}$ [cm^{-1}] 2952 (m), 1596 (vs), 1538 (m), 1486 (m), 1427 (m), 1397 (w), 1362 (m), 1335 (w), 1286 (m), 1234 (m), 1192 (s), 1145 (s).

HRMS (ESI): m/z = 444.2260 [M+H$^+$] (calculated: 444.2257).

M.Pt.: 96.7 – 98.3 °C.

7.5.5 6-((Dimethylphenyl)(neopentyl)amino)-2-(trifluoromethyl)pyrimidin- 4(1*H*)-one (98)

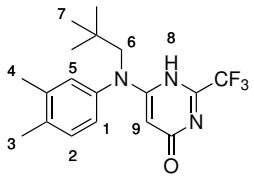

This reaction was done by adapting the method by Gärtner *et al.*[32]: Benzyloxy derivative **97** (1.50 g, 3.39 mmol) was suspended in MeOH (20.0 mL) and Pd/C (10%, 188 mg, 176 μmol, 0.05 eq) was added. The mixture was set under H_2 atmosphere and stirred vigorously for 4 h before filtration and evaporation of the solvent. After purification of the residue *via* FC (CH_2Cl_2/MeOH 95:5), the product was isolated as a colorless powder (1.18 g, 3.33 mmol, 98%).

R_f (CH_2Cl_2/MeOH 95:5): 0.29.

^{1}H-NMR (300 MHz, chloroform-*d*) δ 7.18 (d, J = 7.8 Hz, 1H, H-2), 7.03 – 6.91 (m, 2H, H-1,5), 5.50 (s, 1H, H-9), 3.92 (s, 2H, H-6), 2.28 (s, 3H, H-4), 2.27 (s, 3H, H-3), 0.88 (s,

9H, H-7) ppm.

^{13}C{^{1}H}-NMR (75 MHz, chloroform-*d*) δ 168.61, 165.38, 152.18 (q, J = 37.1 Hz), 141.69, 138.66, 136.24, 131.18, 128.91, 125.23, 118.91 (q, J = 276.4 Hz), 87.94, 61.13, 34.37, 28.59, 20.06, 19.53 ppm.

^{19}F{^{1}H}-NMR (282 MHz, chloroform-*d*) δ -71.16 ppm.

IR (Film): $\tilde{\nu}$ [cm^{-1}] 2970 (m), 2659 (w), 1622 (m), 1544 (m), 1497 (m), 1439 (m), 1398 (w), 1364 (m), 1285 (w), 1192 (s), 1146 (m), 1089 (w).

HRMS (ESI): m/z = 354.1792 [M+H^{+}] (calculated: 354.1788).

M.Pt.: 242.4 – 248.9 °C.

7.5.6 7,8-Dimethyl-10-neopentyl-4-oxo-2-(trifluoromethyl)-4,10-dihydrobenzo[*g*]pteridine 5-oxide (99)

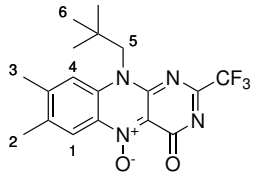

This reaction was done by adapting the method by da Silva Emery *et al.*[109]: Flavin precursor **98** (34.4 mg, 97.3 μmol) was suspended in MeCN (2.00 mL) and the suspension was cooled to -5 °C. $NOBF_4$ (30.1 mg, 258 μmol, 2.7 eq) was added and stirring was continued at -5 °C in the dark for 10 days. After addition of more $NOBF_3$ (106 mg, 909 μmol, 9.3 eq), stirring was continued at -5 °C for 4 days, followed by addition of $NOBF_4$ (126 mg, 1.07 mmol, 11 eq) and stirring at -5 °C for 7 days. Then, the cooling bath was removed and stirring was continued at r.t. for 7 days before addition of ice and water (5 mL). The precipitate was filtered off, washed with water and dried in a desiccator overnight and under high vacuum for 2 days giving the product as an orange powder in a moderate purity not sufficient for yield calculation (19.6 mg). Purification was omitted due to stability reasons.

$\mathbf{R_f}$(CH_2Cl_2/MeOH 95:5): 0.37.

^{1}H-NMR (300 MHz, DMSO-d_6) δ 8.30 (s, 1H, H-1), 8.29 (s, 1H, H-4), 5.36 – 4.37 (m, 2H, H-5), 2.55 (s, 3H, H-3), 2.48 (s, 3H, H-4), 1.01 (s, 9H, H-6) ppm.

^{13}C{^{1}H}-NMR (151 MHz, DMSO-d_6) δ 162.77, 157.14 (d, J = 35.3 Hz), 153.61, 147.34, 138.69, 136.19, 133.74, 127.99, 119.38, 119.07, 118.99 (d, J = 278.0 Hz), 53.51, 34.98, 28.24, 19.80, 18.77 ppm.

^{19}F{^{1}H}-NMR (282 MHz, DMSO-d_6) δ -71.63 ppm.

HRMS (ESI): m/z = 381.1535 [M+H$^+$] (calculated: 381.1533).

M.Pt.: Decomposition >170 °C.

Instruction for cyclization with sodium nitrite:

This reaction was done by adapting the method by Gärtner *et al.*[32]: Flavin precursor **98** (51.7 mg, 146 μmol) was dissolved in AcOH (1.50 mL) followed by addition of $NaNO_2$ (60.1 mg, 871 μmol, 6.0 eq) and stirring at 50 °C overnight. After cooling to r.t., $NaNO_2$ (58.6 mg, 849 μmol, 5.8 eq) was added and stirring at 50 °C was continued overnight. The mixture was cooled to 0 °C and the precipitate was filtered off, washed with water (3.00 mL) and dried in a desiccator yielding an orange powder (24.3 mg). The raw material was used for the next synthetic step without purification.

7.5.7 7,8-Dimethyl-10-neopentyl-2-(trifluoromethyl) benzo[*g*]pteridine-4(10*H*)-one (76)

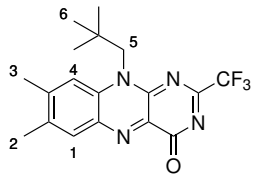

Instruction for deoxygenation using sodium dithionite:

This reaction was done by adapting the method by Gärtner *et al.*[32]: Raw material from cyclization with sodium nitrite (24.3 mg) was suspended in EtOH (5.00 mL) and $Na_2S_2O_4$ (39.0 mg, 224 μmol, 1.5 eq) dissolved in water (5.00 mL) was added slowly. The mixture was stirred at r.t. before the solid was filtered off, washed with degassed water (purged with N_2) and dried in a desiccator overnight to yield a yellow powder that shows two more signals in the ^{1}H-NMR spectrum than expected, which disappeared upon addition of D_2O (16.4 mg).

^{1}H-NMR (300 MHz, DMSO-d_6) δ 11.82 (s, 1H), 7.17 (s, 1H), 6.40 (s, 1H), 6.22 (s, 1H), 3.58 (s, 2H), 1.95 (s, 3H), 1.89 (s, 3H), 0.93 (s, 9H) ppm.

Instruction for deoxygenation *via* heterogeneous catalytic reduction:

Raw material from cyclization with sodium nitrite (44.9 mg) was suspended in MeOH (1.00 mL) and Pd/C (10%, 9.5 mg, 8.9 μmol, 0.08 eq) was added. The mixture was set under H_2 atmosphere and stirred vigorously at r.t. for 30 min. Several work-up and purification procedures were tested. However, no pure material that was sufficient for yield calculation or full characterization was obtained.

MS (APCI): m/z = 365.4 [M+H$^+$] (calculated: 365.2).

Instruction for approach *via* Kuhn condensation:

The reaction was done by adapting a method by Gilch, Czekelius *et al.*[34] and Averill *et al.*[53]: Neopentylnitroaniline **73** (31.1 mg, 131 μmol) was suspended in water (500 μL) and AcOH (1.00 mL) and the suspension was degassed by purging with N_2 for 15 min. Pd/C (10%, 3.8 mg, 3.6 μmol, 0.03 eq) was added, the flask was set under H_2 atmosphere and stirring was continued at r.t. overnight. CF_3-alloxan derivative **72** was dissolved in AcOH (2.00 mL) followed by addition of $B(OH)_3$ (52.5 mg, 849 μmol, 6.5 eq). This mixture was degassed by purging with N_2 for 30 min followed by addition of 1,2-diaminobenzene **74** *via* syringe filter. It was stirred at r.t. for 7 days, at 60 °C for 5 days and at 90 °C for two days. The solvent was removed *in vacuo* and the residue was dissolved in water (5 mL) and $CHCl_3$ (3 mL). The phases were separated and the aqueous phase was extracted with $CHCl_3$ (3 x 3 mL). The combined organic phases were dried over Na_2SO_4, filtered and the solvent was removed *in vacuo*. The residue was subjected to FC (CH_2Cl_2/MeOH 99:1 - 95:5) giving several fractions which were subjected to analysis by mass spectrometry. No desired product could be obtained.

7.5.8 *N*-(4,5-Dimethyl-2-nitrophenyl)pivalamide (117)

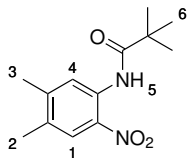

The reaction was done following the method by Mei and Lu [102]: Nitroaniline **28** (10.0 g, 60.2 mmol) was dissolved in CH_2Cl_2 (200 mL) and cooled to 0 °C. NEt_3 (12.6 mL, 9.15 g, 90.4 mmol, 1.5 eq) was added followed by the addition of pivaloyl chloride (8.90 mL, 8.71 g, 72.3 mmol, 1.2 eq). The mixture was stirred at r.t. overnight before dilution with CH_2Cl_2 (50 mL) and sat. NH_4Cl-solution (200 mL), followed by pH adjusting to 1 using 1 M HCl. The phases were separated and the aqueous phase was extracted with CH_2Cl_2, dried over Na_2SO_4, filtered and the solvent was removed *in vacuo*. The raw material was utilized for the next synthetic step without purification.

7.5.9 4,5-Dimethyl-*N*-neopentyl-2-nitroaniline (73)

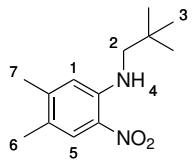

The reaction was done by adjusting a method by Ötvös and Kappe[103]: Pivalamid **117** raw material was dissolved in toluene (200 mL) and cooled to 5 - 10 °C. $BH_3{\cdot}SMe_2$ (6.40 mL, 8.24 g, 108 mmol, 1.8 eq) was added slowly and the mixture was heated to 90 °C for 4 h before addition of 10% Na_2CO_3-solution (30 mL) and stirring at r.t. overnight. The phases were separated and the aqueous phase was extracted with toluene. The combined organic phases were dried over Na_2SO_4, filtered and the solvent was removed *in vacuo*. After purification *via* FC (*n*-hexane/EtOAc 99:1), the product was isolated as a red powder (11.3 g, 47.7 mmol, 79%).

$\mathbf{R}_f$ (*n*-hexane/EtOAc 95:5): 0.49.

^{1}H-NMR (300 MHz, chloroform-*d*) δ 8.20 (s, 1H, H-4), 7.92 (s, 1H, H-5), 6.64 (s, 1H, H-1), 3.06 (d, J = 5.2 Hz, 2H, H-2), 2.26 (s, 3H, H-7), 2.17 (d, 3H, H-6), 1.06 (s, 9H, H-3) ppm.

^{13}C{^{1}H}-NMR (75 MHz, chloroform-*d*) δ 147.40, 144.94, 129.64, 126.47 (d, J = 1.6 Hz), 124.17, 114.22 (d, J = 2.8 Hz), 54.98, 31.87, 27.74, 20.84, 18.65 (d, J = 2.7 Hz) ppm.

IR (Film): $\tilde{\nu}$ [cm^{-1}] 3377 (w), 2959 (s), 2869 (m), 1574 (s), 1514 (m), 1457 (m), 1407 (s), 1367 (m), 1299 (m), 1280 (m), 1242 (s), 1188 (m), 1154 (m), 1058 (m).

HRMS (ESI): m/z = 237.1599 [M+H^{+}] (calculated: 237.1598).

M.Pt.: 94.2 – 96.3 °C.

7.6 Investigated Synthesis of 4-CF_3-Lumiflavin (79)

Scheme 7.4 shows the most promising investigated synthetic approach to 4-CF_3-lumiflavin (**79**).[1]

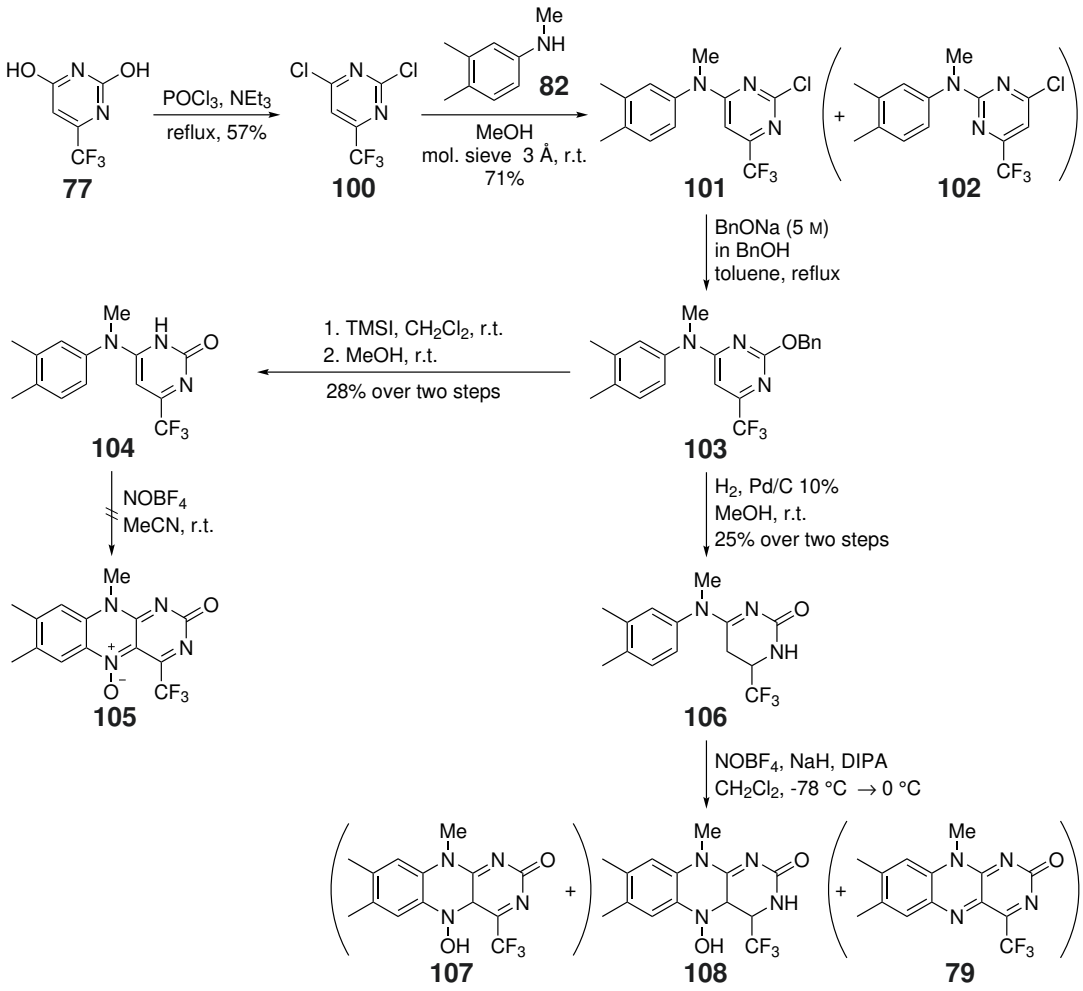

Scheme 7.4 Investigated synthetic approaches to 4-CF_3-lumiflavin (**79**) *via* protecting group strategy. The most promising approach proved to be *via* activation of dihydropyrimidine **106** by deprotonation.[32,99]

The synthetic procedures for the most promising synthetic approach *via* protecting group strategy and activation by deprotonation are described initially followed by the procedures for the synthetic approach *via N*-oxide formation, *via* Kuhn condensation and *via* Tishler condensation. For an overview of the synthetic approaches *via* Kuhn condensation and *via* Tishler condensation see Scheme 5.6 and Scheme 5.8.

1. Parts of the procedures were performed by D. Nürenberg.

7.6.1 2,4-Dichloro-6-(trifluoromethyl)pyrimidine (100)

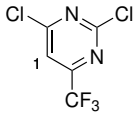

The reaction was done analogous to the method by Madding *et al.*[108]: Pyrimidine **77** (2.00 g, 11.1 mmol) was suspended in $POCl_3$ (5.00 mL, 8.23 g, 53.6 mmol, 4.8 eq) and NEt_3 (3.00 mL, 2.18 g, 21.5 mmol, 1.9 eq) was added over 10 min. The mixture was stirred at 130 °C overnight and after cooling to r.t., it was poured onto an ice/water mixture (60.0 g) in one batch. The aqueous phase was extracted with CH_2Cl_2 (3 x 20 mL), the combined organic layers were dried over $MgSO_4$, filtered and the solvent was removed *in vacuo*. After purification *via* distillation under reduced pressure (50 mbar), the product was isolated as a colorless liquid (1.37 mg, 6.31 mmol, 57%). The spectroscopic data are in agreement with the literature.[120]

$\mathbf{R_f}$ (CH_2Cl_2/MeOH 95:5): 0.92.

^{1}H-NMR (300 MHz, methanol-d_4) δ 8.10 (s, 1H, H-1) ppm.

^{13}C{^{1}H}-NMR (151 MHz, methanol-d_4) δ 166.40, 162.37, 159.63 (q, J = 37.4 Hz), 120.87 (q, J = 274.7 Hz), 118.75 (q, J = 2.9 Hz) ppm.

^{19}F{^{1}H}-NMR (282 MHz, methanol-d_4) δ -71.34 ppm.

7.6.2 2-Chloro-*N*-(3,4-dimethylphenyl)-*N*-methyl-6-(trifluoromethyl)pyrimidin-4-amine (101)

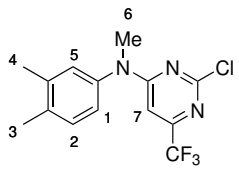

This reaction was done by adapting the method by Gärtner *et al.*[32]: Dichloropyrimidine **100** (400 mg, 1.84 mmol) and aniline **82** (248 mg, 1.84 mmol, 1.0 eq) were dissolved in MeOH (23.6 mL) on molecular sieve (3 Å) and stirred at r.t. for 24 h. The mixture was filtered and the solvent was removed *in vacuo*. After purification *via*

FC (*n*-hexane/EtOAc 99:1 – 95:5), the product was isolated as a white powder (415 mg, 1.31 mmol, 71%).

$\mathbf{R_f}$ (*n*-hexane/EtOAc 8:2): 0.77.

^{1}H-NMR (300 MHz, chloroform-*d*) δ 7.25 (d, J = 7.4 Hz, 1H, H-2), 7.01 – 6.88 (m, 2H, H-1,5), 6.40 (s, 1H, H-7), 3.49 (s, 3H, H-6), 2.32 (s, 3H, H-3/4), 2.30 (s, 3H, H-3/4) ppm.

^{13}C{^{1}H}-NMR (151 MHz, chloroform-*d*) δ 164.24, 161.55, 155.05 (q, J = 35.5 Hz), 140.31, 139.56, 137.56, 131.79, 127.44, 123.75, 120.34 (q, J = 274.9 Hz), 100.00 (d, J = 4.1 Hz), 39.04, 20.00, 19.60 ppm.

^{19}F{^{1}H}-NMR (282 MHz, chloroform-*d*) δ -70.36 ppm.

IR (Film): $\tilde{\nu}$ [cm^{-1}] 2921 (w), 1616 (s), 1508 (s), 1434 (m), 1410 (m), 1323 (m), 1290 (s), 1232 (m), 1209 (m), 1187 (m), 1142 (vs), 1108 (w).

HRMS (ESI): m/z = 316.0826 [M+H$^+$] (calculated: 316.0823).

M.Pt.: 124.6 – 126.2 °C.

7.6.3 2-(Benzyloxy)-*N*-(3,4-dimethylphenyl)-*N*-methyl-6-(trifluoromethyl)pyrimidin-4-amine (103)

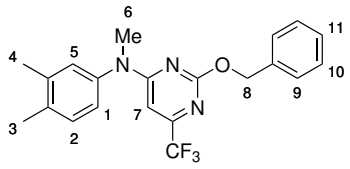

This reaction was done by adapting the method by Gärtner *et al.*[32]. BnONa was prepared following a method by Leonelli, Piancatelli and coworkers[117]: To a pre-cooled flask (0 °C) containing NaH (60% dispersion in mineral oil, 978 mg, 24.4 mmol, 5.1 eq) was added benzyl alcohol (4.80 mL, 5.02 mg, 46.4 mmol, 9.6 eq). Then, the ice-bath was removed and the mixture was stirred at r.t. for 30 min. Toluene (50.0 mL) was added, followed by addition of tertiary amine **101** (1.52 mg, 4.82 mmol) and the mixture was heated to reflux for 3.5 h. Then, it was filtered over celite and the solvent was removed *in vacuo*. After purification *via* FC (*n*-hexane/EtOAc 95:5 – 9:1), a pre-purified product was isolated as a colorless oil (2.22 g) and utilized for the next synthetic step without further purification.

$\mathbf{R}_f$ (*n*-hexane/EtOAc 95:5): 0.23.

^{1}H-NMR (300 MHz, chloroform-*d*) δ 7.55 – 7.46 (m, 2H, H-9), 7.40 – 7.29 (m, 3H, H-10,11), 7.22 (d, *J* = 7.9 Hz, 1H, H-2), 7.00 – 6.88 (m, 2H, H-1,5), 6.19 (s, 1H, H-7), 5.44 (s, 2H, H-8), 3.45 (s, 3H, H-6), 2.31 (s, 3H, H-4), 2.29 (s, 3H, H-3) ppm.

^{19}F{^{1}H}-NMR (282 MHz, chloroform-*d*) δ -70.62 ppm.

7.6.4 4-((3,4-Dimethylphenyl)(methyl)amino)-6-(trifluoromethyl)-5,6-dihydropyrimidin-2(1*H*)-one (106)

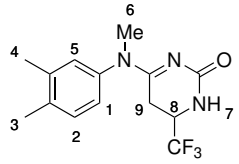

This reaction was done by adapting the method by Gärtner *et al.*[32]: Pre-purified benzyloxy derivative **103** (2.22 g) was dissolved in MeOH (24.0 mL) and Pd/C (10%, 260 mg, 244 μmol, 0.05 eq) was added. The mixture was set under H_2 atmosphere and stirred at r.t. for 4.5 h. After filtration, the solvent was removed *in vacuo*. After purification *via* FC (CH_2Cl_2/MeOH 95:5 - 9:1) followed by recrystallization from toluene, the product was isolated as a colorless powder (362 mg, 1.21 mmol, 25% over two steps).

$\mathbf{R}_f$ (CH_2Cl_2/MeOH 95:5): 0.26.

^{1}H-NMR (300 MHz, chloroform-*d*) δ 7.20 (d, *J* = 7.9 Hz, 1H, H-2), 6.96 – 6.84 (m, 2H, H-1,5), 6.47 (d, *J* = 4.0 Hz, 1H, H-7), 3.98 – 3.80 (m, 1H, H-8), 3.46 (s, 3H, H-6), 2.53 – 2.39 (m, 2H, H-9), 2.29 (s, 6H, H-3,4) ppm.

^{13}C{^{1}H}-NMR (151 MHz, chloroform-*d*) δ 164.91, 160.49, 140.64, 139.01, 137.54, 131.30, 127.79, 124.72 (q, *J* = 283.2 Hz), 124.09, 50.14 (q, *J* = 31.4 Hz), 39.51 (q, *J* = 3.7 Hz), 22.94, 19.80, 19.41 ppm.

^{19}F{^{1}H}-NMR (282 MHz, chloroform-*d*) δ -78.21 (d, *J* = 7.1 Hz) ppm.

IR (Film): $\tilde{\nu}$ [cm^{-1}] 3231 (w), 1669 (m), 1557 (vs), 1505 (w), 1455 (m), 1390 (m), 1259 (s), 1208 (w), 1170 (m), 1127 (m).

HRMS (ESI): m/z = 300.1318 [M+H^+] (calculated: 300.1318).

M.Pt.: 199.1 – 211.2 °C.

Crystallization protocol for X-ray crystallography:

Dihydropyrimidine **106** (575 mg) was dissolved in toluene (15 mL) at 125 °C. The heating bath was removed and the solution was cooled slowly to r.t. followed by chilling in an ice bath to yield crystals suitable for X-ray crystallography.

7.6.5 5-Hydroxy-7,8,10-trimethyl-4-(trifluoromethyl)-4,4a,5,10-tetrahydrobenzo[*g*]pteridin-2(3*H*)-one (108)

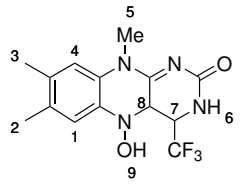

Dihydropyrimidine **106** (31.4 mg, 105 μmol) was dissolved in CH_2Cl_2 (2.70 mL) and cooled to -78 °C. Then, NaH (60% dispersion in mineral oil, 11.0 mg, 275 μmol, 2.6 eq) was added followed by DIPA (1.0 μL, 7.2 mg, 71.4 μmol, 0.68 eq). The mixture was warmed to 0 °C before addition of $NOBF_4$ (72.4 mg, 620 μmol, 5.9 eq). Stirring was continued at 0 °C for 2 days before addition of $NOBF_4$ (118 mg, 1.01 mmol, 9.6 eq) and stirring at 0 °C overnight. Then, the mixture was cooled to -78 °C and NaH (60% dispersion in mineral oil, 104 mg, 2.60 mmol, 24 eq) and DIPA (0.11 mL, 79.4 mg, 785 μmol, 7.5 eq) were added, followed by warming to -40 °C and addition of $NOBF_4$ (113 mg,970 μmol, 18 eq). The mixture was warmed to 0 °C and stirred for 3 days before addition of ice and water (10 mL) and extraction with CH_2Cl_2 (4 x 5 mL). The solvent of the combined organic phases was removed *in vacuo* at ambient temperature to yield a yellow oil (126 mg) which was subjected to mass spectrometry, giving a mass two H^+ lower than expected.

MS (APCI): m/z = 299.9 [**106**+H^+] (calculated for **106**: 300.1), 326.9 [**108**-2H^++H^+] (calculated for **108**: 329.1).

7.6.6 6-((3,4-Dimethylphenyl)(methyl)amino)-4-(trifluoromethyl) pyrimidin-2(1*H*)-one (104)

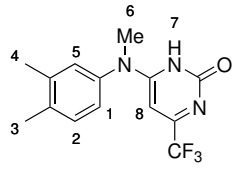

The reaction was done by adapting the method by Schinazi et al.[110]: Pre-purified benzyloxy derivative **103** (85.7 mg) was dissolved in CH_2Cl_2 (2.50 mL) and TMSI (100 μL, 141 mg, 703 μmol, 3.2 eq) was added. The mixture was stirred at r.t. overnight before addition of MeOH (5 mL), followed by evaporation of the solvent *in vacuo*. After purification *via* FC (CH_2Cl_2/MeOH 95:5), the product was isolated as a bright yellow powder (61.5 mg, 207 μmol, 28% over two steps).

R$_f$ (CH_2Cl_2/MeOH 95:5): 0.27.

^{1}H-NMR (300 MHz, chloroform-*d*) δ 12.63 (s, 1H, H-7), 7.22 (d, J = 7.9 Hz, 1H, H-2), 7.00 – 6.88 (m, 2H, H-1,5), 5.78 (s, 1H, H-8), 3.50 (s, 3H, H-6), 2.31 (s, 3H, H-4), 2.30 (s, 3H, H-3) ppm.

^{13}C{^{1}H}-NMR (75 MHz, chloroform-*d*) δ 164.10, 159.33, 143.16 (q, J = 37.0, 36.6 Hz), 140.58, 139.12, 137.35, 131.38, 127.77, 124.12, 119.20 (q, J = 274.7 Hz), 91.80, 39.45 (d, J = 2.0 Hz), 19.91, 19.52 ppm.

^{19}F{^{1}H}-NMR (282 MHz, chloroform-*d*) δ -69.12 ppm.

IR (Film): $\tilde{\nu}$ [cm^{-1}] 2924 (w), 2764 (w), 1644 (s), 1550 (m), 1497 (s), 1447 (m), 1401 (m), 1364 (m), 1281 (m), 1200 (m), 1152 (m).

HRMS (ESI): m/z = 298.1162 [M+H$^+$] (calculated: 298.1162).

M.Pt.: 215.5 – 217.7 °C.

7.6.7 7,8,10-Trimethyl-2-oxo-4-(trifluoromethyl)-2,10-dihydrobenzo[*g*]pteridine 5-oxide (105)

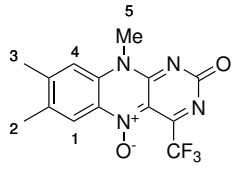

This reaction was done by adapting the method by da Silva Emery *et al.*[109]: Flavin precursor **104** (20.0 mg, 67.3 μmol) was suspended in MeCN (2.00 mL) and cooled to -5 °C before addition of $NOBF_4$ (18.5 mg, 158 μmol, 2.4 eq). The mixture was stirred at -5 °C for 10 days before addition of $NOBF_4$ (17.0 mg, 146 μmol, 2.2 eq) and stirring at r.t. for 4 days and at 50 °C for 7 days. No product formation was observed.

7.6.8 2,5,5-Trihydroxy-6-(trifluoromethyl)pyrimidin-4(5*H*)-one (78)

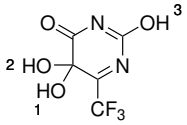

The reaction was done by adapting a synthesis instruction by Holmgren and Wenner[101]: CF_3-Dihydroxypyrimidine **77** (30.3 mg, 168 μmol) was added to a solution of CrO_3 (25.6 mg, 256 μmol, 1.5 eq) in AcOH (500 μL) and water (50 μL). The mixture was stirred at 50 °C overnight and at 80 °C for three days before addition of CrO_3 (17.5 mg, 175 μmol, 1.0 eq). Stirring at 80 °C was continued for 5 days followed by removal of the solvent *in vacuo*. The residue was dissolved in MeOH, filtered and the solvent was removed *in vacuo*. The raw material was utilized for the next synthetic step without purification.

^{1}H-NMR (300 MHz, methanol-d_4): no signals visible.

^{19}F{^{1}H}-NMR (282 MHz, methanol-d_4) δ -73.01, -78.51 ppm.

7.6.9 7,8,10-Trimethyl-4-(trifluoromethyl)benzo[*g*]pteridine-2(10*H*)-one (79)

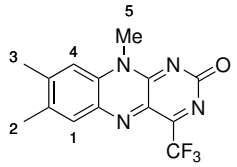

Procedure A: *via* Kuhn condensation:

The reaction was done by adapting a method by Gilch, Czekelius *et al.*[34] and Averill *et al.*[53]: Nitroaniline **29** (22.8 mg, 127 μmol) was suspended in water (400 μL) and AcOH (1.00 mL) and Pd/C (10%, 1.9 μg, 1.8 μmol, 0.01 eq) was added, the flask was set under H_2 atmosphere and the mixture was stirred at r.t. overnight. CF_3-Alloxan derivative **78** raw material was dissolved in AcoH (1.60 mL) followed by addition of $B(OH)_3$ (50.3 mg, 814 μmol, 6.4 eq). This mixture was degassed by purging with N_2 for 30 min followed by addition of 1,2-diaminobenzene **70** *via* syringe filter. It was stirred at r.t. for 2 h and at 100 °C overnight. No product formation was observed.

Procedure B: *via* Tishler condensation:

The reaction was done by adapting a method by Neti and Poulter[91], Folkers *et al.*[118] and Tishler *et al.*[88]:

General procedure: Azo-compound **89** was suspended in the particular solvent and catalyst was added. The conversion of the reaction was monitored *via* TLC.

Table 7.3 Synthetic attempts to 4-CF_3-lumiflavin (**79**) *via* Tishler condensation. With all tested reaction conditions no conversion could be observed.

No.	Solvent	Catalyst	Temperature	Time
1	n-BuOH	AcOH	r.t. - 100 °C	1 d
2	n-BuOH	TFA	r.t. - 100 °C	1 d
3	DMF	$ZnCl_2$	r.t. - 100 °C	3 d
4	DMF	$Yb(Tf)_3$	r.t. - 100 °C	3 d

7.7 Investigated Synthesis of 4-CF_3-NP-Flavin (80)

Scheme 7.5 shows the investigated synthetic approach to 4-CF_3-lumiflavin (**79**). For an overview of the synthetic approach *via* Kuhn condensation see Scheme 5.6.

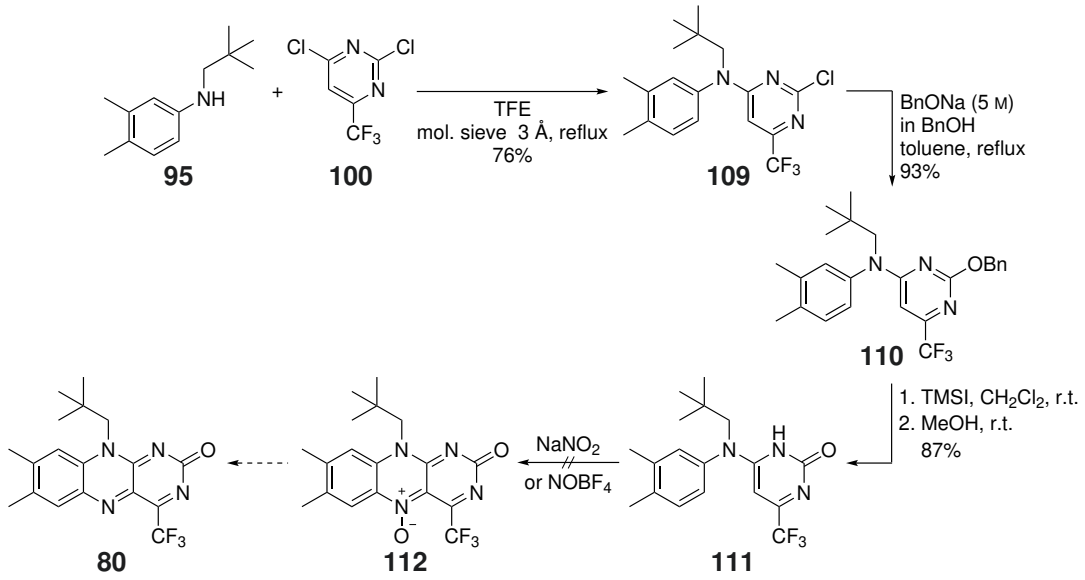

Scheme 7.5 Investigated synthetic approach to 4-CF_3-NP-flavin (**80**) *via* modified protecting group strategy and *N*-oxide formation.

7.7.1 2-Chloro-*N*-(3,4-dimethylphenyl)-*N*-neopentyl-6-(trifluoromethyl)pyrimidin-4-amine (109)

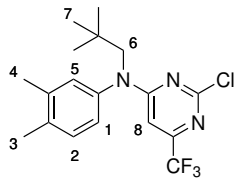

The reaction was done by adapting the method by Gärtner *et al.*[32]: Neopentyl-aniline **95** (32.5 mg, 170 μmol) and dichloropyrimidin **100** (45.3 mg, 186 μmol, 1.1 eq) were dissolved in TFE (4.00 mL) and some 3 Å molecular sieve was added. The mixture was heated to reflux for 3 d before filtration through silica gel and evaporation of the solvent *in vacuo*. After purification of the residue *via* FC (*n*-hexane/EtOAc 98:2), the product was isolated as a pale yellow powder (48.2 mg, 130 μmol, 76%).

R_f (*n*-hexane/EtOAc 9:1): 0.65.

^{1}H-NMR (300 MHz, chloroform-*d*) δ 7.22 (d, *J* = 7.8 Hz, 1H, H-2), 7.02 – 6.91 (m, 2H, H-1,5), 6.39 (s, 1H, H-8), 3.97 (s, 2H, H-6), 2.31 (s, 3H, H-4), 2.30 (s, 3H, H-3), 0.91 (s, 9H, H-7) ppm.

^{13}C{^{1}H}-NMR (75 MHz, chloroform-*d*) δ 165.34, 161.12, 155.17 (q, *J* = 35.3 Hz), 140.51, 139.22, 137.11, 131.44, 128.24, 124.87, 120.35 (q, *J* = 274.8 Hz), 99.70, 61.32, 34.59, 28.65, 20.06, 19.61 ppm.

^{19}F{^{1}H}-NMR (282 MHz, chloroform-*d*) δ -70.33 ppm.

IR (Film): $\tilde{\nu}$ [cm^{-1}] 2955 (m), 1596 (vs), 1497 (s), 1429 (s), 1397 (m), 1365 (w), 1333 (m), 1299 (m), 1283 (m), 1231 (s), 1200 (m), 1150 (s), 1113 (m), 1081 (m).

HRMS (ESI): m/z = 372.1455 [M+H$^+$] (calculated: 372.1449).

M.Pt.: 106.7 – 108.2 °C.

Crystallization protocol for X-ray crystallography:

Tertiary amine **109** (1.47 g) was dissolved in *n*-hexane (2 mL) at 85 °C. The heating bath was removed and the solution was cooled to r.t. followed by chilling in an ice bath to yield crystals suitable for X-ray crystallography.

7.7.2 2-(Benzyloxy)-*N*-(3,4-dimethylphenyl)-*N*-neopentyl-6-(trifluoromethyl)pyrimidin-4-amine (110)

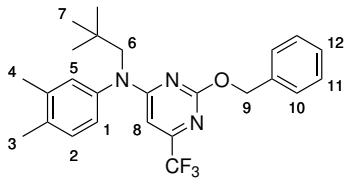

The reaction was done by adapting the method by Gärtner *et al.*[32]. BnONa was prepared following a method by Leonelli, Piancatelli and coworkers[117]: To NaH (60% in mineral oil, 78.1 mg, 1.95 mmol, 7.1 eq) at 0 °C was added BnOH (400 μL, 418 mg, 3.87 mmol, 14 eq) under vigorous stirring. The mixture was stirred at r.t. for 30 min before it was diluted with toluene (2.70 mL). Tertiary amine **109** (102 mg, 274 μmol) was added and the mixture heated to reflux for 1 h. Then, it was directly applied on

FC yielding the product as a colorless resin (113 mg, 255 μmol, 93%).

$\mathbf{R_f}$ (*n*-hexane/EtOAc 95:5): 0.32.

^{1}H-NMR (300 MHz, chloroform-*d*) δ 7.48 (d, *J* = 7.3 Hz, 2H, H-10), 7.42 – 7.28 (m, 3H, H-11,12), 7.19 (d, *J* = 7.8 Hz, 1H, H-2), 7.02 – 6.91 (m, 2H, H-1,5), 6.16 (s, 1H, H-8), 5.43 (s, 2H, H-9), 3.94 (s, 2H, H-6), 2.30 (s, 3H, H-4), 2.28 (s, 3H, H-3), 0.87 (s, 9H, H-7) ppm.

^{13}C{^{1}H}-NMR (151 MHz, chloroform-*d*) δ 166.45, 165.22, 155.75 (q, *J* = 34.3 Hz), 141.51, 138.71, 137.06, 136.39, 131.17, 128.75, 128.47, 128.04, 127.93, 125.32, 120.98 (q, *J* = 274.7 Hz), 95.46 (q, *J* = 3.3 Hz), 69.07, 60.79, 34.29, 28.72, 19.86, 19.42 ppm.

^{19}F{^{1}H}-NMR (282 MHz, chloroform-*d*) δ -70.55 ppm.

IR (Film): $\tilde{\nu}$ [cm^{-1}] 2952 (m), 1599 (s), 1548 (m), 1499 (m), 1441 (s), 1406 (s), 1343 (vs), 1278 (m), 1255 (m), 1200 (m), 1145 (s), 1099 (m), 1067 (m), 1048 (m).

HRMS (ESI): m/z = 444.2257 [M+H$^+$] (calculated: 444.2261).

7.7.3 6-((3,4-Dimethylphenyl)(neopentyl)amino)-4-(trifluoromethyl)pyrimidin-2(1*H*)-one (111)

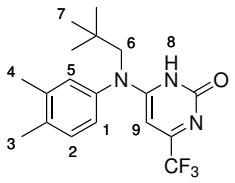

The reaction was done by adapting the method by Schinazi et al.[110]: Benzyloxy derivative **110** (102 mg, 229 μmol) was dissolved in CH_2Cl_2 (2.50 mL). TMSI (100 μL, 141 mg, 703 μmol, 3.1 eq) was added and the mixture stirred at r.t. for 4.5 h. MeOH (5.00 mL) was added and the solvent was removed *in vacuo*. After purification *via* FC (CH_2Cl_2/MeOH 98:2 – 95:5), the product was isolated as a colorless powder (70.0 mg, 198 μmol, 87%).

$\mathbf{R_f}$ (CH_2Cl_2/MeOH 95:5): 0.32.

^{1}H-NMR (300 MHz, chloroform-*d*) δ 7.18 (d, *J* = 7.8 Hz, 1H, H-2), 7.02 – 6.91 (m, 2H, H-1,5), 5.81 (s, 1H, H-9), 4.05 (s, 2H, H-6), 2.29 (s, 3H, H-4), 2.28 (s, 3H, H-3), 0.87 (s,

9H, H-7) ppm.

^{13}C{^{1}H}-NMR (75 MHz, chloroform-*d*) δ 165.35, 159.10, 143.22 (d, J = 38.2 Hz), 140.79, 138.71, 136.90, 130.98, 128.74, 125.42, 119.34 (q, J = 274.8 Hz), 91.92, 60.45, 34.32, 28.59, 20.00, 19.57 ppm.

^{19}F{^{1}H}-NMR (282 MHz, chloroform-*d*) δ -69.10 ppm.

IR (Film): $\tilde{\nu}$ [cm^{-1}] 2925(w), 2758 (w), 1646 (s), 1551 (w), 1477 (s), 1420 (w), 1370 (m), 1336 (s), 1268 (w), 1201 (s), 1154 (s).

HRMS (ESI): m/z = 354.1791 [M+H^{+}] (calculated: 354.1788).

M.Pt.: 247.4 – 261.9 °C.

7.7.4 7,8-Dimethyl-10-neopentyl-2-oxo-4-(trifluoromethyl)-2,10-dihydrobenzo[*g*]pteridine 5-oxide (112)

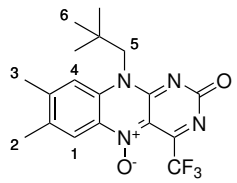

Instruction for the cyclization with sodium nitrite:

This reaction was done by adapting the method by Gärtner *et al.*[32]: Flavin precursor **111** (81.7 mg, 231 μmol) was dissolved in AcOH (4.00 mL) followed by addition of $NaNO_2$ (247 mg, 3.58 mmol, 16 eq) and stirring at 60 °C for 3.5 h, at 70 °C for 1 h and at 140 °C overnight. No product formation was observed.

Instruction for the cyclization with sodium tetrafluoroborate:

This reaction was done by adapting the method by da Silva Emery *et al.*[109]: $NOBF_4$ (20.0 mg, 171 μmol, 2.1 eq) was dissolved in CH_2Cl_2 (2.20 mL) and cooled to 0 °C. Flavin precursor **111** (29.3 mg, 82.9 μmol) was added and the mixture was stirred at r.t. overnight and at 40 °C for 3 h. No product formation was observed.

7.7.5 7,8-Dimethyl-10-neopentyl-4-(trifluoromethyl) benzo[*g*]pteridin-2(10*H*)-one (80)

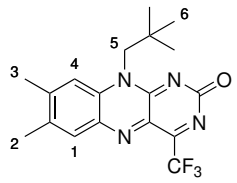

Instruction *via* Kuhn condensation:

The reaction was done by adapting a method by Gilch, Czekelius *et al.*[34] and Averill *et al.*[53]: Neopentylnitroaniline **73** (31.7 mg, 134 μmol) was suspended in water (500 μL) and AcOH (1.00 mL) and the suspension was degassed by purging with N_2 for 15 min. Pd/C (10%, 4.3 mg, 4.0 μmol, 0.03 eq) was added, the flask was set under H_2 atmosphere and stirring was continued at r.t. overnight. CF_3-alloxan derivative **78** was dissolved in AcOH (2.00 mL) followed by addition of $B(OH)_3$ (53.0 mg, 857 μmol, 6.4 eq). This mixture was degassed by purging with N_2 for 15 min followed by addition of 1,2-diaminobenzene **74** *via* syringe filter. It was stirred at 110 °C for 3 days. No product formation was observed.

8 | Bibliography

[1] Edwards A. M., In *Flavins and Flavoproteins: Methods and Protocols* (S. Weber, E. Schleicher, eds.), Springer, New York **2014**, pp. 3–13.

[2] Drenth J., Fraaije M. W., In *Flavin-Based Catalysis* (R. Cibulka, M. W. Fraaije, eds.), Wiley-VCH, Weinheim, Germany **2021**, pp. 29–65.

[3] Massey V., *Biochem. Soc. Trans.* **2000**, *28*, 283–296.

[4] Gadda G., In *Encyclopedia of Biophysics* (G. C. K. Roberts, ed.), Springer, Berlin, Heidelberg **2013**, pp. 771–775.

[5] Svoboda J., Schmaderer H., König B., *Chem. Eur. J.* **2008**, *14*, 1854–1865.

[6] Pavlovska T., Cibulka R., In *Flavin-Based Catalysis* (R. Cibulka, M. W. Fraaije, eds.), Wiley-VCH, Weinheim, Germany **2021**, pp. 1–27.

[7] Mukherjee A., Schroeder C. M., *Curr. Opin. Biotechnol.* **2015**, *31*, 16–23.

[8] Revuelta J. L., Ledesma-Amaro R., Jiménez A., In *Industrial Biotechnology of Vitamins, Biopigments, and Antioxidants* (E. J. Vandamme, J. L. Revuelta, eds.), Wiley-VCH, Weinheim, Germany **2016**, pp. 15–40.

[9] van der Horst M. A., Hellingwerf K. J., *Acc. Chem. Res.* **2004**, *37*, 13–20.

[10] Crosson S., Rajagopal S., Moffat K., *Biochemistry* **2003**, *42*, 2–10.

[11] Losi A., Gärtner W., *Annu. Rev. Plant Biol.* **2012**, *63*, 49–72.

[12] Liscum E., Hodgson D. W., Campbell T. J., *Plant Physiol.* **2003**, *133*, 1429–1436.

[13] Losi A., *Photochem. Photobiol.* **2007**, *83*, 1283–1300.

[14] Cashmore A. R., Jarillo J. A., Wu Y.-J., Liu D., *Science* **1999**, *284*, 760–765.

[15] Briggs W. R., Christie J. M., *Trends Plant Sci.* **2002**, *7*, 204–210.

[16] Tokonami S., Onose M., Nakasone Y., Terazima M., *J. Am. Chem. Soc.* **2022**, *144*, 4080–4090.

[17] Cantrill S., *Nat. Chem.* **2008**.

[18] Drepper T., Eggert T., Circolone F., Heck A., Krauß U., Guterl J.-K., Wendorff M., Losi A., Gärtner W., Jaeger K.-E., *Nat. Biotechnol.* **2007**, *25*, 443–445.

[19] Chudakov D. M., Lukyanov S., Lukyanov K. A., *Trends Biotechnol.* **2005**, *23*, 605–613.

[20] Tsien R. Y., *Annu. Rev. Biochem.* **1998**, *67*, 509–544.

[21] Buckley A. M., Petersen J., Roe A. J., Douce G. R., Christie J. M., *Curr. Opin. Chem. Biol.* **2015**, *27*, 39–45.

[22] Jullien L., Gautier A., *Methods Appl. Fluoresc.* **2015**, *3*, 042007.

[23] Mukherjee A., Walker J., Weyant K. B., Schroeder C. M., *PLoS One* **2013**, *8*, e64753.

[24] Chapman S., Faulkner C., Kaiserli E., Garcia-Mata C., Savenkov E. I., Roberts A. G., Oparka K. J., Christie J. M., *Proc. Natl. Acad. Sci.* **2008**, *105*, 20038–20043.

[25] Christie J. M., Hitomi K., Arvai A. S., Hartfield K. A., Mettlen M., Pratt A. J., Tainer J. A., Getzoff E. D., *J. Biol. Chem.* **2012**, *287*, 22295–22304.

[26] Wingen M., Potzkei J., Endres S., Casini G., Rupprecht C., Fahlke C., Krauss U., Jaeger K. E., Drepper T., Gensch T., *Photochem. Photobiol. Sci.* **2014**, *13*, 875–883.

[27] Crosson S., Moffat K., *Proc. Natl. Acad. Sci.* **2001**, *98*, 2995–3000.

[28] Mathes T., Vogl C., Stolz J., Hegemann P., *J. Mol. Biol.* **2009**, *385*, 1511–1518.

[29] Mansurova M., Scheercousse P., Simon J., Kluth M., Gärtner W., *ChemBioChem* **2011**, *12*, 641–646.

[30] Zirak P., Penzkofer A., Mathes T., Hegemann P., *Chem. Phys.* **2009**, *358*, 111–122.

[31] Tyagi A., Penzkofer A., Mathes T., Hegemann P., *J. Photochem. Photobiol. B: Biol.* **2010**, *101*, 76–88.

[32] Mansurova M., Simon J., Salzmann S., Marian C. M., Gärtner W., *ChemBioChem* **2013**, *14*, 645–654.

[33] Koziar J. C., Cowan D. O., *Acc. Chem. Res.* **1978**, *11*, 334–341.

[34] Reiffers A., Torres Ziegenbein C., Engelhardt A., Kühnemuth R., Gilch P., Czekelius C., *Photochem. Photobiol.* **2018**, *94*, 667–676.

[35] Bracker M., Dinkelbach F., Weingart O., Kleinschmidt M., *Phys. Chem. Chem. Phys.* **2019**, *21*, 9912–9923.

[36] Kubitz M. K., Haselbach W., Sretenović D., Bracker M., Kleinschmidt M., Kühnemuth R., Seidel C. A. M., Gilch P., Czekelius C., *ChemPhotoChem* **2023**, *7*, e202200334.

[37] Salzmann S., Tatchen J., Marian C. M., *J. Photochem. Photobiol. A: Chem.* **2008**, *198*, 221–231.

[38] Bracker M., Kubitz M. K., Czekelius C., Marian C. M., Kleinschmidt M., *ChemPhotoChem* **2022**, e202200040.

[39] IUPAC, In *The "Gold Book"* (A. D. McNaught, A. Wilkinson, eds.), 2. ed., Blackwell Scientific Publications, Oxford **1997**, online version (2019-) created by S. J. Chalk. ISBN 0-9678550-9-8. https://doi.org/10.1351/goldbook.

[40] Medina B. M., Beljonne D., Egelhaaf H.-J., Gierschner J., *J. Chem. Phys.* **2007**, *126*, 111101.

[41] Smart B. E., *J. Fluor. Chem.* **2001**, *109*, 3–11.

[42] Biffinger J. C., Kim H. W., DiMagno S. G., *ChemBioChem* **2004**, *5*, 622–627.

[43] Englman R., Jortner J., *Mol. Phys.* **1970**, *18*, 145–164.

[44] Fukuzumi S., Tanii K., Tanaka T., *J. Chem. Soc, Perk. Trans. 2* **1989**, 2103–2108.

[45] Rehpenn A., Walter A., Storch G., *Synthesis* **2021**, *53*, 2583–2593.

[46] König B., Kümmel S., Svobodová E., Cibulka R., *Phys. Sci. Rev.* **2018**, *3*.

[47] Mironova K. E., Proshkina G. M., Ryabova A. V., Stremovskiy O. A., Lukyanov S. A., Petrov R. V., Deyev S. M., *Theranostics* **2013**, *3*, 831–840.

[48] Qi Y. B., Garren E. J., Shu X., Tsien R. Y., Jin Y., *Proc. Natl. Acad. Sci.* **2012**, *109*, 7499–7504.

[49] Ryumina A. P., Serebrovskaya E. O., Shirmanova M. V., Snopova L. B., Kuznetsova M. M., Turchin I. V., Ignatova N. I., Klementieva N. V., Fradkov A. F., Shakhov B. E., Zagaynova E. V., Lukyanov K. A., Lukyanov S. A., *Biochim. Biophys. Acta Gen. Subj.* **2013**, *1830*, 5059–5067.

[50] Mansurova M., Koay M. S., Gärtner W., *Eur. J. Org. Chem.* **2008**, *2008*, 5401–5406.

[51] Imada Y., Iida H., Ono S., Masui Y., Murahashi S.-I., *Chem. Asian J.* **2006**, *1*, 136–147.

[52] Kuhn R., Reinemund K., Weygand F., Ströbele R., *Ber. Dtsch. Chem. Ges. (A and B Series)* **1935**, *68*, 1765–1774.

[53] Kumar V., Woode K. A., Bryan R. F., Averill B. A., *J. Am. Chem. Soc.* **1986**, *108*, 490–496.

[54] Brown S. A., Rizzo C. J., *Synth. Commun.* **1996**, *26*, 4065–4080.

[55] Rurack K., Spieles M., *Anal. Chem.* **2011**, *83*, 1232–1242.

[56] Cheng K., Li S., Lv X., Tian Y., Kong H., Huang X., Duan Y., Han J., Xie Z., Liao C., *Bioorg. Med. Chem. Lett.* **2019**, *29*, 1012–1018.

[57] Wojciechowski F., Hudson R. H. E., *J. Org. Chem.* **2008**, *73*, 3807–3816.

[58] Hasford J. J., Rizzo C. J., *J. Am. Chem. Soc.* **1998**, *120*, 2251–2255.

[59] FisherScientific, 4-fluoro-5-methoxy-2-nitroaniline | 125163-12-4 | mfcd00247494. https://www.fishersci.com/shop/products/4-fluoro-5-methoxy-2-nitro-1g/502190803, accessed: 09/03/2023.

[60] Carlson E. E., Kiessling L. L., *J. Org. Chem.* **2004**, *69*, 2614–2617.

[61] Abdel-Magid A. F., Carson K. G., Harris B. D., Maryanoff C. A., Shah R. D., *J. Org. Chem.* **1996**, *61*, 3849–3862.

[62] Sheraz M. A., Kazi S. H., Ahmed S., Anwar Z., Ahmad I., *Beilstein J. Org. Chem.* **2014**, *10*, 1999–2012.

[63] Metzler D. E., Cairns W. L., *J. Am. Chem. Soc.* **1971**, *93*, 2772–2777.

[64] Smith E. C., Metzler D. E., *J. Am. Chem. Soc.* **1963**, *85*, 3285–3288.

[65] Heim R., Tsien R. Y., *Curr. Biol.* **1996**, *6*, 178–182.

[66] Weissleder R., Ntziachristos V., *Nat. Med.* **2003**, *9*, 123–128.

[67] Marx V., *Nat. Methods* **2014**, *11*, 717–720.

[68] Slavov C., Mansurova M., Holzwarth A. R., Gärtner W., *Photochem. Photobiol.* **2010**, *86*, 31–38.

[69] Salzmann S., Martinez-Junza V., Zorn B., Braslavsky S. E., Mansurova M., Marian C. M., Gärtner W., *J. Phys. Chem. A* **2009**, *113*, 9365–9375.

[70] Silva-Junior M. R., Mansurova M., Gärtner W., Thiel W., *ChemBioChem* **2013**, *14*, 1648–1661.

[71] Ashton W. T., Graham D. W., Brown R. D., Rogers E. F., *Tetrahedron Lett.* **1977**, *18*, 2551–2554.

[72] Wood A. C., Knight D. W., Richter G., *Tetrahedron* **2015**, *71*, 1679–1683.

[73] Umemoto T., Kawada K., Tomita K., *Tetrahedron Lett.* **1986**, *27*, 4465–4468.

[74] Su Q., Boucher P. A., Rokita S. E., *Angew. Chem. Int. Ed.* **2017**, *56*, 10862–10866.

[75] Skibo E. B., Islam I., Heileman M. J., Schulz W. G., *J. Med. Chem.* **1994**, *37*, 78–92.

[76] Nürenberg D., *Preparation and Fluorination of Lumiflavin Derivatives*. Bachelorarbeit, Heinrich-Heine-Universität Düsseldorf **2021**.

[77] Lal G. S., Pez G. P., Syvret R. G., *Chem. Rev.* **1996**, *96*, 1737–1756.

[78] Timofeeva D. S., Ofial A. R., Mayr H., *J. Am. Chem. Soc.* **2018**, *140*, 11474–11486.

[79] Rozatian N., Hodgson D. R. W., *Chem. Commun.* **2021**, *57*, 683–712.

[80] Umemoto T., Fukami S., Tomizawa G., Harasawa K., Kawada K., Tomita K., *J. Am. Chem. Soc.* **1990**, *112*, 8563–8575.

[81] Takeuchi Y., Tarui T., Shibata N., *Org. Lett.* **2000**, *2*, 639–642.

[82] Banks R. E., Mohialdin-Khaffaf S. N., Lal G. S., Sharif I., Syvret R. G., *J. Chem. Soc., Chem. Commun.* **1992**, 595–596.

[83] Rozatian N., Ashworth I. W., Sandford G., Hodgson D. R. W., *Chem. Sci.* **2018**, *9*, 8692–8702.

[84] Shu X., Lev-Ram V., Deerinck T. J., Qi Y., Ramko E. B., Davidson M. W., Jin Y., Ellisman M. H., Tsien R. Y., *PLoS Biol.* **2011**, *9*, e1001041.

[85] König B., Kümmel S., Svobodová E., Cibulka R., *Phys. Sci. Rev.* **2018**, *3*.

[86] Daďová J., Kümmel S., Feldmeier C., Cibulková J., Pažout R., Maixner J., Gschwind R. M., König B., Cibulka R., *Chem. Eur. J.* **2013**, *19*, 1066–1075.

[87] Lambooy J. P., In *Methods Enzymol.*, vol. 18, Academic Press **1971**, pp. 437–447.

[88] Tishler M., Pfister K., Babson R. D., Ladenburg K., Fleming A. J., *J. Am. Chem. Soc.* **1947**, *69*, 1487–1492.

[89] Hemmerich P., Prijs B., Erlenmeyer H., *Helv. Chim. Acta* **1959**, *42*, 1604–1611.

[90] Hemmerich P., Fallab S., Erlenmeyer H., *Helv. Chim. Acta* **1956**, *39*, 1242–1252.

[91] Neti S. S., Poulter C. D., *J. Org. Chem.* **2016**, *81*, 5087–5092.

[92] Becker H. G. O., Berger W., Domschke G., Fanghänel E., Faust J., Fischer M., Gentz F., Gewald K., Gluch R., Mayer R., Müller K., Pavel D., Schmidt H., Schollberg K., Schwetlick K., Seiler E., Zeppenfeld G., Beckert R., Fanghänel E., Habicher W. D., Metz P., *Organikum - Organisch-chemisches Grundpraktikum*, vol. 21. Wiley-VCH, Weinheim **2001**.

[93] Yoneda F., Sakuma Y., Ichiba M., Shinomura K., *Chem. Pharm. Bull. (Tokyo)* **1972**, *20*, 1832–1834.

[94] Yoneda F., Sakuma Y., Ichiba M., Shinomura K., *J. Am. Chem. Soc.* **1976**, *98*, 830–835.

[95] Yoneda F., Mori K., Ono M., Kadokawa Y., Nagao E., Yamaguchi H., *Chem. Pharm. Bull. (Tokyo)* **1980**, *28*, 3514–3520.

[96] Ali H. I., Tomita K., Akaho E., Kambara H., Miura S., Hayakawa H., Ashida N., Kawashima Y., Yamagishi T., Ikeya H., Yoneda F., Nagamatsu T., *Biorg. Med. Chem.* **2007**, *15*, 242–256.

[97] Legrand Y.-M., Gray M., Cooke G., Rotello V. M., *J. Am. Chem. Soc.* **2003**, *125*, 15789–15795.

[98] Šafář P., Považanec F., Čepec P., Prónayová N., *Collect. Czechoslov. Chem. Commun.* **1997**, *62*, 1105–1113.

[99] Fenner H., Hochhuth D., *Arch. Pharm.* **1990**, *323*, 873–879.

[100] Yoneda F., Shinozuka K., Tsukuda K., Koshiro A., *J. Heterocycl. Chem.* **1979**, *16*, 1365–1367.

[101] Holmgren A. V., Wenner W., *Org. Synth.* **1952**, *32*, 6.

[102] Mei C., Lu W., *J. Org. Chem.* **2018**, *83*, 4812–4823.

[103] Ötvös S. B., Kappe C. O., *ChemSusChem* **2020**, *13*, 1800–1807.

[104] Tie C., Gallucci J. C., Parquette J. R., *J. Am. Chem. Soc.* **2006**, *128*, 1162–1171.

[105] Li F., Frett B., Li H.-y., *Synlett* **2014**, *25*, 1403–1408.

[106] Furst A., Berlo R. C., Hooton S., *Chem. Rev.* **1965**, *65*, 51–68.

[107] Dehmlow E. V., Thieser R., Zahalka H. A., Sasson Y., *Tetrahedron Lett.* **1985**, *26*, 297–300.

[108] Madding G. D., Minielli J. L., Mattson R. J., Process of large-scale production of bmy 21502. https://worldwide.espacenet.com/patent/search/family/023695332/publication/US4963678A?q=pn**1990**, uS4963678A.

[109] Gil de Melo S. M., de Rezende L. C. D., Petrilli R., Vianna Lopez R. F., Goulart M. O. F., da Silva Emery F., *Dyes Pigments* **2020**, *173*, 107885.

[110] Goudgaon N. M., Naguib F. N. M., el Kouni M. H., Schinazi R. F., *J. Med. Chem.* **1993**, *36*, 4250–4254.

[111] Malaczynski S. A., *Synthese von Flavinderivaten zur selektiven Tyrosin-oxidation - Anwendung in der CIDNIP-Spektroskopie*. Masterarbeit, Heinrich-Heine-Universität Düsseldorf **2022**.

[112] Fulmer G. R., Miller A. J. M., Sherden N. H., Gottlieb H. E., Nudelman A., Stoltz B. M., Bercaw J. E., Goldberg K. I., *Organometallics* **2010**, *29*, 2176–2179.

[113] Jhulki I., Chanani P. K., Abdelwahed S. H., Begley T. P., *J. Am. Chem. Soc.* **2016**, *138*, 8324–8327.

[114] Lavrard H., Popowycz F., *Eur. J. Org. Chem.* **2017**, *2017*, 600–608.

[115] Chen M., Ren Z.-H., Wang Y.-Y., Guan Z.-H., *J. Org. Chem.* **2015**, *80*, 1258–1263.

[116] Han X., Javanbakht H., Jiang M., Liang C., Wang J., Wang Y., Wang Z., Weikert R. J., Yang S., Zhou C., Novel dihydoquinolizinones for the treatment and prophylaxis of hepatitis b virus infection. https://patentimages. storage.googleapis.com/40/b3/8b/d0f003cb1257b1/US20150210682A1. pdf **2015**, uS20150210682A1.

[117] Leonelli F., Capuzzi M., Bodo E., Passacantilli P., Piancatelli G., *Carbohydr. Res.* **2008**, *343*, 1133–1141.

[118] Heyl D., Chase E. C., Koniuszy F., Folkers K., *J. Am. Chem. Soc.* **1951**, *73*, 3826–3827.

[119] Gao Y., Mao Y., Zhang B., Zhan Y., Huo Y., *Org. Biomol. Chem.* **2018**, *16*, 3881–3884.

[120] Schlosser M., Lefebvre O., Ondi L., *Eur. J. Org. Chem.* **2006**, *2006*, 1593–1598.

[121] Sheldrick G., *Acta Cryst.* **2008**, *A64*, 112–122.

[122] Dolomanov O. V., Bourhis L. J., Gildea R. J., Howard J. A. K., Puschmann H., *J. Appl. Crystallogr.* **2009**, *42*, 339–341.

[123] Macrae C. F., Sovago I., Cottrell S. J., Galek P. T. A., McCabe P., Pidcock E., Platings M., Shields G. P., Stevens J. S., Towler M., Wood P. A., *J. Appl. Crystallogr.* **2020**, *53*, 226–235.

9 | Appendix

9.1 NMR Spectra

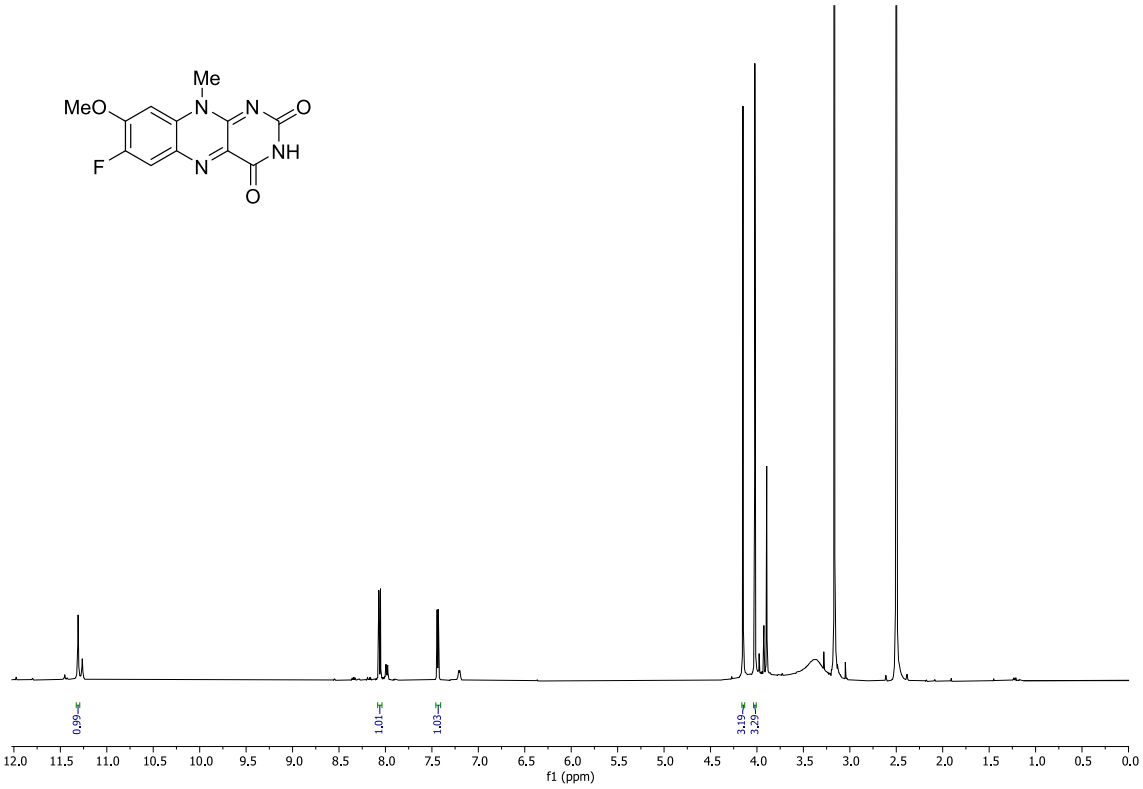

Figure 9.1 ^{1}H-NMR spectrum (600 MHz, DMSO-d_6) of **16**.

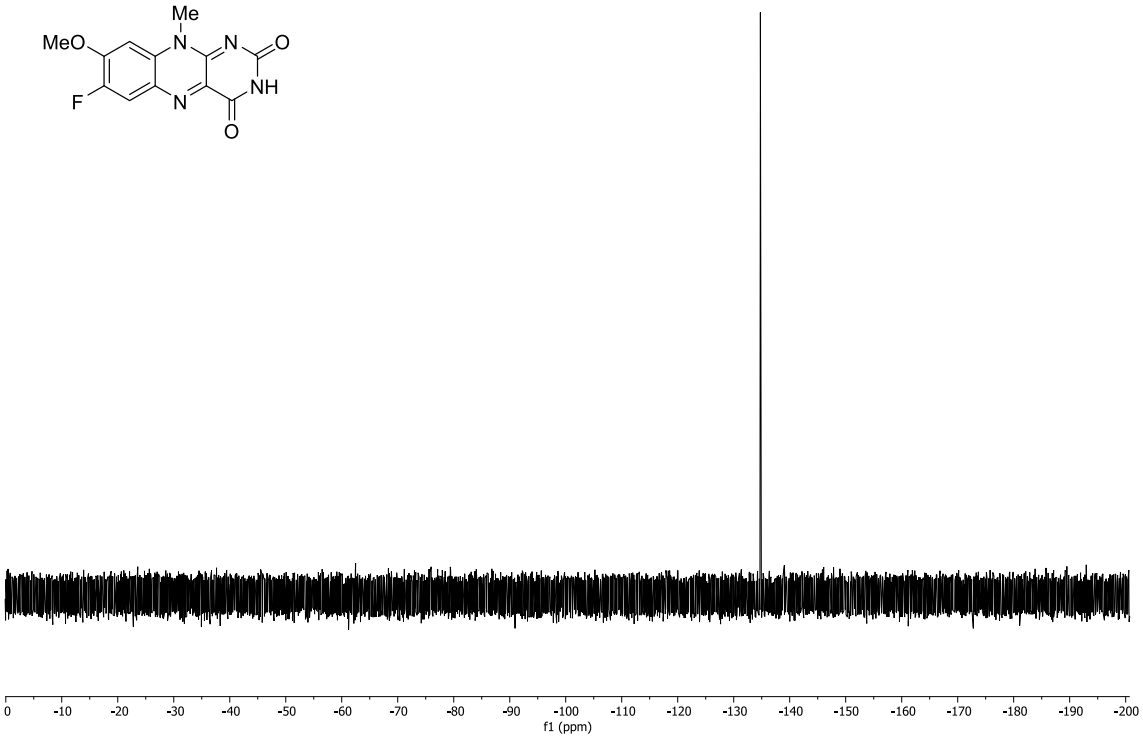

Figure 9.2 ^{19}F{^{1}H}-NMR spectrum (565 MHz, DMSO-d_6) of **16**.

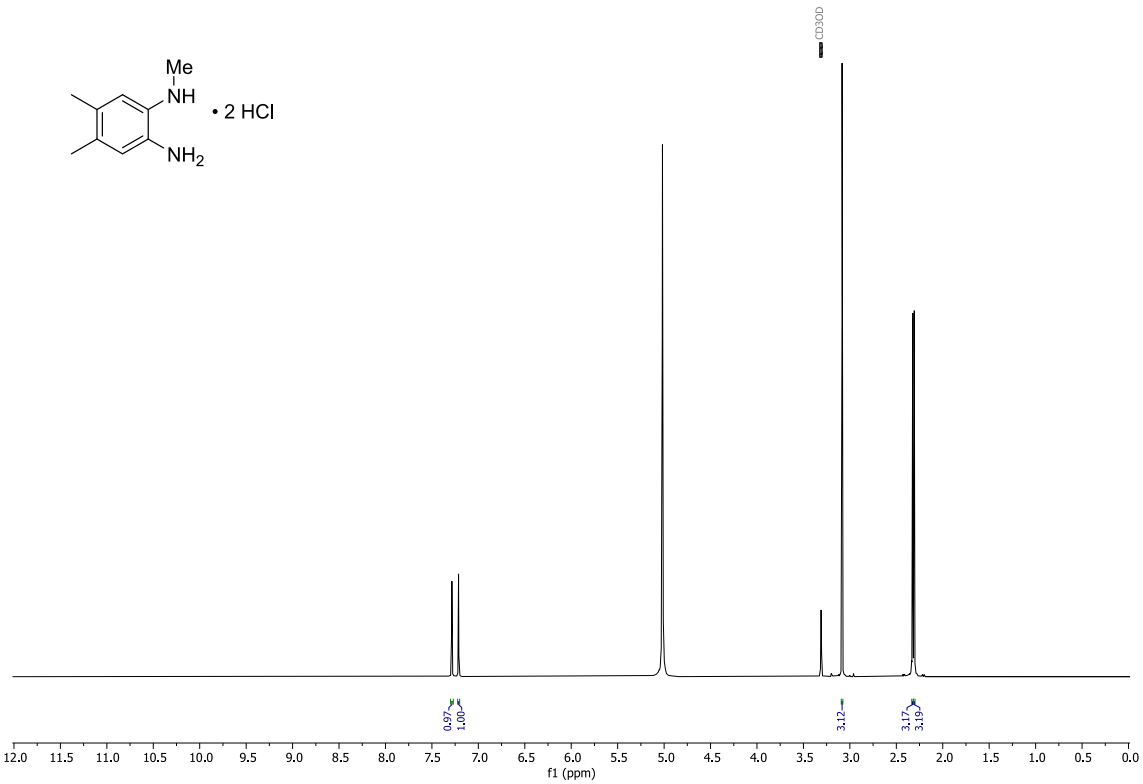

Figure 9.3 ^{1}H-NMR spectrum (600 MHz, methanol-d_4) of **35**.

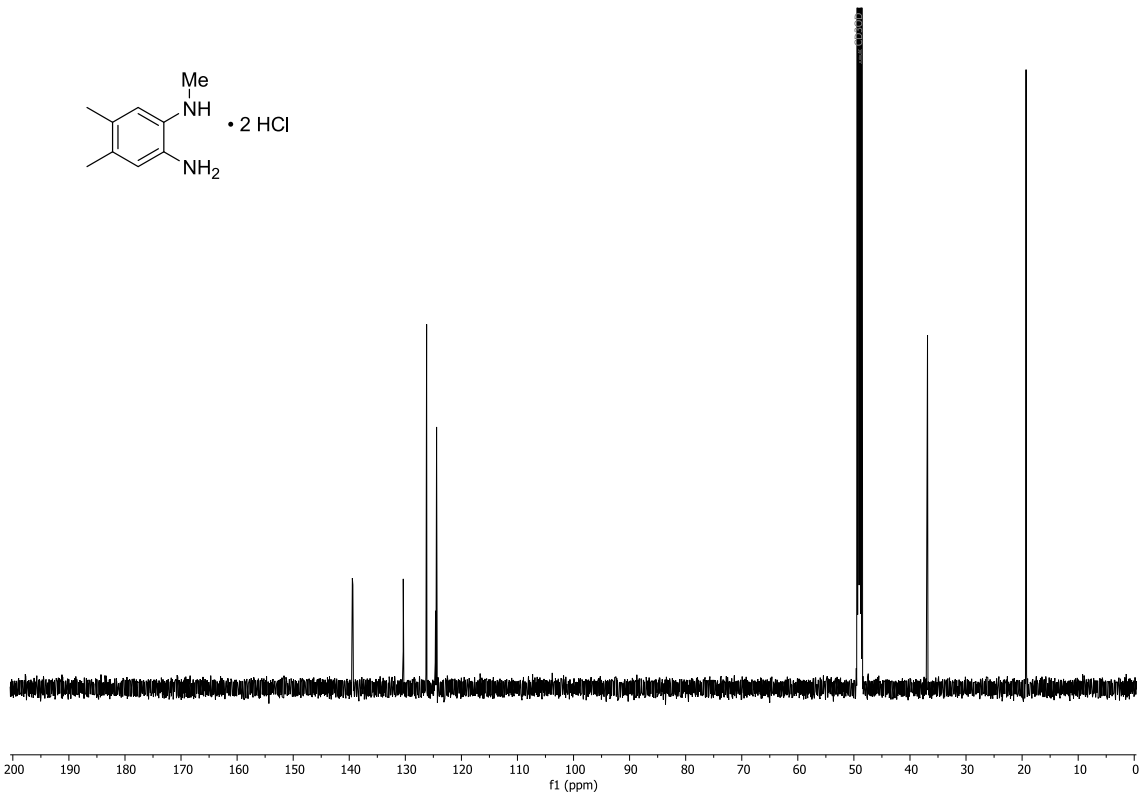

Figure 9.4 ^{13}C{^{1}H}-NMR spectrum (150 MHz, methanol-d_4) of **35**.

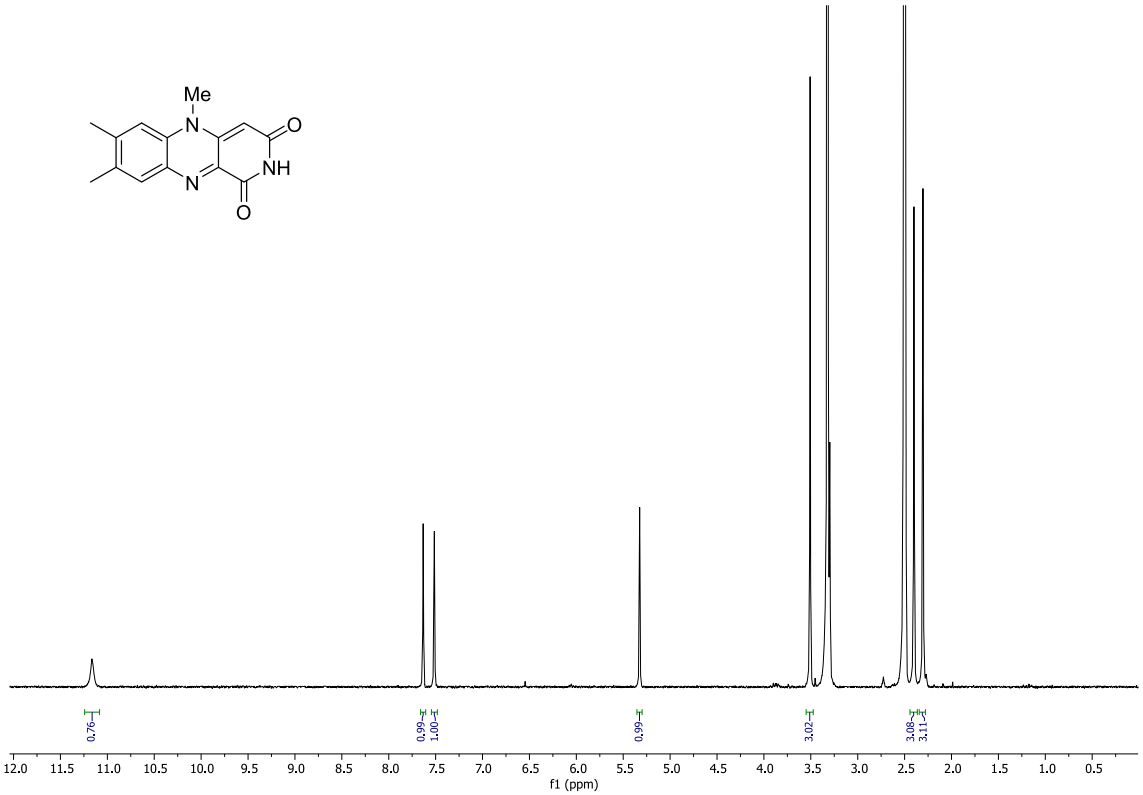

Figure 9.5 ^{1}H-NMR spectrum (300 MHz, DMSO-d_6) of **31**.

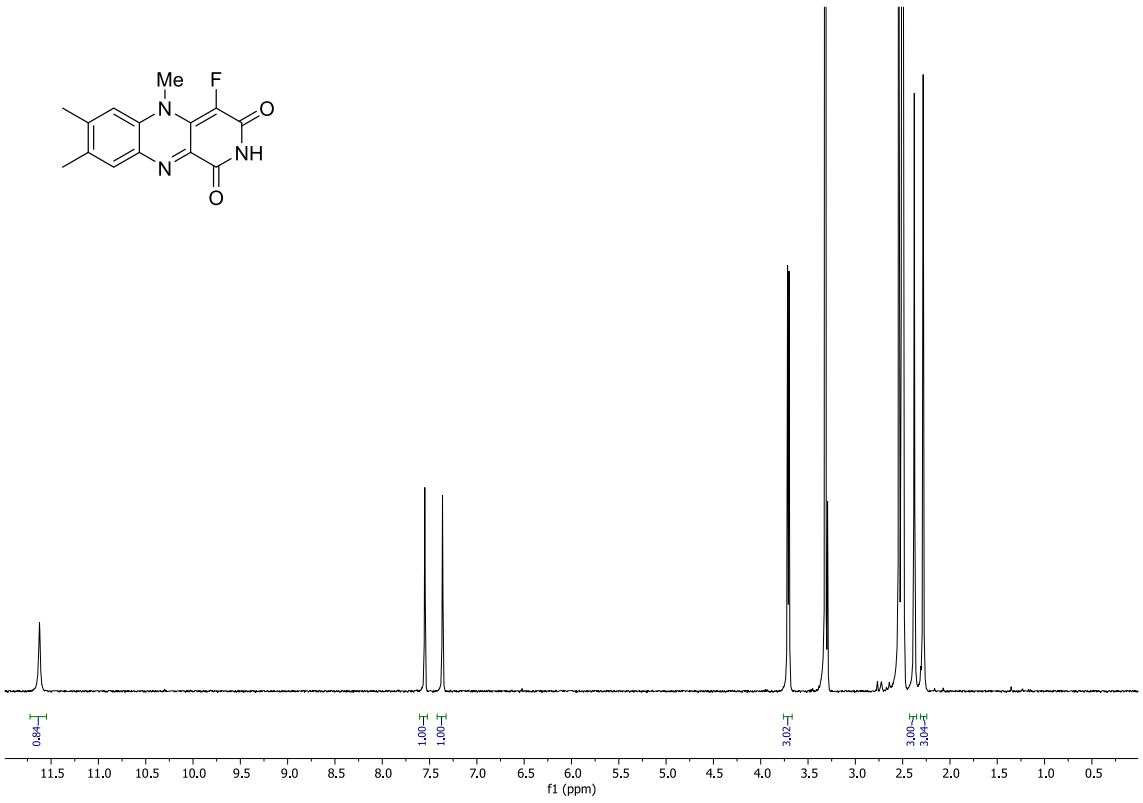

Figure 9.6 ^{1}H-NMR spectrum (300 MHz, DMSO-d_6) of **33**.

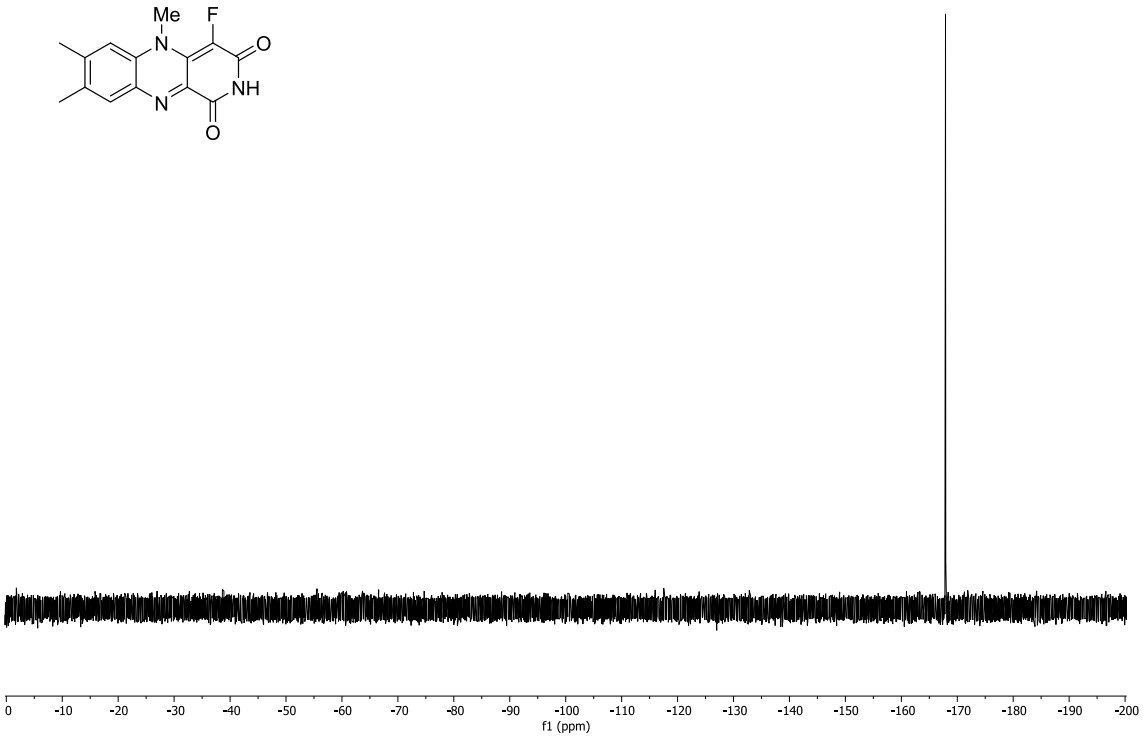

Figure 9.7 $^{19}F\{^{1}H\}$-NMR spectrum (282 MHz, DMSO-d_6) of **33**.

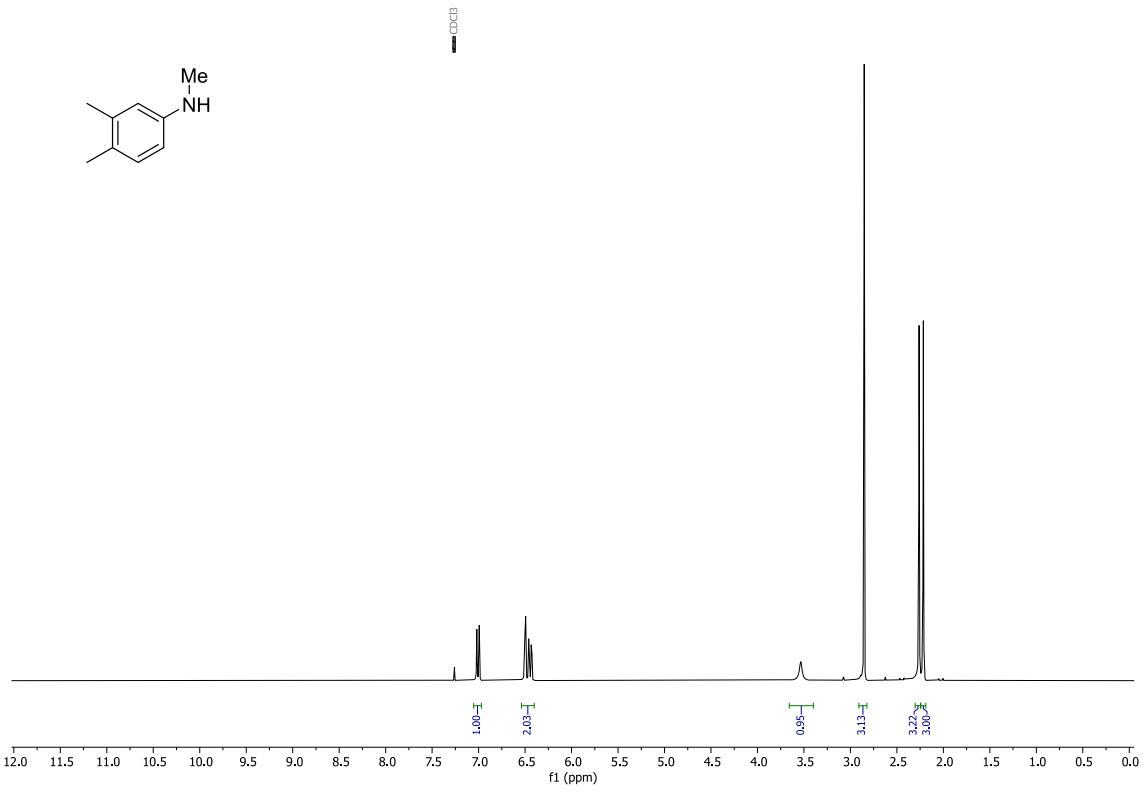

Figure 9.8 ^{1}H-NMR spectrum (300 MHz, chloroform-d) of **82**.

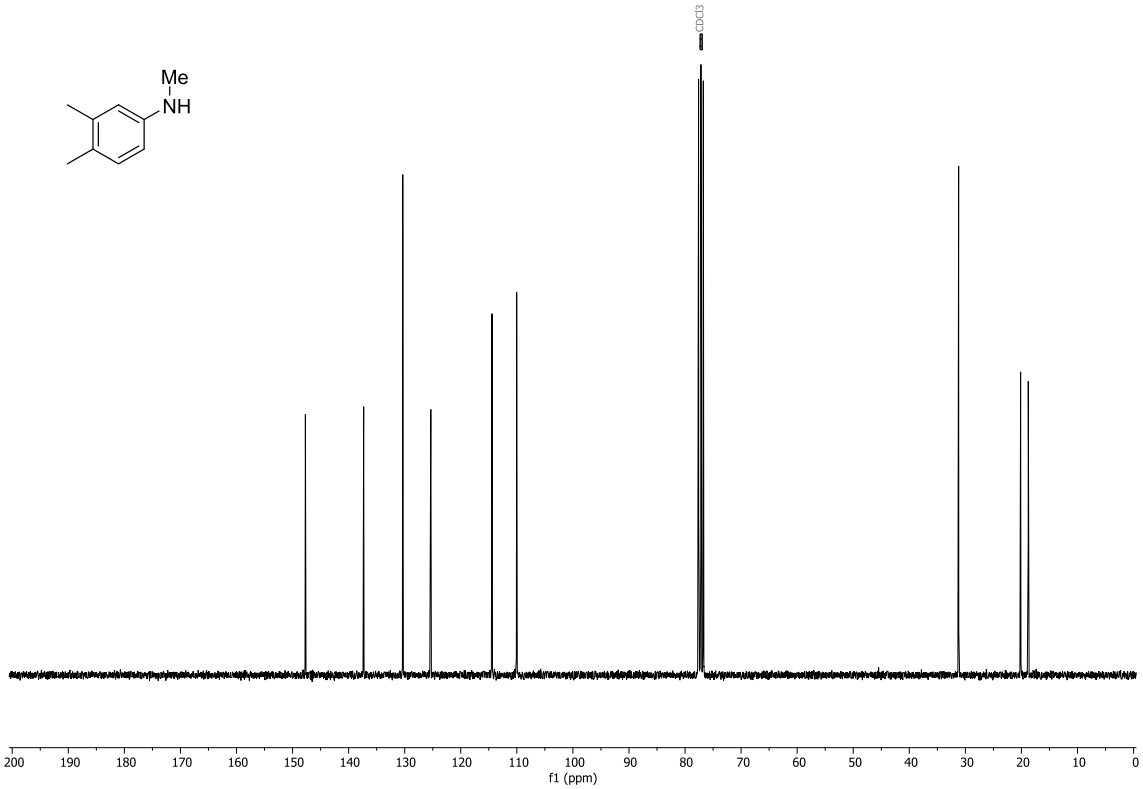

Figure 9.9 $^{13}C\{^{1}H\}$-NMR spectrum (75 MHz, chloroform-*d*) of **82**.

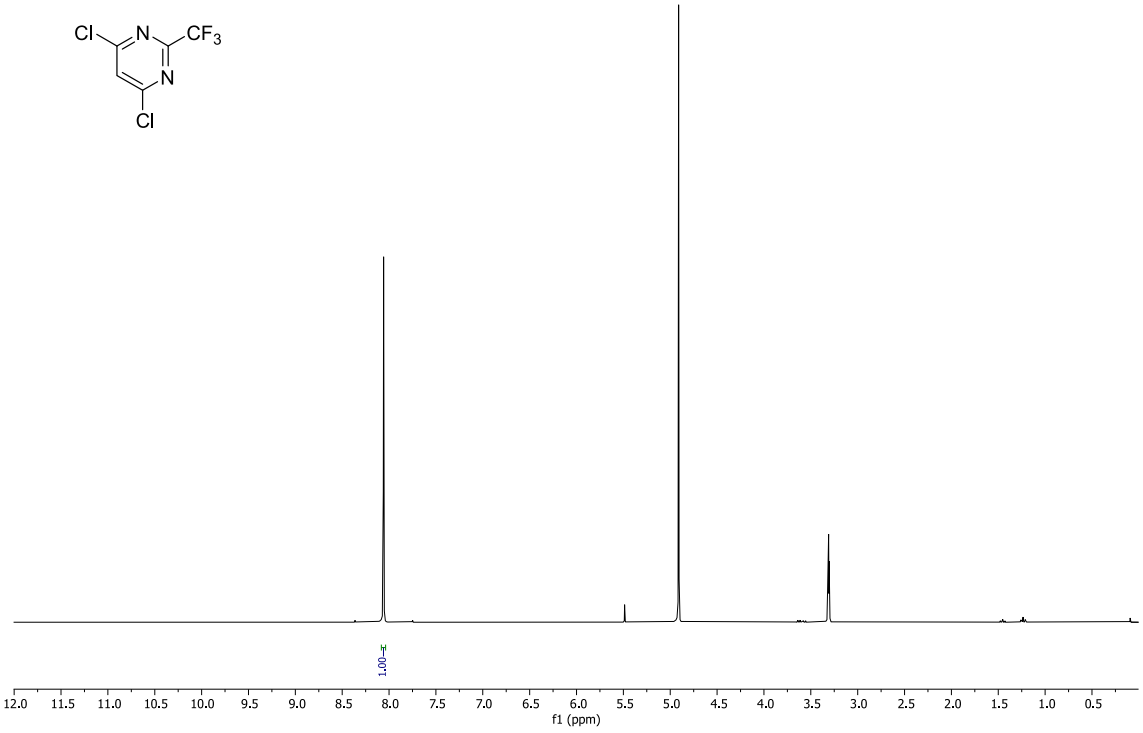

Figure 9.10 ^{1}H-NMR spectrum (300 MHz, methanol-d_4) of **90**.

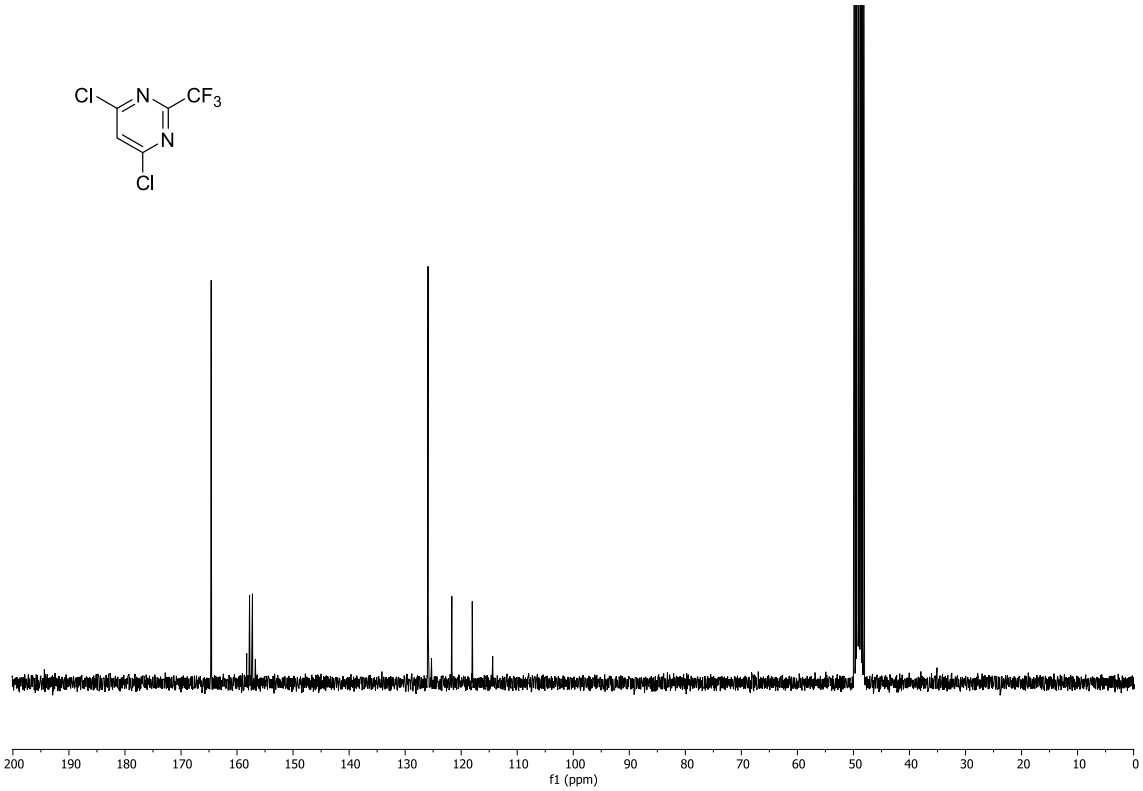

Figure 9.11 $^{13}C\{^{1}H\}$-NMR spectrum (75 MHz, methanol-d_4) of **90**.

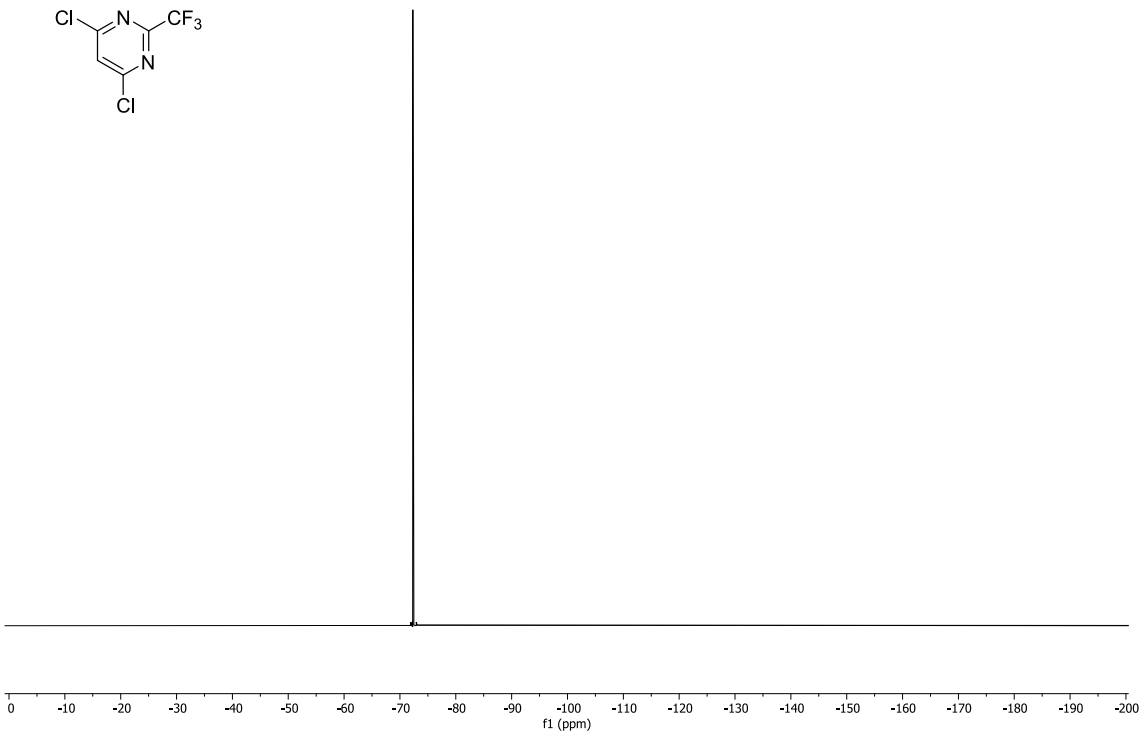

Figure 9.12 $^{19}F\{^{1}H\}$-NMR spectrum (282 MHz, methanol-d_4) of **90**.

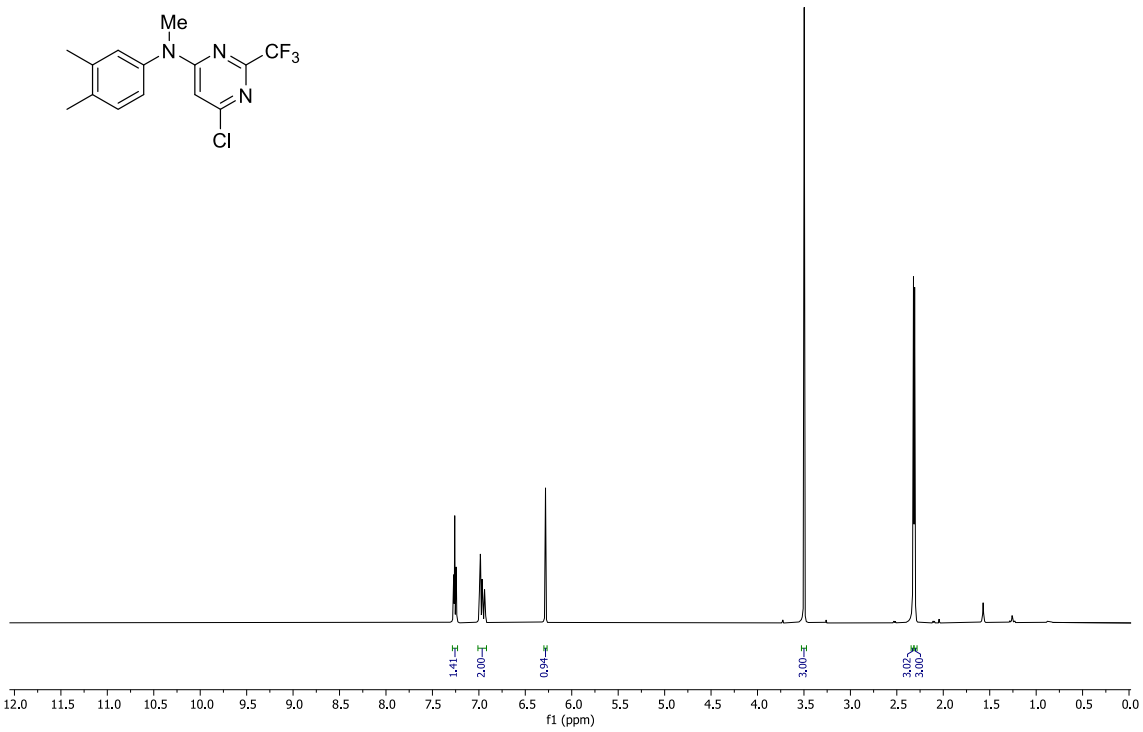

Figure 9.13 ^{1}H-NMR spectrum (300 MHz, chloroform-*d*) of **91**.

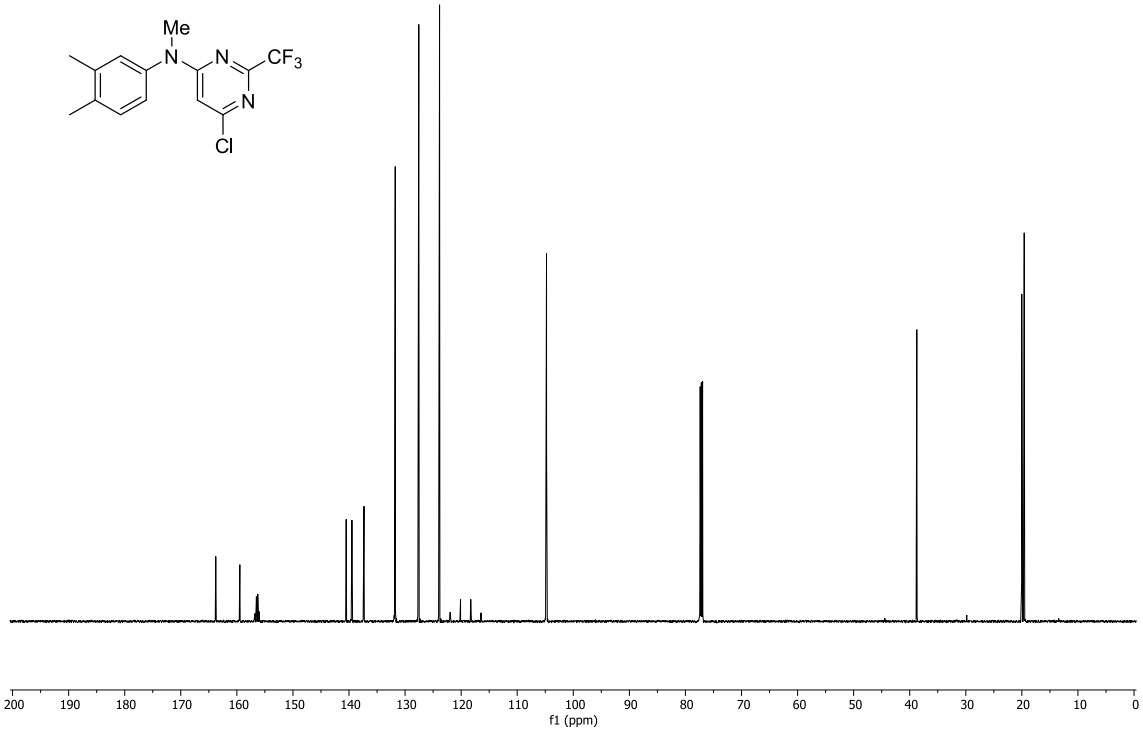

Figure 9.14 ^{13}C{^{1}H}-NMR spectrum (151 MHz, chloroform-*d*) of **91**.

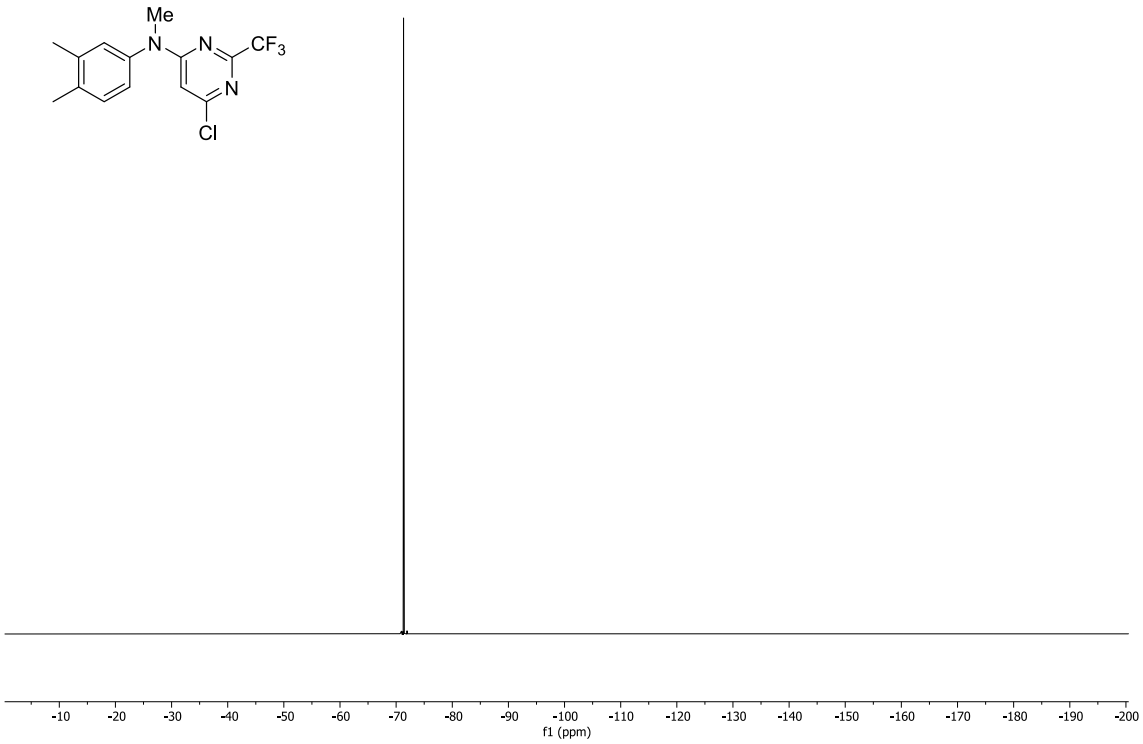

Figure 9.15 $^{19}F\{^{1}H\}$-NMR spectrum (282 MHz, chloroform-*d*) of **91**.

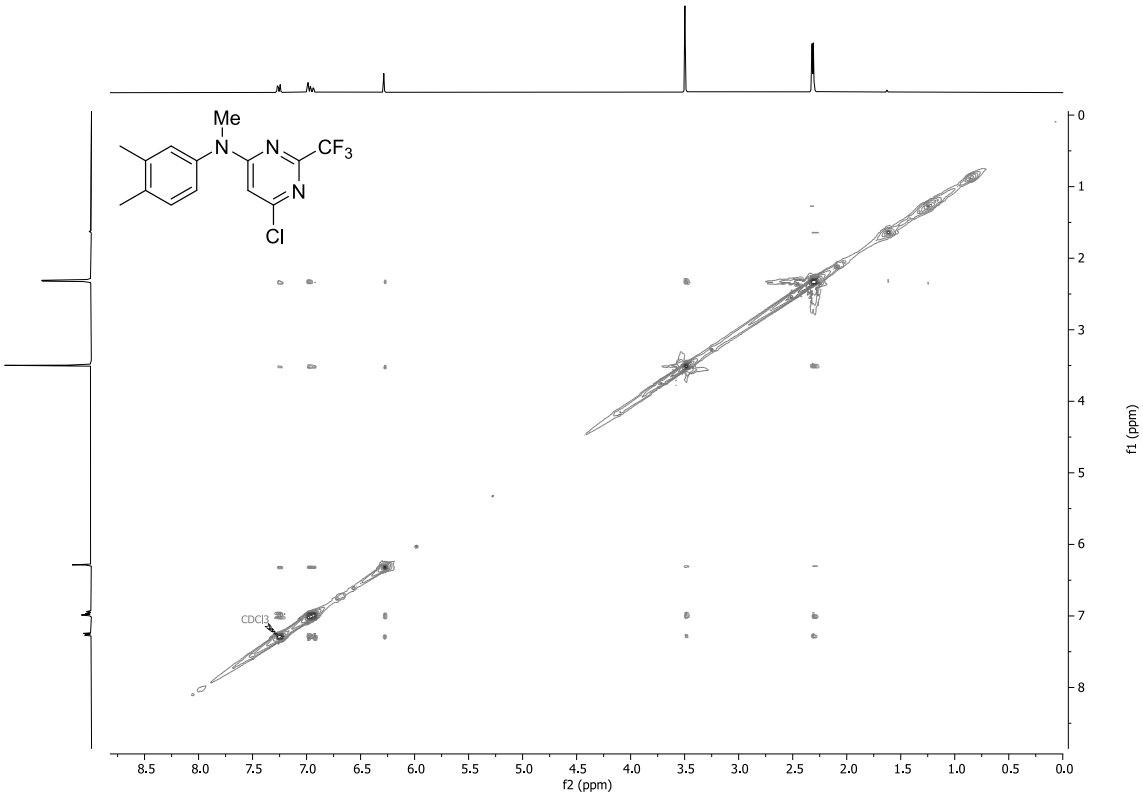

Figure 9.16 NOESY spectrum (300 MHz, chloroform-*d*) of **91**.

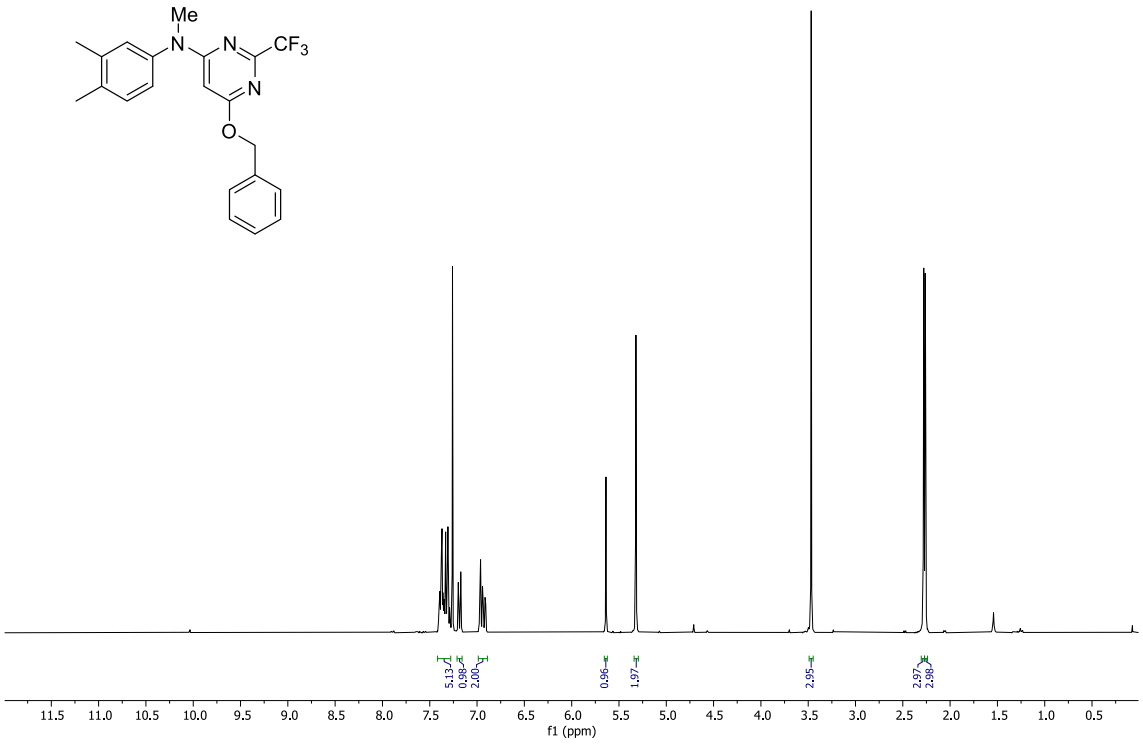

Figure 9.17 ^{1}H-NMR spectrum (300 MHz, chloroform-*d*) of **92**.

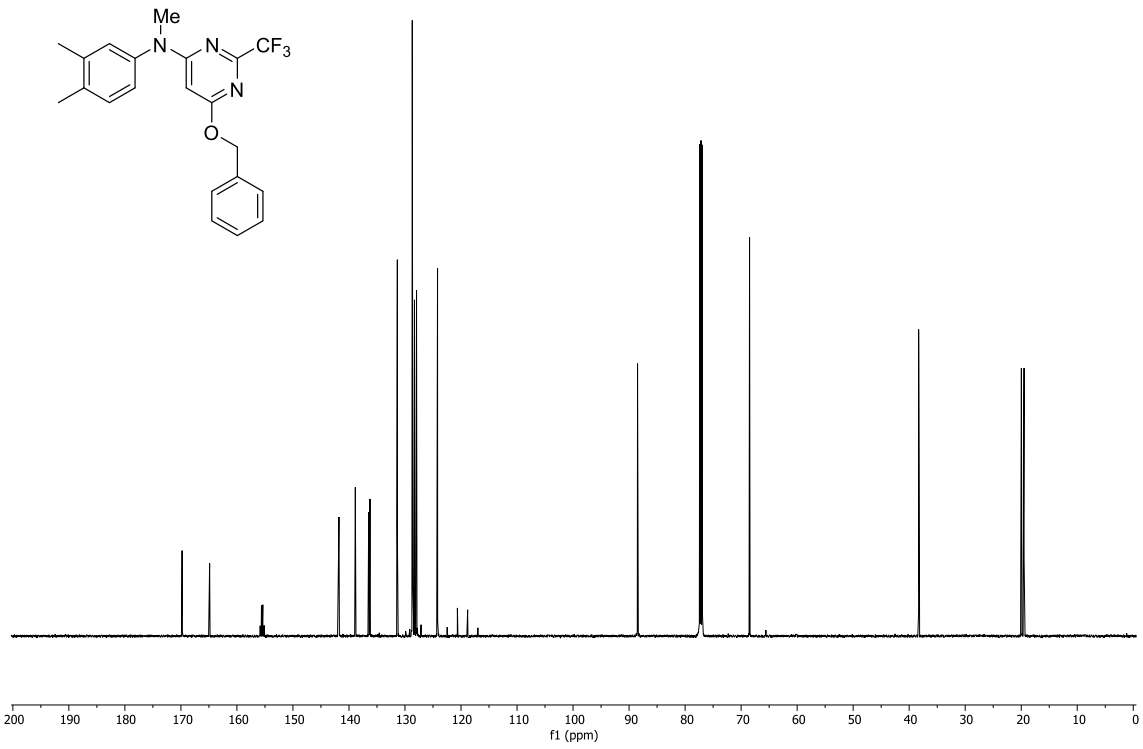

Figure 9.18 ^{13}C{^{1}H}-NMR spectrum (151 MHz, chloroform-*d*) of **92**.

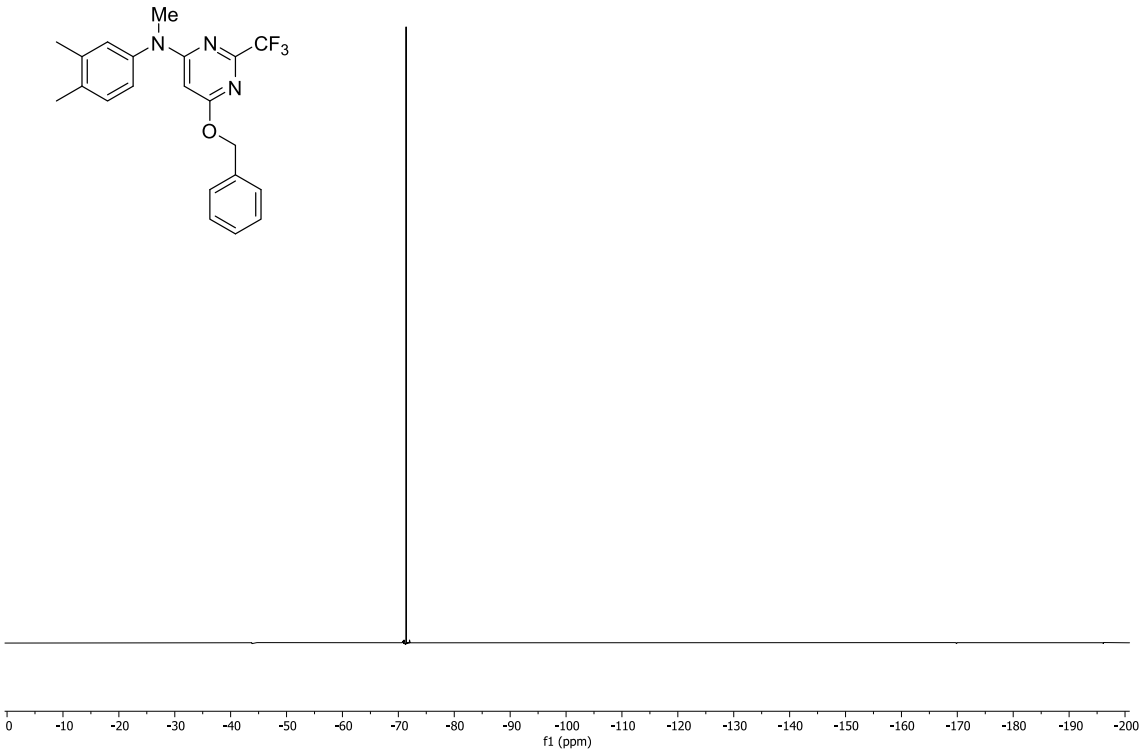

Figure 9.19 $^{19}F\{^{1}H\}$-NMR spectrum (282 MHz, chloroform-*d*) of **92**.

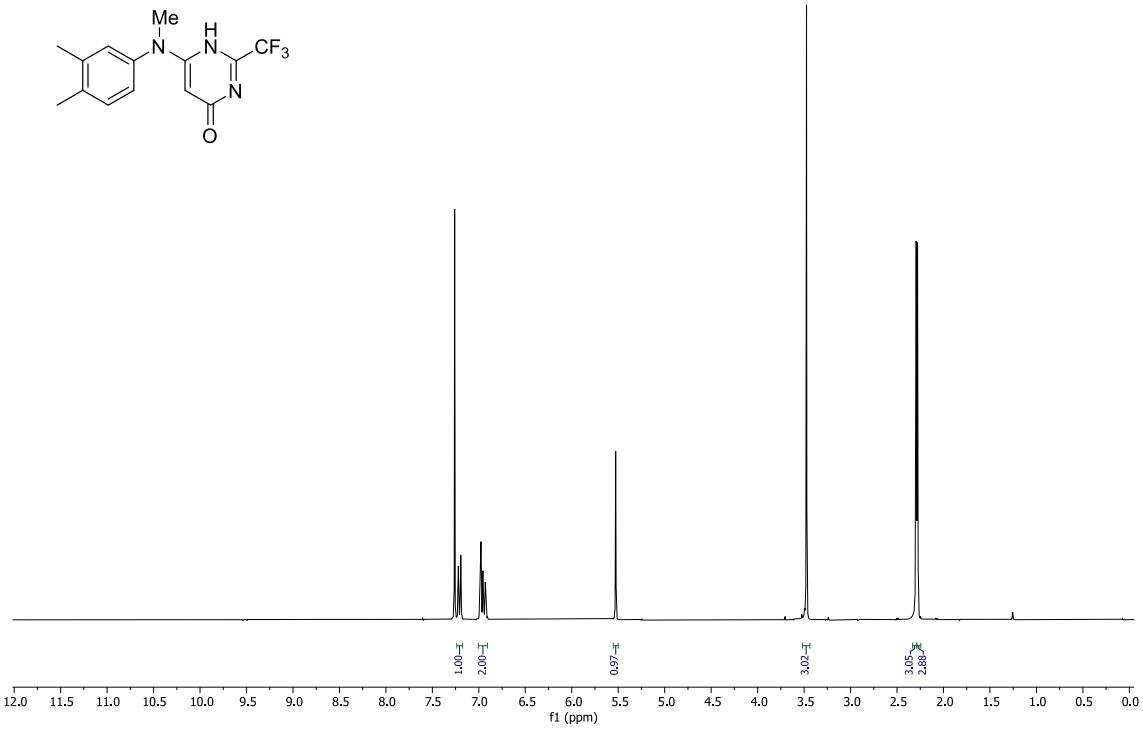

Figure 9.20 ^{1}H-NMR spectrum (300 MHz, chloroform-*d*) of **93**.

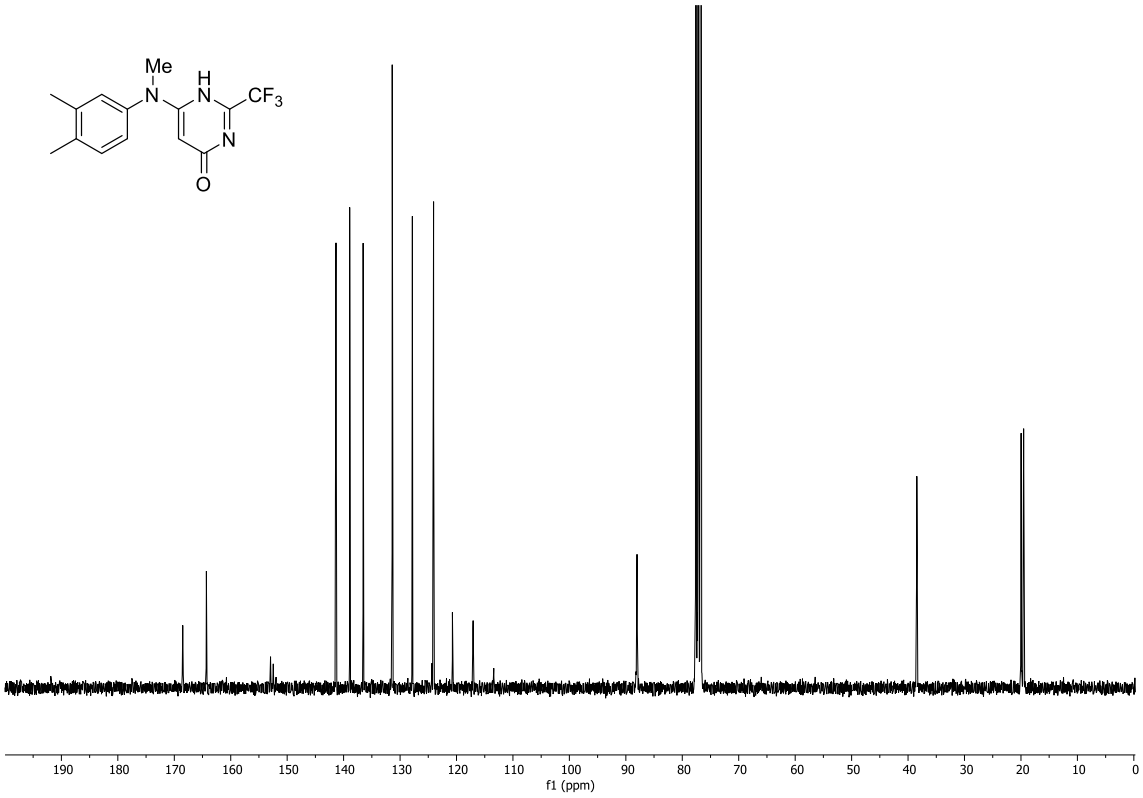

Figure 9.21 $^{13}C\{^{1}H\}$-NMR spectrum (75 MHz, chloroform-*d*) of **93**.

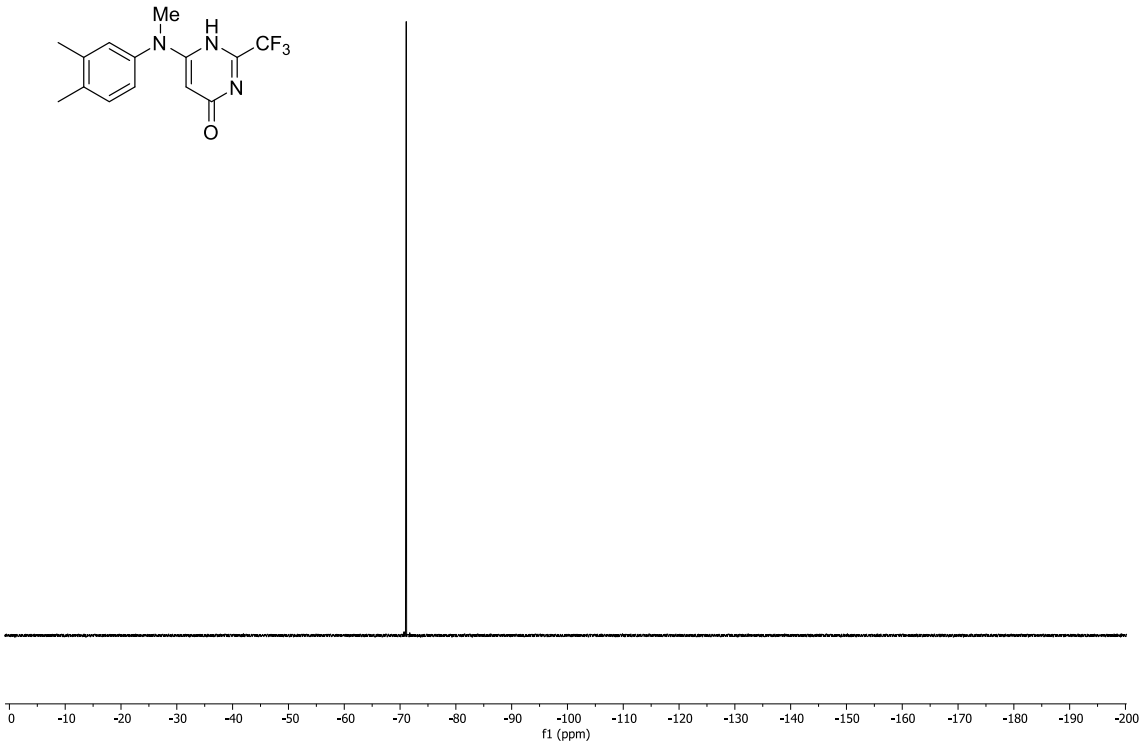

Figure 9.22 $^{19}F\{^{1}H\}$-NMR spectrum (282 MHz, chloroform-*d*) of **93**.

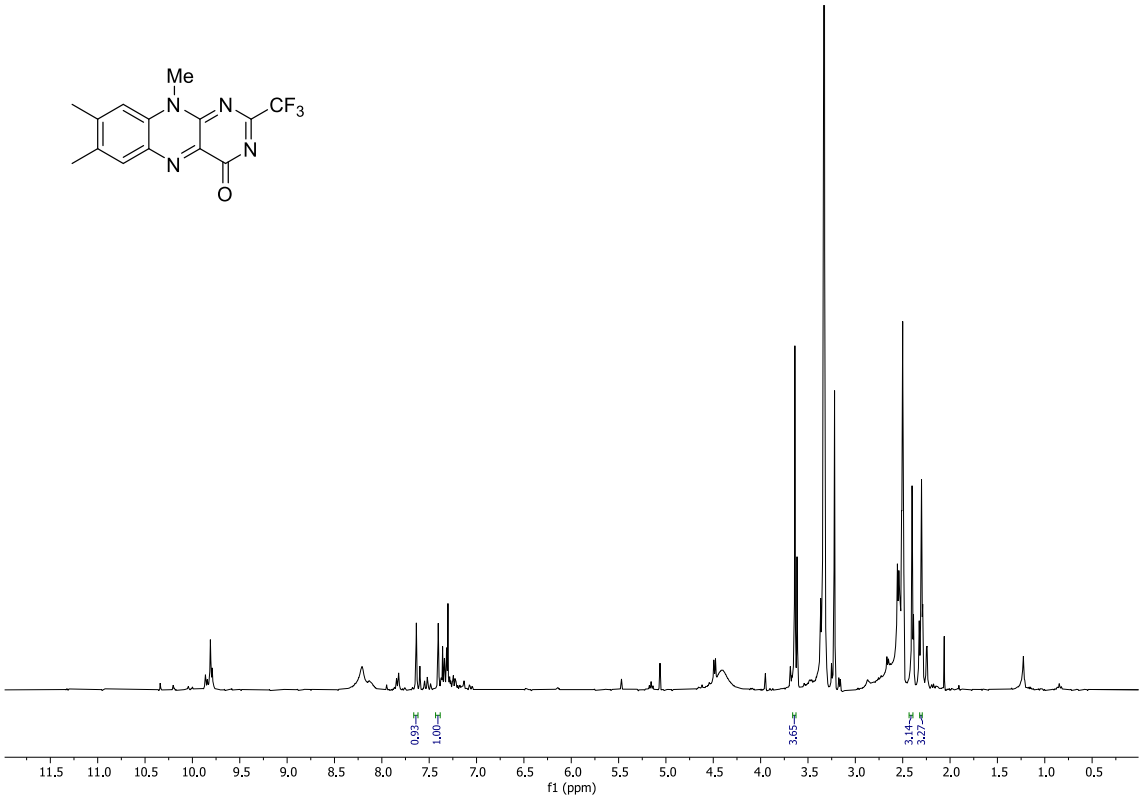

Figure 9.23 ^{1}H-NMR spectrum (300 MHz, DMSO-d_6) of **75**.

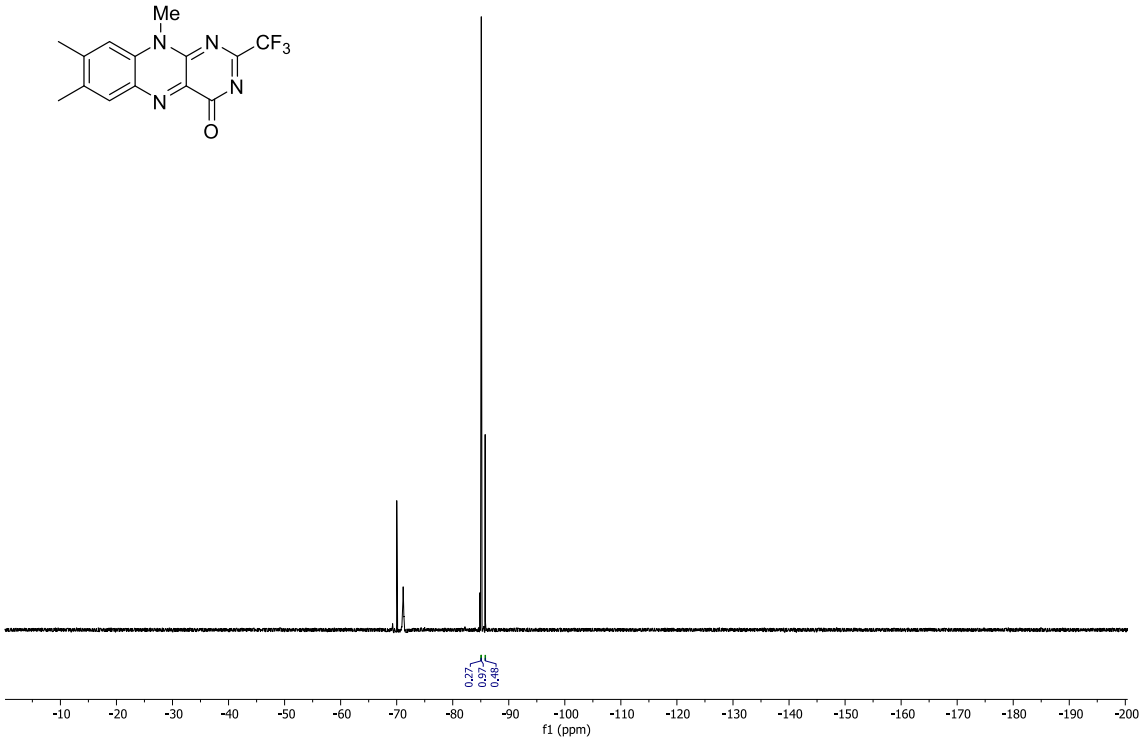

Figure 9.24 ^{19}F{^{1}H}-NMR spectrum (282 MHz, DMSO-d_6) of **75**.

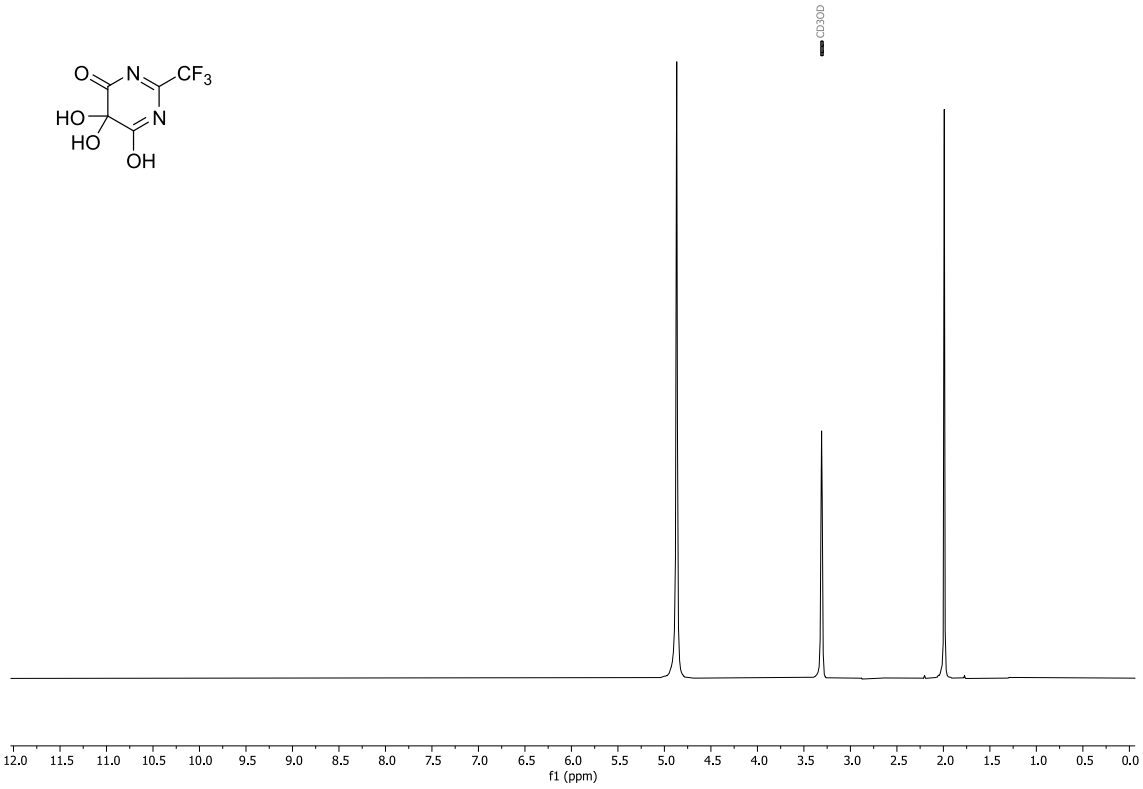

Figure 9.25 ^{1}H-NMR spectrum (300 MHz, methanol-d_4) of **72**.

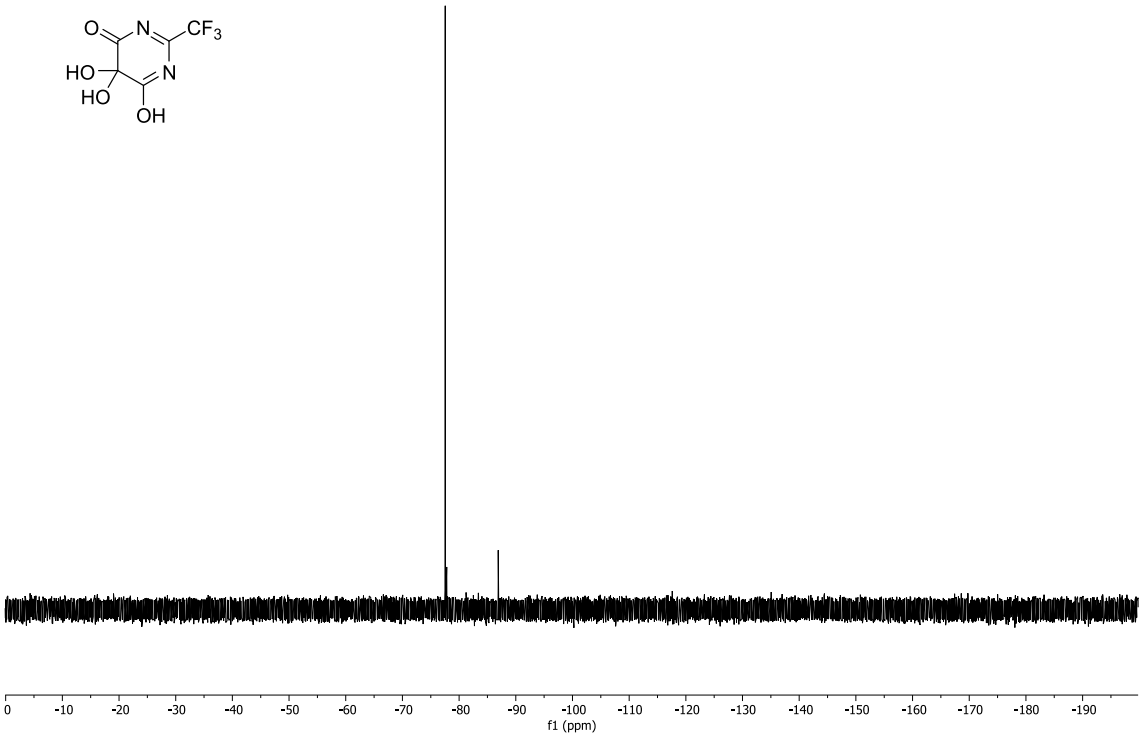

Figure 9.26 ^{19}F{^{1}H}-NMR spectrum (282 MHz, methanol-d_4) of **72**.

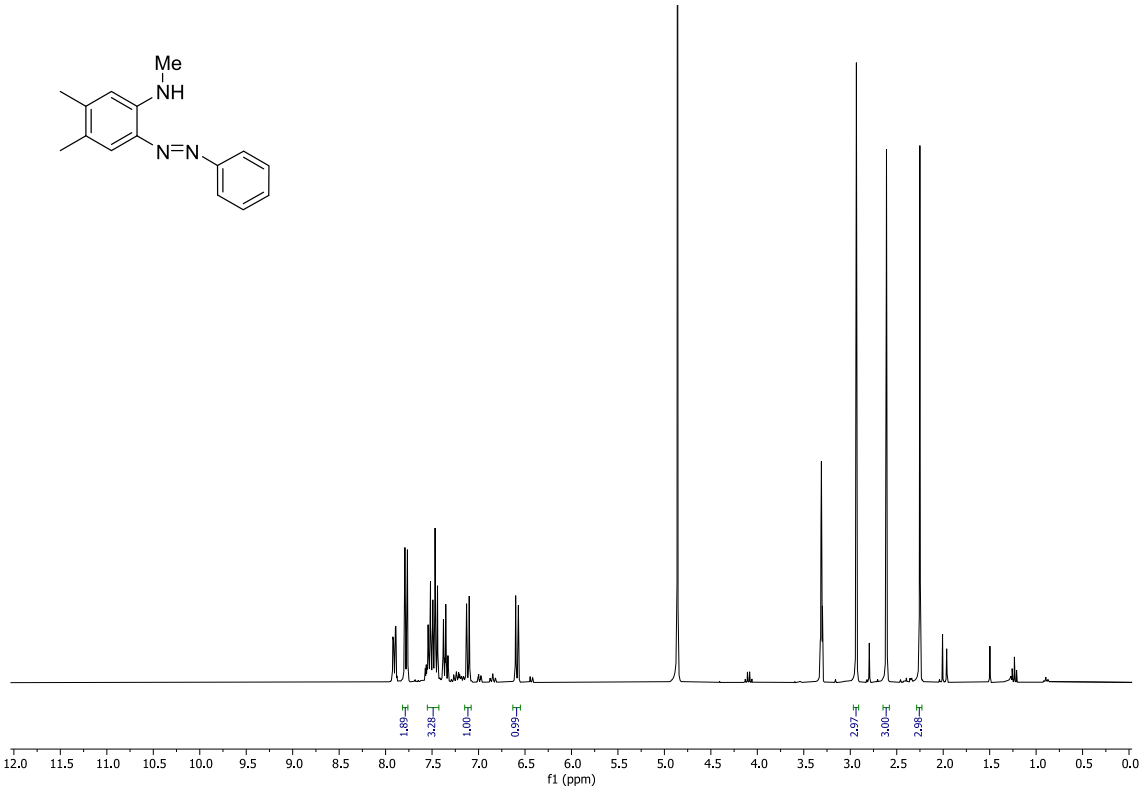

Figure 9.27 ^{1}H-NMR spectrum (300 MHz, methanol-d_4) of **85**.

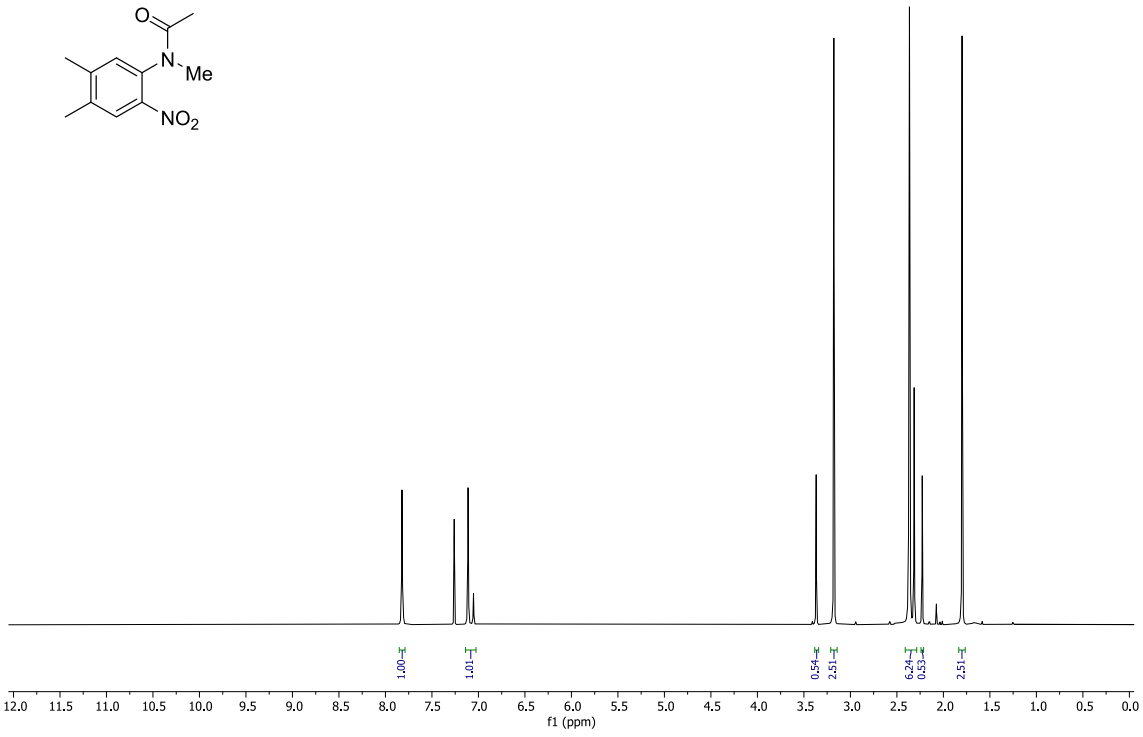

Figure 9.28 ^{1}H-NMR spectrum (300 MHz, chloroform-d) of **86**.

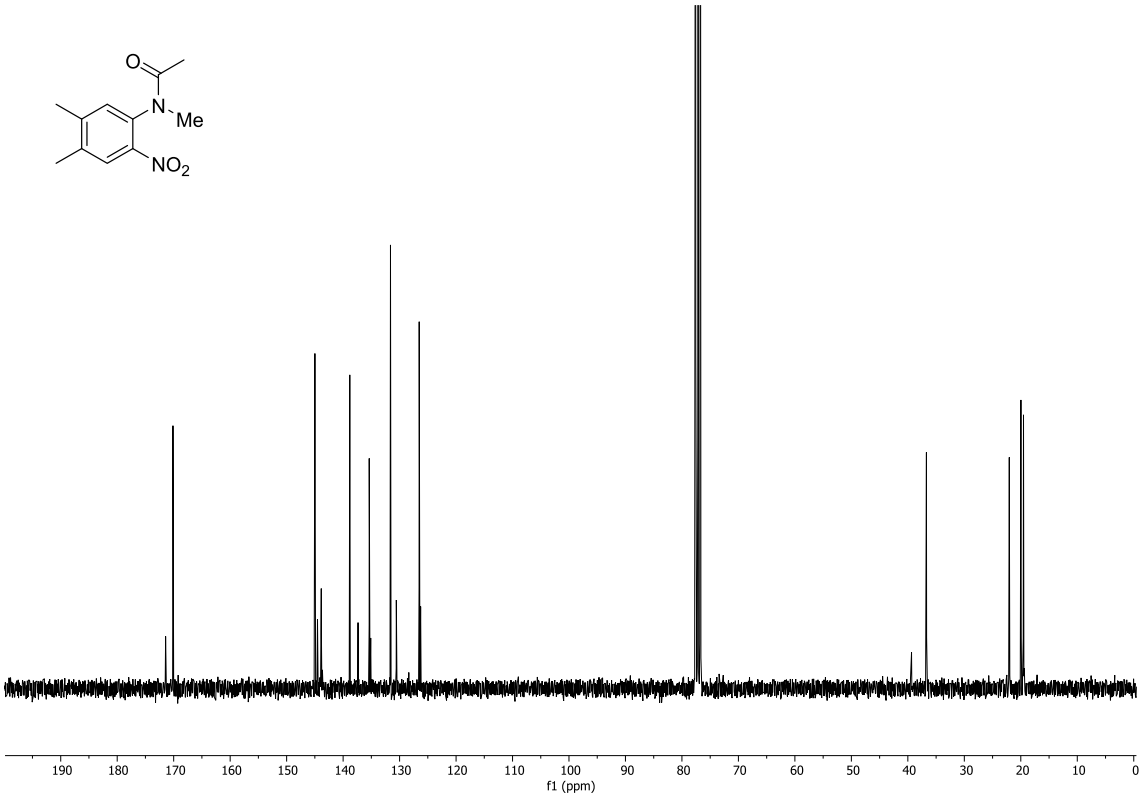

Figure 9.29 $^{13}C\{^{1}H\}$-NMR spectrum (75 MHz, chloroform-*d*) of **86**.

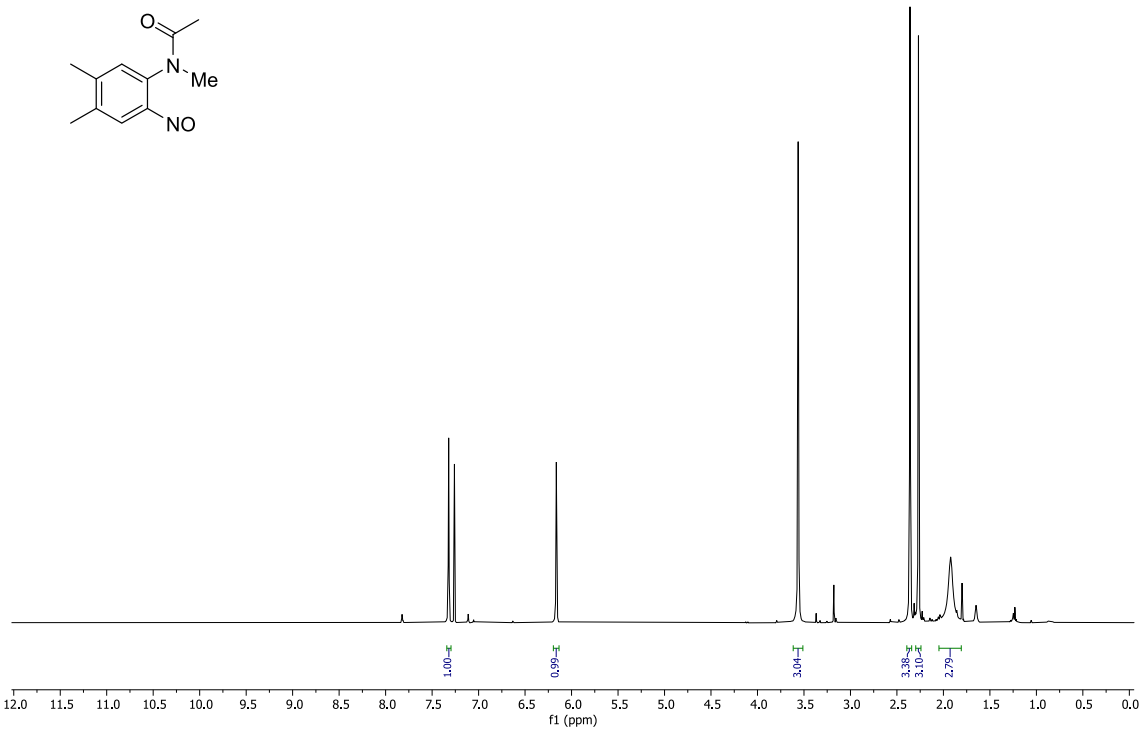

Figure 9.30 ^{1}H-NMR spectrum (300 MHz, chloroform-*d*) of **87**.

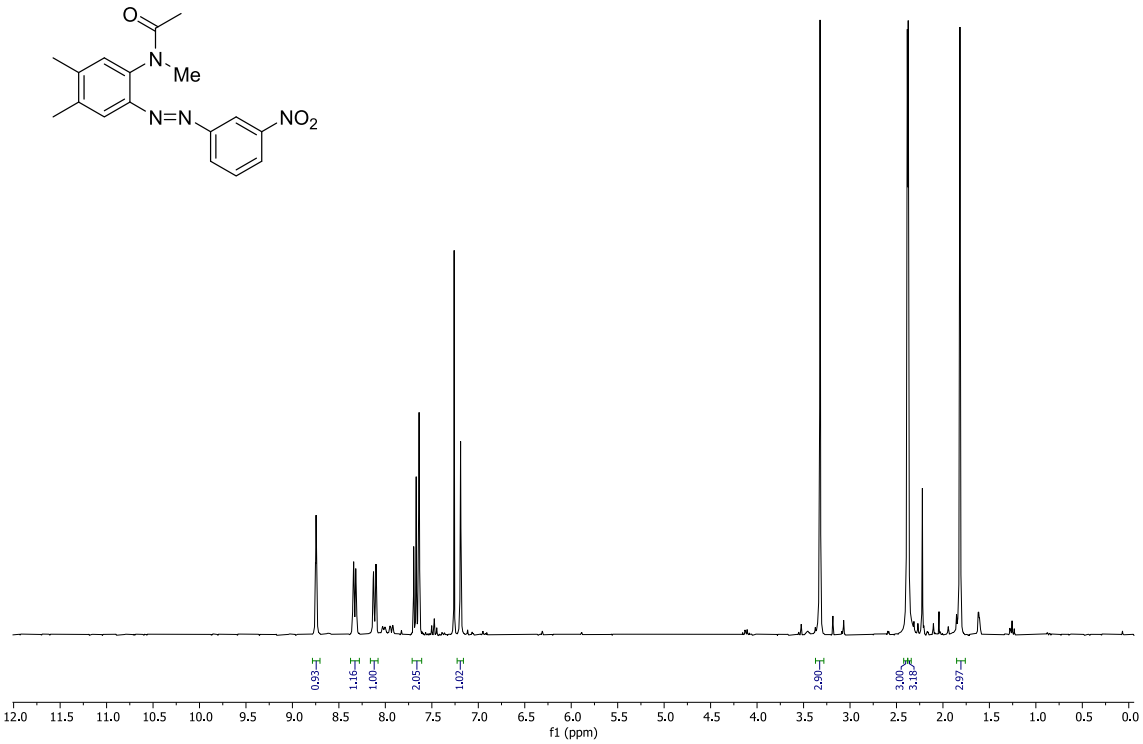

Figure 9.31 ^{1}H-NMR spectrum (300 MHz, chloroform-*d*) of **88**.

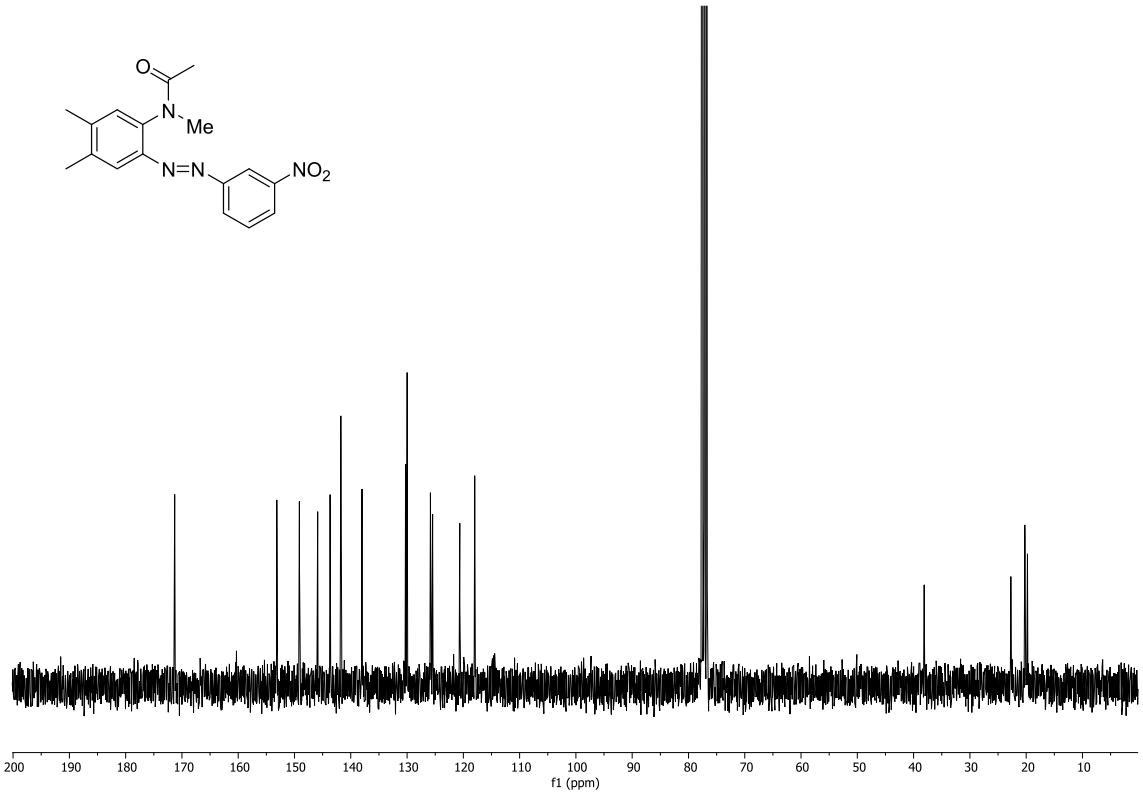

Figure 9.32 ^{13}C{^{1}H}-NMR spectrum (75 MHz, chloroform-*d*) of **88**.

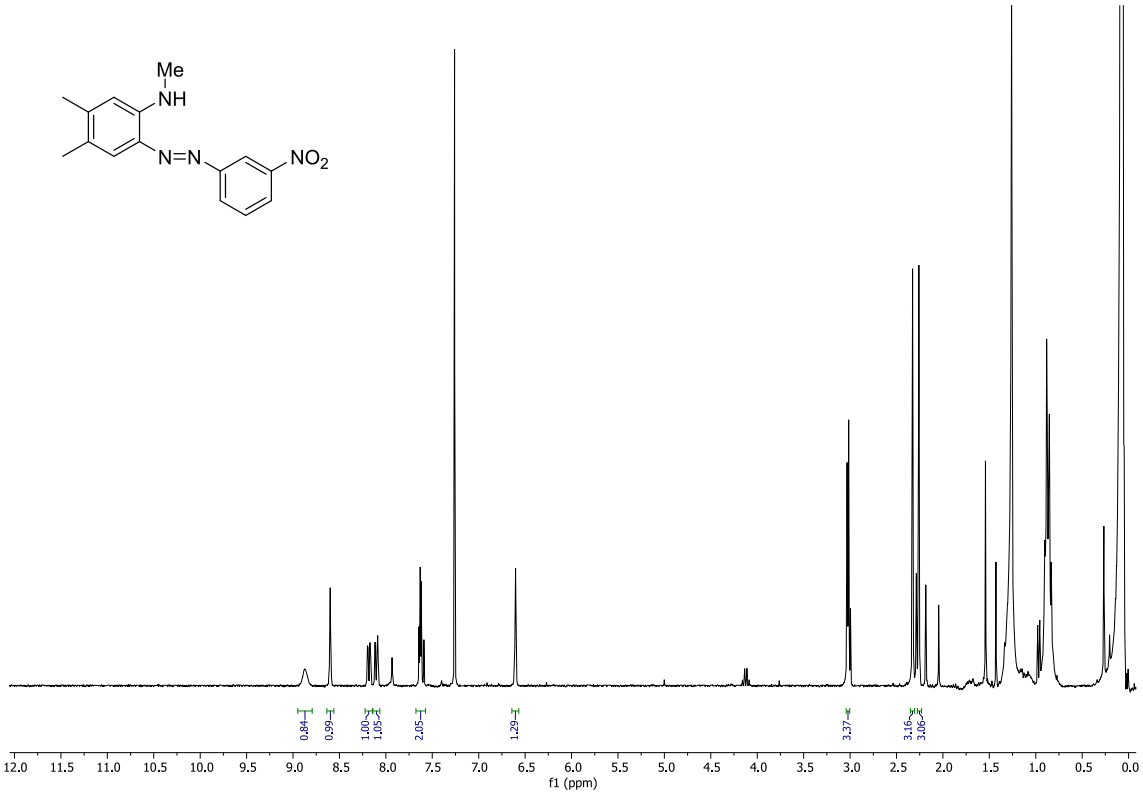

Figure 9.33 ^{1}H-NMR spectrum (300 MHz, chloroform-*d*) of **89**.

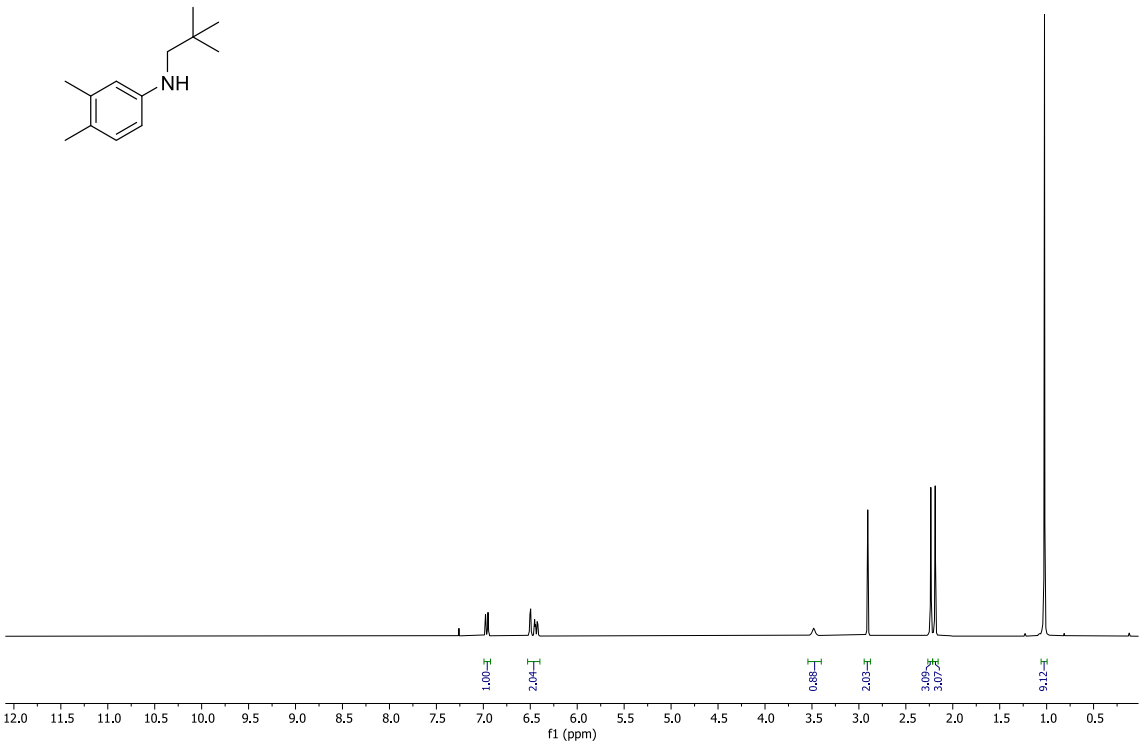

Figure 9.34 ^{1}H-NMR spectrum (300 MHz, chloroform-*d*) of **95**.

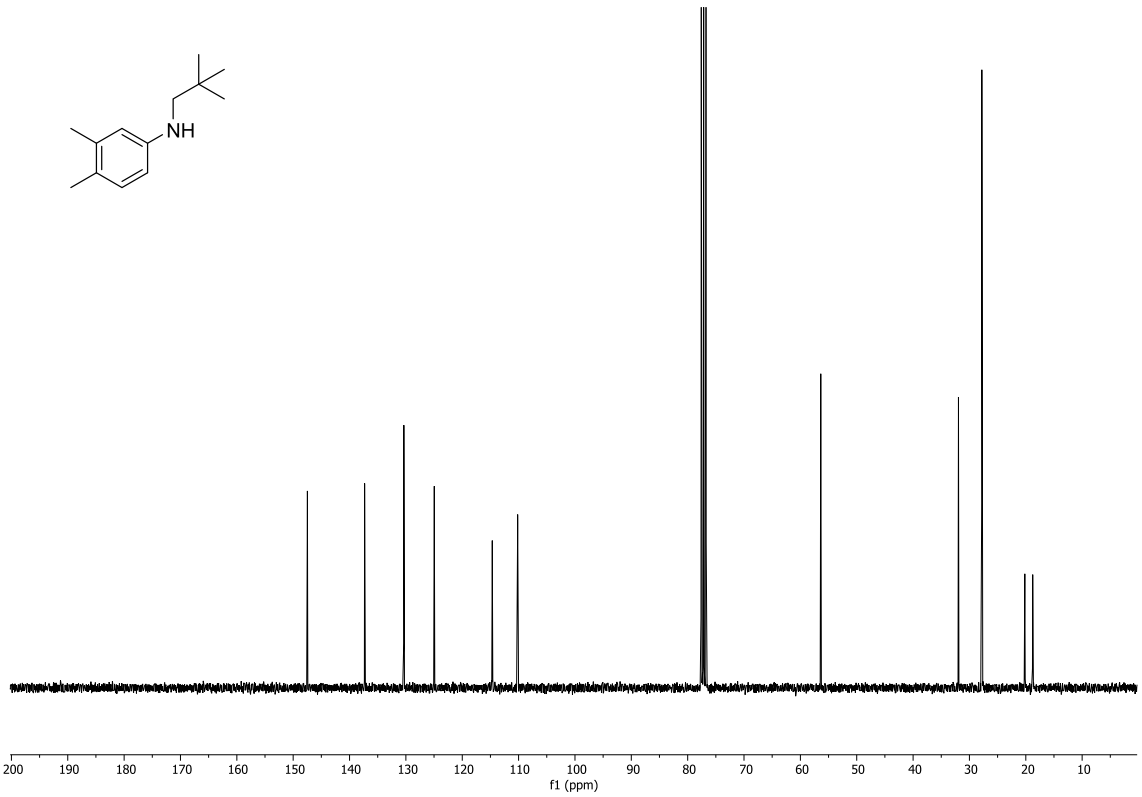

Figure 9.35 $^{13}C\{^{1}H\}$-NMR spectrum (75 MHz, chloroform-*d*) of **95**.

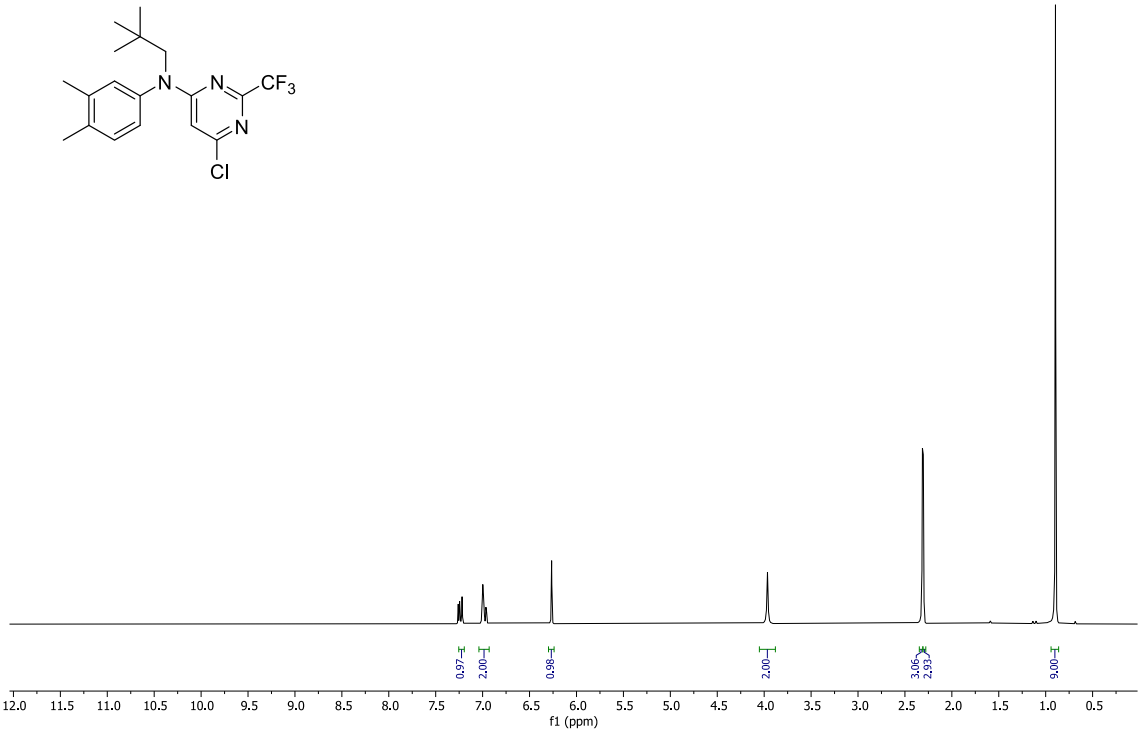

Figure 9.36 ^{1}H-NMR spectrum (300 MHz, chloroform-*d*) of **96**.

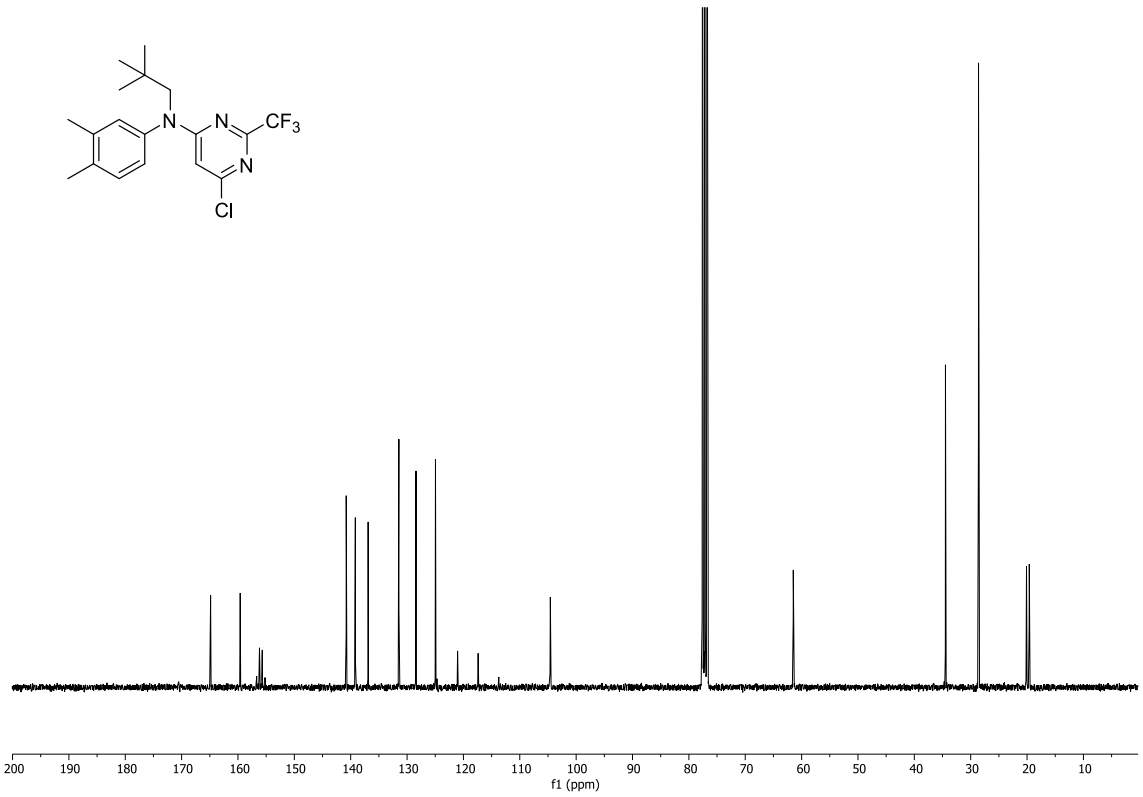

Figure 9.37 $^{13}C\{^{1}H\}$-NMR spectrum (75 MHz, chloroform-*d*) of **96**.

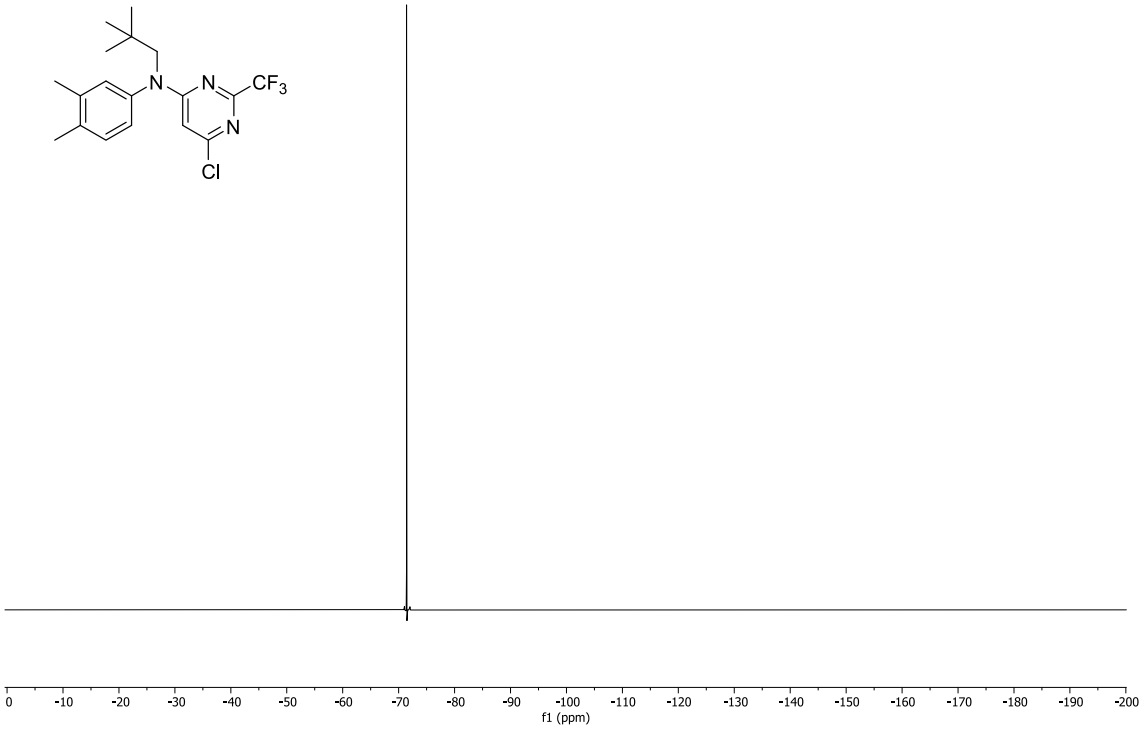

Figure 9.38 $^{19}F\{^{1}H\}$-NMR spectrum (282 MHz, chloroform-*d*) of **96**.

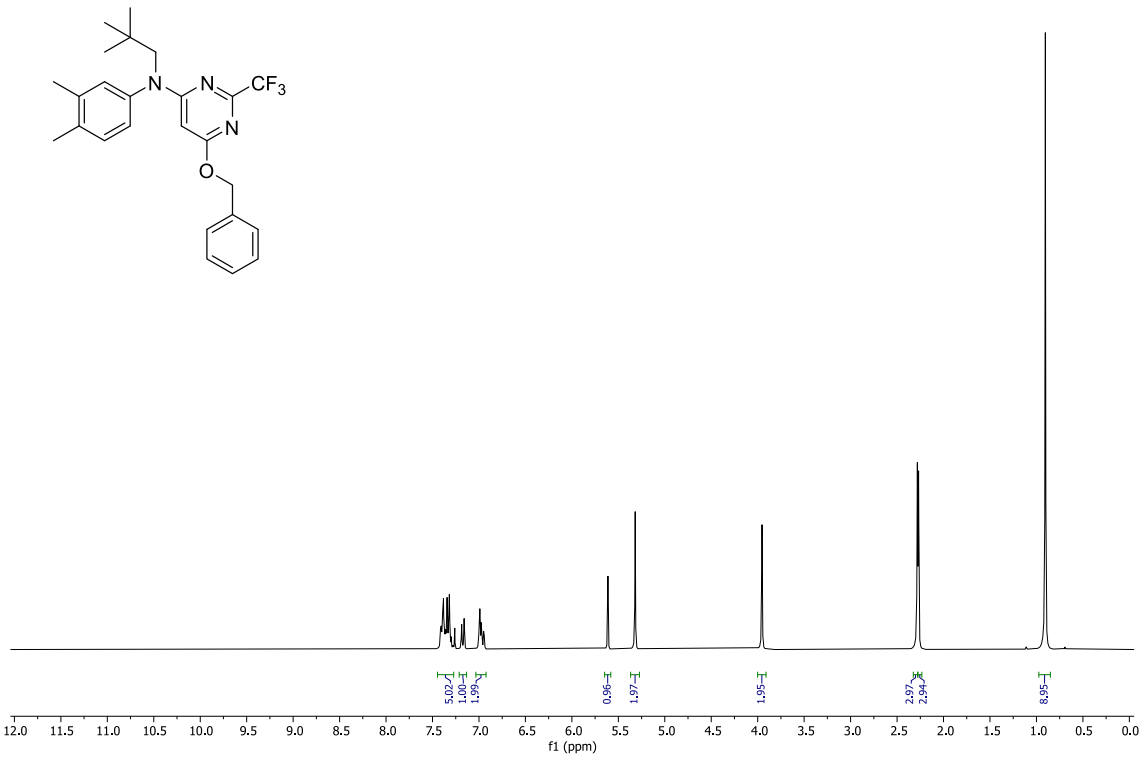

Figure 9.39 ^{1}H-NMR spectrum (300 MHz, chloroform-*d*) of **97**.

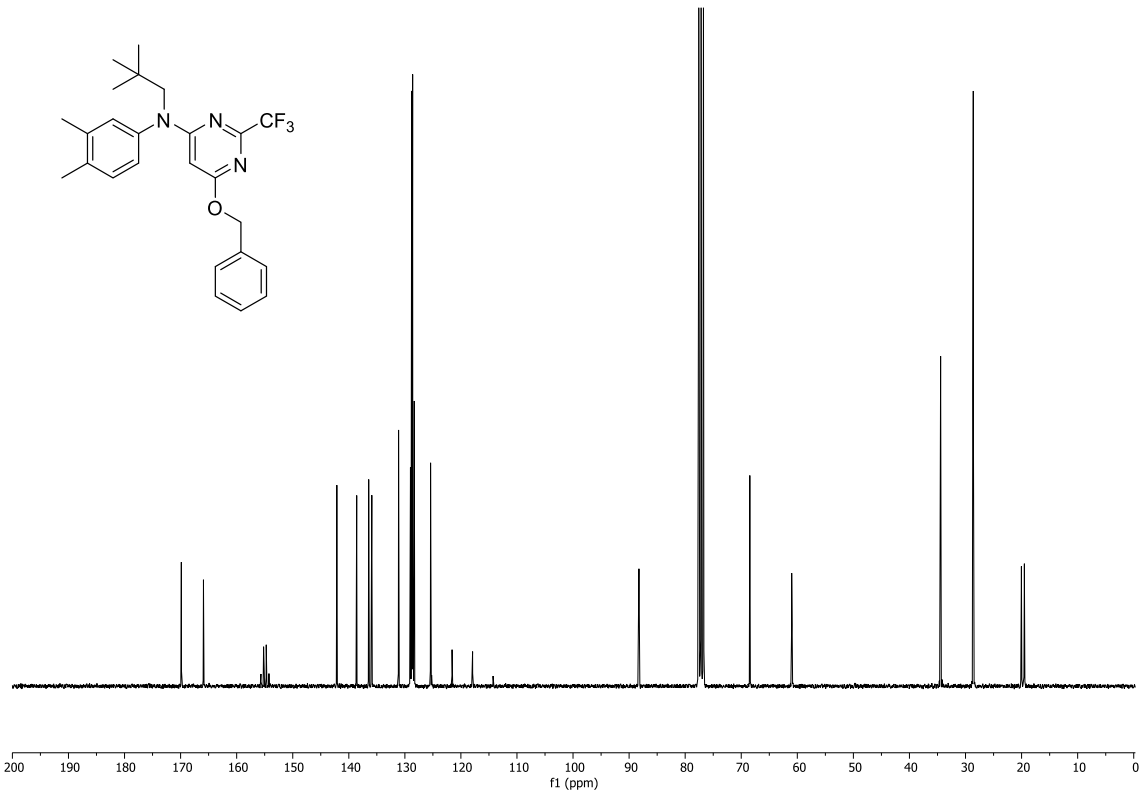

Figure 9.40 ^{13}C{^{1}H}-NMR spectrum (75 MHz, chloroform-*d*) of **97**.

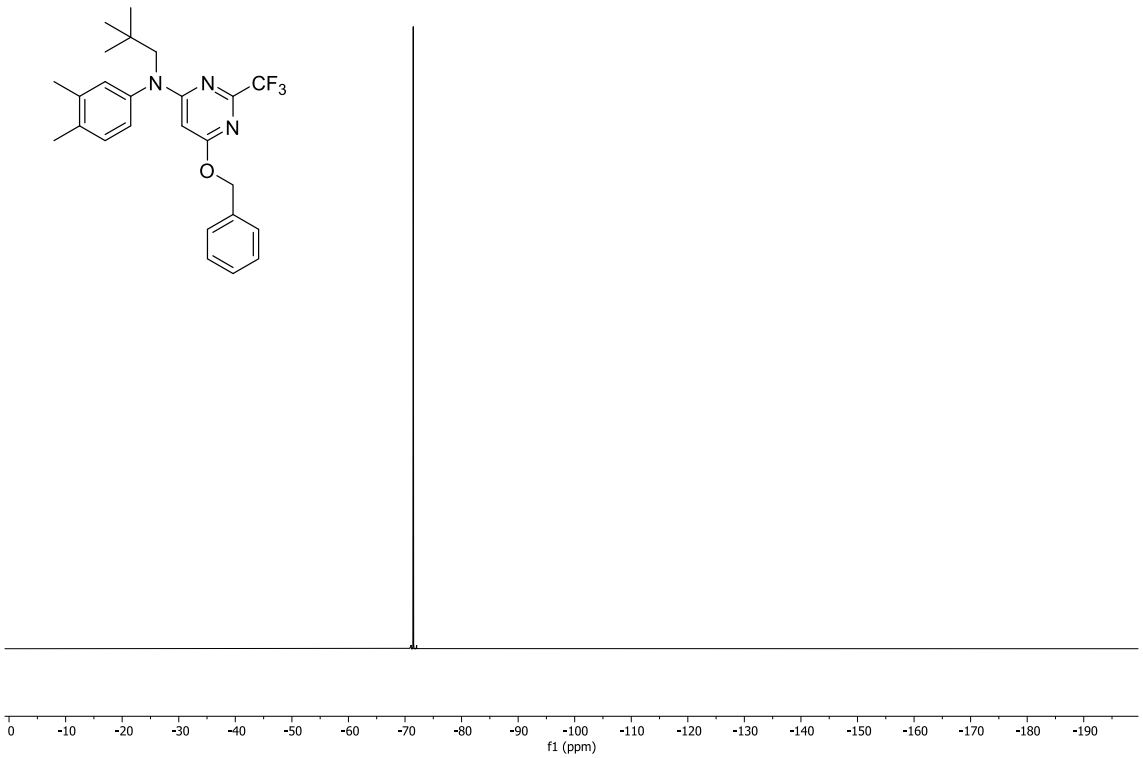

Figure 9.41 $^{19}F\{^{1}H\}$-NMR spectrum (282 MHz, chloroform-*d*) of **97**.

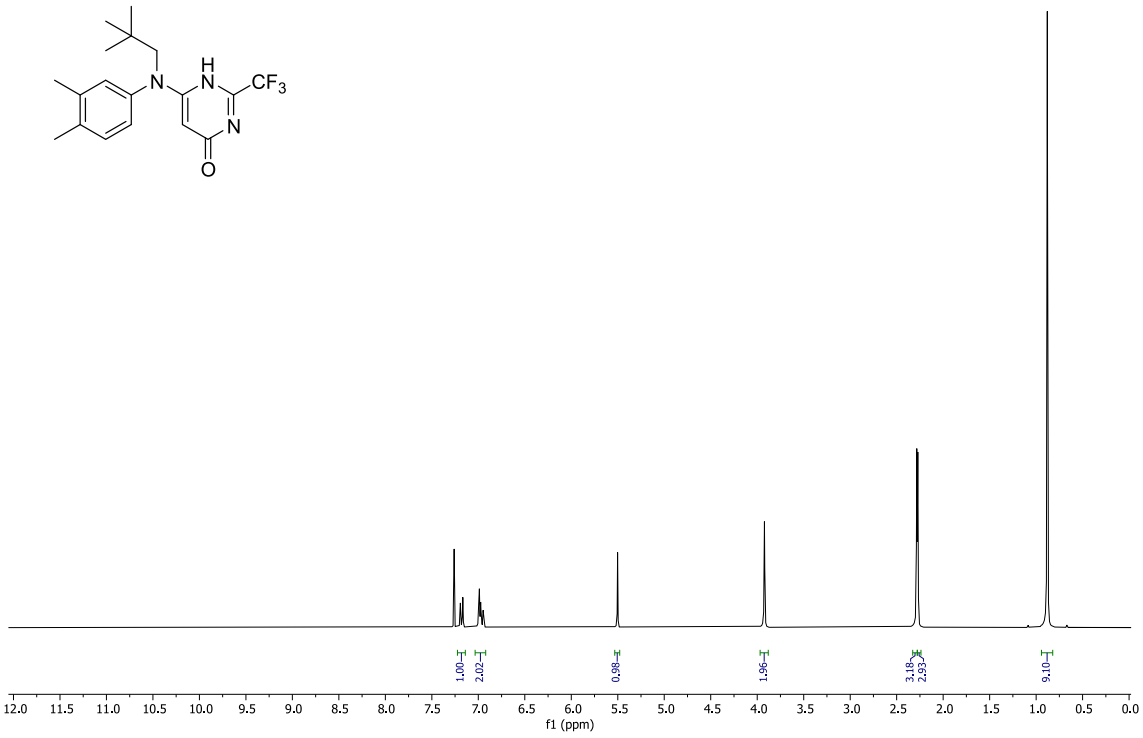

Figure 9.42 ^{1}H-NMR spectrum (300 MHz, chloroform-*d*) of **98**.

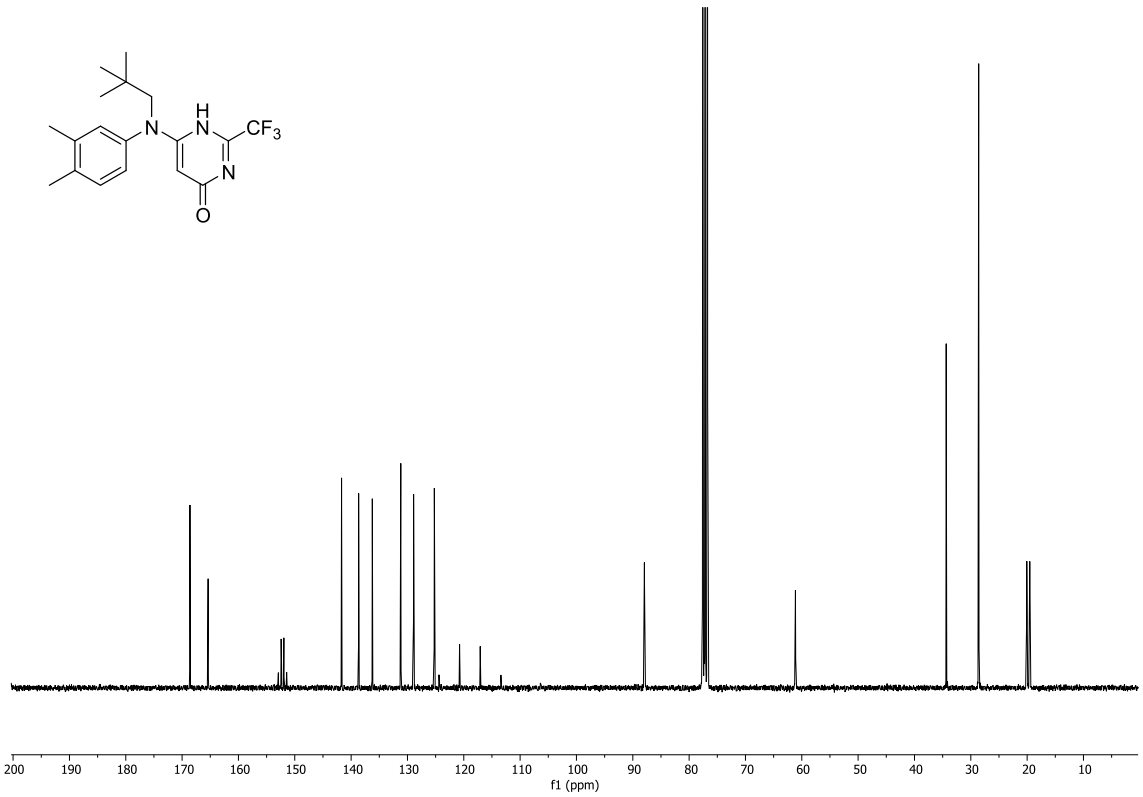

Figure 9.43 $^{13}C\{^{1}H\}$-NMR spectrum (75 MHz, chloroform-*d*) of **98**.

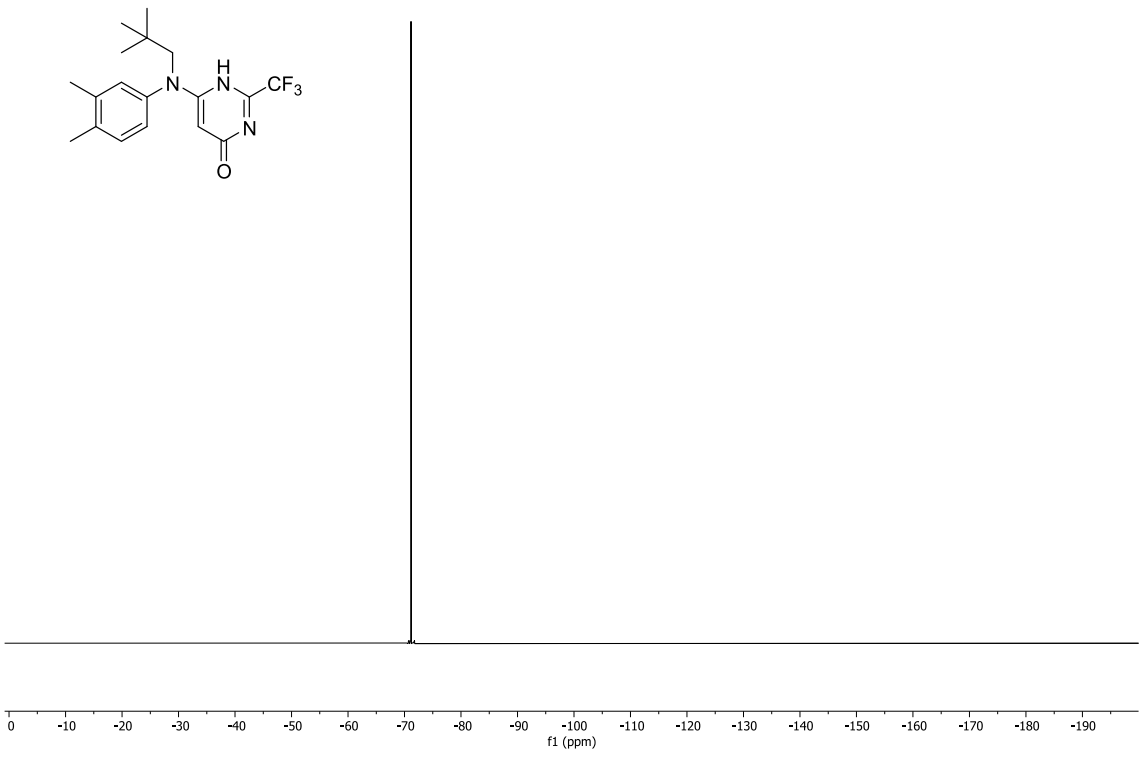

Figure 9.44 $^{19}F\{^{1}H\}$-NMR spectrum (282 MHz, chloroform-*d*) of **98**.

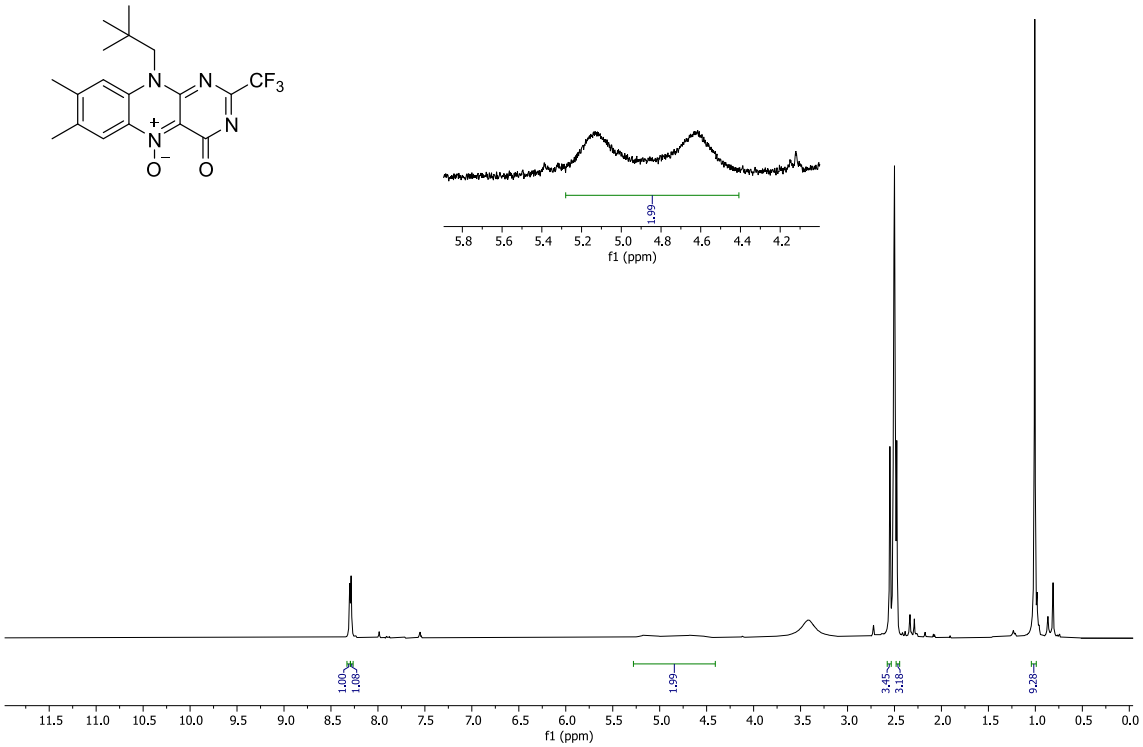

Figure 9.45 ^{1}H-NMR spectrum (300 MHz, DMSO-d_6) of **99**.

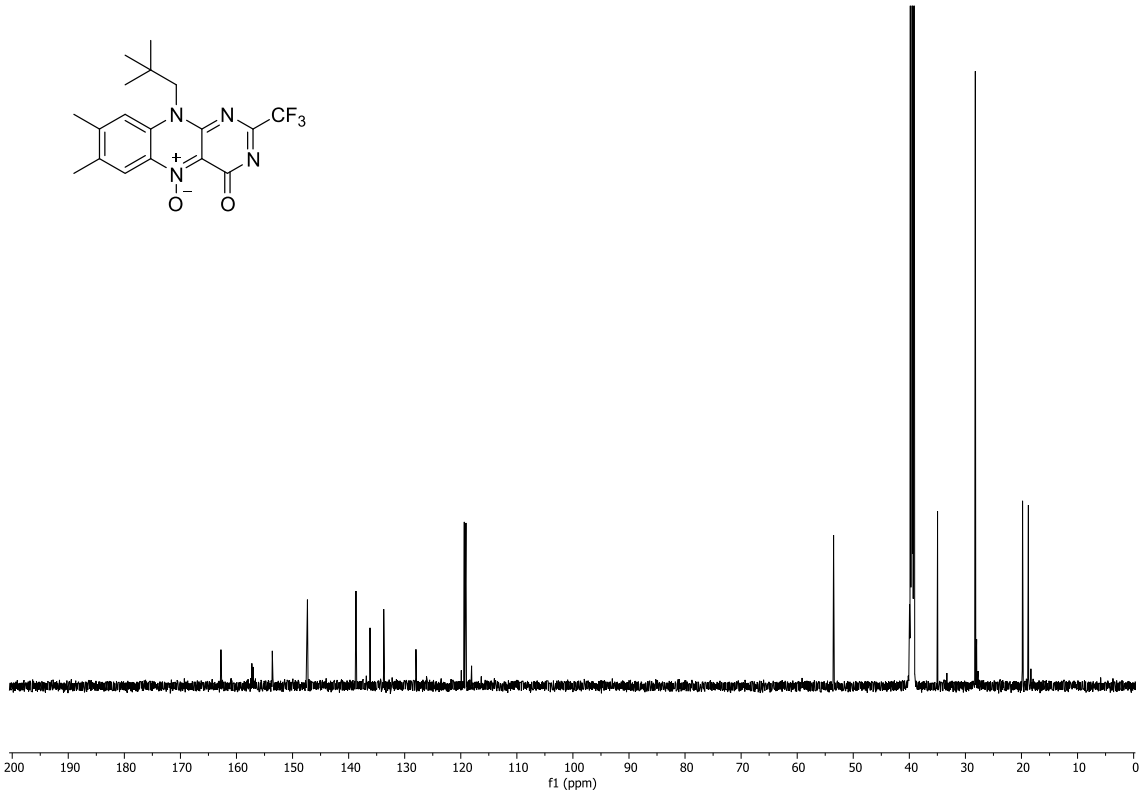

Figure 9.46 ^{13}C{^{1}H}-NMR spectrum (151 MHz, DMSO-d_6) of **99**.

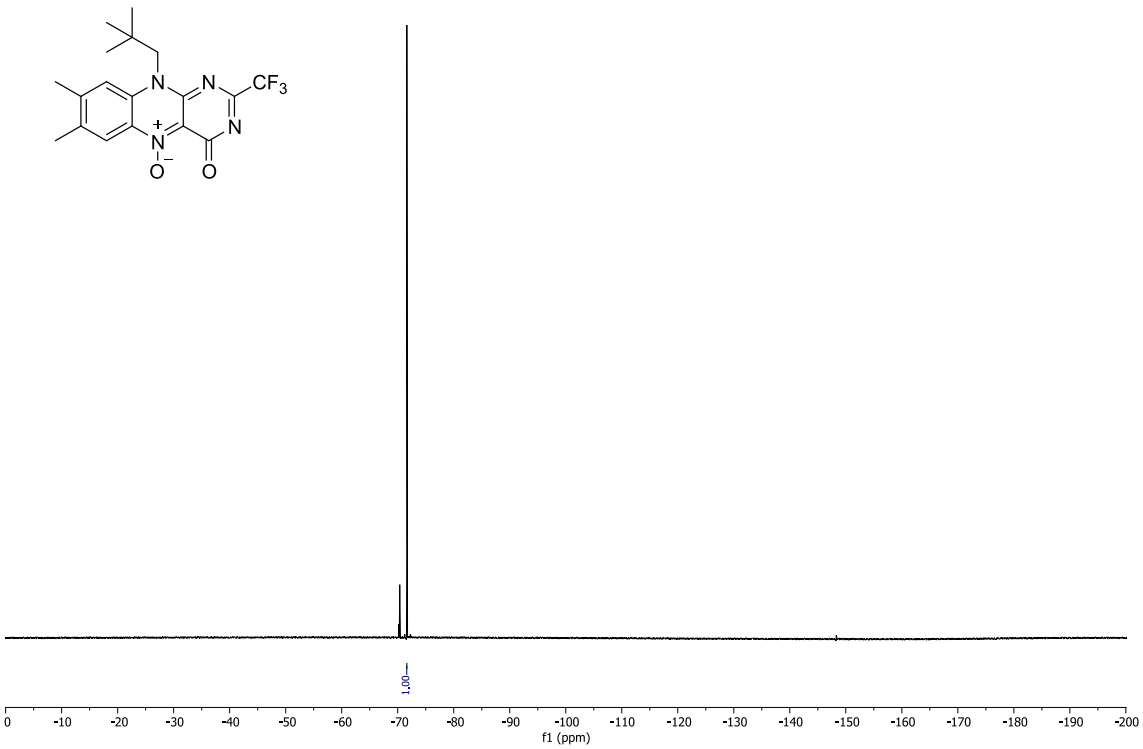

Figure 9.47 $^{19}F\{^{1}H\}$-NMR spectrum (282 MHz, DMSO-d_6) of **99**.

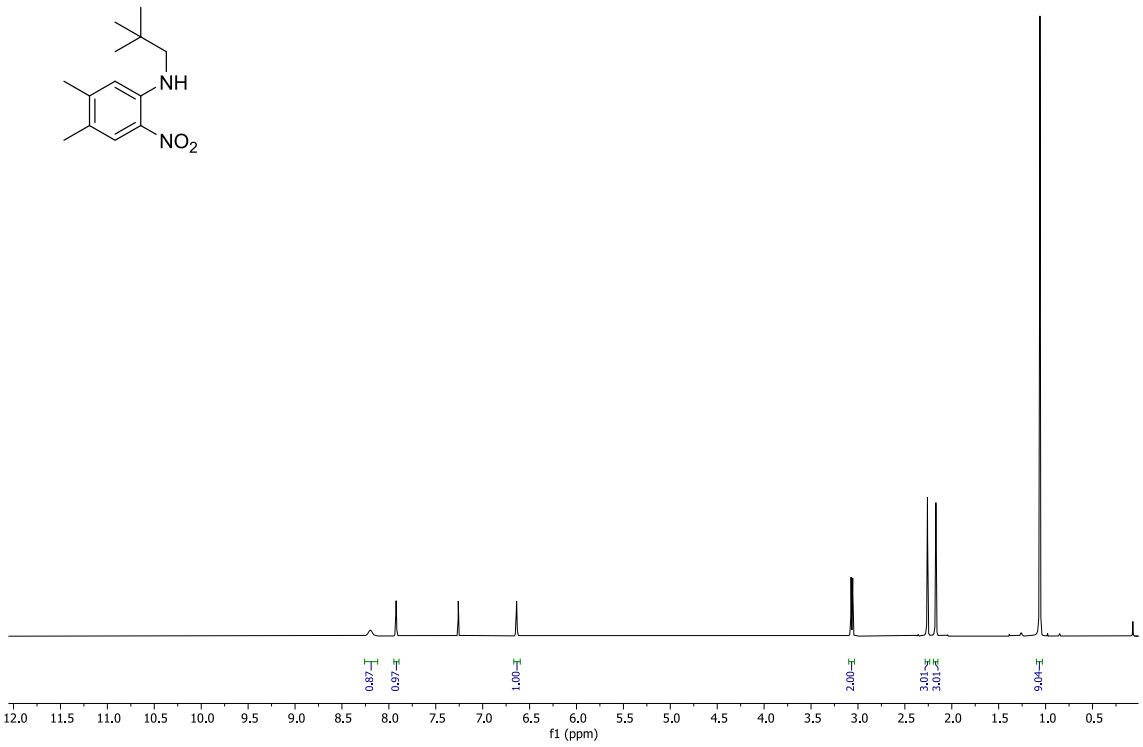

Figure 9.48 ^{1}H-NMR spectrum (300 MHz, chloroform-d) of **73**.

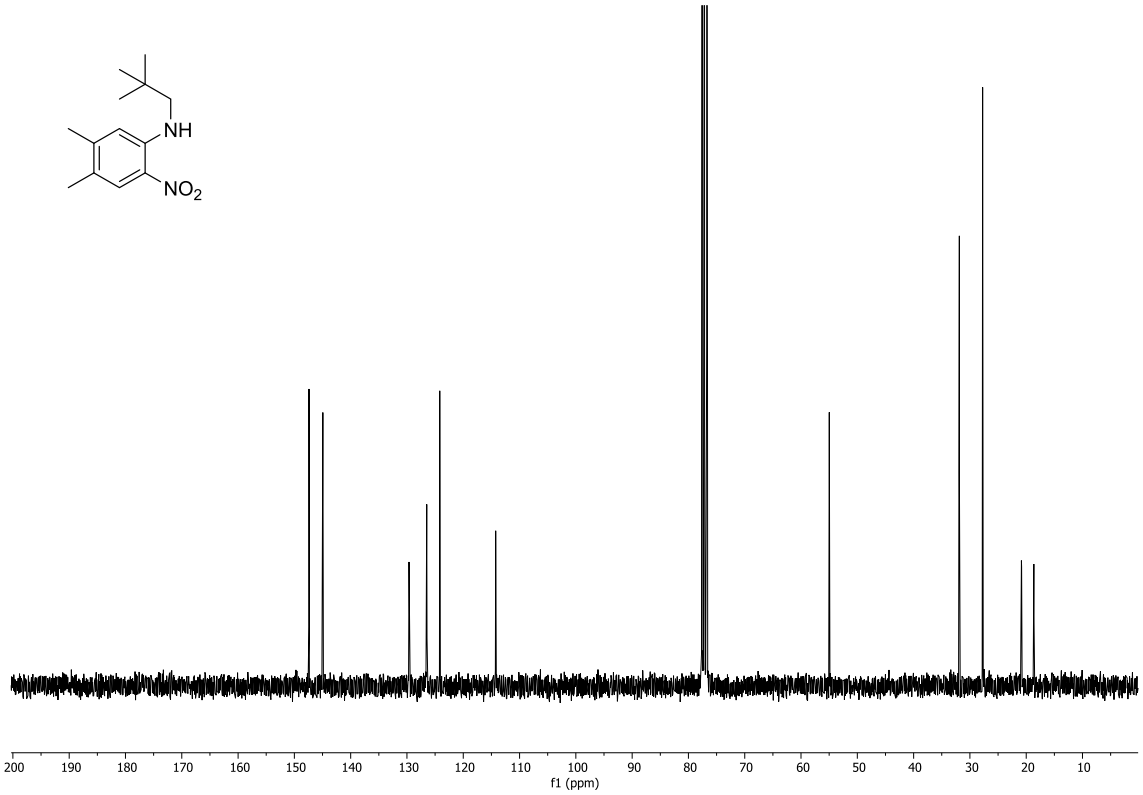

Figure 9.49 $^{13}C\{^{1}H\}$-NMR spectrum (75 MHz, chloroform-*d*) of **73**.

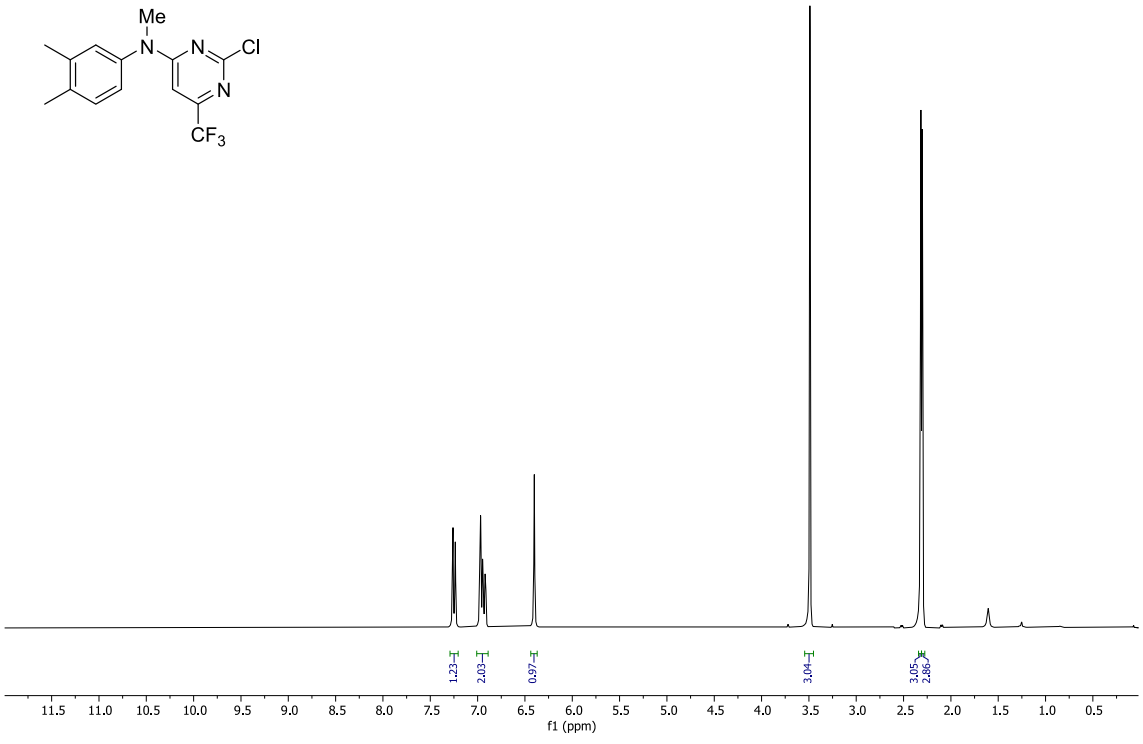

Figure 9.50 ^{1}H-NMR spectrum (300 MHz, chloroform-*d*) of **101**.

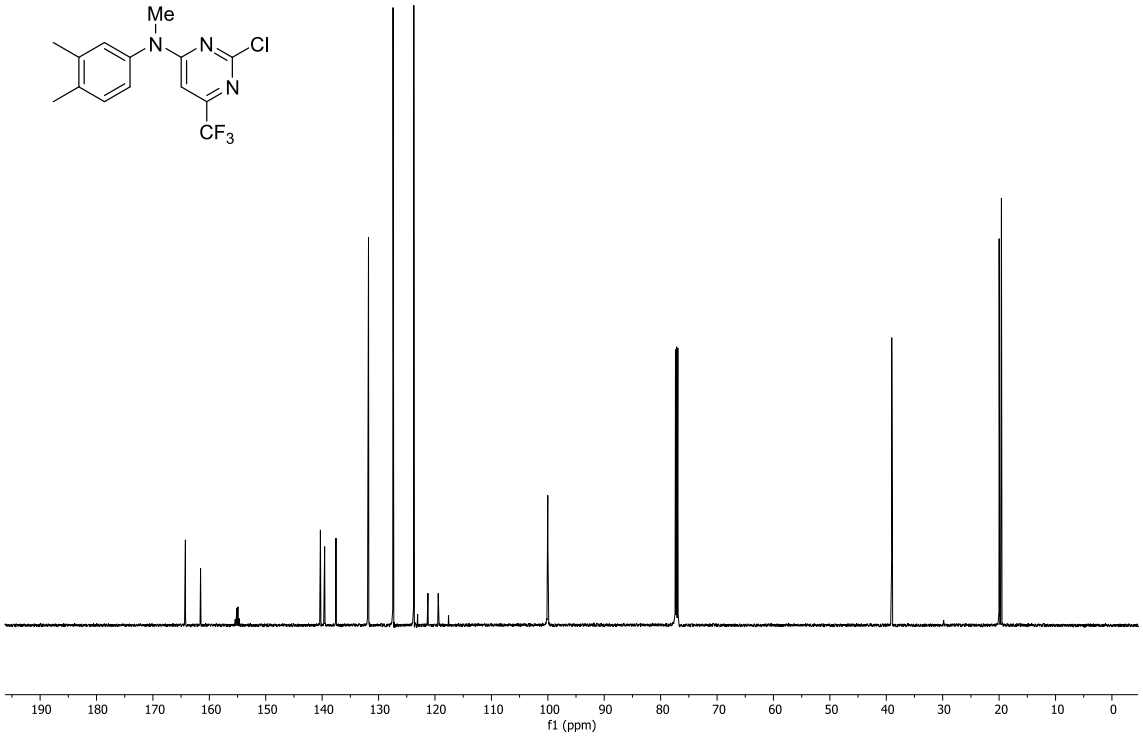

Figure 9.51 $^{13}C\{^{1}H\}$-NMR spectrum (151 MHz, chloroform-*d*) of **101**.

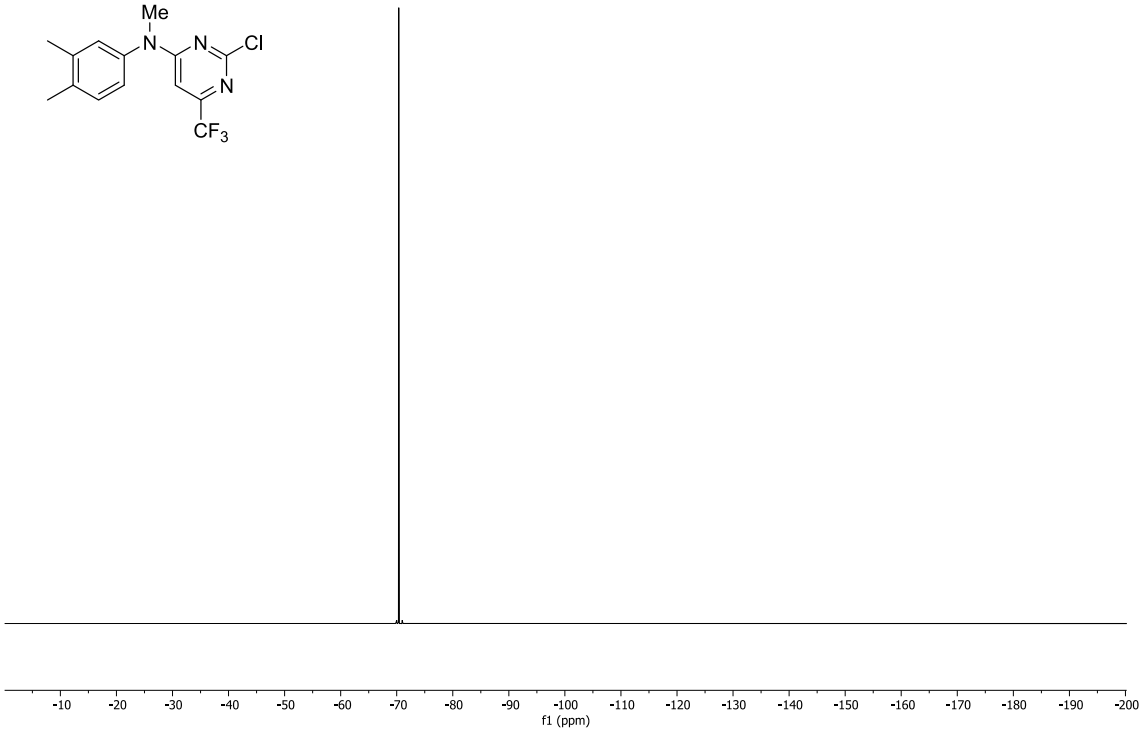

Figure 9.52 $^{19}F\{^{1}H\}$-NMR spectrum (282 MHz, chloroform-*d*) of **101**.

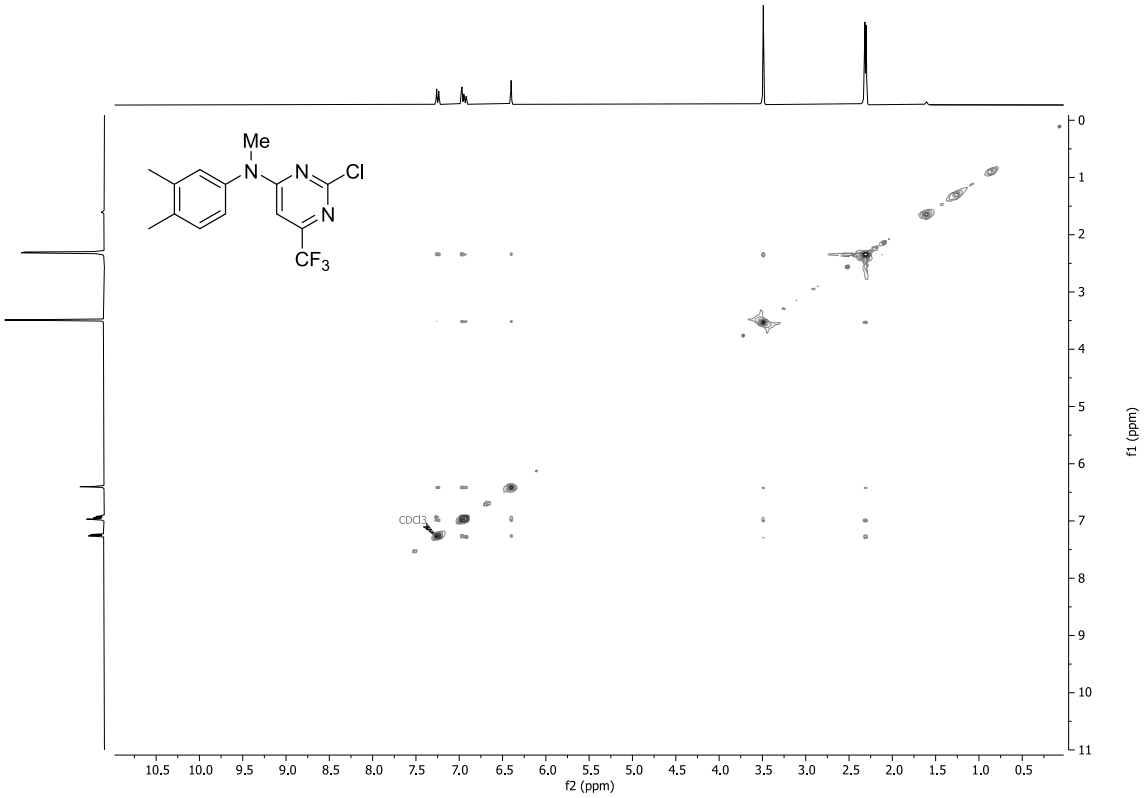

Figure 9.53 NOESY spectrum (300 MHz, chloroform-*d*) of **101**.

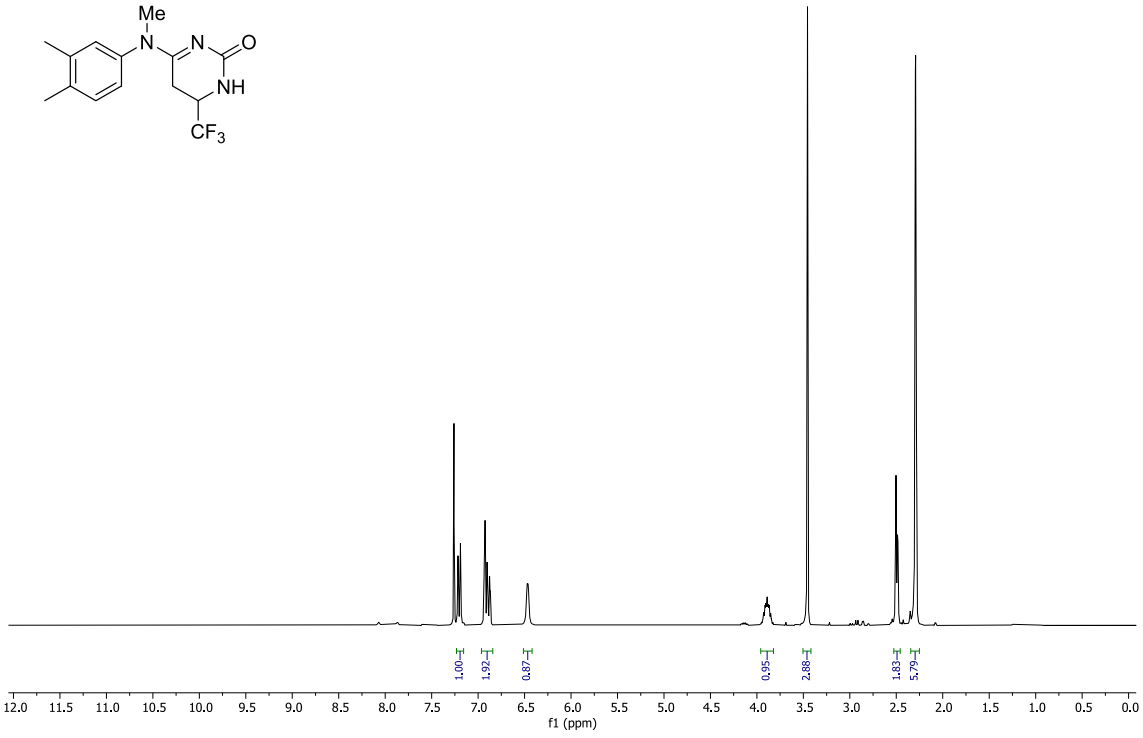

Figure 9.54 ^{1}H-NMR spectrum (300 MHz, chloroform-*d*) of **106**.

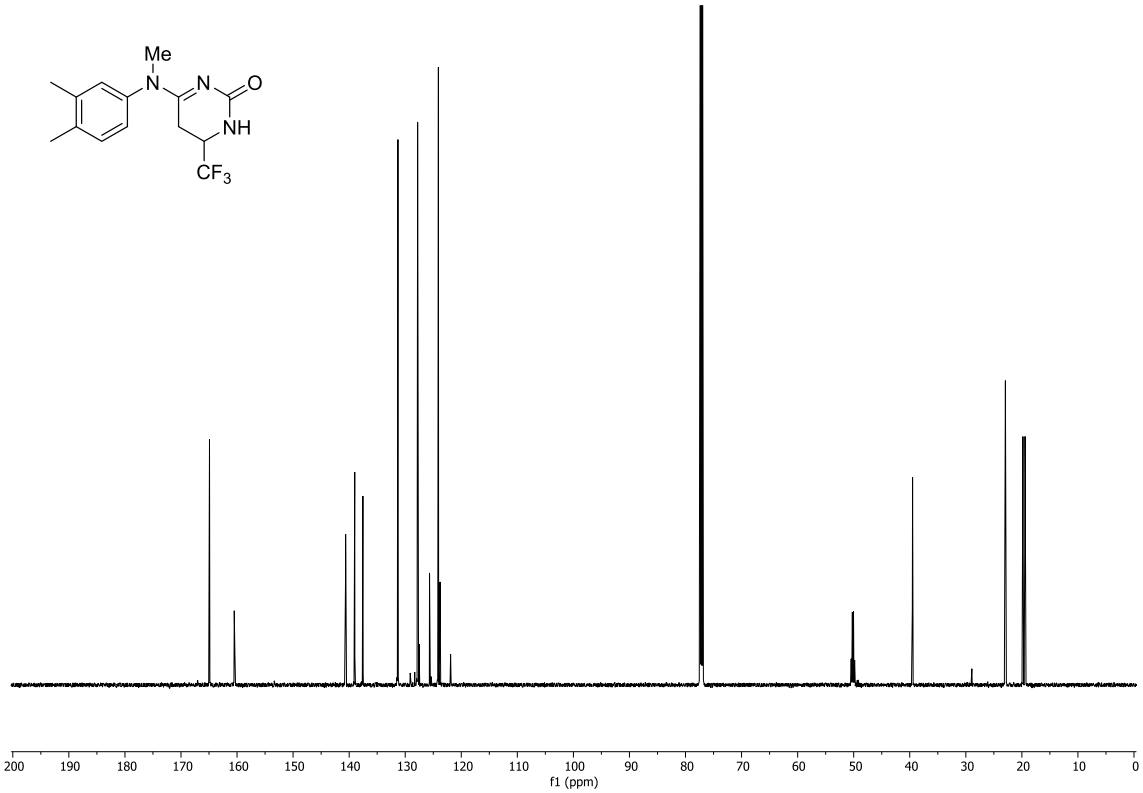

Figure 9.55 $^{13}C\{^{1}H\}$-NMR spectrum (151 MHz, chloroform-*d*) of **106**.

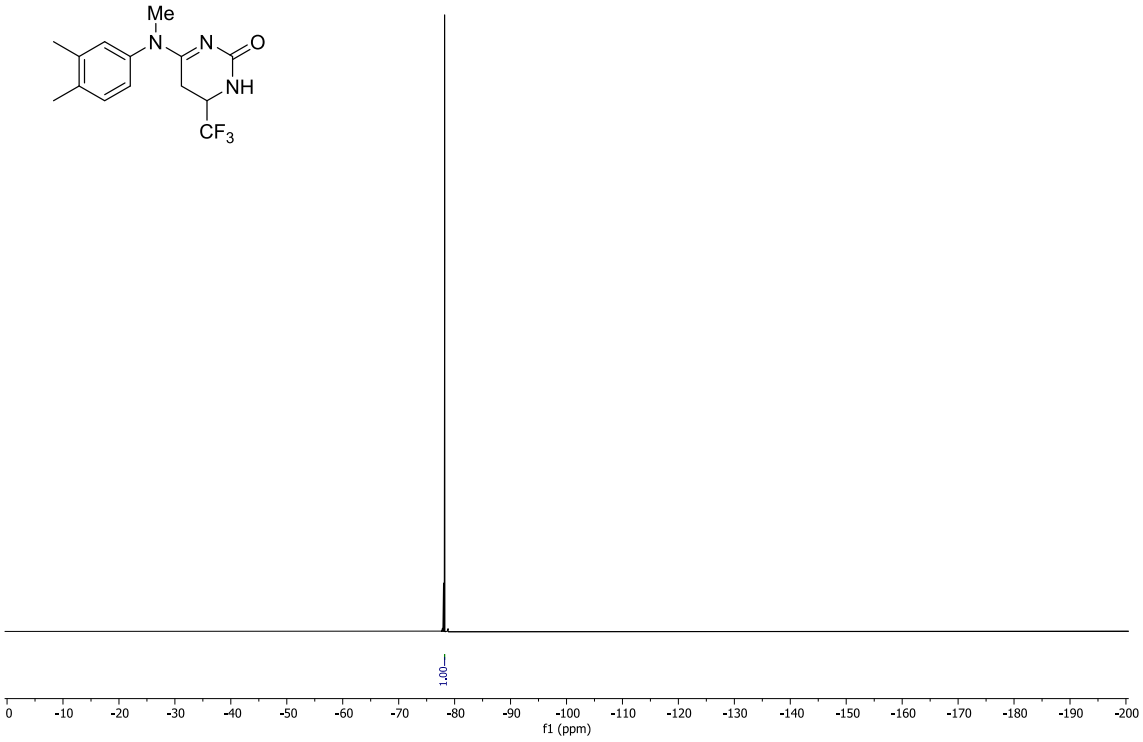

Figure 9.56 $^{19}F\{^{1}H\}$-NMR spectrum (282 MHz, chloroform-*d*) of **106**.

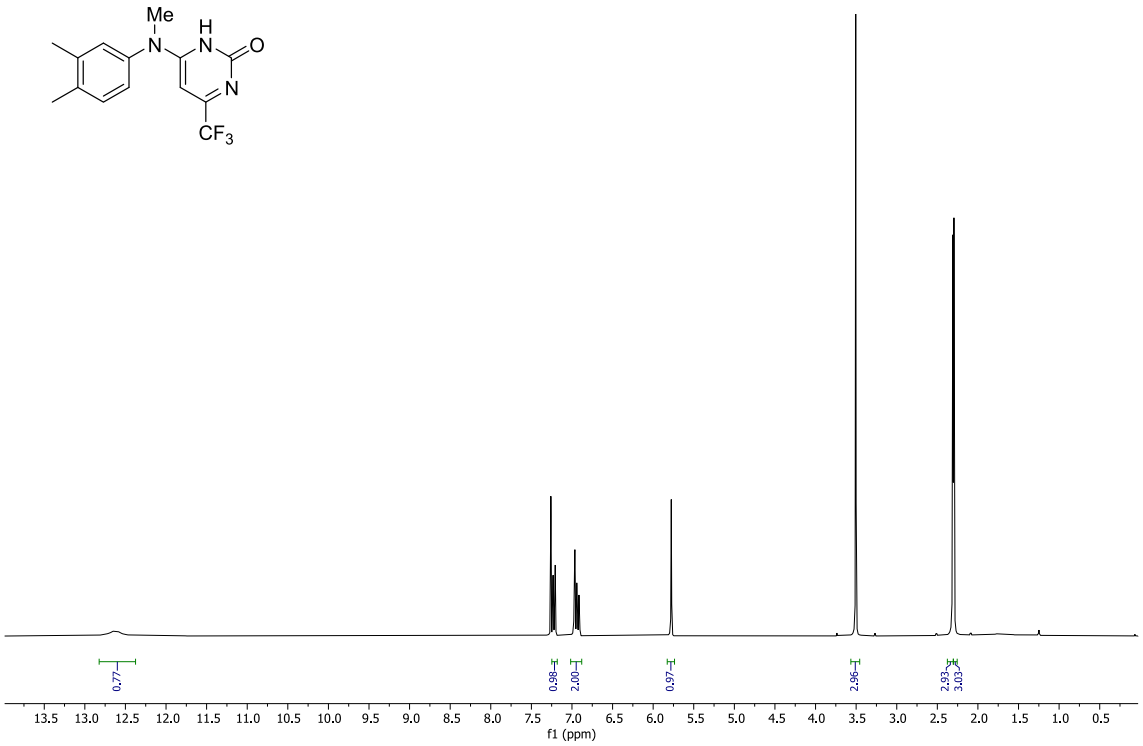

Figure 9.57 ^{1}H-NMR spectrum (300 MHz, chloroform-*d*) of **104**.

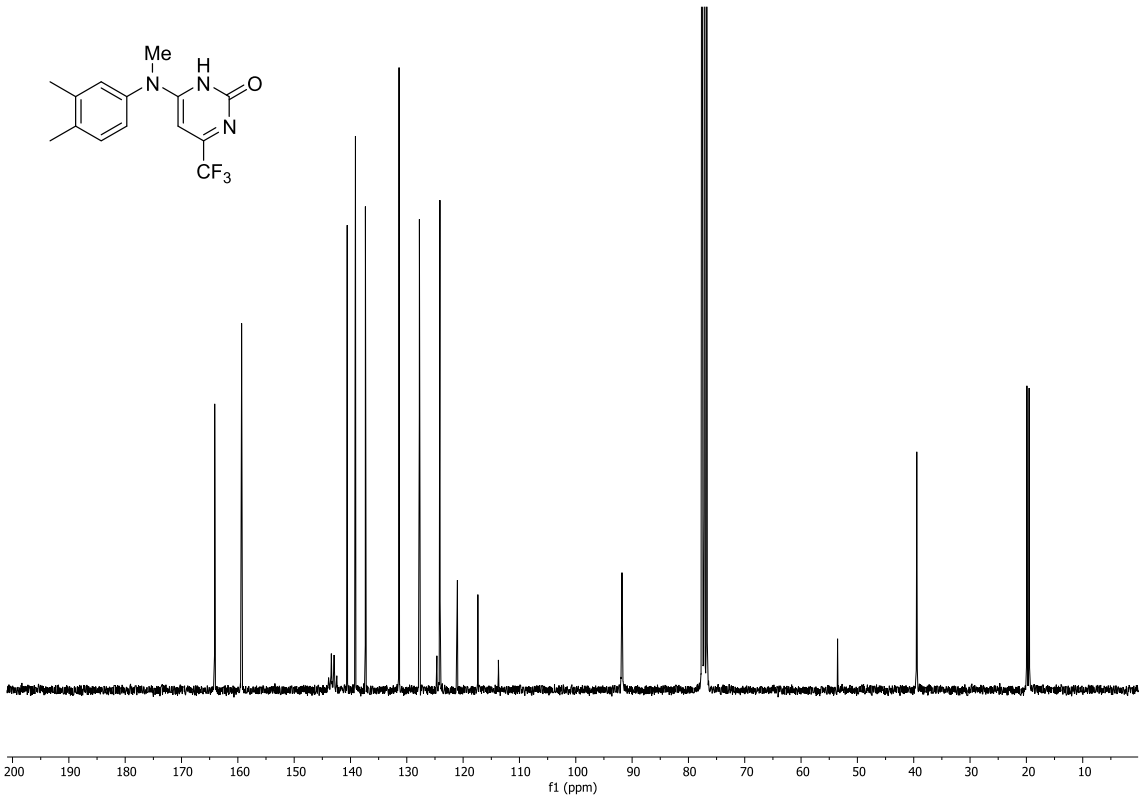

Figure 9.58 ^{13}C{^{1}H}-NMR spectrum (75 MHz, chloroform-*d*) of **104**.

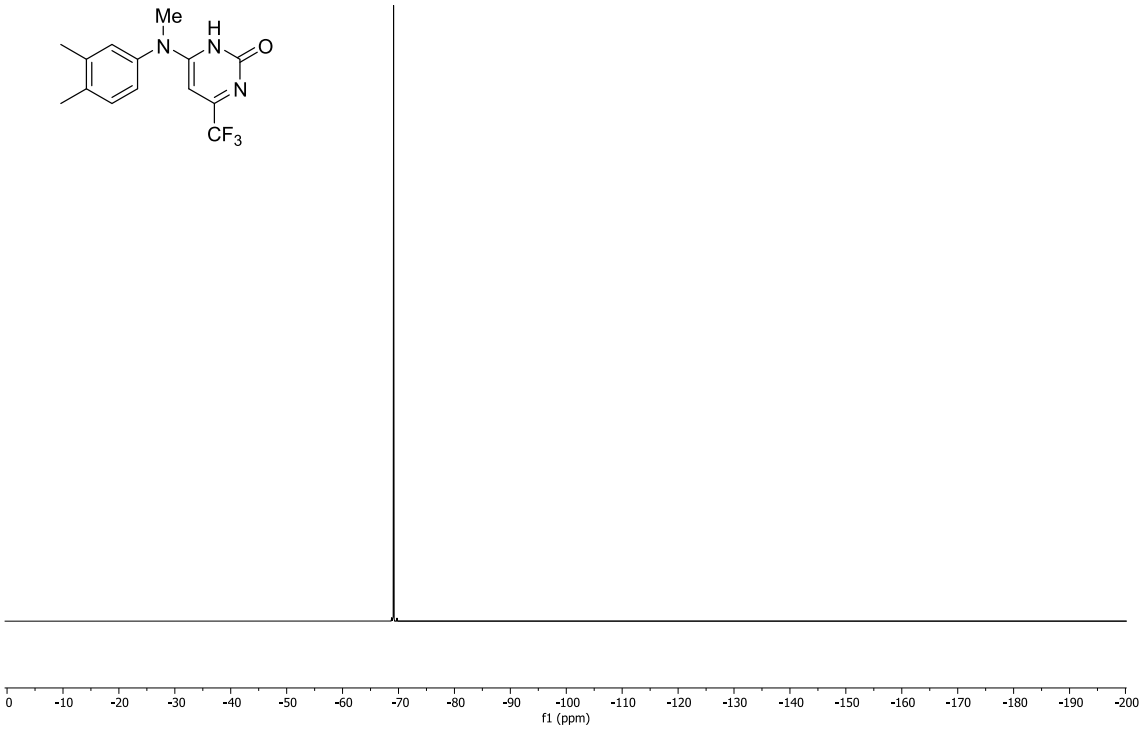

Figure 9.59 $^{19}F\{^{1}H\}$-NMR spectrum (282 MHz, chloroform-*d*) of **104**.

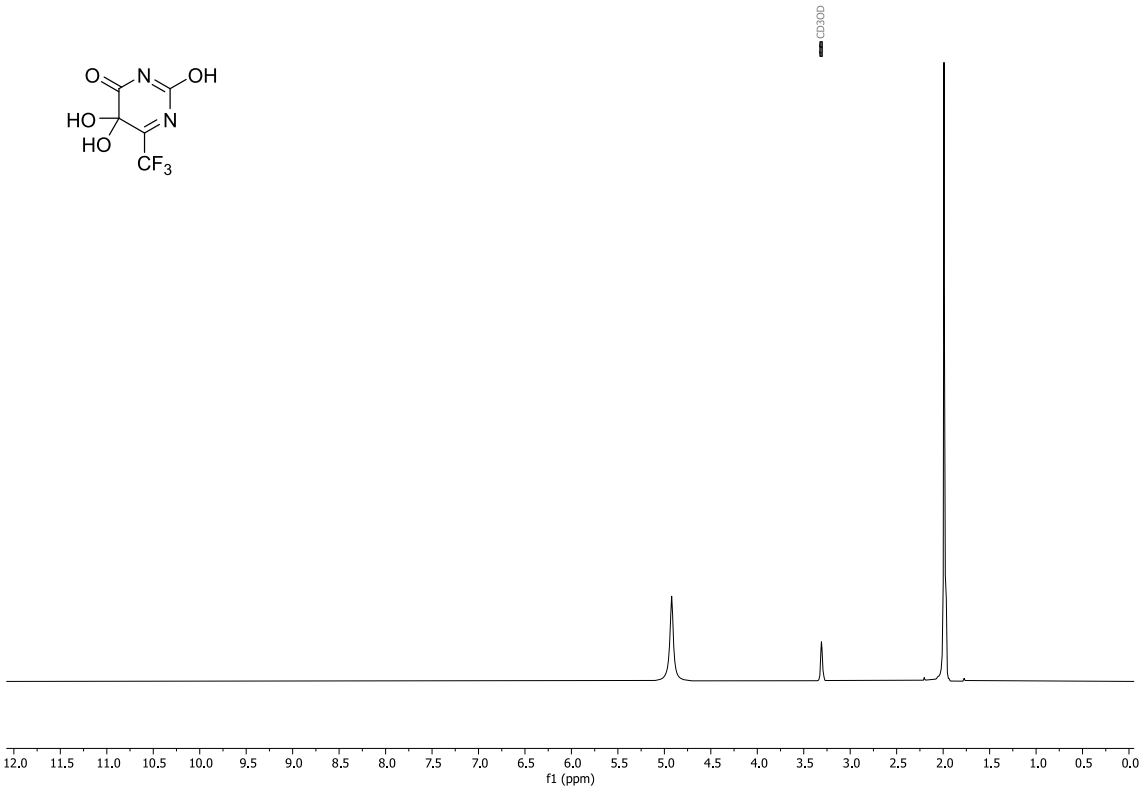

Figure 9.60 ^{1}H-NMR spectrum (300 MHz, methanol-d_4) of **78**.

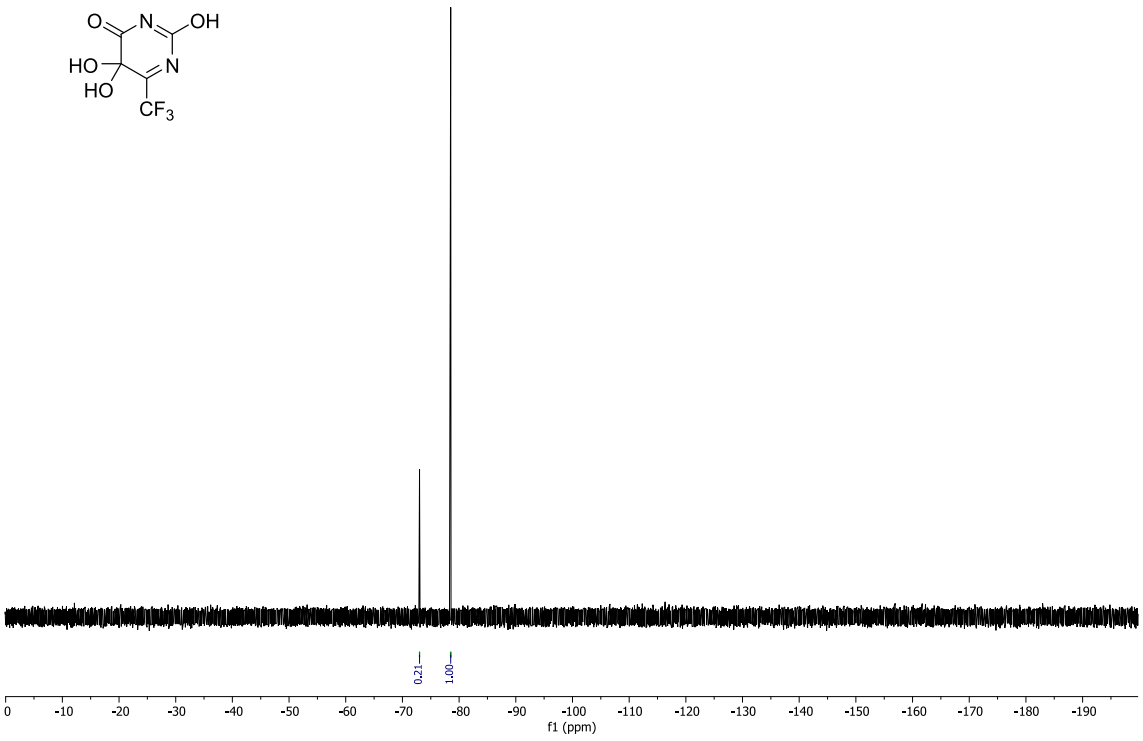

Figure 9.61 $^{19}F\{^{1}H\}$-NMR spectrum (282 MHz, methanol-d_4) of **78**.

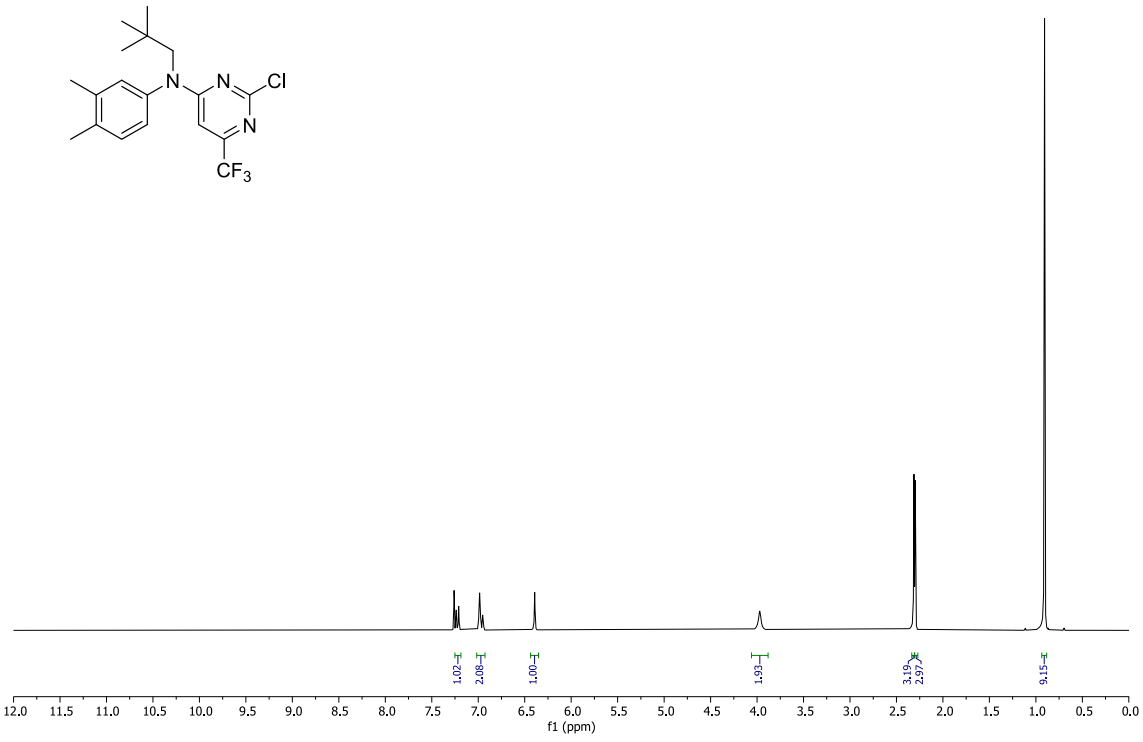

Figure 9.62 ^{1}H-NMR spectrum (300 MHz, chloroform-d) of **109**.

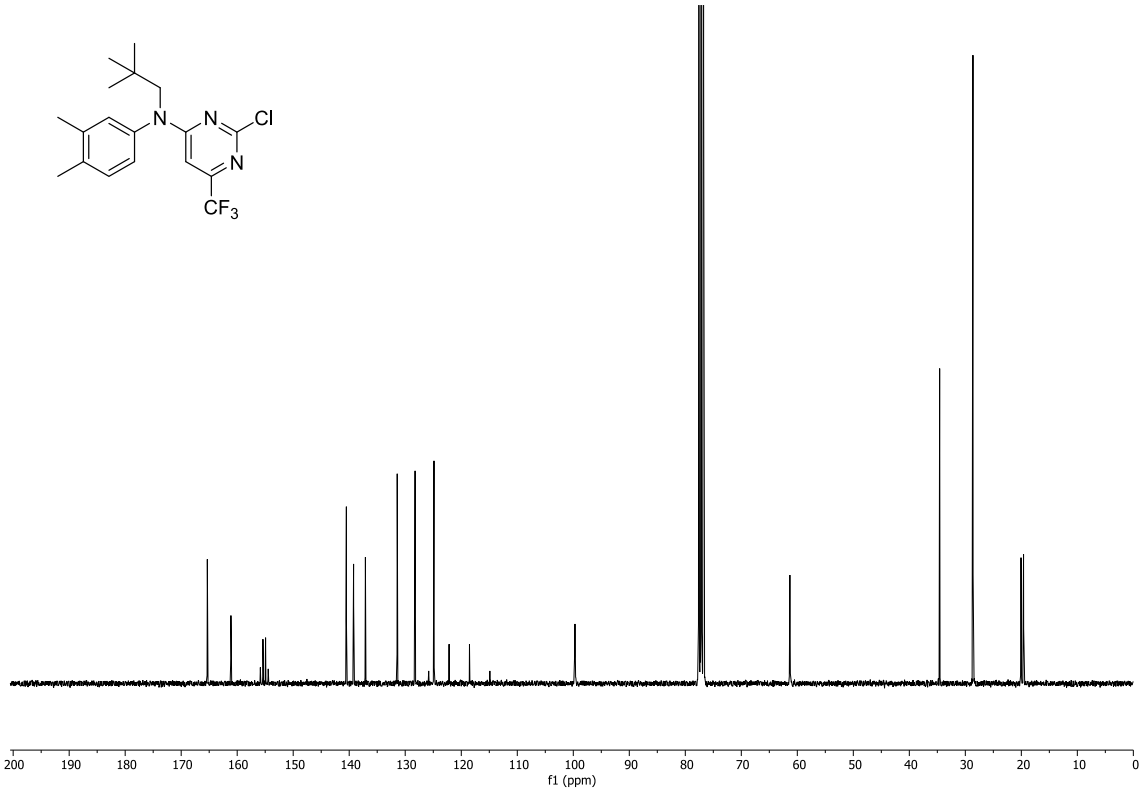

Figure 9.63 $^{13}C\{^{1}H\}$-NMR spectrum (75 MHz, chloroform-*d*) of **109**.

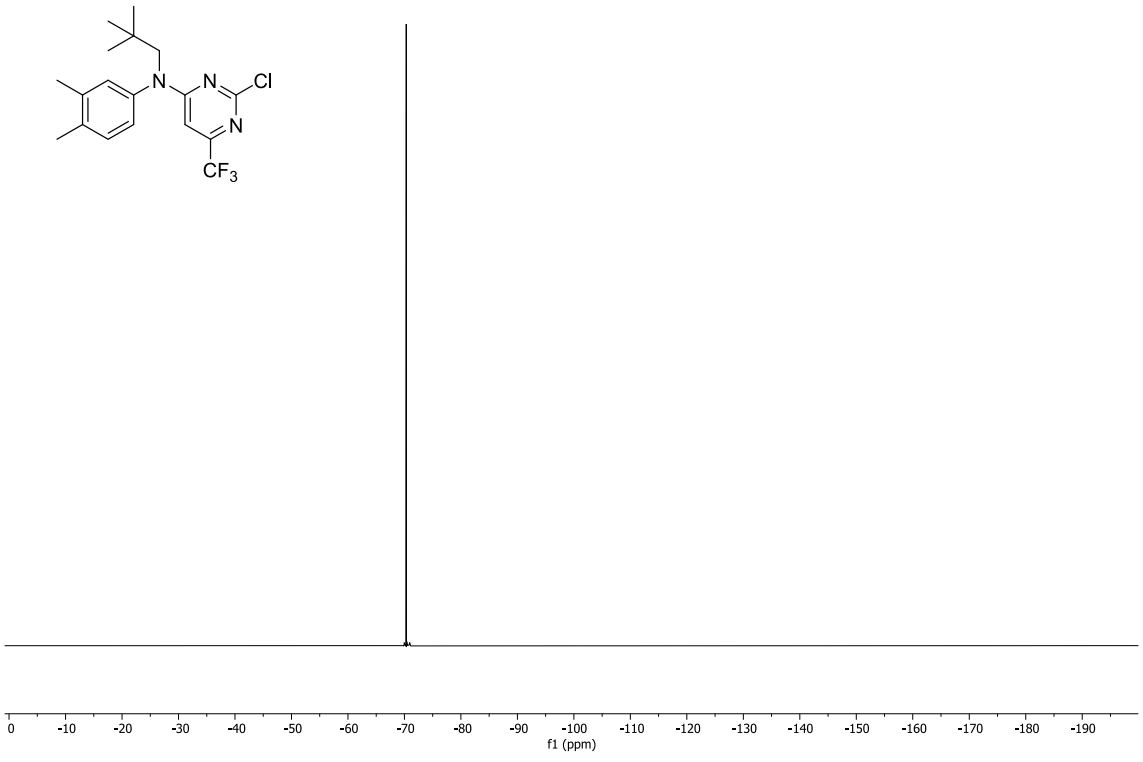

Figure 9.64 $^{19}F\{^{1}H\}$-NMR spectrum (282 MHz, chloroform-*d*) of **109**.

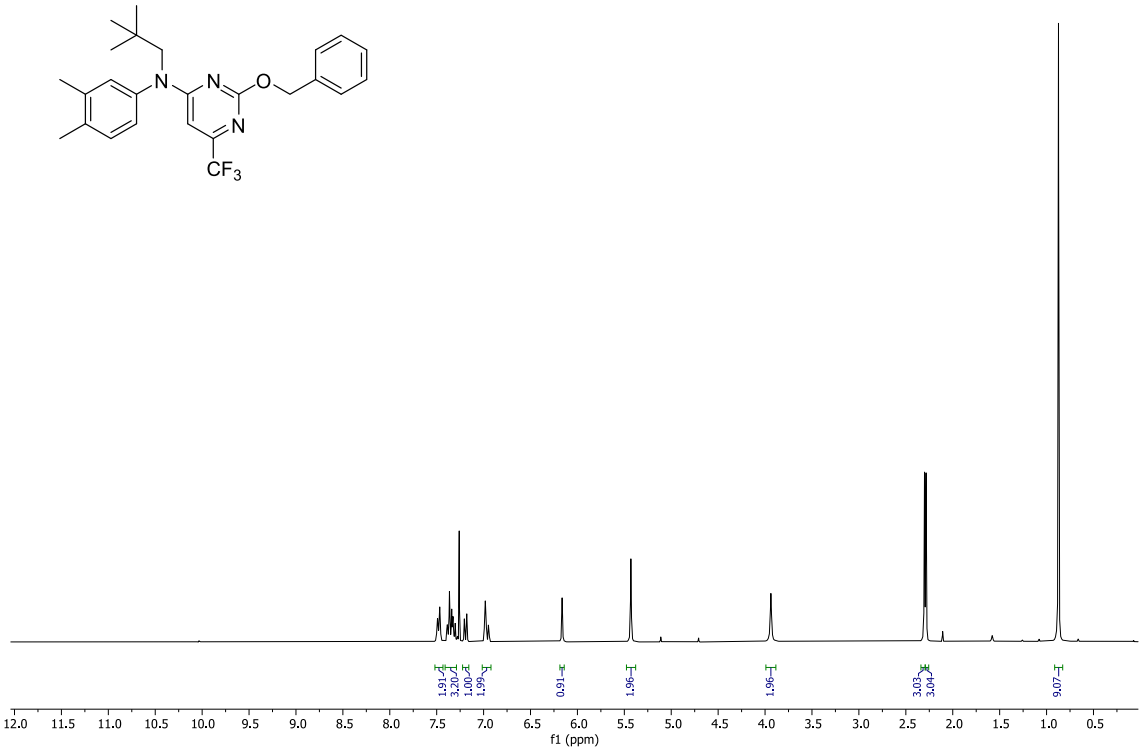

Figure 9.65 ^{1}H-NMR spectrum (300 MHz, chloroform-*d*) of **110**.

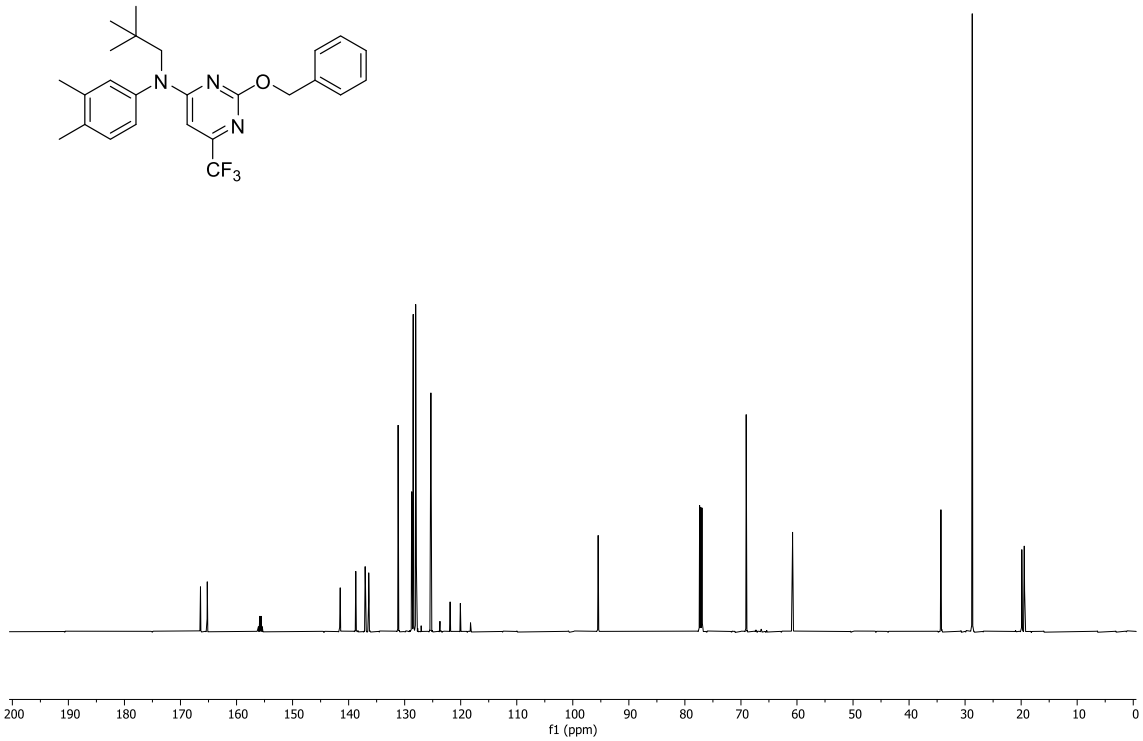

Figure 9.66 ^{13}C{^{1}H}-NMR spectrum (151 MHz, chloroform-*d*) of **110**.

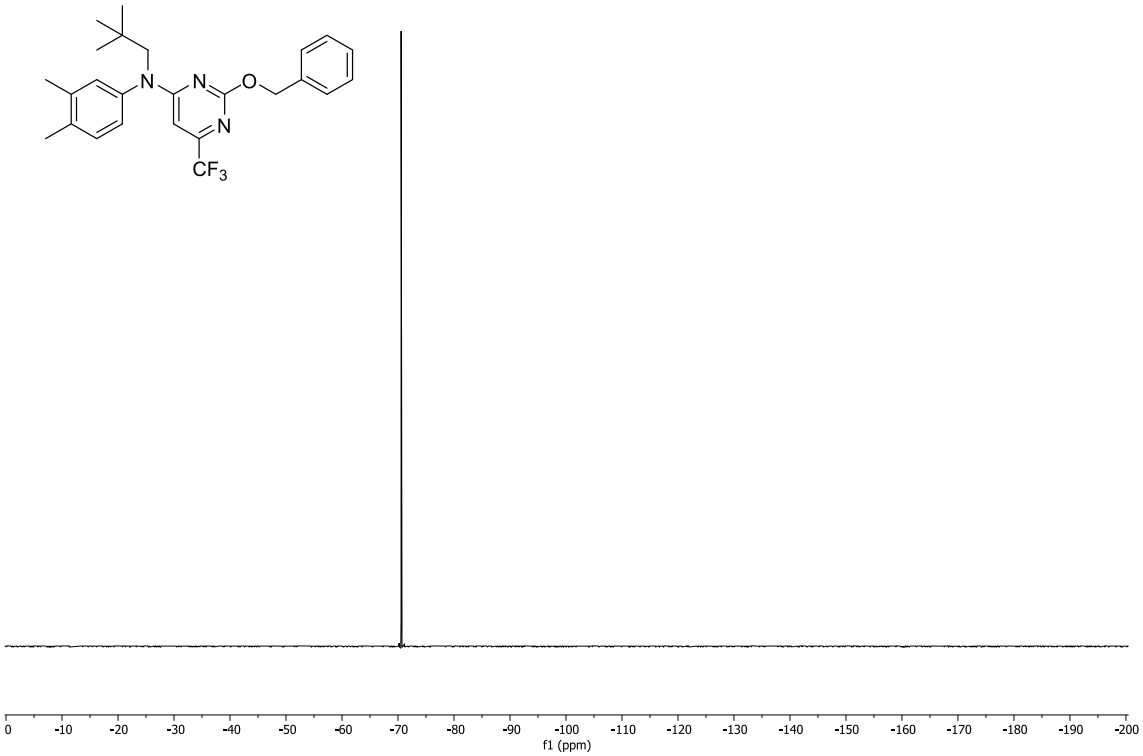

Figure 9.67 $^{19}F\{^{1}H\}$-NMR spectrum (282 MHz, chloroform-*d*) of **110**.

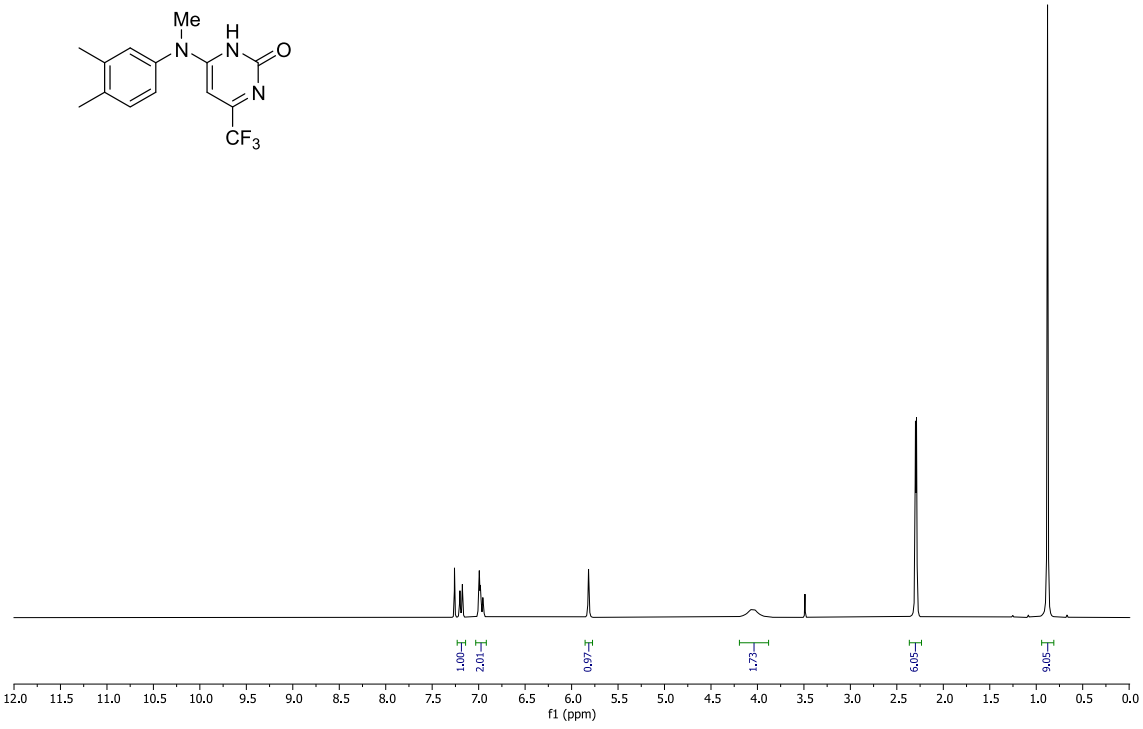

Figure 9.68 ^{1}H-NMR spectrum (300 MHz, chloroform-*d*) of **111**.

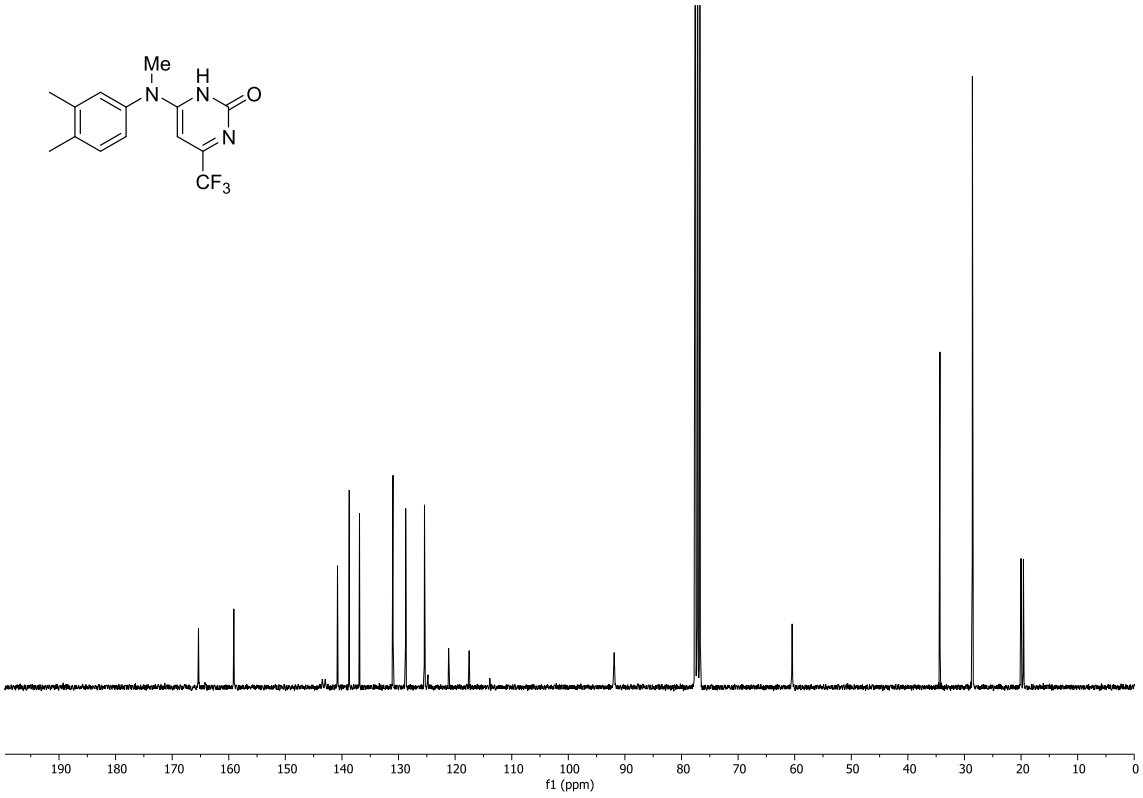

Figure 9.69 $^{13}C\{^{1}H\}$-NMR spectrum (75 MHz, chloroform-*d*) of **111**.

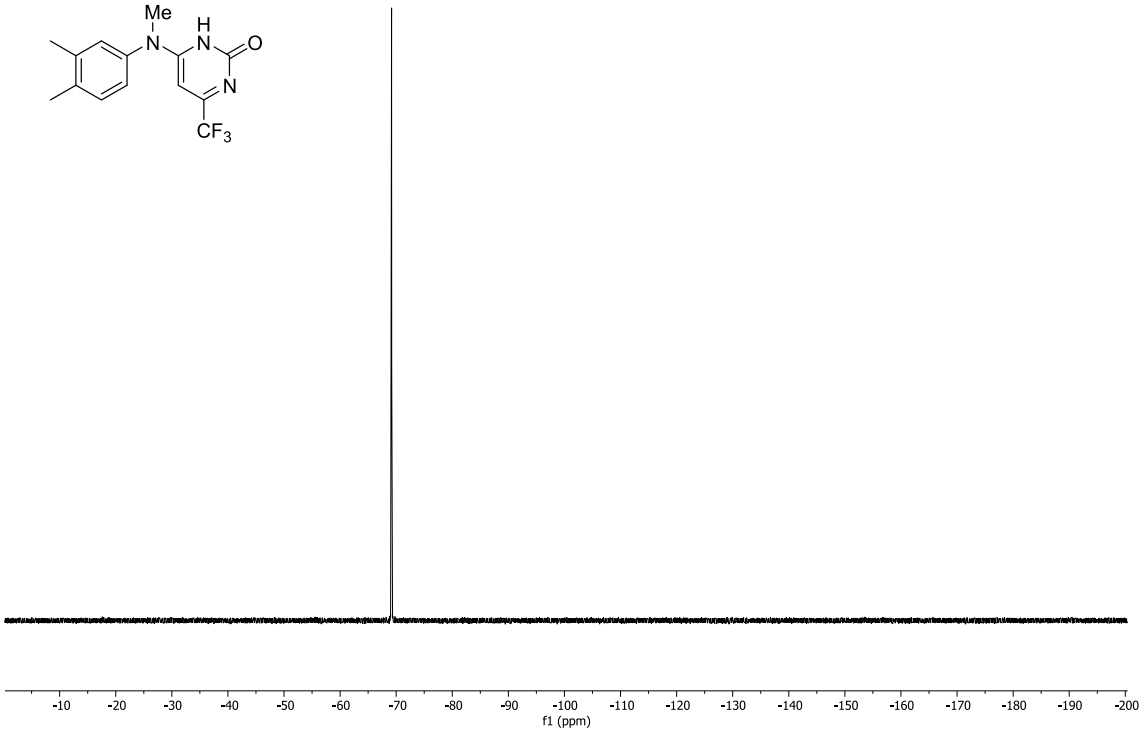

Figure 9.70 $^{19}F\{^{1}H\}$-NMR spectrum (282 MHz, chloroform-*d*) of **111**.

9.2 Crystallographic Data

Crystal Structure Determination

Crystal structures were measured by P. Schmeinck on a Rigaku XtaLAB-Synergy S diffractometer. Structure solution and refinement was done with Olex2 by OlexSys Ltd. and SHELX.[121,122] Structure solution of 1-F-lumiflavin (**33**) was supported by L. Karl. The figures (thermal ellipsoid plots) were created with Mercury by the Cambridge Crystallograpic Data Centre.[123]

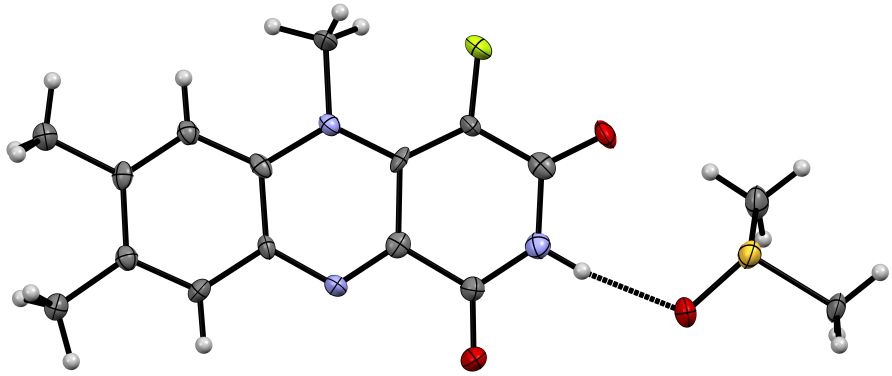

Figure 9.71 Molecular structure of 1-F-lumiflavin (**33**) with DMSO. Thermal displacement ellipsoids are drawn at the 50% probability level.

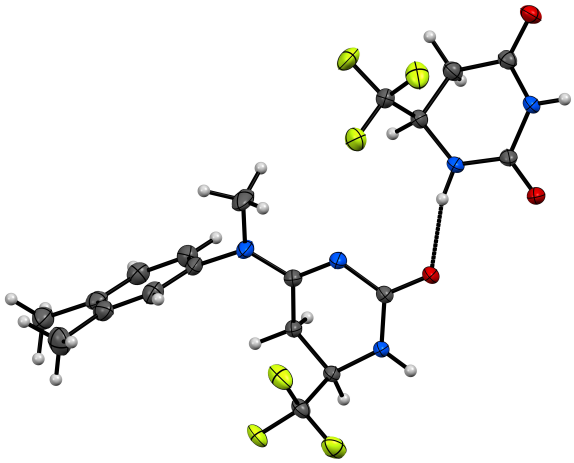

Figure 9.72 Molecular structure of dihydropyrimidine **106** with incorporated reduced dihydroxypyrimidine **77**. Thermal displacement ellipsoids are drawn at the 50% probability level.

Crystal Structure Table

Compound	**33**	**106**	**109**
Empirical formula	$C_{16}H_{18}FN_3O_3S$	$C_{19}H_{21}F_6N_5O_3$	$C_{18}H_{21}ClF_3N_3$
Formula weight [g/mol]	351.39	481.41	371.36
Crystal shape and color	needle, dark purple	block, colorless	block, colorless
Size [mm^3]	0.5 × 0.1 × 0.1	0.5 × 0.1 × 0.1	0.5 × 0.5 × 0.1
Temperature [K]	100.15	100.15	99.97(14)
Crystal system	monoclinic	triclinic	monoclinic
Space group	$P2_1/c$	P-1	$I2/a$
Lattice parameters [Å]	a = 7.4254(6) b = 31.689(4) c = 6.8984(7)	a = 9.0590(3) b = 9.4978(3) c = 13.7425(5)	a = 19.2990(9) b = 10.0635(5) c = 19.9488(11)
Angles [°]	β = 101.983(9)	α = 108.784(3) β = 91.287(3) γ = 97.502(2)	β = 103.850(5)
Volume [$Å^3$]	1587.8(3)	1107.23(7)	3761.7(3)
Z	4	2	8
ρ_{calc} [g/cm^3]	1.470	1.444	1.311
μ [mm^{-1}]	2.103	1.172	2.101
F(000)	736.0	496.0	1550.0
Radiation	Cu $K\alpha$ (λ = 1.54184)	Cu $K\alpha$ (λ = 1.54184)	Cu $K\alpha$ (λ = 1.54184)
2Θ range [°]	5.578 to 104.184	6.81 to 157.966	9.132 to 142.866
Index ranges	-7 ≤ h ≤ 7 -17 ≤ k ≤ 29 -5 ≤ l ≤ 7	-11 ≤ h ≤ 10 -12 ≤ k ≤ 12 -17 ≤ l ≤ 17	-23 ≤ h ≤ 23 -12 ≤ k ≤ 10 -23 ≤ l ≤ 24
Reflections collected	3062	13724	9356
Independent reflections	1601 (R_{int} = 0.0344, R_{sigma} = 0.0516)	4390 (R_{int} = 0.0256, R_{sigma} = 0.0254)	3474 (R_{int} = 0.0583, R_{sigma} = 0.0648)
Final R-value [I>=2σ(I)][a]	R_1 = 0.0822 wR_2 = 0.2257	R_1 = 0.0430 wR_2 = 0.1159	R_1 = 0.0987 wR_2 = 0.2603
Final R-value (all data)[a]	R_1 = 0.0953 wR_2 = 0.2367	R_1 = 0.0467 wR_2 = 0.1193	R_1 = 0.1449 wR_2 = 0.2960
Completeness	89.9	99.9	99.5
Data/restraints/ parameters	1601/0/222	4390/0/301	3474/0/231
Goodness-of-fit on F^2 [b]	1.066	1.042	1.038
Largest diff. peak, hole [e $Å^{-3}$]	0.80, -0.38	0.71, -0.30	1.04, -0.43

[a] $R1 = \Sigma||F_o|-|F_c||/\Sigma|F_o|$; $wR2 = [\Sigma w(F_o^2-F_c^2)^2/\Sigma wF_o^2]^{1/2}$; $w = 1/[\sigma^2F_o^2+(aP)^2+bP]$ with $P = (F_o^2+2F_c^2)/3$

[b] $GooF = [\Sigma w(F_o^2-F_c^2)^2/(N_R-N_P)]^{1/2}$ with N_R = Number of reflexes and N_P = Number of parameters

10 | Publications

Check for updates

ChemPhotoChem

Research Articles
doi.org/10.1002/cptc.202200334

Chemistry Europe
European Chemical Societies Publishing

www.chemphotochem.org

Special Collection

Increasing the Fluorescence Quantum Yield and Lifetime of the Flavin Chromophore by Rational Design

Mira K. Kubitz,[a] Wiebke Haselbach,[b] Dragana Sretenović,[c] Mario Bracker,[d] Martin Kleinschmidt,[d] Ralf Kühnemuth,[c] Claus A. M. Seidel,*[c] Peter Gilch,*[b] and Constantin Czekelius*[a]

A previous quantum chemical study (M. Bracker et al., *Phys. Chem. Chem. Phys.* **2019**, *21*, 9912–9923) on the excited state properties of fluorinated derivatives of the flavin chromophore promised an increased fluorescence performance of the derivative 7,8-difluoro-10-methyl-isoalloxazine (7,8-dF-MIA). Here, we describe the synthesis of 7,8-dF-MIA, its ribityl derivative, and for reason of comparison 9-F-MIA. The compounds dissolved in water (H_2O and D_2O) were characterized by steady state, time resolved, and fluorescence correlation spectroscopy. The experiments confirm the increase of the fluorescence quantum yield of 7,8-dF-MIA (0.42 in H_2O) compared to MIA (0.22) predicted by quantum chemistry. The anticipated reduction of the fluorescence quantum yield for 9-F-MIA is also confirmed experimentally. The quantum chemical computations as well as the spectroscopic observations attribute the increased fluorescence quantum yield of 7,8-dF-MIA predominantly to a decrease of the rate constant of intersystem crossing. Switching from H_2O to D_2O as a solvent is shown to increase fluorescence quantum yields (0.53 for 7,8-dF-MIA) and lifetimes of all fluorinated MIA derivatives. This can be attributed to a Förster type energy transfer from the excited chromophore to vibrational overtones of water and further water-mediated deactivation processes.

Introduction

Flavins, a class of yellow redox-active chromophores, are an essential moiety of many photoreceptor proteins like cryptochromes, phototropins or photoactivated adenylyl cyclase.[1–7] Upon absorption of blue light, photochemical processes of biological importance are induced. Among others, the circadian rhythm or the induction of flowering are related to flavin compounds.[1,3–10] Flavin derivatives bound to these proteins are most often flavin mononucleotide (FMN) or flavin adenine dinucleotide (FAD).[1,3–10] Both are ubiquitous in nature and are also known to act as cofactors in enzyme catalysis. Due to their redox activity, they can participate in both one- and two-electron transfer processes and have therefore been employed in photo-redox catalysis.[4–6,10–18]

By modifying the isoalloxazine core system, their photophysical properties can be altered.[19–22] If the fluorescence quantum yield Φ_{fl} and peak absorption coefficient of the first transition (1^{st} ε_{max}) are maximized, application areas like optical imaging, where a high sensitivity (1^{st} $\varepsilon_{max} \times \Phi_{fl}$) is needed, will benefit while high triplet quantum yields could be useful in terms of singlet oxygen production, photodynamic therapy and photochemically induced radical reactions.[23–25]

Fluorine substituents are highly suited for electronic modifications as they exert a strong electron-withdrawing effect.[26–27] When they are introduced at different positions of the core system, shifts of absorption as well as an increase/decrease of fluorescence and triplet quantum yields are observed.[19–21] At the same time, the sterical impact on protein binding and associated biological activity should be comparably small.[28–30]

As shown in our previous studies,[19] substitution of hydrogen with fluorine substituents at the left A-ring of the 10-methyl-isoalloxazine (MIA) core system (6-, 7- and 8-position) led to a distinct impact on the photophysical properties, depending on the position of fluorination (Figure 1). In particular, for 6-F- as well as 7-F-MIA bathochromic and for 8-F-MIA hypsochromic shifts of up to 500 cm^{-1} were observed. The

[a] M. K. Kubitz, Prof. Dr. C. Czekelius
Institut für Organische Chemie und Makromolekulare Chemie
Heinrich-Heine-Universität Düsseldorf
Universitätsstraße 1, 40225 Düsseldorf (Germany)
E-mail: Constantin.Czekelius@hhu.de
[b] W. Haselbach, Prof. Dr. P. Gilch
Institut für Physikalische Chemie
Heinrich-Heine-Universität Düsseldorf
Universitätsstraße 1, 40225 Düsseldorf (Germany)
E-mail: Peter.Gilch@hhu.de
[c] D. Sretenović, Dr. R. Kühnemuth, Prof. Dr. C. A. M. Seidel
Institut für Physikalische Chemie
Heinrich-Heine-Universität Düsseldorf
Universitätsstraße 1, 40225 Düsseldorf (Germany)
E-mail: cseidel@hhu.de
[d] Dr. M. Bracker, Dr. M. Kleinschmidt
Institut für Theoretische Chemie und Computerchemie
Heinrich-Heine-Universität Düsseldorf
Universitätsstraße 1, 40225 Düsseldorf (Germany)

Supporting information for this article is available on the WWW under https://doi.org/10.1002/cptc.202200334

An invited contribution to a Special Collection on Emissive Materials for Organic Light Emitting Diodes

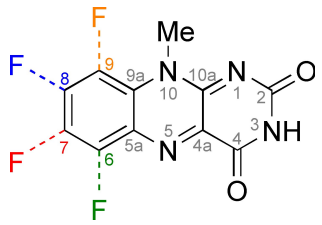

Figure 1. Chemical structure of 10-methylisoalloxazine (MIA). Fluorine substitution positions are color coded, and the coding was continued from the reference[19] and is used throughout the paper.

derivative with fluorine in 7-position proved particularly interesting due to its 50% increased fluorescence quantum yield compared to the non-fluorinated MIA. These experimental observations were reproduced by quantum chemical computations.[20]

According to this study the S_1 state of $\pi\pi^*$ character is separated from its triplet counterpart T_1 by ca. 0.5 eV in MIA and its fluorinated derivatives in aqueous medium. Intersystem crossing (ISC) to this triplet state is El-Sayed-forbidden and the large energetic separation also leads to small vibronic rate constants for ISC (ca. $5 \cdot 10^6\ s^{-1}$). In vacuum, the second triplet state T_2 is of $n\pi^*$ character, energetically below the S_1 state and ISC to this state is El-Sayed-allowed and fast (ca. $2 \cdot 10^9\ s^{-1}$), but in aqueous medium, this state is so strongly destabilized that it plays no role for radiationless deactivation of the S_1 state anymore. The next triplet state T_3 is of $\pi\pi^*$ character again. In water, it is shifted energetically below the T_2 state and also slightly below the S_1 state (0.0–0.2 eV depending on the mono-fluorination pattern). ISC to this state is also El-Sayed-forbidden, but the close energetic vicinity of the S_1 state as well as of the T_2 state (causing admixture of $n\pi^*$ character by out-of-plane vibrations) leads to considerable vibronic ISC rate constants (ca. $3 \cdot 10^8\ s^{-1}$). The T_3 state is considered to be decisive for non-radiative decay by ISC. Therefore, the energetic upshift of the T_3 state above the S_1 state decreases the non-radiative decay and increases the fluorescence yield.

Fluorination in 7- and 8-position both cause a blue shift of this T_3 state. For vertical energies, it was shown that the effect of multiple fluorination on the photophysical properties can be predicted by simply adding the shifts of the mono-fluorinated derivatives.[20] According to this analysis, it is expected that difluorination in 7- and 8-position will bring the T_3 state energetically above the S_1 state, effectively hindering ISC and thus increasing fluorescence quantum yield. The computational study also predicts a decrease in fluorescence quantum yield for 9-F-MIA, a derivative that was not previously available and is also considered in this paper.

In this work, 7,8-dF-MIA as well as 9-F-MIA were synthesized and their photophysical properties were investigated experimentally to compare them with computational ones. This demonstrates that the spectroscopic properties of chromophores can be tuned using a rational design approach. Following the work of Klehs et al.,[31] we tested whether the fluorescence properties of all fluorinated MIA derivatives can be increased even further by using heavy water (D_2O) as a solvent. For potential applications in fluorescence microscopy in analogy to riboflavin, the corresponding equivalent 7,8-difluoro-10-ribityl-isoalloxazin (7,8-dF-RIA) was synthesized and its fluorescence properties were also characterized.

Results and Discussion

Synthesis

Following the reported synthesis route,[19,32–33] 9-F-MIA (**3**) was obtained starting from the corresponding fluorinated nitroaniline. As illustrated in Scheme 1, nitroaniline **1** was methylated in a two-step-one-pot reaction. Then, reduction of the nitro group and condensation with alloxan monohydrate gave 9-F-MIA (**3**) in an overall yield of 43%. For spectroscopic measurements particularly high purity of material is mandatory. Due to the generally low solubility of MIA derivatives, recrystallization methods often employ solvents such as formic acid or acetic acid. However, the concomitant formation of alloxazines by demethylation, which is commonly observed upon heating with traces of acid, renders the purification quite challenging. By screening other solvents trifluoroethanol proved to be highly suitable as it is very polar and not particularly acidic or nucleophilic.

In contrast to the monofluorinated derivatives, methylation of 4,5-Difluoro-*N*-methyl-2-nitroaniline (**4**) following the one-pot procedure shown above[32] proved to be troublesome due to a high propensity for fluorine substitution in *para*-position to the nitro group. Therefore, a modified synthesis route via Boc-protection and alkylation with methyl *p*-toluenesulfonate was developed.[34] Finally, reduction of the nitro group and condensation with alloxan monohydrate[19,33] gave 7,8-dF-MIA (**8**) as the main product in a mixture with the corresponding alloxazine **9** in a ratio of 1:0.4 (Scheme 2).

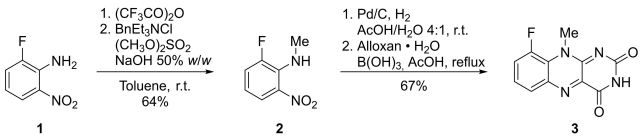

Scheme 1. Synthesis route to 9-F-methylisoalloxazine (**3**).

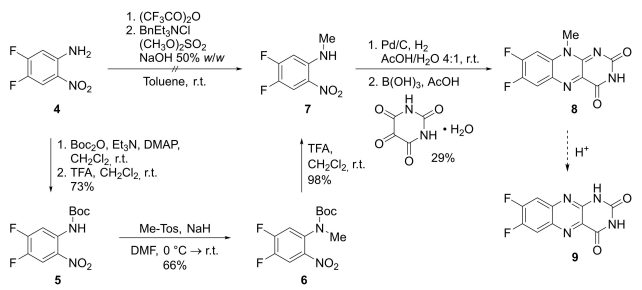

Scheme 2. Synthesis route to 7,8-dF-methylisoalloxazine (**8**) and formation of alloxazine by-product **9**.

The already mentioned formation of the alloxazine by-product turned out to be very problematic for the purification of this MIA derivative. Since alloxazines are less soluble than methylisoalloxazines, recrystallization was again the first choice. However, slow precipitation and fast formation of alloxazine by-product **9** during recrystallization were observed along with substantial degradation by nucleophilic fluorine substitution. Finally, using a combination of optimized reaction conditions[35] and work-up and purification methods, spectroscopically pure product was obtained (see Supporting Information Chapter 1 for details). Specifically, heating should be avoided in general for this delicate compound and solvents evaporated only under high vacuum conditions. It was further found that a flash chromatography method applying the raw product as a solution in trifluoroethanol/methanol proved to be essential for purification.

7,8-Difluoro-10-ribityl-isoalloxazin (referred to as 7,8-dF-RIA, **13**) was synthesized following a modified protocol by Mansurova et al.[36] as illustrated in Scheme 3. To avoid nucleophilic substitution of fluorine substituents, the nitro group was reduced first. Since the diamine was highly air-sensitive, Boc-protection was performed in situ to give the less sensitive protected derivative **10**. Ribitylated diamine **11** was obtained via reductive amination with D-ribose. Boc-deprotection was followed by condensation with alloxan monohydrate which is best performed under inert conditions in order to prevent fast oxidation of the 1,2-diaminobenzene derivative. Additionally, 7,8-dF-RIA **13** showed pronounced light sensitivity which made its purification in combination with the well-known continuous formation of poorly soluble alloxazines and the sensitivity of the fluorine substituents towards nucleophiles even more challenging. Therefore, it was renounced to heat the product at any point due to a very fast formation of side products. Instead, the solvent of the reaction mixture was solely removed at ambient temperature using high vacuum conditions. Multiple recrystallizations from different solvents led to a pre-purified product, which was finally purified by HPLC.

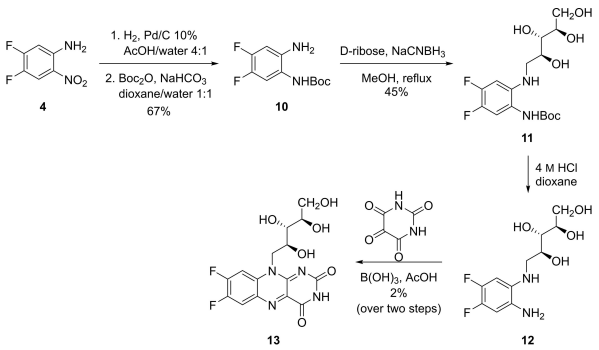

Scheme 3. Synthesis route to 7,8-difluor-10-ribityl-isoalloxazin (7,8-dF-RIA, **13**).

Spectroscopy

Steady state spectroscopy

First, we studied the impact of the fluorine substitution pattern on the optical properties of the two fluorinated derivatives 9-F-MIA and 7,8-dF-MIA in water. The absorption spectra exhibit two strong bands in the visible and near UV region (Figure 2 and Table 1). The position of these bands is close to the ones of MIA.[19–20,37] For MIA, the lowest-energy absorption maxima were reported at 431 nm ($\pi_{HOMO} \rightarrow \pi_{LUMO}$ transition, absorption coefficient $\varepsilon_{431} = 8470\ M^{-1}\,cm^{-1}$)[19] and 345 nm ($\varepsilon_{431} = 6250\ M^{-1}\,cm^{-1}$).[19] Quantum chemical calculations predict the first excited state to be unaltered upon fluorination in the 9- and 7,8-positions.[20] Experimentally, a slight redshift of $-54\ cm^{-1}$ for 9-F-MIA is observed compared to MIA, the absorption coefficient decreases by ~21 %. For 7,8-dF-MIA, the peak wavelength of 431 nm is retained and the absorption strength for the lowest energy absorption increases by ~31 %.

For MIA, the emission peak is at 524 nm.[19] 7,8-dF-MIA has a higher energy for the fluorescence peak (519 nm) and 9-F-MIA has a lower energy (535 nm) compared to MIA. This translates into a lower Stokes shift for 7,8-dF-MIA and a higher one for 9-F-MIA.

As shown in the previous work by Reiffers et al.[19] and Bracker et al.,[20] fluorination also has an effect on the fluorescence quantum yields Φ_{fl}. The yield was determined using coumarin 153 in ethanol as a reference ($\Phi_{fl}^{r} = 0.544$)[38] and is clearly the highest for 7,8-dF-MIA (0.42) of all fluorinated derivatives studied so far. The yield decreases with fluorination at position 9 (0.12) compared to MIA (0.22). This finding was predicted by quantum chemical computations.[20]

Values for the 0–0 energies $\tilde{\nu}_{00}$, Stokes shifts $\Delta\tilde{\nu}_s$ and radiative rate constants k_{rad}^{SB} were derived from the steady-state

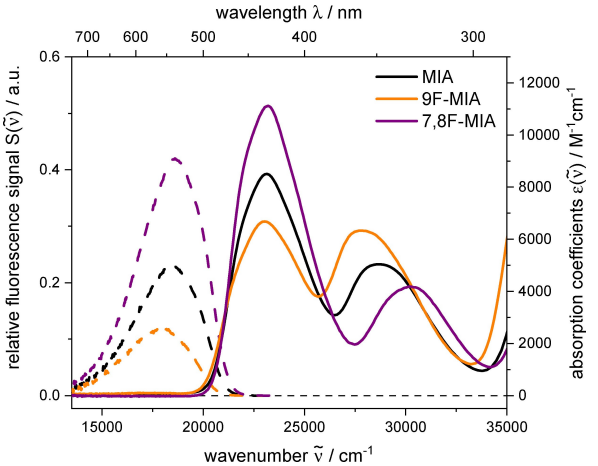

Figure 2. Absorption (absorption coefficients) and fluorescence emission spectra (recorded with constant wavelength bandpass and converted to constant wavenumber bandpass) of 9-F-MIA and 7,8-dF-MIA in water. For the fluorescence emission spectra, the excitation was tuned to 420 nm. The corresponding spectra of MIA in water[19] are shown for comparison. The fluorescence spectra are scaled according to their fluorescence quantum yield.

Table 1. Spectroscopic and photophysical parameters for MIA and various fluorinated MIA derivatives in H_2O.[a]

Parameters	MIA[19]	6-F-MIA[19]	7-F-MIA[19]	8-F-MIA[19]	9-F-MIA	7,8-dF-MIA
1^{st} λ_{max} [nm]	431	430	441	422	432	431
1^{st} ε_{max} [$M^{-1}cm^{-1}$]	8470	7880	9400	10220	6669	11117
1^{st} f	–	–	–	–	0.185	0.251
λ_{em} [nm]	524	524	533	534	535	519
2^{nd} λ_{max} [nm]	345	364	331	348	357	328
2^{nd} ε_{max} [M^{-1} cm^{-1}]	6250	8630	6640	5420	7679	5468
$\tilde{\nu}_{00}$ [cm^{-1}]	20750	20590	20300	21320	20393	20894
$\Delta\tilde{\nu}_s$ [cm^{-1}]	4640	5030	4520	4740	4900	4150
Φ_{fl} (±5%)	0.22	0.12	0.38[c]	0.24	0.12	0.42
1^{st} ε_{max} $\times\Phi_{fl}$ [$M^{-1}cm^{-1}$]	1863	946	3572	2453	800	4669
k_{rad}^{SB} [10^7 s^{-1}] (±5%)	4.45	3.94	4.66	5.94	3.51	5.94
τ_{fl}^{SB} [ns][d] (±10%)	4.94	3.04	7.08	4.04	3.40	7.01
τ_{fl}[ns] (± < 10%)	5.00	3.56	7.74	4.46	3.64	7.31
Φ_T (±20%)	0.5	0.4	0.2	0.5	0.4	0.3
k_{ISC} [10^7 s^{-1}] (±20%)[b]	10.0	11.2	2.6	11.2	11.0	4.1
Φ_{IC} (±20%)	0.3	0.5	0.4	0.3	0.5	0.3
k_{IC} [10^7 s^{-1}] (±20%)[b]	5.6	13.5	5.2	5.8	13.2	3.8
τ_T [μs] (±10%)[e]	5 (0.5); 39 (0.5)	11 (0.5); 44 (0.5)	44 (1)	10 (0.5); 47 (0.5)	21 (1)	43 (1)

[a] Wavelength maximum for the 1^{st} and 2^{nd} bands with the lowest absorption energies and the fluorescence maximum were determined via a Gaussian fit. The values given refer to spectra in the wavelength domain. The wavelength for absorption and emission were received from measurements with constant wavelength bandpass. Stokes shifts $\Delta\tilde{\nu}_s$ and 0–0 excitation energies $\tilde{\nu}_{00}$ are derived from spectra redrawn according to the transition dipole representation.[39] Fluorescence quantum yields Φ_{fl} were determined using coumarin 153 in ethanol as a reference (Φ'_{fl} =0.544).[38] Radiative rate constants k_{rad}^{SB} were obtained from Strickler-Berg analysis.[39–40] A prediction of the fluorescence lifetime τ_{fl}^{SB} can be achieved via $\tau_{fl}^{SB} = \Phi_{fl}/k_{rad}^{SB}$ and compared to the τ_{fl}measured by TCSPC. Triplet yields Φ_T were obtained from nanosecond transient absorption measurements with thioxanthone in methanol as a reference. [b] The values were calculated by using $k_{ISC} = \Phi_T/\tau_{fl}$ and $k_{IC} = \Phi_{IC}/\tau_{fl}$ and the specified Φ_T. Using the yields Φ_F and Φ_{ICS}, intersystem crossing rate constants k_{ISC} internal conversion quantum yields Φ_{IC} could be determined. [c] The value was updated by measurements in this study. [d] The fluorescence lifetime measurements have an average precision < 0.05% and an accuracy given by instrument calibration and linearity < 1%. [e] The relative amplitudes for the respective compounds are given for 550 nm.

spectra. For the 0–0 energies, absorption and fluorescence were redrawn as a function of wavenumber $\tilde{\nu}$ to arrive at the transition dipole representation.[39] In this representation, the absorption spectrum is redrawn according to $\varepsilon(\tilde{\nu})/\tilde{\nu}$ and the fluorescence spectrum according to $S(\tilde{\nu})/\tilde{\nu}^3$. These spectra were then normalized to their maximum. The intersection of these spectra was taken as the experimentally measured value for the 0–0 energy (here reported in wavenumber units, $\tilde{\nu}_{00}$, see Table 1). The 0–0 energy of 9-F-MIA obtained in this fashion is shifted by -357 cm^{-1} compared to the one of MIA. 7,8-dF-MIA exhibits an upshift of $+144$ cm^{-1}. Shifts of these magnitudes and signs were predicted quantum chemically.[20] The Stokes shift $\Delta\tilde{\nu}_s$ of 9-F-MIA is larger than the one of MIA, and it is the other way around for 7,8-dF-MIA. Quantum chemical computations predict a smaller Stokes shift for 9-F-MIA (4436 cm^{-1}) and 7,8-dF-MIA (4033 cm^{-1}).

The radiative rate constants k_{rad}^{SB} were determined from the spectra using the Strickler-Berg approach.[39–40] In this analysis, an integral needs to be computed that covers the lowest electronic transition in the absorption spectrum. A procedure requiring the use of the respective fluorescence spectrum was used here (see ref.[39,41] for details). According to this analysis, all derivatives feature rate constants of ~$5\cdot10^7$ s^{-1}. The one of 7,8-dF-MIA ($5.94\cdot10^7$ s^{-1}) is higher compared to MIA ($4.45\cdot10^7$ s^{-1}), whereas 9-F-MIA ($3.51\cdot10^7$ s^{-1}) has a lower one. The quantum chemical computation for 7,8-dF-MIA ($5.87\cdot10^7$ s^{-1}) is in excellent agreement.

The computed value for 9-F-MIA ($4.01\cdot10^7$ s^{-1}) deviates by only 14% from the experimental one. Together with the fluorescence quantum yield, the radiative rate constants allow predictions for the fluorescence lifetime τ_{fl}^{SB} using $\tau_{fl}^{SB} = \Phi_{fl}/k_{rad}^{SB}$. The corresponding fluorescence lifetimes are expected in the range of 3–7 ns.

Time-resolved spectroscopy

The fluorescence lifetimes were measured experimentally by time-correlated single photon counting (TCSPC) (Figure 3). Measured decays are characterized by a single-exponential function (see Methods) and obtained fluorescence lifetimes τ_{fl} are given in Table 1.

The lifetimes measured by TCSPC are longer than the ones calculated via the Strickler-Berg method, but the deviations are rather small (< 10 %). Together with previously[19] reported values we see a characteristic influence of the fluorination substitution. For 6-F-MIA, 8-F-MIA and 9-F-MIA the fluorescence lifetime is reduced and for 7-F-MIA is prolonged in comparison to MIA (5.00 ns). Interestingly, the fluorescence lifetime of the difluorinated derivative 7,8-dF-MIA is prolonged. It is in between its mono-fluorinated counterparts, but it is closer to 7-F-MIA than to 8-F-MIA.

For all MIA derivatives studied, the fluorescence quantum yields are well below one. Therefore, the non-radiative decay processes dominate. To specify the type of non-radiative decay (ISC or internal conversion (IC)), measurements were performed on a nanosecond transient absorption instrument. From these experiments, the triplet quantum yields Φ_T and hence the rate constants for ISC can be derived. The effects of fluorination on triplet yields were investigated using a relative method detailed in Ref. [19]. The difference absorption signals at time zero of the sample ($\Delta A_{t=0}(\lambda_{Pr})$) and a reference ($\Delta A^r_{t=0}(\lambda_{Pr})$) (see Supporting Information, chapter 4, Figure S3) were recorded. Thioxanthone in methanol served as a reference. The respective difference absorption coefficient spectra $\Delta\varepsilon_T(\lambda_{Pr})$ and $\Delta\varepsilon^r_T(\lambda_{Pr})$ of the sample and reference were obtained from the signals $\Delta A_{t=0}(\lambda_{Pr})$ as well as $\Delta A^r_{t=0}(\lambda_{Pr})$ and the respective ground state bleaches (see Supporting Information, chapter 4, Figure S4). With these inputs and the triplet quantum yield of the reference Φ^r_T, the yield was calculated via Equation (1):

$$\Phi_T = \frac{\Delta A_{t=0}(\lambda_{Pr})}{\Delta\varepsilon_T(\lambda_{Pr})}\frac{\Delta\varepsilon^r_T(\lambda_{Pr})}{\Delta A^r_{t=0}(\lambda_{Pr})}\Phi^r_T \quad (1)$$

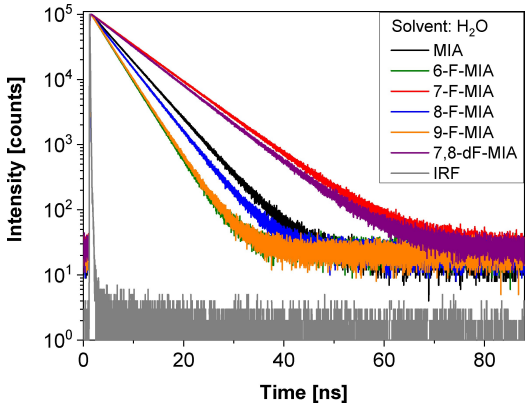

Figure 3. Fluorescence decays in H_2O measured by TCSPC. The corresponding decays in D_2O are shown in Supporting Information Figure S1.

The triplet yields Φ_T obtained in this fashion are lower for 9-F-MIA (0.4) and 7,8-dF-MIA (0.3) compared to MIA (0.5).

By using the triplet quantum yields and fluorescence lifetimes, the rate constants for ISC k_{ISC} can be computed via $k_{ISC} = \Phi_T/\tau_{fl}$. For 9-F-MIA ($11.0\cdot10^7\ s^{-1}$), a higher rate constant was computed than for MIA ($10.0\cdot10^7\ s^{-1}$), 7,8-dF-MIA ($4.1\cdot10^7\ s^{-1}$) has a lower rate constant. The magnitude $\sim10^8\ s^{-1}$ of the ISC rate constants match the previously published data of Bracker et al.[20]

For the fluorinated MIA derivatives studied, the determined quantum yields of fluorescence and triplet do not sum up to one. Thus, the derivatives also undergo the IC process in competition with the radiative decays and the ISC process. The IC quantum yield derived from $\Phi_{IC} = 1 - \Phi_{fl} - \Phi_T$ is larger for 9-F-MIA (0.5) compared to MIA (0.3) and comparable for 7,8-dF-MIA (0.3). Using the relation $k_{IC} = \Phi_{IC}/\tau_{fl}$, the respective IC rate constants can be determined. 9-F-MIA ($13.2\cdot10^7\ s^{-1}$) has a higher IC rate constant compared to MIA ($5.6\cdot10^7\ s^{-1}$), while 7,8-dF-MIA ($3.8\cdot10^7\ s^{-1}$) has a lower one.

Finally, we want to discuss the experimental sensitivity[42] ($1^{st}\ \varepsilon_{max}\times\Phi_{fl}$) in potential bioanalytical applications that is governed by the product of the absorption coefficient $1^{st}\ \varepsilon_{max}$ and the fluorescence quantum yield Φ_{fl}. According to Table 1, fluorine substitution at the positions 7 and 8 of MIA result in increased absorption coefficients. This effect is even additive, so that 7,8-dF-MIA has the largest value $1^{st}\ \varepsilon_{max} = 11117\ M^{-1}\ cm^{-1}$. At the same time, the fluorescence quantum yield stays very high due to the small rate constant of intersystem crossing. Altogether, the newly designed derivative 7,8-dF-MIA has the highest sensitivity ($1^{st}\ \varepsilon_{max}\times\Phi_{fl}$) $=4669\ M^{-1}\,cm^{-1}$ of all MIA and flavin derivatives studied in this work.

Impact of the deuterated solvent D_2O on the fluorescence

Next, we measured the fluorescence lifetimes in both H_2O and D_2O with a very high precision (< 0.05 %) to characterize the non-radiative deactivation processes in more detail. Similar to Maillard et al.,[43] we observed longer fluorescence lifetimes in D_2O for all MIA derivatives (Table 2) which indicates that the MIA derivatives are between 13 to 33 % brighter, while the absorption and fluorescence spectra as well as the absorption coefficients remain unchanged. For 7-F-MIA and 7,8-dF-MIA the fluorescence enhancement in D_2O is largest so that their fluorescence quantum yields are raised to 0.51 and 0.53, respectively.

To analyse the nature of the quenching reaction by H_2O in more detail, we consider H_2O molecules as quenchers with an effective pseudo-first order rate constant k_{qw} of the bulk (given by the water concentration). The fluorophores dissolved in D_2O are considered as "unquenched". The measured fluorescence lifetime τ_{fl} in H_2O and D_2O relate to all deactivation processes [Eq. (2)]:

$$\tau_{fl}^{(H_2O)} = \frac{1}{k_{rad} + k_{ISC}^{(H_2O)} + k_{IC}^{(H_2O)} + k_{qw}}$$

and

$$\tau_{fl}^{(D_2O)} = \frac{1}{k_{rad} + k_{ISC}^{(D_2O)} + k_{IC}^{(D_2O)}} \quad (2)$$

As absorption and fluorescence spectra are not affected by switching from H_2O to D_2O, the same radiative rate constant k_{rad} applies for both situations. This allows us to compute k_{qw} and the corresponding quenching yields, Φ_{qw}, according to Eq. (3) for all compounds.

$$k_{qw} = 1/\tau_{fl}^{(H_2O)} - 1/\tau_{fl}^{(D_2O)}$$

and

$$\Phi_{qw} = k_{qw} \cdot \tau_{fl}^{(H_2O)} \quad (3)$$

We became interested, to which extent the quenching constant has a systematic dependency and whether this is a universal feature[43] for all fluorinated MIA derivatives. Therefore, we formulate a Stern–Volmer correlation like Equation (4) (see Supporting Information, chapter 2) with an average quenching constant $\overline{k_{qw}}$, which is equivalent to Equation (3).

$$\tau_{fl}^{(D_2O)}/\tau_{fl}^{(H_2O)} = 1 + \overline{k_{qw}} \cdot \tau_{fl}^{(D_2O)}$$

assuming

$$\frac{k_{rad} + k_{ISC}^{(D_2O)} + k_{IC}^{(D_2O)}}{k_{rad} + k_{ISC}^{(H_2O)} + k_{IC}^{(H_2O)}} = 1 \quad (4)$$

Here, we also implicitly test the validity of the underlying assumption that the ratio of the sums for the internal radiative and non-radiative rate constants in H_2O and D_2O is unity for the distinct derivatives. In the following, we apply eq. 4 to the MIA derivatives (a) to (f) (filled dots in Figure 4). Indeed, in Figure 4 we observe a linear relation with an average quenching constant $\overline{k_{qw}} = 0.029\ ns^{-1}$ and an intercept, which is very close to unity. This value is in good agreement with the mean value of the individual quenching constants for MIA and its fluorinated derivatives of $0.033\ ns^{-1}$ (see Table 2). Notably, the small deviations from linearity confirm our approximation in eq. 3 and at the same time display its limits. From this we can conclude that, although the water quenching rate constants are quite similar ($\overline{k_{qw}} = 2.9 \cdot 10^7\ s^{-1} \pm 19\%$) for all MIA derivatives, the resulting water quenching yields $\Phi_{qw} = 0.17 \pm 27\%$ and the corresponding enhancement factors in D_2O vary slightly more because of the different fluorescence lifetimes.

Our analysis confirms the hypothesis that the quenching reaction of water is roughly comparable for all fluorinated MIA compounds and that the quenching yields depend on the specific S_1 lifetimes. This result is in very good agreement with studies of Maillard et al.[43] on the universal quenching by water and alcohols for 42 common organic fluorophores emitting in over the whole visible spectrum. Considering dyes with similar singlet energies of $\tilde{\nu}_{00} \approx 20500\ cm^{-1}$ (2.5 eV), the authors report values of k_{qw} in the range of $3 \pm 1 \cdot 10^7\ s^{-1}$, that excellently agree with our values in Table 2.

In view of the structural diversity of the studied fluorophores, we tested the hypothesis that the universal quenching process by water is majorly mediated by internal conversion[44] and that intersystem crossing can be modulated to a minor extent (visible by the observed small deviations that are larger than our experimental uncertainties). Therefore, we applied full fluorescence correlation spectroscopy (FCS)[45–47] to study the influence of H_2O and D_2O on the stationary triplet population T_{eq} and characteristic triplet relaxation time t_T of 7-F-MIA. We

Table 2. Fluorescence lifetimes τ_{fl} of MIA derivatives in H_2O and D_2O measured by TCSPC.

Parameters	MIA	6-F-MIA	7-F-MIA	8-F-MIA	9-F-MIA	7,8-dF-MIA
$\tau_{fl}^{(H_2O)}$ [ns][a]	5.00	3.56	7.74	4.46	3.64	7.31
$\tau_{fl}^{(D_2O)}$ [ns][a]	5.76	4.20	10.32	5.01	4.24	9.29
$\Phi_{fl}^{(D_2O)}$	0.25	0.14	0.51	0.27	0.14	0.53
Φ_{qw} [b]	0.13	0.15	0.25	0.11	0.14	0.21
k_{qw} [$10^7\ s^{-1}$][c]	2.6	4.3	3.2	2.5	3.9	2.9

[a] The fluorescence lifetime measurements have an average precision $< 0.05\%$ and an accuracy given by instrument calibration and linearity $< 1\%$. [b] The water quenching yields [Eq. (3)] have an average precision $< 0.15\%$ and an accuracy given by the fluorescence lifetime measurement $< 1\%$. [c] The quenching constant of water k_{qw} was computed by Eq. (3) with a precision of $< 0.15\%$.

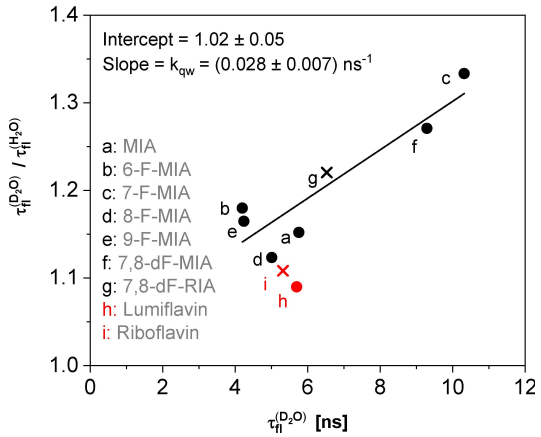

Figure 4. Stern–Volmer plot: The ratio of fluorescence lifetimes in D_2O over H_2O against the lifetimes in D_2O. Compounds with a methyl group at position 10 of the isoalloxazine are depicted as dots and compounds with a ribityl group with the cross. The symbols of fluorinated compounds are displayed in black and the compounds with the naturally occurring 7,8-dimethyl-isoalloxazine (flavin) core are displayed in red. The linear regression is only applied to compounds of MIA family (a to f, filled dots). The slope corresponds to an average quenching constant in water, $\overline{k_{qw}} = 0.028\ ns^{-1}$. The standard errors were not shown as they are smaller than the symbol size.

selected 7-F-MIA for several reasons: (1) very high brightness, (2) a strong fluorescence enhancement in D_2O, and (3) the rate constants k_{qw} and k_{ISC} are approximately equal in H_2O, so that a potential change of intersystem crossing in D_2O could be detected with high sensitivity. The normalized full correlation curves $G(t_c)$ of 7-F-MIA are displayed as a function of the correlation time t_c in Figure 5.

In both solvents, the correlation curves exhibit similar distinctive features in the three characteristic time regimes antibunching, triplet and translational diffusion. The rise term in D_2O is slower because the excited state lifetime is prolonged. Notably, the triplet terms in H_2O and D_2O are quite similar in air-saturated solution. Thus, a significant difference of the underlying key triplet parameters, rate constant for intersystem crossing k_{ISC} and triplet depopulation k_T, can be excluded. The value of k_{ISC} of $2.58 \cdot 10^7\ s^{-1}$ recovered by FCS for both conditions excellently agrees with result obtained by transient absorption spectroscopy in Table 1. The triplet decay is faster in the FCS experiment due to oxygen from air. The kinetic scheme (Figure 6) and a detailed description of analysis procedure for determining the triplet parameters is given in the experimental section. The final decay of $G(t_c)$ due to translational diffusion is slightly longer in D_2O, because its viscosity is approximately

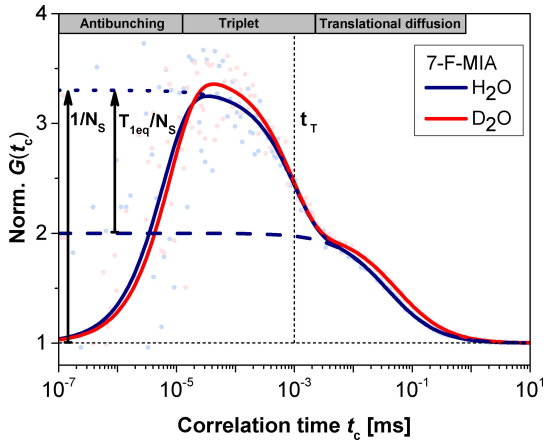

Figure 5. Normalized and averaged full correlation curves $G(t_c)$ of 7-F-MIA in air-saturated H_2O and D_2O at nanomolar concentrations. The detailed analysis and the fitted model function [solid lines, Equations (6), (7)] are described in the experimental section. The overall and unnormalized amplitude of $G(t_c)$ is related to the inverse number of bright molecules in the singlet state N_s. The obtained triplet parameters were the triplet fraction $T_{1eq} = 0.56 \pm 0.01$ and the triplet relaxation time $t_T = (1.02 \pm 0.06)$ µs for H_2O and $T_{1eq} = 0.59 \pm 0.01$ and $t_T = (0.92 \pm 0.07)$ µs for D_2O. The dashed lines represent the contributions of the translational diffusion and triplet term to the fitted model function [Eq. (6)] with the following additional parameters: $t_d = 37$ µs, $z_0/\omega_0 = 6$ (fixed), $AB = 1$ (fixed), $t_{AB} = 6.0$ ns for H_2O and $t_d = 54$ µs, $z_0/\omega_0 = 6$ (fixed), $AB = 1$ (fixed), $t_{AB} = 8.1$ ns for D_2O.

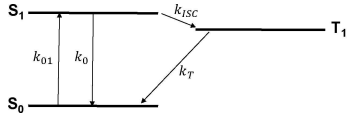

$$\begin{pmatrix} -k_{01} & k_0 & k_T \\ k_{01} & -(k_0 + k_{ISC}) & 0 \\ 0 & k_{ISC} & -k_T \end{pmatrix}$$

Figure 6. Assumed kinetic scheme (left side) and the rate matrix (right side). The solution of the kinetic scheme is given in Equations (7)–(9).

25% higher.[48–49] To conclude, our FCS measurements show that the triplet properties of 7-F-MIA are not majorly changed in D_2O, i.e. FCS confirms our hypothesis that the fluorescence enhancement in D_2O cannot be caused by a reduction of rate of intersystem crossing but by a reduction of internal conversion.

Impact of the ribityl group

Finally, we studied the effect of the ribityl residue at position 10 of the isoalloxazine ring. For this, we compared the fluorescence lifetimes of 7,8-dF-RIA (**13**) with the natural analogue riboflavin and studied the accord with the corresponding derivatives incorporating a methyl group at position 10 (7,8,10-trimethyl-isoalloxine referred to as lumiflavin) (Table 3). In both ribityl derivatives, the fluorescence lifetime in H_2O is reduced and the quenching constant of water k_{qw} is increased by approx. 20% as compared to the corresponding methyl-substituted compounds 7,8-dF-MIA and lumiflavin (Table 3). Moreover, from the comparison between the 10-ribityl- and 10-methyl derivatives, it obvious that the ribityl substitution leads to a reduction of fluorescence with the rate constant k_{qRib} that has a similar order of magnitude as water quenching k_{qw} and is solvent independent. It is remarkable that both quenching constants k_{qw} and k_{qRib} are three times smaller for non-fluorinated flavin derivatives as compared to fluorinated derivatives. Notably, the significantly lower fluorescence reduction of non-fluorinated flavin derivatives by the ribityl substituent is also visible in the Stern–Volmer analysis in Figure 4 (red symbols).

Again, we applied FCS to investigate which non-radiative deactivation process is influenced by the ribityl substituent. The analysis of the correlation functions of 7,8-dF-MIA and 7,8-dF-RIA in D_2O (see Supporting Information, Figure S2 and chapter 3) shows that k_{ISC} ($1.54 \cdot 10^7\ s^{-1} \pm 21\%$) of 7,8-dF-RIA is

Table 3. Fluorescence lifetimes τ_{fl} of 7,8-dF-RIA in relation to flavins in H_2O and D_2O measured by TCSPC.

Parameters	7,8-dF-MIA	7,8-dF-RIA	Lumi-flavin	Ribo-flavin
$\tau_{fl}^{(H_2O)}$ [ns][a]	7.31	5.35	5.23	4.80
$\tau_{fl}^{(D_2O)}$ [ns][a]	9.29	6.53	5.70	5.32
Φ_{qw} [b]	0.21	0.18	0.07	0.08
k_{qw} /[$10^7\ s^{-1}$][c]	2.9	3.4	1.6	2.0
$k_{qRib}^{(H_2O)}$ [$10^7\ s^{-1}$][d]		5.0		1.7
$k_{qRib}^{(D_2O)}$ [$10^7\ s^{-1}$][d]		4.6		1.3

[a] The fluorescence lifetime measurements have an average precision < 0.05% and an accuracy given by instrument calibration and linearity < 1%. [b] The water quenching yields [Eq. (1)] have an average precision < 0.15% and an accuracy given by the fluorescence lifetime measurement < 1%. [c] The quenching constant of water k_{qw} was computed by Equation (3) with a precision of < 0.15%. [d] The quenching constant of the ribityl chain k_{qRib} was computed by $k_{qRib} = 1/\tau_{fl}^{(Rib-derivative)} - 1/\tau_{fl}^{(Me-derivative)}$ with a precision of < 0.15%.

not increased with respect to 7,8-dF-MIA. Thus, the reduction of the fluorescence lifetime by the ribityl substituent is caused by additional internal conversion processes.

Conclusion

To develop bright fluorophores, it is essential to minimize non-radiative deactivation processes that compete with fluorescence.

In previous work,[19–20] we have demonstrated that rational design regarding the photophysical properties of new flavin derivatives using quantum chemical calculations works to predict state energies as well as radiative and ISC rate constants. To find even brighter MIA derivatives, we had applied these methodologies and computed the properties of the electronic states of further MIA compounds, 9-F-MIA and 7,8-dF-MIA. Here, these derivatives were also synthesized and characterized experimentally. The predicted similarity of 9-F-MIA with 6-F-MIA was reproduced experimentally. Moreover, the predicted high fluorescence quantum yield of 7,8-dF-MIA was also experimentally confirmed. The small rate constant of intersystem crossing due to a higher energy of the $^3\pi\pi^{*u}$ state can be rationalized by the additivity of the energy shifts of both 7-F-MIA and 8-F-MIA (Figure 7).

This shows that quantum chemical calculations are already on a very high level to make tailor design of fluorescence probes for microscopy feasible. Additionally, the fluorinated flavin derivative 7,8-dF-RIA as a first example of a fluorescent probe for analytical applications and fluorescence microscopy was synthesized. The fluorescence lifetime measurements of 7,8-dF-RIA revealed that the incorporation of the ribityl group reduces its fluorescence by 27%, so that its fluorescence quantum yield drops to 0.31 (Table 3). Nevertheless, it is still brighter than natural flavin with $\Phi_{fl} = 0.20$.[50] The fluorescence enhancement of all MIA derivatives in D_2O demonstrates that the quenching by protic solvents is also significant. The FCS measurements of 7-F-MIA in H_2O and D_2O (Figure 5) reveal that internal conversion is the main process caused by water quenching. Millard et al.[43] studied the fluorescence quenching of 42 distinct dyes by protic solvents in detail. For dyes with $E_{0,0} < 2.1$ eV, they suggest that an efficient universal and water-specific deactivation by dipolar coupling between the fluorophore and water by Förster resonance energy transfer from the electronic (vibronic) excited fluorophore state and isoenergetic vibrational oscillators of the solvent. Comparing D_2O with H_2O, the absorbance by O–D stretching vibrations is more than order of magnitude smaller.[51] For other fluorophores and our flavin derivatives with $E_{0,0} \approx 2{,}6$ eV, the predicted rate constant of FRET quenching drops to $\approx 2 \cdot 10^6\ s^{-1}$ so that additional solvent-mediated deactivation processes are proposed.[43–44]

Altogether, we predicted and synthesized the new MIA derivative 7,8-dF-MIA that has the highest sensitivity $(1^{st}\ \varepsilon_{max} \times \Phi_{fl}) = 4669\ M^{-1}cm^{-1}$ of all MIA and flavin derivatives studied in this work. Its fluorescence quantum yield is enhanced even further in D_2O ($\phi_{fl}^{(D_2O)} = 0.53$) in concord with a very long fluorescence lifetime ($\tau_{fl}^{(D_2O)} = 9.3\ ns$) that makes 7,8-dF-MIA a promising probe for bioanalytical applications.

Experimental Section

Steady-state measurements

Absorption spectra were carried out with a two-beam absorption spectrometer from PerkinElmer (Lambda 19). Steady-state fluorescence measurements were carried out using a HORIBA Scientific instrument (FluoroMax-4). The spectral sensitivity of the instrument as well as the solvent background were corrected. Absorbance was adjusted for all fluorescence measurements to be less than 0.05 per cm at the excitation wavelength (420 nm) to avoid inner filter effects.

Time-correlated single photon counting

Time-correlated single photon counting (TCSPC) was performed using a fluorescence lifetime and steady-state spectrometer (FT300 with hybrid PMT detector, PicoQuant, Germany). Excitation was

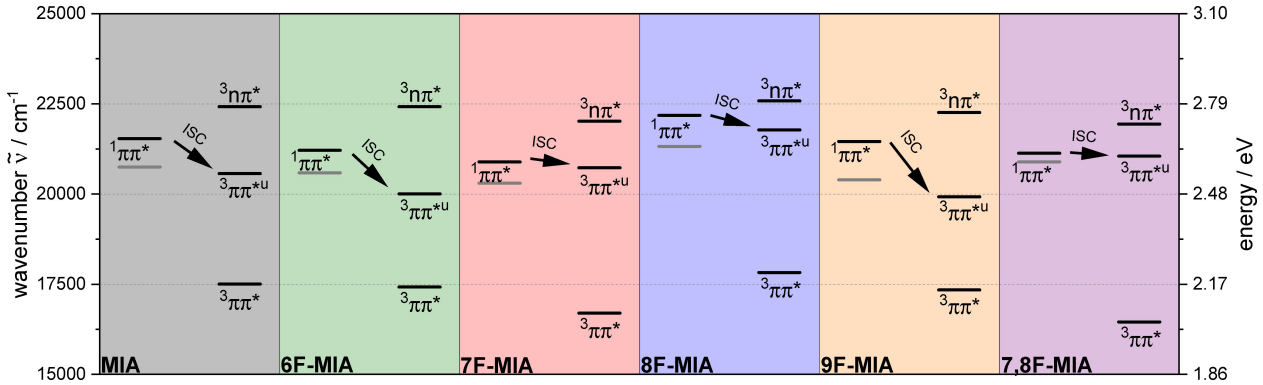

Figure 7. Schematic representation of experimental and calculated adiabatic energies for MIA as reference and the fluorinated derivatives in aqueous solution.[20] Gray bars represent experimental 0–0 energies of the singlet states for the respective compounds. Black bars represent the quantum chemical ones.[20] The values include zero-point vibrational energy (ZPVE) corrections for the equilibrium geometries.[20] Note that the changes in the rate constant of the intersystem crossing correlate with the energetic transition between the $^1\pi\pi^*$ and $^3\pi\pi^{*u}$ states in the mono-fluorinated derivatives. The additive behaviour of the energy shifts explains the small rate constant of the intersystem crossing in the di-fluorinated compound.

achieved with a supercontinuum laser excitation source (EXW-12 with EXTEND-UV spectral extension unit, NKT Photonics, Denmark) running at a repetition rate of 11.1 MHz. Excitation wavelengths were set by tuning the frequency doubler. They were selected to match the absorption maxima. MIA, 6-F-MIA, 9-F-MIA and 7,8-dF-MIA were excited at 430 nm, 7-F-MIA at 440 nm, and 8-F-MIA at 420 nm. Emission was detected under magic angle conditions (excitation polarizer 0 – emission polarizer 54.7). Input and output slit widths were set to 1000 μm which corresponds to a detection bandpass of 5.4 nm. Detection wavelengths were selected to match the fluorescence maxima, i.e. 525 nm, 530 nm, 535 nm, 510 nm, 540 nm, and 520 nm for MIA, 6-F-MIA, 7-F-MIA, 8-F-MIA, 9-F-MIA, and 7,8-dF-MIA respectively. Measurements were performed at 20 C. All samples were measured in Quartz Macro Cell type 111-QS cuvettes (Hellma) with a light path of 1 cm and a sample volume of 3 mL. As solvents, double-distilled water (H_2O) and heavy water (D_2O) from Aldrich (99.9 atom % D) were used. The concentration of the sample was in the range of 10^{-6} to 10^{-5} M in all measurements. For the instrument response function (IRF), Ludox HS-30 colloidal silica water suspension (Aldrich) with a zero lifetime was used. Fitting was performed with the program ChiSurf.[52] The instrument response function (IRF) full width at half maximum was around 100 ps, and it was taken into account in the fit via convolution. A single exponential fit function including a constant offset to account for detector dark counts and afterpulsing was applied to the data to obtain the fluorescence lifetime of a sample.

Nanosecond transient absorption spectrometer

Nanosecond transient absorption data were acquired using a transient absorption spectrometer from Edinburgh Instruments in a right-angle geometry (LP980).[53] The excitation source was a Nd:YAG laser (Spitlight 600, InnoLas, repetition rate 5 Hz, pulse duration of 12 ns (FWHM), diameter of the pump beam ~8 mm) with an excitation wavelength of 355 nm which was generated by frequency-tripling. The average pulse energy amounted to 0.5 mJ. A pulsed xenon lamp (Osram XBO 150 W/CR OFR) was used as a probe beam. Fused silica flow-through cuvettes from the manufacturer Hellma were used, with a path length of 5 mm in the pump and 10 mm in the probe direction. The absorption was adjusted to 0.65 per cm at the excitation wavelength. The transmitted probe light was dispersed with a grating monochromator and detected by using a Hamamatsu photomultiplier covering the UV/Vis spectral range (PMT-900). To acquire transient spectra, kinetic traces were recorded every 5 nm and averaged over 80 acquisitions. Typical data are shown in Supporting Information Figures S3 and S4. The nanosecond transient absorption data $\Delta A(\lambda, t)$ were analysed by global multi-exponential fit function via Equation (5).[54–55]

$$\Delta A(\lambda, t) = \mathrm{IRF} \otimes \sum_{i=1}^{n} \Delta A_i(\lambda) e^{-t/\tau_i} \tag{5}$$

The exponential decay functions were convoluted with the response function (IRF) of the instrument (FWHM; 12 ns). $\Delta A_i(\lambda)$ stand for the decay associated difference spectra with the respective time constants τ_i.

Fluorescence correlation spectroscopy (FCS)

Fluorescence correlation spectroscopy (FCS) measurements were performed using a confocal fluorescence microscope (FV1000, Olympus) with extension for time-resolved experiments.[56] The samples were excited by a laser diode at 440 nm (LDH-D-C 440, PicoQuant) in continuous wave mode. The laser beam was directed by a dichroic beam splitter into the microscope objective (Olympus 60X, NA 1.20, water immersion) and focused in the sample close to the diffraction limit. The emitted light was separated into polarisations parallel and perpendicular relative to the excitation beam (PBS 101, Thorlabs). In each channel the light, after passing a dichroic beam splitter (BS 560, AHF) and a bandpass filter (HC520/35, AHF) was focused on a single photon sensitive detector (PDM50-CTC, Micro Photon Devices). The photon trace was recorded by a TCSPC module (HydraHarp 400, PicoQuant). Custom software (LabVIEW based) was used to analyse the received data. The full correlation curves were measured in air at nanomolar concentrations of 7-F-MIA at 23 C for 30 minutes and repeated four times each.

The setup was calibrated measuring the translational diffusion times of Rhodamine 110 in H_2O and D_2O ($t_d = 45$ μs and 56 μs, respectively). To this end, the following model function was fitted to the FCS curves [Equation (6)]:

$$G(t_c) = \mathrm{offset} + \frac{1}{N_S} \cdot \frac{1}{1+\frac{t_c}{|t_d|}} \cdot \frac{1}{\sqrt{\left(1+\frac{t_c}{\left(\frac{z_0}{\omega_0}\right)^2 \cdot |t_d|}\right)}} \cdot \left(1 - |T_{1eq}| + |T_{1eq}| \cdot e^{-\left(\frac{t_c}{|t_T|}\right)}\right) \cdot \left(1 - |AB| \cdot e^{-\left(\frac{t_c}{|t_{AB}|}\right)}\right) \tag{6}$$

with the number of bright molecules in the singlet state N_S, their translational diffusion time t_d, the axial ratio of the detection volume element z_0/ω_0 and T_{1eq}, t_T, AB and t_{AB} the amplitude and relaxation time corresponding to the triplet kinetics and the antibunching, respectively.

The known diffusion coefficient of Rhodamine 110 of $4.3 \cdot 10^{-6}$ cm^2 s^{-1} at 22.5 C in water[57] was rescaled to the experimental conditions using Stokes-Einstein equation and the temperature-dependent viscosity of the two solvents (H_2O: 0.9321 mPa·s at 23 C;[48] D_2O: 1.1562 mPa·s at 23 C.[49] A constant hydrodynamic radius of R110 was assumed. This way the radial extension of the confocal detection volume element $\omega_0 = 0.276$ μm was confirmed to be identical within the experimental error (±5 %) in both cases.

We used the reported absorption coefficient of $\varepsilon = 9400$ M^{-1} cm^{-1} at 441 nm[19] to compute excitation rate k_{01} in the next step. In agreement with Maillard et al.,[43] we find no differences for the absorption spectra and absorption coefficients of 7-F-MIA between H_2O and D_2O.

To avoid losses by reflection, we measured the laser power P at the sample with an immersion power meter: $P = 65$ μW. Widengren et al.[45] showed that the size of the confocal observation volume defined by the pinhole slightly affects the effective value for the average irradiance I_{av} in the top hat approximation. As lower limit for the mean irradiance, we estimate $I_{av} = 1.2\ P/(\pi\ \omega_0^2) = 32.6$ kW/cm^2 for H_2O and D_2O, which results in an excitation rate constant of $k_{01} = 0.26 \cdot 10^7$ s^{-1}. This is a slight underestimation of the absolute value of I_{av}, since a confocal aperture of about 1.5 AU was used to collect photons most efficiently. Thus, we compute also an upper limit for the mean irradiance by $I_{av} = 1.6\ P/(\pi\ \omega_0^2) = 43.5$ kW/cm^2, which results in an excitation rate of $k_{01} = 0.35 \cdot 10^7$ s^{-1}. The characteristic rise time of the antibunching term t_{AB} describing the population of the S_1 state is related to the whole kinetic scheme according to Equation (9). The time regime of the antibunching was too noisy to give reproducible results but served to stabilize the fit.

To relate the FCS observables, the amplitude connected to the triplet fraction T_{1eq} and the triplet relaxation time t_T, the kinetic

scheme (left side) with the corresponding rate matrix (right) must be solved.

$$T_{1eq} = \frac{k_{ISC}}{k_T} S_{1eq} = \frac{k_{ISC} \cdot k_{01}}{k_{01} \cdot (k_{ISC} + k_T) + k_T \cdot (k_0 + k_{ISC})} \tag{7}$$

$$\frac{1}{t_T} = \frac{1}{2}\left(-\sqrt{(k_0 + k_{01} + k_{ISC} + k_T)^2 - 4(k_0 k_T + k_{01} k_{ISC} + k_{01} k_T + k_{ISC} k_T)} + k_0 + k_{01} + k_{ISC} + k_T\right) \tag{8}$$

$$\frac{1}{t_{AB}} = \frac{1}{2}\left(\sqrt{(k_0 + k_{01} + k_{ISC} + k_T)^2 - 4(k_0 k_T + k_{01} k_{ISC} + k_{01} k_T + k_{ISC} k_T)} + k_0 + k_{01} + k_{ISC} + k_T\right) \tag{9}$$

Considering the independently measured fluorescence lifetimes ($= 1/k_0$) of 7.74 ns (H_2O) and 10.32 ns (D_2O), the experimental results are consistent with an intersystem crossing rate of $k_{ISC} = 2.58 \cdot 10^7\ s^{-1}$ and a triplet depopulation rate of $k_T = 0.043 \cdot 10^7\ s^{-1}$ for both cases, assuming excitation rates $k_{01} = 0.34 \cdot 10^7\ s^{-1}$ (H_2O) and $k_{01} = 0.31 \cdot 10^7\ s^{-1}$ (D_2O). This would correspond to a 10% smaller focal area in H_2O, well within the experimental error. A significant difference in triplet depopulations has not been observed for the two solvents.

Acknowledgements

Funding by the Deutsche Forschungsgemeinschaft (DFG, German Research Foundation) – 396890929/GRK 2482 (ModISC) is most gratefully acknowledged. We also thank the CeMSA@HHU (Center for Molecular and Structural Analytics @ Heinrich Heine University) for recording the NMR- and MS-spectroscopic data. CAMS thanks Alexandre Fürstenberg for the stimulating discussions on the fluorescence enhancement induced by D_2O. Open Access funding enabled and organized by Projekt DEAL.

Conflict of Interest

The authors declare no conflict of interest.

Data Availability Statement

The data that support the findings of this study are available in the supplementary material of this article.

Keywords: flavin · fluorine · intersystem crossing · fluorescence time-resolved spectroscopy

[1] A. Losi, *Photochem. Photobiol.* **2007**, *83*, 1283–1300.
[2] L. O. Björn, *Photobiology: The Science of Life and Light*; Springer: New York, **2007**.
[3] M. A. van der Horst, K. J. Hellingwerf, *Acc. Chem. Res.* **2004**, *37*, 13–20.
[4] E. Silva, A. M. Edwards, *Flavins: Photochemistry and Photobiology*; The Royal Society of Chemistry: Cambridge, UK, **2006**.
[5] A. R. Cashmore, J. A. Jarillo, Y.-J. Wu, D. Liu, *Science* **1999**, *284*, 760–765.
[6] R. Banerjee, A. Batschauer, *Planta* **2005**, *220*, 498–502.
[7] A. Losi, W. Gärtner, *Annu. Rev. Plant Biol.* **2012**, *63*, 49–72.
[8] R. P. Sinha, D.-P. Häder, *Photochem. Photobiol. Sci.* **2002**, *1*, 225–236.
[9] W. R. Briggs, J. M. Christie, *Trends Plant Sci.* **2002**, *7*, 204–210.
[10] E. Liscum, D. W. Hodgson, T. J. Campbell, *Plant Physiol.* **2003**, *133*, 1429–1436.
[11] T. Pavlovska, R. Cibulka, *Structure and Properties of Flavins. In Flavin-Based Catalysis*, **2021**, S. 1–27.
[12] V. Massey, *Biochem. Soc. Trans.* **2000**, *28*, 283–296.
[13] J. Svoboda, H. Schmaderer, B. König, *Chem. Eur. J.* **2008**, *14*, 1854–1865.
[14] N. A. Romero, D. A. Nicewicz, *Chem. Rev.* **2016**, *116*, 10075–10166.
[15] T. Hering, B. Mühldorf, R. Wolf, B. König, *Angew. Chem. Int. Ed.* **2016**, *55*, 5342–5345; *Angew. Chem.* **2016**, *128*, 5428–5431.
[16] S. Fukuzumi, K. Tanii, T. Tanaka, *J. Chem. Soc. Perkin Trans. 2* **1989**, 2103–2108.
[17] A. Rehpenn, A. Walter, G. Storch, *Synthesis* **2021**, *53*, 2583–2593.
[18] A. Kormányos, M. S. Hossain, G. Ghadimkhani, J. J. Johnson, C. Janáky, N. R. de Tacconi, F. W. Foss, Jr., Y. Paz, K. Rajeshwar, *Chem. Eur. J.* **2016**, *22*, 9209–9217.
[19] A. Reiffers, C. Torres Ziegenbein, A. Engelhardt, R. Kühnemuth, P. Gilch, C. Czekelius, *Photochem. Photobiol.* **2018**, *94*, 667–676.
[20] M. Bracker, F. Dinkelbach, O. Weingart, M. Kleinschmidt, *Phys. Chem. Chem. Phys.* **2019**, *21*, 9912–9923.
[21] M. Bracker, M. K. Kubitz, C. Czekelius, C. M. Marian, M. Kleinschmidt, *ChemPhotoChem* **2022**, e202200040.
[22] M. Mansurova, J. Simon, S. Salzmann, C. M. Marian, W. Gärtner, *ChemBioChem* **2013**, *14*, 645–654.
[23] L. Jullien, A. Gautier, *Methods Appl. Fluoresc.* **2015**, *3*, 042007.
[24] T. Drepper, T. Eggert, F. Circolone, A. Heck, U. Krauß, J.-K. Guterl, M. Wendorff, A. Losi, W. Gärtner, K.-E. Jaeger, *Nat. Biotechnol.* **2007**, *25*, 443–445.
[25] X. Shu, V. Lev-Ram, T. J. Deerinck, Y. Qi, E. B. Ramko, M. W. Davidson, Y. Jin, M. H. Ellisman, R. Y. Tsien, *PLoS Biol.* **2011**, *9*, e1001041.
[26] B. M. Medina, D. Beljonne, H.-J. Egelhaaf, J. Gierschner, *J. Chem. Phys.* **2007**, *126*, 111101.
[27] B. E. Smart, *J. Fluorine Chem.* **2001**, *109*, 3–11.
[28] A. Bondi, *J. Phys. Chem.* **1964**, *68*, 441–451.
[29] J. C. Biffinger, H. W. Kim, S. G. DiMagno, *ChemBioChem* **2004**, *5*, 622–627.
[30] B. Cordero, V. Gómez, A. E. Platero-Prats, M. Revés, J. Echeverría, E. Cremades, F. Barragán, S. Alvarez, *Dalton Trans.* **2008**, 2832–2838.
[31] K. Klehs, C. Spahn, U. Endesfelder, S. F. Lee, A. Fürstenberg, M. Heilemann, *ChemPhysChem* **2014**, *15*, 637–641.
[32] S. A. Brown, C. J. Rizzo, *Synth. Commun.* **1996**, *26*, 4065–4080.
[33] V. Kumar, K. A. Woode, R. F. Bryan, B. A. Averill, *J. Am. Chem. Soc.* **1986**, *108*, 490–496.
[34] K. Cheng, S. Li, X. Lv, Y. Tian, H. Kong, X. Huang, Y. Duan, J. Han, Z. Xie, C. Liao, *Bioorg. Med. Chem. Lett.* **2019**, *29*, 1012–1018.
[35] J. J. Hasford, C. J. Rizzo, *J. Am. Chem. Soc.* **1998**, *120*, 2251–2255.
[36] M. Mansurova, M. S. Koay, W. Gärtner, *Eur. J. Org. Chem.* **2008**, *2008*, 5401–5406.
[37] S. Salzmann, J. Tatchen, C. M. Marian, *J. Photochem. Photobiol. A* **2008**, *198*, 221–231.
[38] K. Rurack, M. Spieles, *Anal. Chem.* **2011**, *83*, 1232–1242.
[39] W. W. Parson, *Modern optical spectroscopy, Vol. 2*, Springer, **2007**.
[40] S. J. Strickler, R. A. Berg, *J. Chem. Phys.* **1962**, *37*, 814–822.
[41] J. Mooney, P. Kambhampati, *J. Phys. Chem. Lett.* **2013**, *4*, 3316–3318.
[42] C. R. Cantor, P. R. Schimmel, *Biophysical Chemistry, Part II: Techniques for the study of biological structure and function*, Freeman and Company: New York, **1980**, S. 443.
[43] J. Maillard, K. Klehs, C. Rumble, E. Vauthey, M. Heilemann, A. Fürstenberg, *Chem. Sci.* **2021**, *12*, 1352–1362.
[44] P. Fita, M. Fedoseeva, E. Vauthey, *J. Phys. Chem. A* **2011**, *115*, 2465–2470.
[45] J. Widengren, U. Mets, R. Rigler, *J. Phys. Chem.* **1995**, *99*, 13368–13379.
[46] S. Felekyan, R. Kühnemuth, V. Kudryavtsev, C. Sandhagen, W. Becker, C. A. M. Seidel, *Rev. Sci. Instrum.* **2005**, *76*, 083104.
[47] P. A. W. van den Berg, J. Widengren, M. A. Hink, R. Rigler, A. J. W. G. Visser, *Spectrochim. Acta Part A* **2001**, *57*, 2135–2144.

[48] M. L. Huber, R. A. Perkins, A. Laesecke, D. G. Friend, J. V. Sengers, M. J. Assael, I. N. Metaxa, E. Vogel, R. Mareš, K. Miyagawa, *J. Phys. Chem. Ref. Data* **2009**, *38*, 101–125.
[49] M. J. Assael, S. A. Monogenidou, M. L. Huber, R. A. Perkins, J. V. Sengers, *J. Phys. Chem. Ref. Data* **2021**, *50*, 033102.
[50] A. Kotaki, K. Yagi, *J. Biochem.* **1970**, *68*, 509–516.
[51] W. C. Waggener, *Anal. Chem.* **1958**, *30*, 1569–1570.
[52] T.-O. Peulen, O. Opanasyuk, C. A. M. Seidel, *J. Phys. Chem. B* **2017**, *121*, 8211–8241.
[53] W. Haselbach, J. M. Kaminski, L. N. Kloeters, T. J. J. Müller, O. Weingart, C. M. Marian, P. Gilch, B. E. Nogueira de Faria, *Chem. Eur. J.* **2023**, *29*, e202202809.
[54] H. Satzger, W. Zinth, *Chem. Phys.* **2003**, *295*, 287–295.
[55] I. H. M. van Stokkum, D. S. Larsen, R. van Grondelle, *Biochim. Biophys. Acta Bioenerg.* **2004**, *1657*, 82–104.
[56] S. Weidtkamp-Peters, S. Felekyan, A. Bleckmann, R. Simon, W. Becker, R. Kühnemuth, C. A. M. Seidel, *Photochem. Photobiol. Sci.* **2009**, *8*, 470–480.
[57] P. O. Gendron, F. Avaltroni, K. J. Wilkinson, *J. Fluoresc.* **2008**, *18*, 1093–1101.

Manuscript received: March 21, 2022
Revised manuscript received: March 24, 2023
Accepted manuscript online: March 27, 2023
Version of record online: May 15, 2023

ChemPhotoChem

Supporting Information

Increasing the Fluorescence Quantum Yield and Lifetime of the Flavin Chromophore by Rational Design

Mira K. Kubitz, Wiebke Haselbach, Dragana Sretenović, Mario Bracker, Martin Kleinschmidt, Ralf Kühnemuth, Claus A. M. Seidel,* Peter Gilch,* and Constantin Czekelius*

Table of contents

1 Synthesis

1.1 General description

Chemicals and equipment

In all experiments chemicals by the companies MERCK, ACROS, FLUKA, SIGMA ALDRICH, TCI, FLUOROCHEM, J&K, EURISOTOP, APOLLO SCIENTIFIC, CARBOLUTION and BLDPHARM were used and if necessary purified by recrystallisation or distillation before use. The solvents *n*-hexane, ethyl acetate, dichloromethane and acetone for work-up and purification were purchased in technical purity and distilled before use by a rotary evaporator ROTAVAPOR R-210 by the company BÜCHI and diaphragm pumps by VACUUBRAND. All other solvents as well as those used for syntheses were purchased in analytical purity, dried over molecular sieve if necessary and used without further purification. Dry solvents like dichloromethane and toluene were taken from a solvent drying system MBRAUN MB SPS-800.

Air-sensitive reactions were carried out under exclusion of oxygen and water on a combined vacuum-nitrogen line using conventional Schlenk techniques. Glass appliances were dried in a compartment dryer overnight at 120 °C and then additionally heated under high vacuum with a heat gun by METERK. High vacuum was generated by a rotary vane oil pump by VACUUBRAND. Nitrogen was dried by molecular sieve (3 Å) and orange gel before use and nitrogen flow was checked by a bubble counter. Liquids were transferred by syringe through a septum and solids were added to the reaction flask in nitrogen countercurrent. If necessary, reaction mixtures or solvents were degassed by purging nitrogen through or by freeze-pump-thaw method.

For stirring, a PTFE-coated stirring bar and magnetic stirrers with heating plates by IKA RCT or HEIDOLPH MR were used, which were equipped with a thermometer and a silicone oil bath. Room temperature reactions are considered within a range of 18-30 °C. An ice-water bath and an acetone dry ice bath were used to generate temperatures of 0 °C and -78 °C, respectively. The rotary evaporator ROTAVAPOR R-210 by BÜCHI and a diaphragm pump by VACUUBRAND were used to remove solvents *in vacuo*.

Chromatography

Thin layer chromatography was performed on ALUGRAM® XTRA SIL G/UV_{254} standard silica aluminum plates by MACHEREY-NAGEL to check the progress of reactions and flash chromatography. The spots were detected by means of UV light (254 nm) and/or by staining with a potassium permanganate solution of the composition 3.0 g $KMnO_4$, 20 g K_2CO_3, 5.0 ml 5% NaOH and 300 ml H_2O and then developed with a heat gun by METERK. For flash

chromatography silica gel 60M by MACHEREY-NAGEL was used. Flash chromatography was either performed manually with nitrogen pressure or by using a MPLC system by BÜCHI including a CONTROL UNIT C-620, a FRACTION COLLECTOR C-660, a UV PHOTOMETER C-640 and PUMP MODULES C-605. Reversed Phase HPLC was performed using the following devices: KNAUER HPLC PUMP 64, MERCK-HITACHI L-6250 INTELLIGENT PUMP, KNAUER DYNAMIC MIXING CHAMBER, KNAUER AUTOMATIC HPLC VALVE, LATEK HMV-P, KNAUER VARIABLE WAVELENGTH MONITOR, MERCK-HITACHI L-4000 UV DETECTOR, ERMA DEGASSER ERC-3510, WATERS FRACTION COLLECTOR II, LICHROSPHER® 100 RP-18 (5 MM) SORBENT LOT NO. HX391811 HIBAR® RT 250-25, KNAUER EUROSPHER 100-C18 (5 MM), 4.0 MMID. For data processing, the program CLARITY was used.

Analytics

For NMR-spectroscopy chloroform-*d*, methanol-d_4 and dimethylsulfoxide-d_6 were used. The standardization of the NMR spectra was performed using the following (residual) proton signals of the solvents:[1]

Chloroform-*d*:	^{1}H-NMR	δ = 7.26 ppm.
	^{13}C-NMR	δ = 77.16 ppm.
Methanol-d_4:	^{1}H-NMR	δ = 3.31 ppm.
	^{13}C-NMR	δ = 49.00 ppm.
Dimethylsulfoxide-d_6:	^{1}H-NMR	δ = 2.50 ppm.
	^{13}C-NMR	δ = 39.52 ppm.

For evaluation, the multiplicities of the NMR-Signals were abbreviated as follows: singlet = s, doublet = d, triplet = t, quartet = q and multiplet = m and combinations of these. Coupling constants *J* are given in Hertz (Hz) and chemical shifts *δ* in ppm. The following devices were used for recording of the NMR-spectra:

NMR-Spectroscopy	^{1}H-NMR	BRUKER AVANCE III – 300, 300 MHz
		BRUKER AVANCE III – 600, 600 MHz
	^{13}C-NMR	BRUKER AVANCE III – 300, 75 MHz
		BRUKER AVANCE III – 600, 151 MHz

For IR-spectroscopy a JASCO FT/IR-6200 spectrometer was used. Infrared spectra were recorded from samples as a film on a sodium chloride single crystal or on a diamond plate. For

evaluation, the intensities of the absorption bands were designated with the following abbreviations: very strong = vs, strong = s, medium = m and weak = w.

Melting points were measured on a BÜCHI B-540 melting point apparatus and are uncorrected. For mass spectra (HRMS) a BRUKER DALTONICS UHR-QTOF MAXIS 4G spectrometer was used.

1.2 Experimental details

1) Synthesis of 9-F-MIA (**3**)

9-F-MIA was synthesized *via* the following route (Supporting Scheme 1).

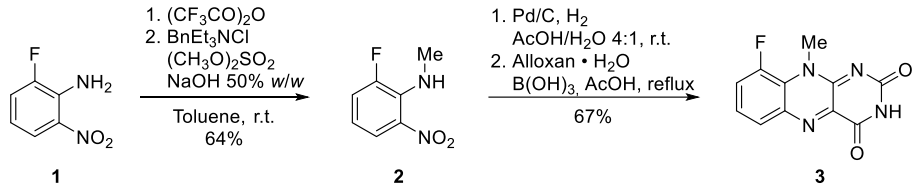

Supporting Scheme 1. Synthesis route to 9-F-MIA.

2-Fluoro-*N*-methyl-6-nitroaniline (2).

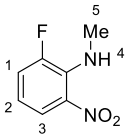

Analogous to the method by Brown and Rizzo[2], 6-fluoro-2-nitroaniline (**1**) (1.02 g, 6.55 mmol) was suspended in toluene (15.0 mL) and the mixture cooled down to 0 °C. Trifluoroacetic anhydride (1.80 mL, 2.72 g, 12.9 mmol, 2.0 eq) was added and the reaction mixture stirred for 80 min at r.t. resulting in formation of colorless crystals. To the mixture were successively added benzyltriethylammonium chloride (1.50 g, 6.57 mmol, 1.0 eq) and dimethyl sulfate (0.780 mL, 1.04 g, 8.24 mmol, 1.3 eq) and the mixture stirred for 25 min before 50% *w*/*w* NaOH (6.60 mL) was added. The mixture was stirred for 3 d at r.t. before sat. NH_4Cl-solution (30 mL) and CH_2Cl_2 (20 mL) were added. The layers were separated and the aqueous layer extracted with CH_2Cl_2 (4 x 20 mL). The combined organic layers were dried over Na_2SO_4, filtered and the solvent removed *in vacuo*. Purification *via* flash chromatography (*n*-hexane, then *n*-hexane/EtOAc 6:4) gave the product as red crystals (715 mg, 4.20 mmol, 64%). The spectroscopic data are in agreement with the literature[3]: **^{1}H-NMR** (300 MHz, $CDCl_3$) δ 7.94 (dt, *J* = 8.8, 1.6, 1.6 Hz, 1H, H-3), 7.83 (s, 1H, H-4), 7.17 (dddd, *J* = 13.9, 7.8, 1.6, 0.6 Hz, 1H, H-1), 6.55 (ddd, *J* = 8.8, 7.8, 4.5 Hz, 1H, H-2), 3.25 (dd, *J* = 7.5, 5.5 Hz, 3H, H-5) ppm.

9-Fluoro-10-methylbenzo[*g*]pteridine-2,4(3*H*,10*H*)-dione (3).

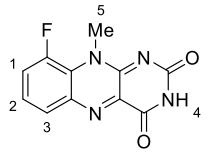

Analogous to the method by Gilch and Czekelius *et al.*[4] and Averill *et al*.[5], a solution of nitroaniline **2** (499 mg, 2.93 mmol) in AcOH/H_2O 4:1 (14.0 mL) was degassed by purging N_2 for 30 min. Pd/C 10% (40.5 mg, 38.1 mmol, 0.01 eq related to Pd) was added and the mixture stirred vigorously under H_2 atmosphere overnight. Then, it was filtered through a syringe filter directly into a degassed (30 min) mixture of alloxan monohydrate (611 mg, 3.81 mmol, 1.3 eq) and $B(OH)_3$ (1.14 g, 18.5 mmol, 6.3 eq) in AcOH (37.0 mL). After refluxing for 1 h, the product was obtained by filtration. Addition of water (150 mL) in this step turned out to be helpful for precipitation. The raw product was obtained as a green powder (494 mg, 1.97 mmol, 67%) with a purity of 98% and 2% of AcOH incorporated. **mp:** Decomposition >280 °C. **^{1}H-NMR** (300 MHz, DMSO-d_6) δ 11.49 (s, 1H, H-4), 7.97 (dt, *J* = 8.1, 1.2 Hz, 1H, H-3), 7.83 (ddd, *J* = 14.4, 8.2, 1.5 Hz, 1H, H-1), 7.60 (td, *J* = 8.2, 4.8 Hz, 1H, H-2), 4.09 (d, *J* = 7.2 Hz, 3H, H-5) ppm. **^{13}C{^{1}H}-NMR** (151 MHz, DMSO-d_6) δ 158.53, 154.48, 151.13, 149.71 (d, *J* = 250.3 Hz), 138.83, 135.97, 127.66 (d, *J* = 3.6 Hz), 125.06 (d, *J* = 8.9 Hz), 122.80 (d, *J* = 6.2 Hz), 120.75 (d, *J* = 23.2 Hz), 35.41 (d, *J* = 15.9 Hz) ppm. **^{19}F{^{1}H}-NMR** (282 MHz, DMSO-d_6) δ -120.48 ppm. **IR (Film):** $\tilde{\upsilon}$ [cm^{-1}] 3186 (w), 3067 (w), 1665 (m), 1614 (w), 1582 (m), 1547 (m), 1508 (m), 1466 (s), 1400 (m), 1271 (m), 1246 (m), 1204 (s), 1065 (w), 1022 (w). **HRMS (ESI):** m/z = 247.0626 [$M+H^+$] (calculated: 247.0626).

Purification procedure for photophysical measurements:

The raw product (198 mg) was dissolved in CF_3CH_2OH (90 mL) by heating to 80 °C and the solution filtered hot through a BÜCHNER funnel. The filtrate was cooled to 0 °C for 7 days before the product was filtered off through a BÜCHNER funnel giving a pre-purified product (118 mg). Then, this material was again dissolved in CF_3CH_2OH (40 mL) by heating to 80 °C, EtOAc (10 mL) was layered on top, and the two-layer system stored at 0 °C overnight. The product was filtered off, giving the product in >99% purity as a green powder with <1% CF_3CH_2OH incorporated (59.8 mg).

2) Synthesis of 7,8-dF-MIA (**8**)

7,8-dF-MIA was synthesized *via* the following route (Supporting Scheme 2):

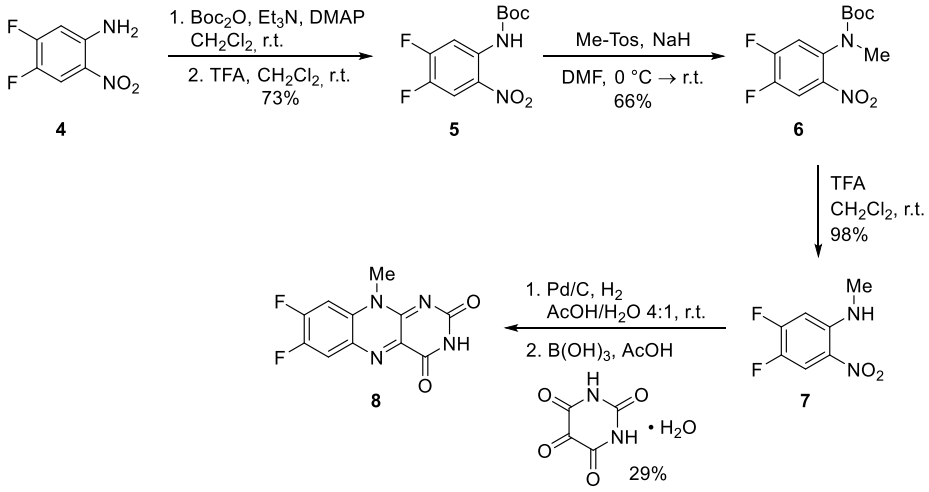

Supporting Scheme 2. Synthesis route to 7,8-dF-MIA (**8**).

***tert*-Butyl (4,5-difluoro-2-nitrophenyl)carbamate (5).**

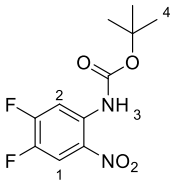

Analogous to the protocol by Xie and Liao *et al.*[6] 4,5-fluoro-2-nitroaniline (**4**) (296 mg (1.70 mmol) was dissolved in CH_2Cl_2 (4.20 mL) and Boc_2O (830 µL, 789 mg, 3.61 mmol, 2.1 eq) as well as NEt_3 (360 µL, 261 mg, 2.58 mmol, 1.5 eq) were added dropwise. The mixture was stirred at r.t. for 5 min before addition of DMAP (20.8 mg, 170 µmol, 0.1 eq) and stirring for 35 min continued. Then, the solvent was evaporated and the residue dissolved in CH_2Cl_2 (780 µL). To the solution cooled to 0 °C TFA (200 µL, 298 mg, 2.61 mmol, 1.5 eq) was added slowly and the mixture stirred at 0 °C for 5 min and at r.t. for 2 h. To complete conversion, additional TFA (200 µL, 298 mg, 2.61 mmol, 1.5 eq) was added, and the mixture stirred at r.t. for 10 min. Then, sat. Na_2CO_3-solution (6.00 mL) was added, the phases separated, and the aqueous phase extracted with CH_2Cl_2 (4 x 3 mL). The combined organic phases were dried over Na_2SO_4, filtered and the solvent removed *in vacuo*. Purification *via* flash chromatography (*n*-hexane/EtOAc 99:1) gave the product as a yellow powder 339 mg (1.24 mmol, 73%). **m.p.** 94.5 – 97.3 °C. **^{1}H-NMR** (600 MHz, $CDCl_3$) δ 9.76 (s, 1H, H-3), 8.59 (dd, *J* = 13.0, 7.5 Hz, 1H, H-1), 8.09 (dd, *J* = 10.1, 8.0 Hz, 1H, H-2), 1.54 (s, 9H, H-4) ppm. **^{13}C{^{1}H}-NMR** (151 MHz, $CDCl_3$) δ 155.02 (dd, *J* = 259.4, 12.9 Hz), 152.03, 144.28 (dd, *J* = 249.2, 14.3 Hz), 134.65 – 134.28 (m), 130.97, 114.96 (dd, *J* = 22.5, 3.2 Hz), 109.29 (d, *J* =

25.4 Hz), 82.80, 28.28 ppm. **^{19}F{^{1}H}-NMR** (565 MHz, $CDCl_3$) δ -121.14 (d, *J* = 23.0 Hz), -141.64 (d, *J* = 23.0 Hz) ppm. **IR (Film):** $\tilde{\nu}$ [cm^{-1}] 3366 (m), 3104 (w), 3088 (w), 2983 (m), 2936 (w), 1739 (vs), 1599 (s), 1530 (vs), 1456 (s), 1343 (s), 1312 (s), 1285 (vs), 1232 (s), 1148 (vs), 1069 (m). **HRMS (ESI):** m/z = 297.0653 [M+Na^+] (calculated: 297.0657).

***tert*-Butyl (4,5-difluoro-2-nitrophenyl)(methyl)carbamate (6).**

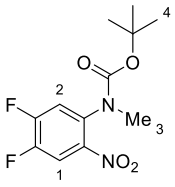

The reaction was done analogous to the method by Xie and Liao *et al*.[6]: To a pre-cooled (0 °C) solution of Boc-protected amine **5** (4.91 g, 17.9 mmol) in DMF (90.0 mL) NaH, 60% dispersion in mineral oil (1.47 g, 36.8 mmol, 2.1 eq) was added. The mixture was stirred for 10 min at 0 °C before methyl *p*-toluenesulfonate (3.00 mL, 3.70 g, 19.9 mmol, 1.1 eq) was added and the mixture stirred for another 10 min at 0 °C before being stirred at r.t. for 5 h. Finally, ice was added in small portions followed by water (180 mL) and EtOAc (80 mL). The phases were separated and the aqueous phase extracted with EtOAc (2 x 80 mL). The combined organic layers were dried over Na_2SO_4, filtered, and the solvent removed *in vacuo*. Purification *via* flash chromatography (*n*-hexane/EtOAc 99:1 – 9:1) gave the product as a yellow powder (3.41 g, 11.8 mmol, 66%). **m.p.** 75.2 – 76.5 °C. **^{1}H-NMR** (300 MHz, $CDCl_3$) δ 7.83 (t, *J* = 8.6 Hz, 1H, H-1), 7.18 (dd, *J* = 10.2, 7.1 Hz, 1H, H-2), 3.25 (s, 3H, H-3), 1.55 – 1.20 (m, 9H, H-4) ppm. **^{13}C{^{1}H}-NMR** (75 MHz, $CDCl_3$) δ 152.80 (dd, *J* = 260.0, 13.6 Hz), 152.79, 147.76 (dd, *J* = 254.0, 13.6 Hz), 142.11, 135.15, 118.06 (d, *J* = 19.2 Hz), 114.86 (d, *J* = 22.2 Hz), 82.26, 37.58 (d, *J* = 33.4 Hz), 28.06 (d, *J* = 32.5 Hz) ppm. **^{19}F{^{1}H}-NMR** (282 MHz, $CDCl_3$) δ -126.15 (dd, *J* = 84.8, 21.6 Hz), -135.07 (dd, *J* = 89.6, 21.7 Hz) ppm. **IR (Film):** $\tilde{\nu}$ [cm^{-1}] 2979 (w), 2362 (w), 1714 (s), 1605 (w), 1543 (s), 1346 (s), 1263 (m), 1153 (m). **HRMS (ESI):** m/z = 289.0994 [M+H^+] (calculated: 289.0990).

4,5-Difluoro-*N*-methyl-2-nitroaniline (7).

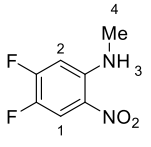

The reaction was done analogous to the method by Xie and Liao *et al*.[6]: To a pre-cooled (0 °C) solution of methylated Boc-protected amine **6** (603 mg, 2.09 mmol) in CH_2Cl_2 (1.00 mL) TFA (250 µL, 372 mg, 3.26 mmol, 1.6 eq) was added and the mixture stirred at r.t. for 3.5 h. Then, additional TFA (120 µL, 179 mg, 1.57 mmol, 0.8 eq) was added and the mixture stirred at r.t. for 2.5 h. Sat. Na_2CO_3-solution (10 mL) was added, the phases separated, and the aqueous phase extracted with CH_2Cl_2 (5 x 3 mL). The combined organic layers were dried over Na_2SO_4, filtered, and the solvent removed *in vacuo*. Purification *via* flash chromatography (*n*-hexane/EtOAc 99:1) gave the product as a yellow powder (386 mg, 2.05 mmol, 98%). **m.p.** 114.6 – 116.0 °C. **^{1}H-NMR** (300 MHz, $CDCl_3$) δ 8.05 (m, 2H, H-1,3), 6.60 (dd, *J* = 12.5, 6.7 Hz, 1H, H-2), 3.00 (d, *J* = 5.1 Hz, 3H, H-4) ppm. **^{13}C{^{1}H}-NMR** (75 MHz, $CDCl_3$) δ 156.50 (dd, *J* = 259.4, 14.5 Hz), 144.89 (d, *J* = 11.0 Hz), 140.88 (dd, *J* = 241.8, 14.8 Hz), 126.60 (m), 115.25 (dd, *J* = 21.6, 3.7 Hz), 100.95 (d, *J* = 22.6 Hz), 30.22 ppm. **^{19}F{^{1}H}-NMR** (282 MHz, $CDCl_3$) δ -121.86 (d, *J* = 23.2 Hz), -150.91 (d, *J* = 23.9 Hz) ppm. **IR (Film):** $\tilde{\nu}$ [cm^{-1}] 3384 (m), 3074 (w), 1648 (m), 1578 (s), 1527 (vs), 1457 (m), 1407 (s), 1310 (m), 1262 (s), 1235 (s), 1028 (s). **HRMS (ESI):** m/z = 189.0469 [$M+H^+$] (calculated: 189.0470).

7,8-Difluoro-10-methylbenzo[*g*]pteridine-2,4(3*H*,10*H*)-dione (8).

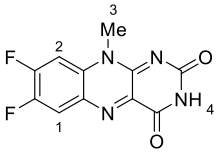

The reaction was done following the method by Gilch and Czekelius *et al*.[4] and Averill *et al*.[5]: A solution of *N*-methyl-nitroaniline **7** (1.39 g, 7.39 mmol) in AcOH (36.0 mL) and water (9.00 mL) was degassed by purging N_2 through for 20 min. Then, Pd/C (10%, 111 mg, 105 µmol, 0.01 eq) was added, the reaction vessel set under H_2-atmosphere and the mixture stirred at r.t. overnight. The colorless mixture was filtered through a syringe filter directly into a degassed mixture (N_2-purge for 30 min) of alloxan monohydrate (1.53 g, 9.56 mmol, 1.3 eq) and $B(OH)_3$ (2.88 g, 46.5 mmol, 6.3 eq) in AcOH (90.0 mL). It was stirred for 1 h at r.t. before the solution was concentrated using high vacuum to 5-10 mL. The residue was suspended with cold water and filtered using a glass frit. The precipitate was washed with cold water and cold EtOH in small portions giving the raw product as a green powder (2.26 g). NMR-spectroscopy showed a mixture of product, alloxazine and unknown monofluorinated side product 1:0.4:0.2. A fraction of the raw material (1.93 g) was submitted to the optimized purification protocol (see below) and the yield of pure product calculated accordingly (482 mg, 1.82 mmol, 29% orange-yellow powder). **m.p.** decomposition >200 °C. **^{1}H-NMR** (300 MHz, DMSO-d_6) δ 11.45 (s, 1H, H-4), 8.35 (dd, *J* = 10.5, 8.4 Hz, 1H, H-1), 8.18 (dd, *J* = 12.5, 7.4 Hz,

1H, H-2), 3.93 (s, 3H, H-3) ppm. **^{13}C{^{1}H}-NMR** (75 MHz, DMSO-d_6) 159.40, 155.38, 153.59 (dd, J = 271.1, 14.4 Hz), 150.84, 147.55 (dd, J = 248.3, 15.3 Hz), 139.08 (d, J = 3.7 Hz), 131.64 (d, J = 10.7 Hz), 131.33 (d, J = 10.7 Hz), 118.77 (d, J = 17.7 Hz), 105.61 (d, J = 24.0 Hz), 32.68 ppm. **^{19}F{^{1}H}-NMR** (282 MHz, DMSO-d_6) δ -124.56 (d, J = 23.6 Hz), -139.03 (d, J = 23.8 Hz) ppm. **IR (Film):** $\tilde{\nu}$ [cm^{-1}] 3028 (w), 1712 (m), 1643 (m), 1547 (s), 1537 (s), 1504 (s), 1395 (m), 1298 (m), 1275 (s) 1238 (vs), 1211 (s). **HRMS (ESI):** m/z = 265.0532 [M+H$^+$] (calculated: 265.0532).

*Purification procedure of 7,8-dF-MIA (**8**) for photophysical measurements:*

1.93 g of raw product **8** was subsequently suspended in ca. 5 mL CF_3CH_2OH and ca. 5 mL MeOH and the supernatant solution applied onto a prepacked column (silica gel). Flash chromatography was performed with EtOAc/MeOH 95:5 as eluent. The undissolved residue of material was dried *in vacuo* and suspended again in CF_3CH_2OH and MeOH, respectively. With this procedure 15 consecutive flash chromatographies were performed giving a total yield of 482 mg product with a purity of >99% and <1% CF_3CH_2OH incorporated.

2) Synthesis of 7,8-dF-riboflavin (**13**)

7,8-dF-Riboflavin (7,8-dF-RIA) was synthesized following a modified protocol by Gärtner *et al*.[7] according to the synthesis route shown in Supporting Scheme 3.

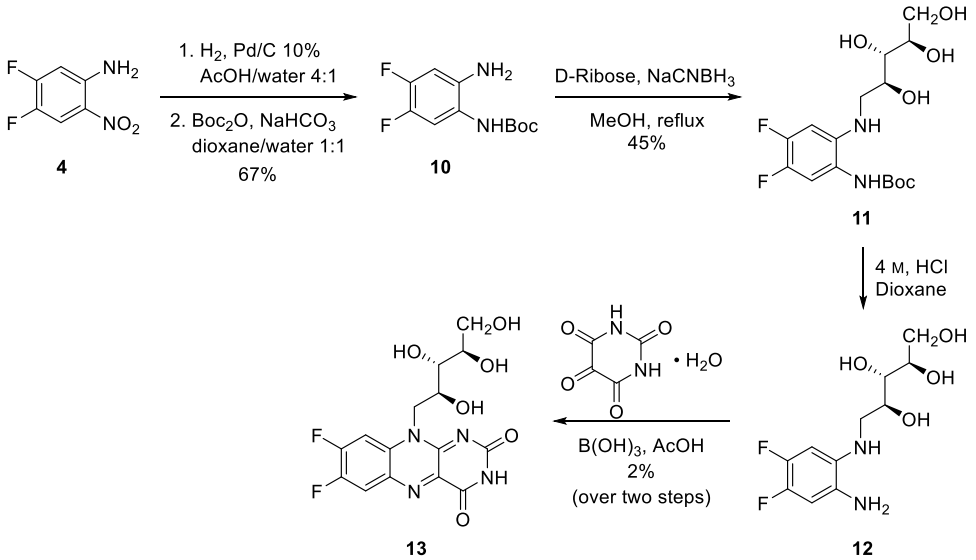

Supporting Scheme 3. Synthesis route to 7,8-dF-RIA (**13**).

***tert*-Butyl(2-amino-4,5-difluorophenyl)carbamate (10)**

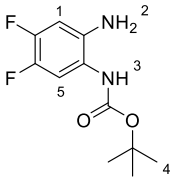

Nitroaniline **4** (3.00 g, 17.2 mmol) was dissolved in a mixture of AcOH (85.0 mL) and water (21 mL) and Pd/C (10%, 246 mg, 231 µmol, 0.01 eq) was added. The mixture was degassed by purging N_2 through for 30 min before purging with H_2 for 5 min and finally setting the flask under H_2 atmosphere. After stirring at r.t. for 5.5 h, the flask was set under nitrogen atmosphere overnight. The mixture was filtered through a syringe filter into a new flask and the solvent was removed under inert conditions using high vacuum. Dissolving the residue in a degassed mixture of dioxane (120 mL) and water (120 mL) was followed by addition of $NaHCO_3$ (1.45 g, 17.3 mmol, 1.0 eq) and Boc_2O (4.00 mL, 3.80 g, 17.4 mmol, 1.0 eq). After stirring at r.t. for 24 h and 42 h additional Boc_2O (1st: 1.50 mL, 1.43 g, 6.53 mmol, 0.38 eq; 2nd: 1.00 mL, 950 mg, 4.35 mmol, 0.25 eq) was added. After stirring for 44 h altogether, water (210 mL) was added and the product extracted with 3 x 150 mL CH_2Cl_2. The combined organic phases were washed with 100 mL sat. $NaHCO_3$-solution and 100 mL brine, dried over Na_2SO_4, filtered, and the solvent removed *in vacuo*. Flash chromatography (*n*-hexane/EtOAc 9:1 – 6:4) furnished carbamate **10** as a beige powder (2.81 g, 11.5 mmol, 67%). **m.p.** 142.2 – 144.9°C. **^{1}H-NMR** (300 MHz, $CDCl_3$) δ 7.31 – 7.18 (m, 1H, H-5), 6.57 (dd, *J* = 11.4, 7.6 Hz, 1H, H-1), 6.15 (brs, 1H, H-3), 3.59 (brs, 2H, H-2), 1.51 (s, 9H, H-4) ppm. **^{13}C{^{1}H}-NMR** (75 MHz, $CDCl_3$) δ 153.69, 147.98 (dd, *J* = 244.5, 13.4 Hz), 143.64 (dd, *J* = 239.1, 13.4 Hz), 136.13, 120.85, 113.43 (d, *J* = 20.3 Hz), 105.96 (d, *J* = 20.1 Hz), 81.22, 28.40 ppm. **^{19}F{^{1}H}-NMR** (282 MHz, $CDCl_3$) δ -141.22, -148.31 ppm. **IR (Film):** $\tilde{\upsilon}$ [cm^{-1}] 3440 (m), 3361 (m), 3290 (s), 3049 (w), 2993 (m), 1677 (vs), 1508 (vs), 1439 (s), 1369 (m), 1282 (m), 1221 (m), 1156 (m). **HRMS (ESI):** m/z = 245.1099 [M+H$^+$] (calculated: 245.1096).

***tert*-Butyl(4,5-difluoro-2-(((2*S*,3*S*,4*R*)-2,3,4,5-tetrahydroxypentyl)amino)phenyl) carbamate (11)**

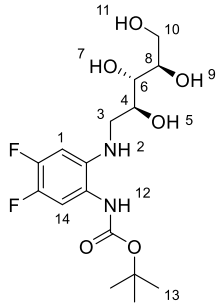

Boc-protected aniline **10** (1.43 g, 5.85 mmol) was dissolved in MeOH (120 mL) and D-ribose (3.43 g, 22.9 mmol, 3.9 eq) and $NaCNBH_3$ (1.47 g, 23.4 mmol, 4.0 eq) were added. The mixture was purged with N_2 for 30 min and refluxed overnight before evaporation of the solvent. To the residue was slowly added 1 M HCl (60 mL) until gas formation stopped and subsequently neutralized using sat. $NaHCO_3$-solution. After extraction with 4 x 90 mL EtOAc were the combined organic phases dried over Na_2SO_4, filtered and the solvent removed *in vacuo*. Flash chromatography (CH_2Cl_2/MeOH 95:5 – 9:1) gave the desired riboaniline **11** as a white powder (1.01 g, 2.66 mmol, 45%; recovery starting material: 423 mg, 1.73 mmol, 30%). **m.p.** 49.8 – 53.4 °C. **^{1}H-NMR** (300 MHz, MeOD) δ 7.09 (dd, *J* = 11.6, 8.4 Hz, 1H, H-14), 6.62 (dd, *J* = 13.3, 7.8 Hz, 1H, H-1), 3.93 (ddd, *J* = 7.6, 6.1, 3.3 Hz, 1H, H-4), 3.84 – 3.57 (m, 4H, H-6,8,10), 3.38 (dd, *J* = 12.9, 3.4 Hz, 1H, H-3), 3.16 (dd, *J* = 12.8, 7.7 Hz, 1H, H-3'), 1.50 (s, 9H, H-13) ppm. **^{13}C{^{1}H}-NMR** (75 MHz, MeOD) δ 156.68, 149.97 (dd, *J* = 241.3, 12.9 Hz), 142.50 (dd, *J* = 234.6, 13.7 Hz), 142.07, 120.60 (dd, *J* = 7.5, 3.0 Hz), 115.96 (d, *J* = 19.6 Hz), 101.06 (d, *J* = 22.3 Hz), 81.41, 74.47, 74.38, 71.87, 64.64, 47.32, 28.65 ppm. **^{19}F-NMR** (282 MHz, MeOD) δ -142.89 (d, *J* = 22.3 Hz), -155.70 (d, *J* = 22.5 Hz) ppm. **IR (Film):** $\tilde{\nu}$ [cm^{-1}] 3312 (w), 2972 (w), 1685 (m), 1525 (s), 1368 (m), 1233 (m), 1155 (s), 1051 (s). **HRMS (ESI):** m/z = 379.1682 [M+H$^+$] (calculated: 379.1675).

7,8-Difluoro-10-((2*S*,3*S*,4*R*)-2,3,4,5-tetrahydroxypentyl)benzo[*g*]pteridine-2,4-(3*H*,10*H*)-dione (13)

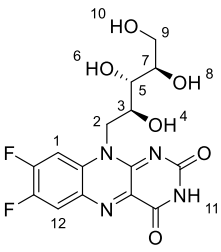

Boc-protected riboaniline **11** (500 mg, 1.32 mmol) was dissolved in dioxane (15.0 mL) and conc. HCl (7.50 mL) was added slowly. The mixture was degassed by purging N_2 through for 15 min and then stirred at r.t. under N_2 atmosphere for 2.5 h. The solvent was removed *in vacuo*, the residue dissolved in water (150 mL) and extracted with 3 x 30 mL Et_2O. The aqueous phase was lyophilized and the ribitylated aniline **12** as the residue directly dissolved in AcOH/water 4:1 (11 mL). Alloxan monohydrate (40.7 mg, 254 µmol, 3.6 eq) and $B(OH)_3$ (16.4 mg, 265 µmol, 3.8 eq) were added, the mixture degassed by purging N_2 through for 30 min and stirred at r.t. overnight. The solvent was removed *in vacuo* and the residue suspended in toluene/water 1:1 (20 mL). It was stirred for 10 min before removal of the solvent *in vacuo* to give 337 mg raw product. A fraction of the raw material (80.0 mg) was submitted to the optimized purification protocol (see below) and the yield of pure product calculated accordingly (11.0 mg, 28.5 µmol, 2.2% yellow powder). **^{1}H-NMR** (300 MHz, MeOD) δ 8.13 (dd, *J* = 12.4, 7.4 Hz, 1H, H-12), 8.01 (dd, *J* = 10.0, 8.3 Hz, 1H, H-1), 4.93 – 4.77 (m, 2H, C*H*OH), 4.32 (dt, *J* = 9.0, 3.7 Hz, 1H, C*H*OH), 3.81 – 3.52 (m, 4H, H-2,9) ppm. **^{19}F{^{1}H}-NMR** (282 MHz, MeOD) δ -124.22 (d, *J* = 21.7 Hz), -139.10 (d, *J* = 21.8 Hz) ppm. **HRMS (ESI):** m/z = 385.0954 [M+H$^+$] (calculated: 385.0954).

Purification method for photophysical measurements:

80.0 mg raw product was dissolved in water (150 mL) and the solution concentrated at max. 38 °C stepwise in a 50 mL flask to an amount of ~5 mL. The residue was stored in a fridge overnight. The precipitate was filtered off using a glass frit. The filtrate was disposed and the solid (54.5 mg) redissolved in water (50 mL). Evaporation of water was performed following the described procedure and the concentrate (~4 mL) stored in the fridge until precipitation occurred. The solvent was removed *via* pipette and retained (filtrate 1). The precipitate was dissolved again in water (30 mL), evaporated to ~4 mL and stored in the fridge until precipitation occurred. The solvent was removed *via* pipette, combined with filtrate 1 and the solvent was removed *in vacuo*. The residue was dissolved in MeOH (6 mL), filtered and the solvent removed *in vacuo* before dissolving in MeOH (4 mL) again and addition of Et_2O (80 mL) in one batch. The solvent was removed *via* pipette and the residue dissolved in 8.0 mL CF_3CH_2OH, filtered, and evaporated. The residue was dissolved in MeOH (2 mL) and purified *via* two separate HPLC runs with water/MeOH 95:5 – 9:1 (60 min). The product was obtained in pure form as a yellow powder (2.6 mg).

2 Impact of the deuterated solvent D_2O on the fluorescence

Fluorescence lifetimes were measured by time-correlated single photon counting (TCSPC) in both H_2O and D_2O. All the investigated dyes have significantly longer fluorescence lifetimes in D_2O. Fluorescence decays in D_2O are shown in **Supporting Figure 1**.

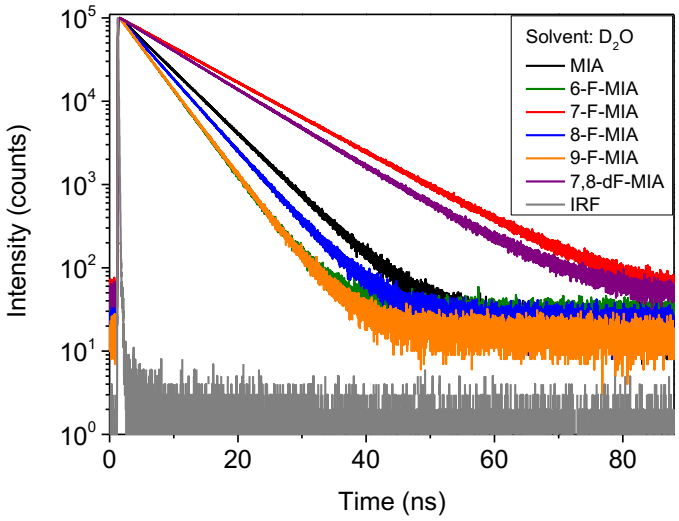

Supporting Figure 1. Fluorescence decays in D_2O measured by TCSPC.

In order to elucidate the impact of the deuterated solvent D_2O on the fluorescence lifetimes, we need to introduce a quenching constant in water, k_{qw}. Since we are interested in a systematic dependency for all MIA derivatives, we assume that all the derivatives have the same quenching constant and therefore, the term average quenching constant, $\overline{k_{qw}}$ is used. Assuming that quenching is present in water, the rate constants of S1 depopulation k_{S1} in H_2O and D_2O differ by the quenching constant:

$$k_{S1}^{(H_2O)} = k_{rad}^{(H_2O)} + k_{IC}^{(H_2O)} + k_{ISC}^{(H_2O)} + \overline{k_{qw}} \quad \text{(S1)}$$

$$k_{S1}^{(D_2O)} = k_{rad}^{(D_2O)} + k_{IC}^{(D_2O)} + k_{ISC}^{(D_2O)} \quad \text{(S2)}$$

The solvent is marked in the superscript. The radiative rate constant k_{rad} is obtained from the Strickler-Berg analysis and presents the rate constant for the emitter with no non-radiative transitions. The internal conversion and intersystem crossing rates are given in Table 1, and for the sake of simplicity, a non-radiative rate constant is introduced as a sum of these two constants (eq. S3).

$$k_{nr} = k_{IC} + k_{ISC} \quad \text{(S3)}$$

Finally, the respective lifetimes in H_2O and D_2O can be expressed as following using the experimental observation that the shape of the spectra in H_2O an D_2O does change (i.e. $k_{rad}^{(H_2O)} = k_{rad}^{(D_2O)} = k_{rad}$

$$\tau_{fl}^{(H_2O)} = \frac{1}{k_{S1}^{(H_2O)}} = \frac{1}{k_{rad} + k_{nr}^{(H_2O)} + \overline{k_{qw}}} \quad \text{(S4)}$$

$$\tau_{fl}^{(D_2O)} = \frac{1}{k_{S1}^{(D_2O)}} = \frac{1}{k_{rad} + k_{nr}^{(D_2O)}} \quad \text{(S5)}$$

Their ratio is equal to:

$$\frac{\tau_{fl}^{(D_2O)}}{\tau_{fl}^{(H_2O)}} = \frac{k_{rad} + k_{nr}^{(H_2O)} + \overline{k_{qw}}}{k_{rad} + k_{nr}^{(D_2O)}}. \quad \text{(S6)}$$

Taking into account the following assumption:

$$k_{rad} + k_{nr}^{(D_2O)} = k_{rad} + k_{nr}^{(H_2O)}, \quad \text{(S7)}$$

we gain:

$$\frac{\tau_{fl}^{(D_2O)}}{\tau_{fl}^{(H_2O)}} = 1 + \frac{\overline{k_{qw}}}{k_{rad} + k_{nr}^{(D_2O)}}. \quad \text{(S8)}$$

This equation can be rewritten as a Stern-Volmer type equation:

$$\frac{\tau_{fl}^{(D_2O)}}{\tau_{fl}^{(H_2O)}} = 1 + \overline{k_{qw}} \cdot \tau_{fl}^{(D_2O)} \quad \text{(S9)}$$

The dependency $\tau_{fl}^{(D_2O)}/\tau_{fl}^{(H_2O)}$ against $\tau_{fl}^{(D_2O)}$ is called the Stern-Volmer plot, and it is shown in Figure 4 in the main text of the manuscript. The average quenching constant in water $\overline{k_{qw}}$ is obtained as the slope of the linear regression.

3 Impact of the ribityl group

7,8-dF-MIA and 7,8-dF-RIA in D_2O were measured at 20.5 °C, excited with P = 96 µW and detected employing Hybrid PMTs (HPM-100-40, Becker&Hickl) under otherwise identical conditions as 7-F-MIA. Besides the formal fit (combination of eqs. 1-4) was fit to the averaged FCS-curves using a custom script in ORIGIN 8.6 (OriginLab Corporation) to directly yield the rate constants corresponding to the kinetic model in Figure 7. In these fits the fluorescence rate constants k_0 were fixed using the independently measured fluorescence lifetimes in D_2O (7,8-dF-MIA: τ_{fl} = 9.29 ns, 7,8-dF-RIA: τ_{fl} = 6.53 ns). Due to the high correlation between the fit parameters also the excitation rate needed to be approximated and fixed in the fit. To that end, the best fit of the excitation rate from 7-F-MIA measured in D_2O was scaled for the different excitation power and the different extinction coefficient (ε = 10560 $M^{-1}cm^{-1}$ at 440 nm for 7,8-dF-MIA in H_2O, the ratio for the two molecules is assumed to be identical in D_2O and H_2O). Thus an excitation rate for 7,8-dF-MIA of k_{01} = 0.51 10^7 s^{-1} is estimated. This assumption yields an intersystem crossing rate of k_{ISC} = 2.3 10^7 s^{-1} (± 13%) and a triplet depopulation rate of k_T = 0.039 10^7 s^{-1} (± 10%) for 7,8-dF-MIA in D_2O. Under our measurements conditions, we observe a high triplet fraction of 7,8-dF-MIA, so that the signal in the centre of the detection volume is saturated. This results in a broadened correlation function and a systematically smaller k_{ISC}.[8] Under these circumstances the values of k_{ISC} obtained by FCS and transient absorption spectroscopy (Table 1) are consistent. Notably, FCS obtains very similar values of 7-F-MIA in water k_{ISC} = 2.58 10^7 s^{-1}.

Assuming the same excitation rate for 7,8-dF-RIA in D_2O, k_{ISC} = 1.54 10^7 s^{-1} (± 21%) and k_T = 0.051 10^7 s^{-1} (± 17%) are obtained. Error bars are standard errors of the fit and do not include possible systematic errors due to uncertainties in the excitation rate or the inhomogeneous illumination profile (see description in Methods). The corresponding quantum yields for intersystem crossing for 7,8-dF-MIA and 7,8-dF-RIA in D_2O are Φ_{ISC} = 0.22 and Φ_{ISC} = 0.10, respectively.

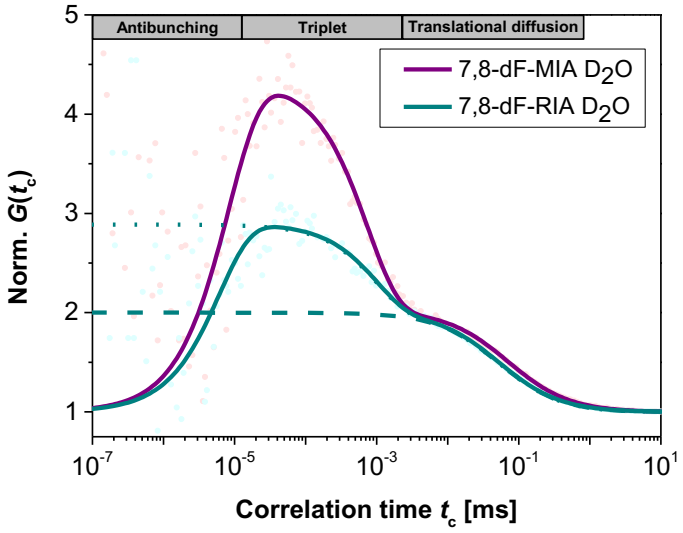

Supporting Figure 2. Normalized and averaged full correlation curves $G(t_c)$ of 7,8-dF-MIA and 7,8-dF-RIA in D_2O. The dashed lines represent the contributions of the translational diffusion and triplet term to the fitted model function (eq. 6) with additional parameters listed in Supporting Table 1.

Supporting Table 1. Parameters of formal fits (eq. 6) to the averaged curves

Sample	N_s	t_d / µs	z_0/ω_0	T_{1eq}	t_T / µs	AB	t_{AB} / ns
7,8-dF-MIA / D_2O	25.1	70 [a]	10 (fixed)	0.69	0.75	1 (fixed)	8.7
7,8-dF-RIA / D_2O	3.5	52	10 (fixed)	0.47	1.01	1 (fixed)	6.2

[a] due to the high triplet fraction, the signal is saturated that results in a broadened correlation function with increased apparent diffusion time t_d. Due to the smaller fluorescence quantum yield of 7,8-dF-RIA, the triplet population is significantly smaller, so that $G(t_c)$ is much less saturated.

4 Triplet quantum yield (relative method)

Nanosecond transient absorption data were acquired as described in the methods section. Typical data are shown in Supporting Figures 3 and 4.

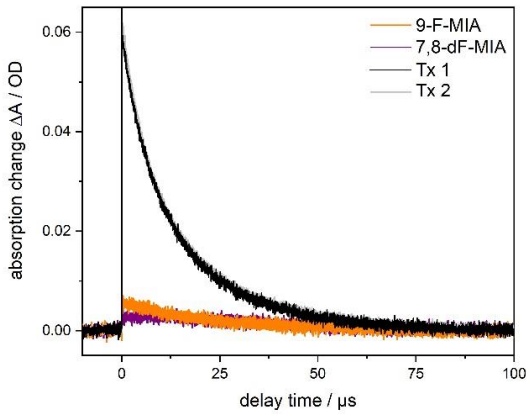

Supporting Figure 3. Nanosecond transient absorption time trace at 600 nm for the samples and the reference. The recorded time zero signals of the samples ($\Delta A_{t=0}(\lambda_{Pr})$) and the reference ($\Delta A^{r}_{t=0}(\lambda_{Pr})$) were on the order of ~5 mOD and 60 mOD, respectively. The sample solutions (nitrogen-purged water) as well as the reference (thioxanthone (Tx)) solution (nitrogen-purged methanol) were excited at 355 nm. Tx was measured before the sample solutions (Tx 1) and afterwards (Tx 2).

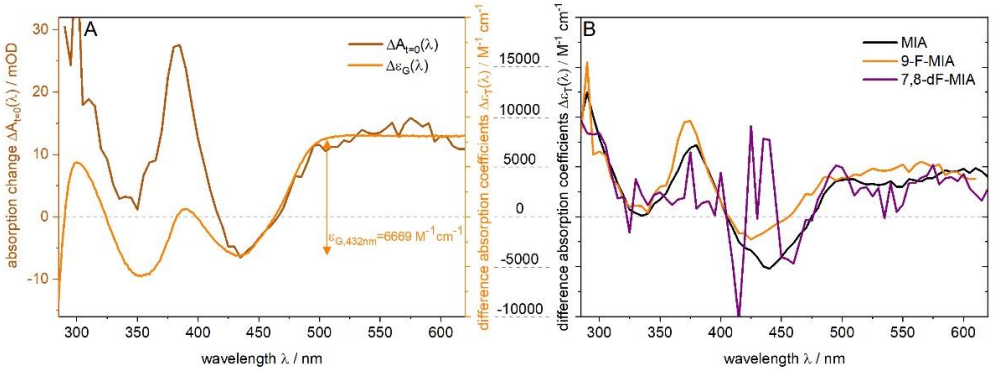

Supporting Figure 4. Relative method for determining difference absorption coefficients $\Delta\varepsilon_T(\lambda)$. A: The ground state bleach of the time zero spectrum $\Delta A_{t=0}(\lambda)$ (dark orange) is aligned with the ground state absorption spectrum (orange), respectively, exemplified for 9-F-MIA. B: Triplet difference absorption coefficients $\Delta\varepsilon_T(\lambda)$ for all MIA derivatives studied in this paper.

5 References

[1] G. R. Fulmer, A. J. M. Miller, N. H. Sherden, H. E. Gottlieb, A. Nudelman, B. M. Stoltz, J. E. Bercaw, K. I. Goldberg, *Organometallics* **2010**, *29*, 2176-2179.

[2] S. A. Brown, C. J. Rizzo, *Synth. Commun.* **1996**, *26*, 4065-4080.

[3] N. E. Kanitz, T. Lindel, *Z. Naturforsch., B: Chem. Sci.* **2016**, *71*, 1287-1300.

[4] A. Reiffers, C. Torres Ziegenbein, A. Engelhardt, R. Kühnemuth, P. Gilch, C. Czekelius, *Photochem. Photobiol.* **2018**, *94*, 667-676.

[5] V. Kumar, K. A. Woode, R. F. Bryan, B. A. Averill, *J. Am. Chem. Soc.* **1986**, *108*, 490-496.

[6] K. Cheng, S. Li, X. Lv, Y. Tian, H. Kong, X. Huang, Y. Duan, J. Han, Z. Xie, C. Liao, *Bioorg. Med. Chem. Lett.* **2019**, *29*, 1012-1018.

[7] M. Mansurova, M. S. Koay, W. Gärtner, *Eur. J. Org. Chem.* **2008**, *2008*, 5401-5406.

[8] J. Widengren, U. Mets, R. Rigler, *J. Phys. Chem.* **1995**, *99*, 13368-13379.

6 Spectra

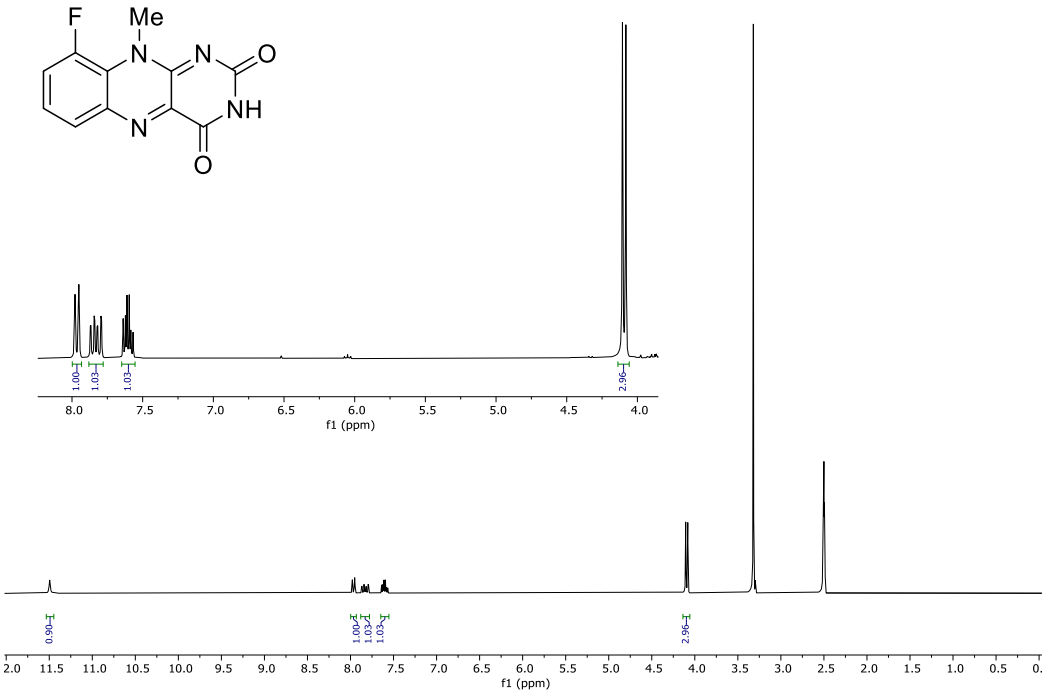

Spectrum 1 ^{1}H-NMR spectrum (300 MHz, DMSO-d_6) of 9-fluoro-10-methylbenzo[*g*]pteridine-2,4(3*H*,10*H*)-dione (**3**).

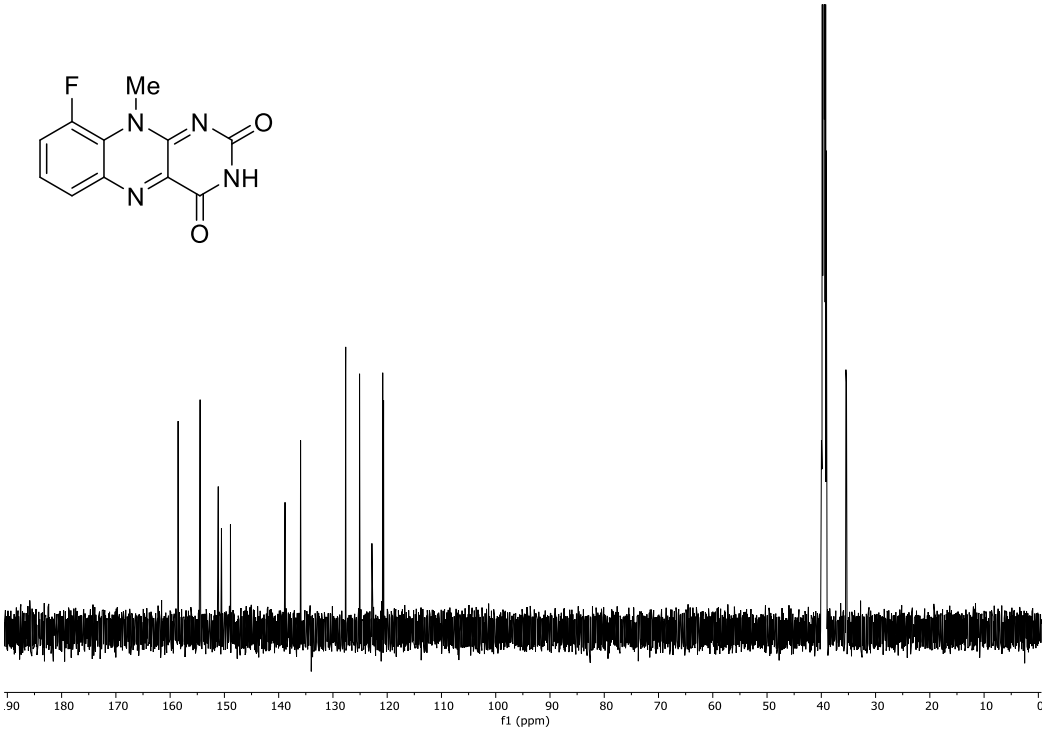

Spectrum 2 $^{13}C\{^{1}H\}$-NMR spectrum (151 MHz, DMSO-d_6) of 9-fluoro-10-methylbenzo[*g*]pteridine-2,4(3*H*,10*H*)-dione (**3**).

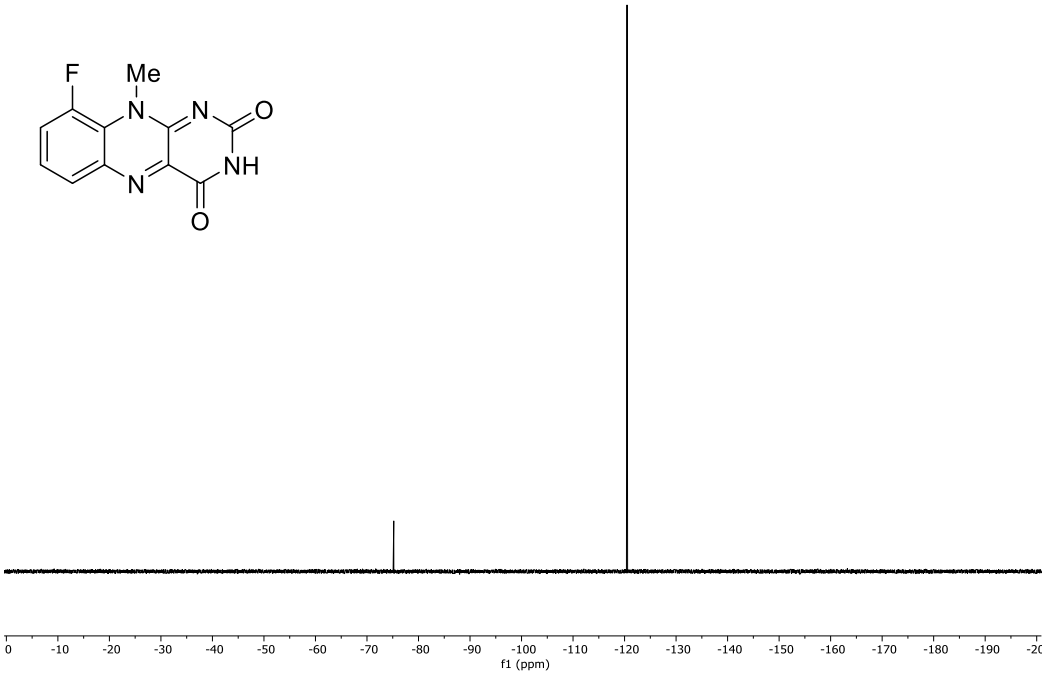

Spectrum 3 $^{19}F\{^{1}H\}$-NMR spectrum (282 MHz, DMSO-d_6) of 9-fluoro-10-methylbenzo[*g*]pteridine-2,4(3*H*,10*H*)-dione (**3**).

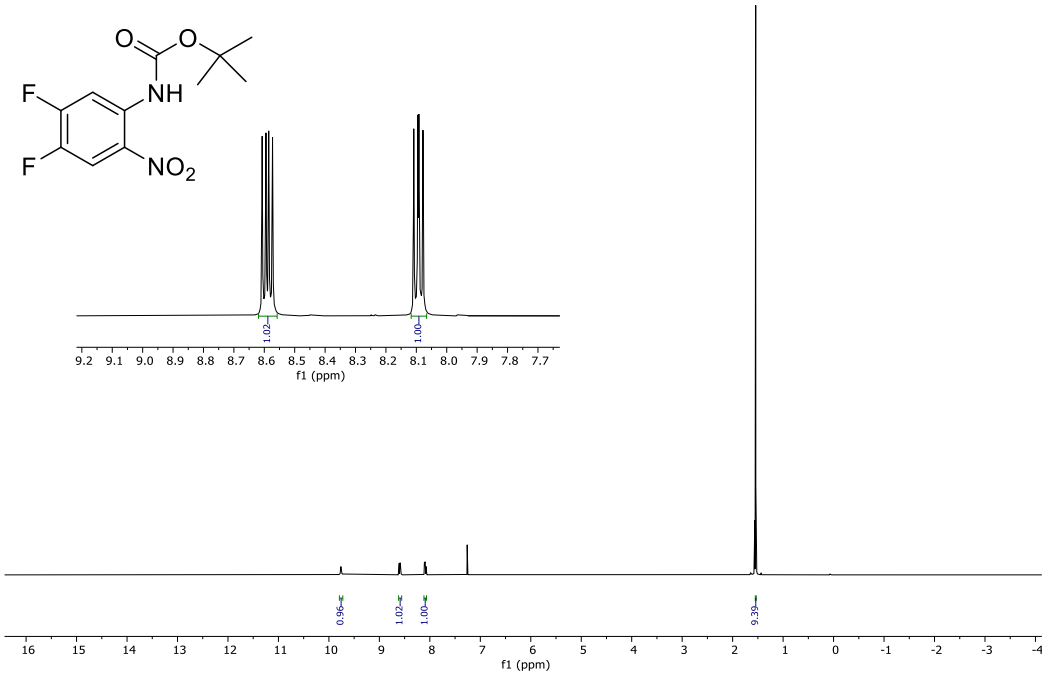

Spectrum 4 ^{1}H-NMR spectrum (600 MHz, $CDCl_3$) of *tert*-butyl (4,5-difluoro-2-nitrophenyl)carbamate (**5**).

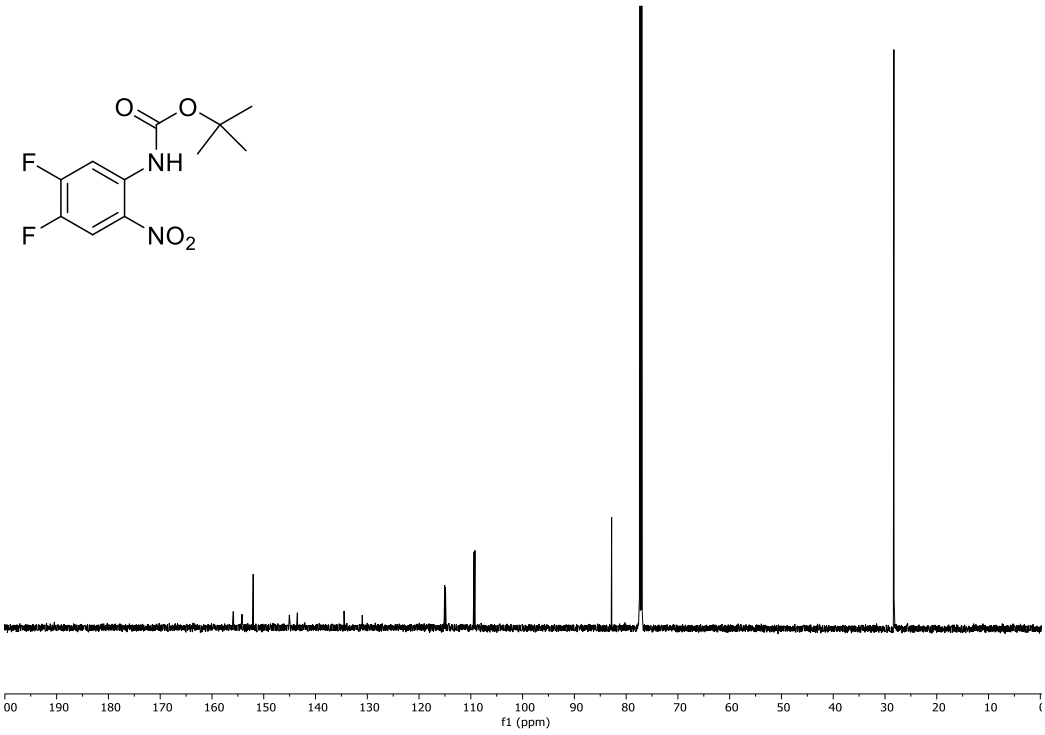

Spectrum 5 ^{13}C{^{1}H}-NMR spectrum (151 MHz, $CDCl_3$) of *tert*-butyl (4,5- difluoro-2-nitrophenyl)carbamate **5**).

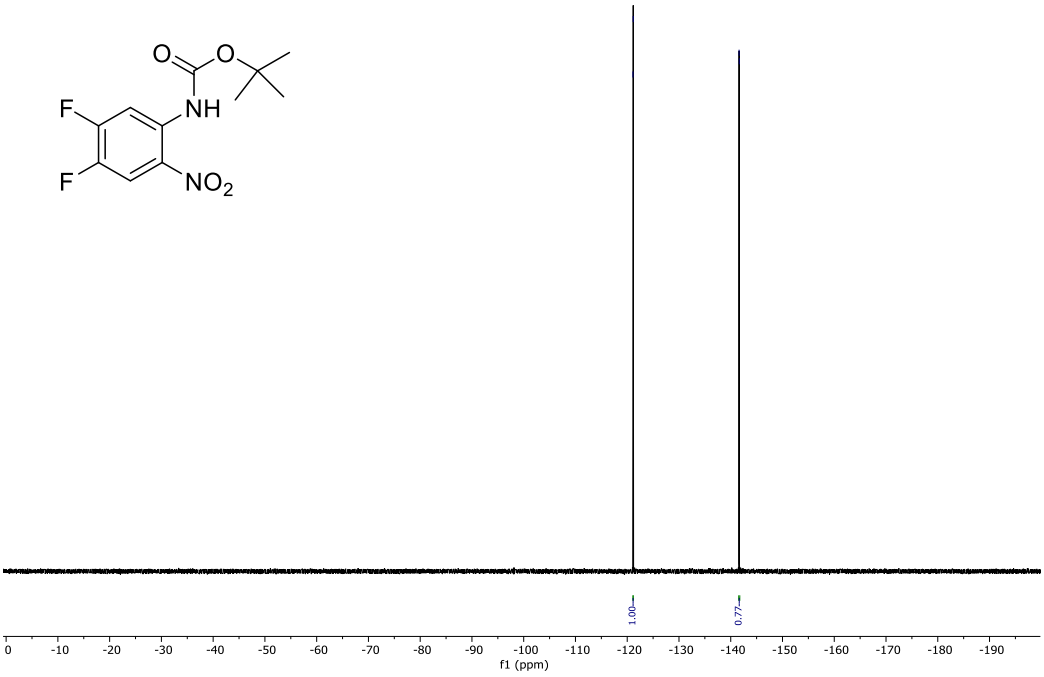

Spectrum 6 $^{19}F\{^{1}H\}$-NMR spectrum (565 MHz, $CDCl_3$) of *tert*-butyl (4,5-difluoro-2-nitrophenyl)carbamate (**5**).

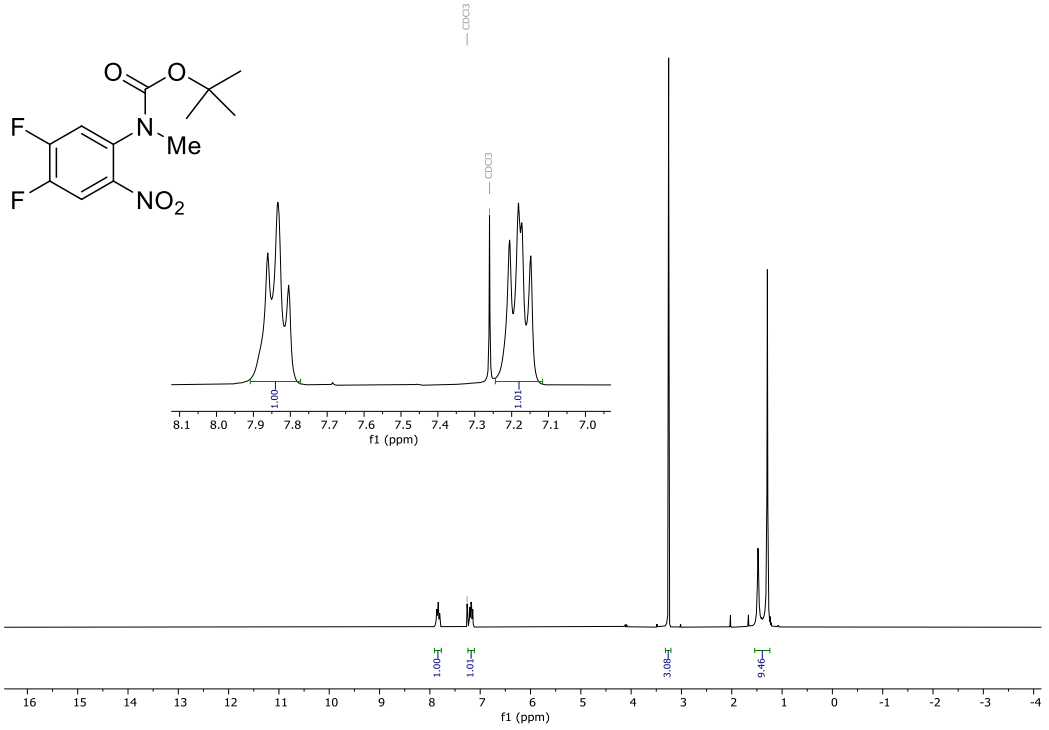

Spectrum 7 ^{1}H-NMR spectrum (300 MHz, $CDCl_3$) of *tert*-butyl (4,5-difluoro-2-nitrophenyl)(methyl)carbamate (**6**).

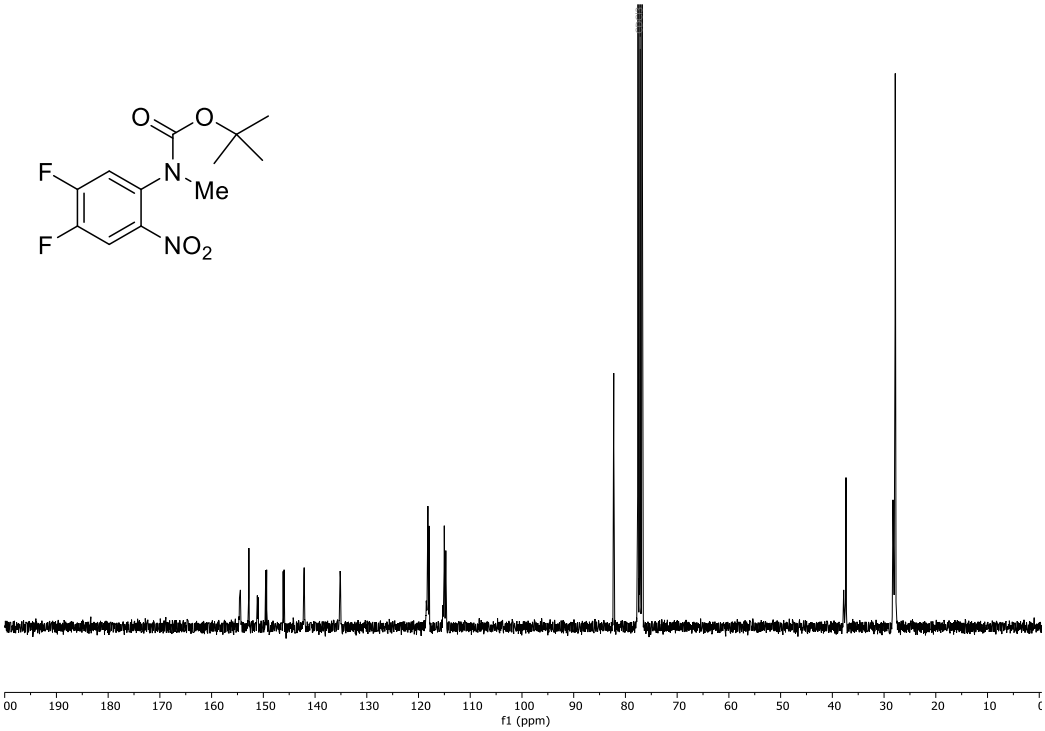

Spectrum 8 $^{13}C\{^1H\}$-NMR spectrum (75 MHz, $CDCl_3$) of
tert-butyl (4,5-difluoro-2-nitrophenyl)(methyl)carbamate (**6**).

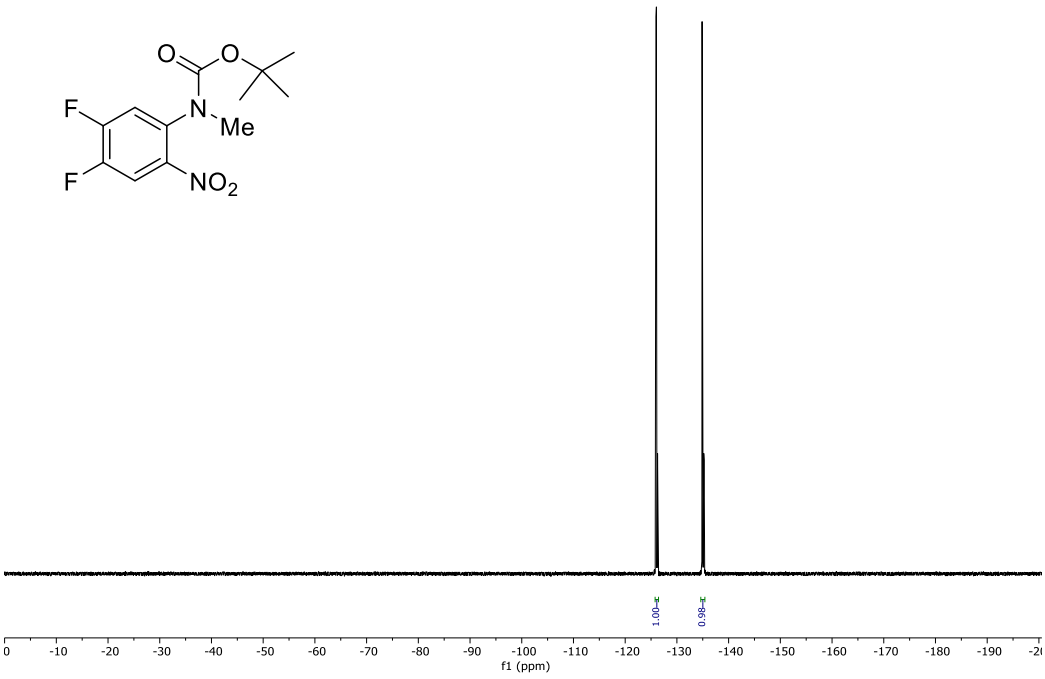

Spectrum 9 $^{19}F\{^1H\}$-NMR spectrum (282 MHz, $CDCl_3$) of
tert-butyl (4,5-difluoro-2-nitrophenyl)(methyl)carbamate (**6**).

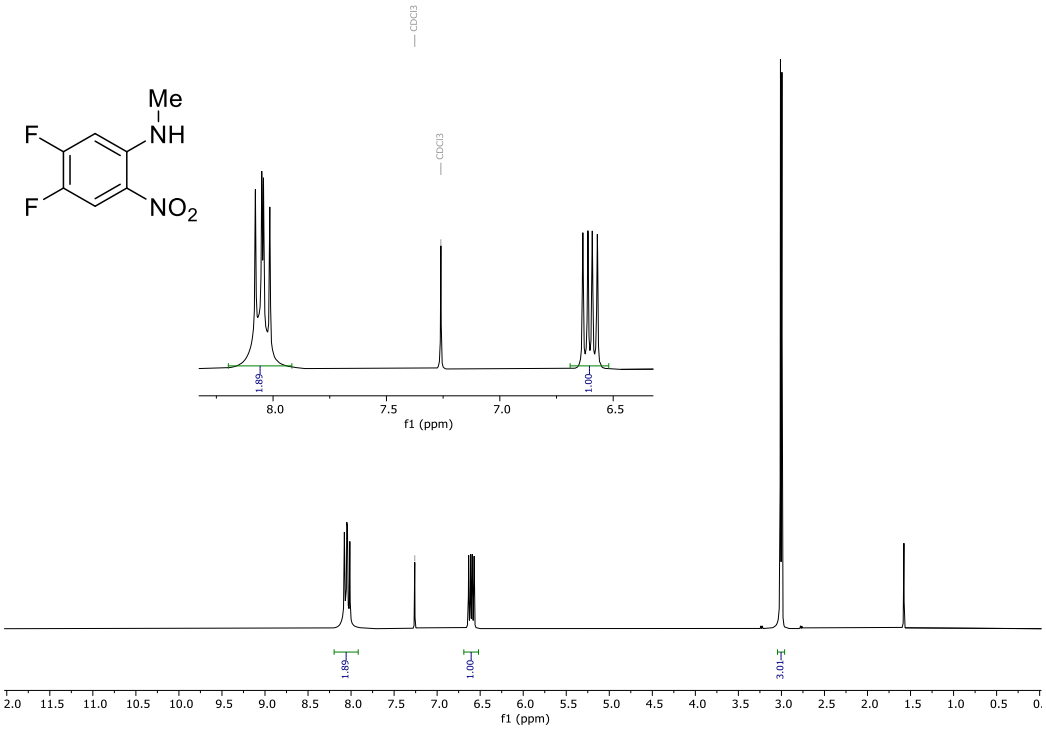

Spectrum 10 ^{1}H-NMR spectrum (300 MHz, $CDCl_3$)
of 4,5-difluoro-*N*-methyl-2-nitroaniline (**7**).

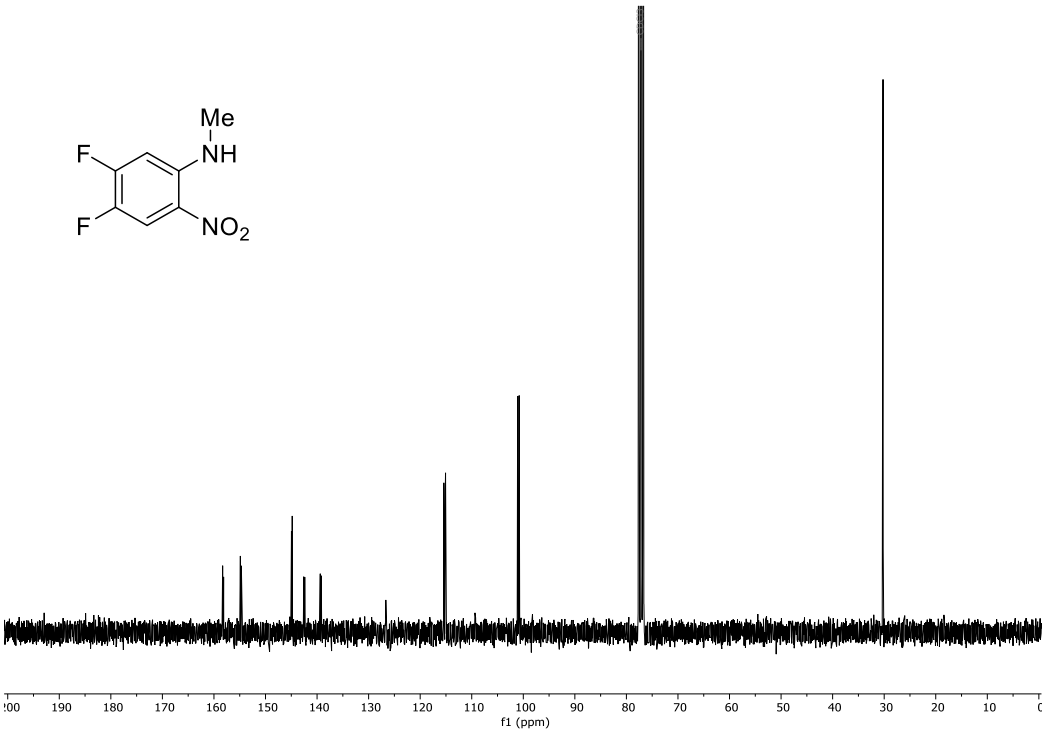

Spectrum 11 ^{13}C{^{1}H}-NMR spectrum (75 MHz, $CDCl_3$)
of 4,5-difluoro-*N*-methyl-2-nitroaniline (**7**).

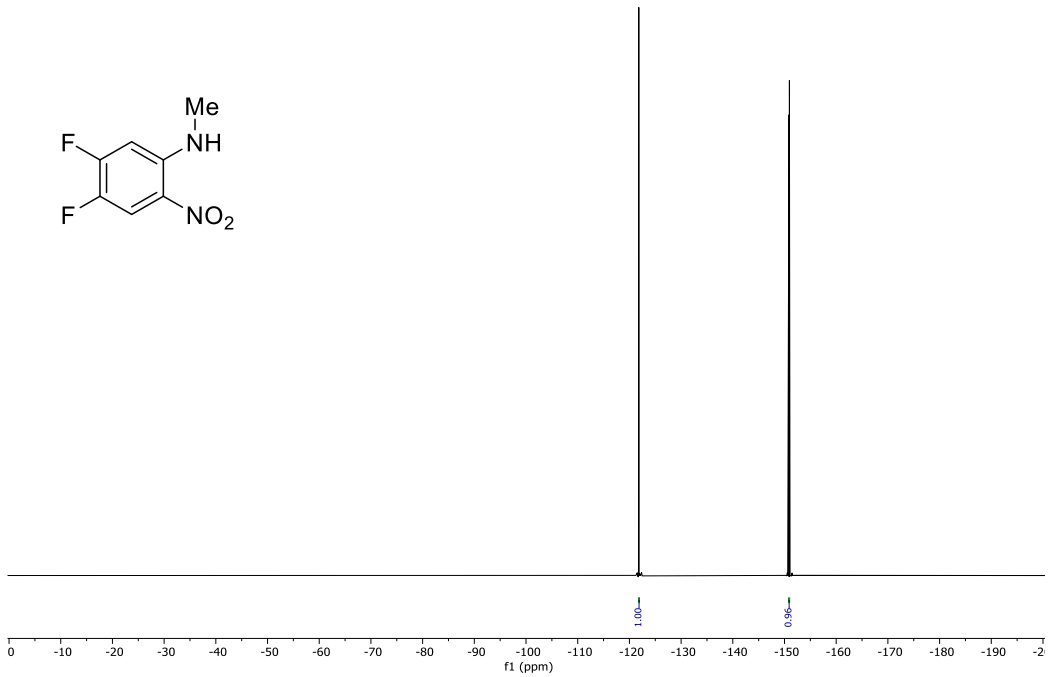

Spectrum 12 $^{19}F\{^{1}H\}$-NMR spectrum (282 MHz, $CDCl_3$)
of 4,5-difluoro-*N*-methyl-2-nitroaniline (**7**).

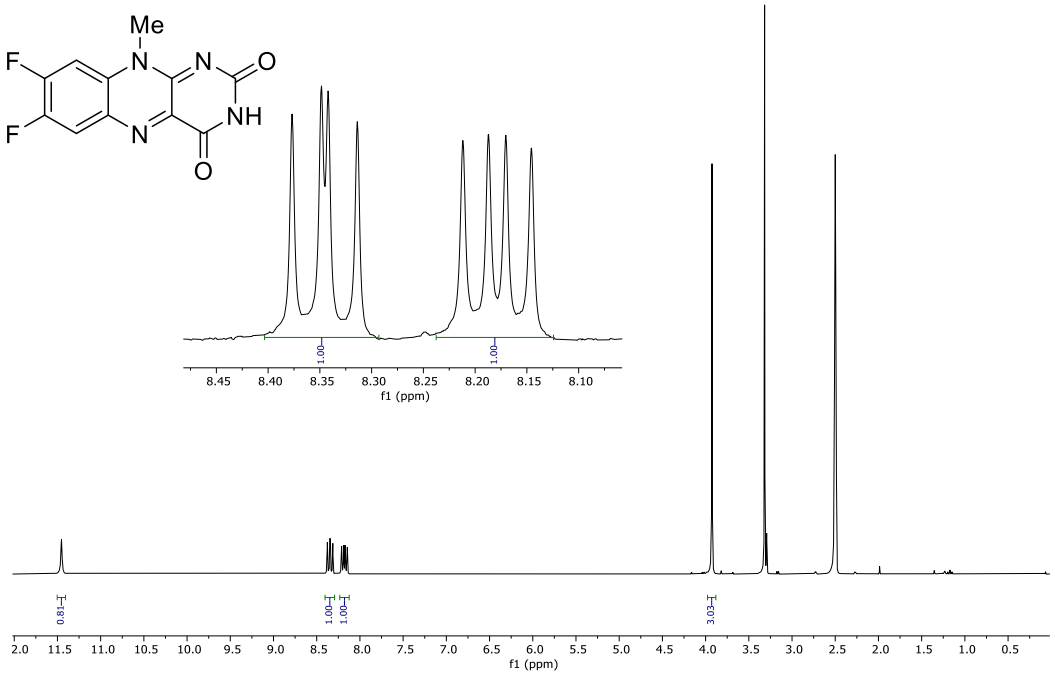

Spectrum 13 ^{1}H-NMR-spectrum (300 MHz, DMSO-d_6) of 7,8-difluoro-
10-methylbenzo[*g*]pteridine-2,4(3*H*,10*H*)-dione (**8**).

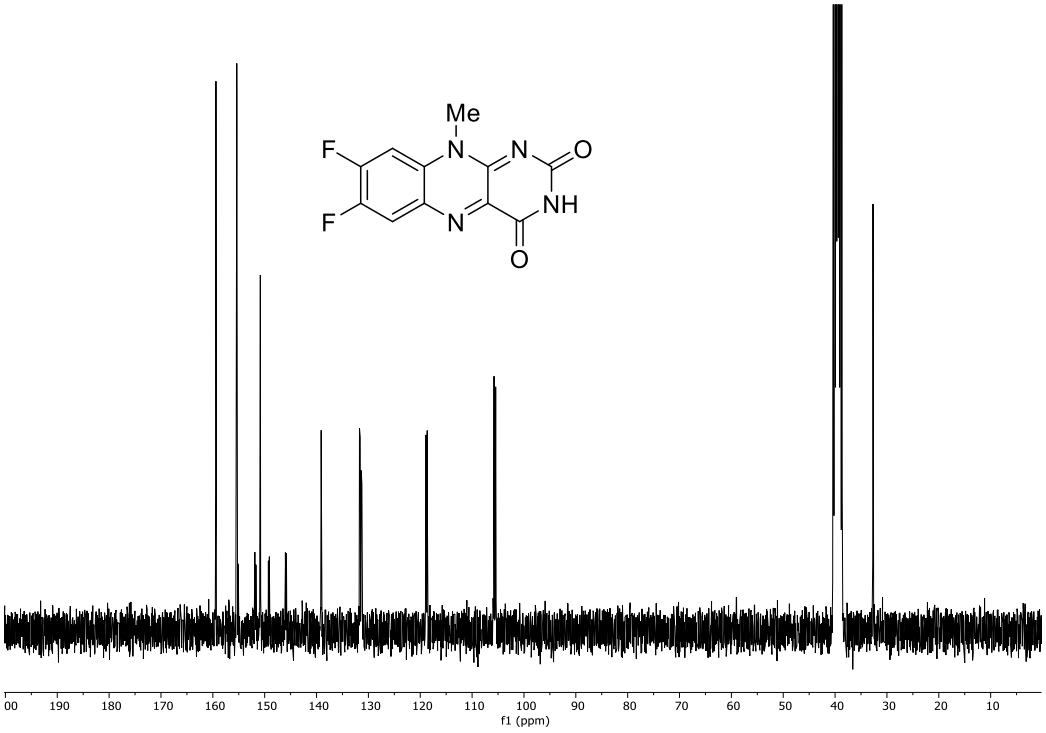

Spectrum 14 $^{13}C\{^{1}H\}$-NMR-spectrum (75 MHz, DMSO-d_6) of 7,8-difluoro-10-methylbenzo[*g*]pteridine-2,4(3*H*,10*H*)-dione (**8**).

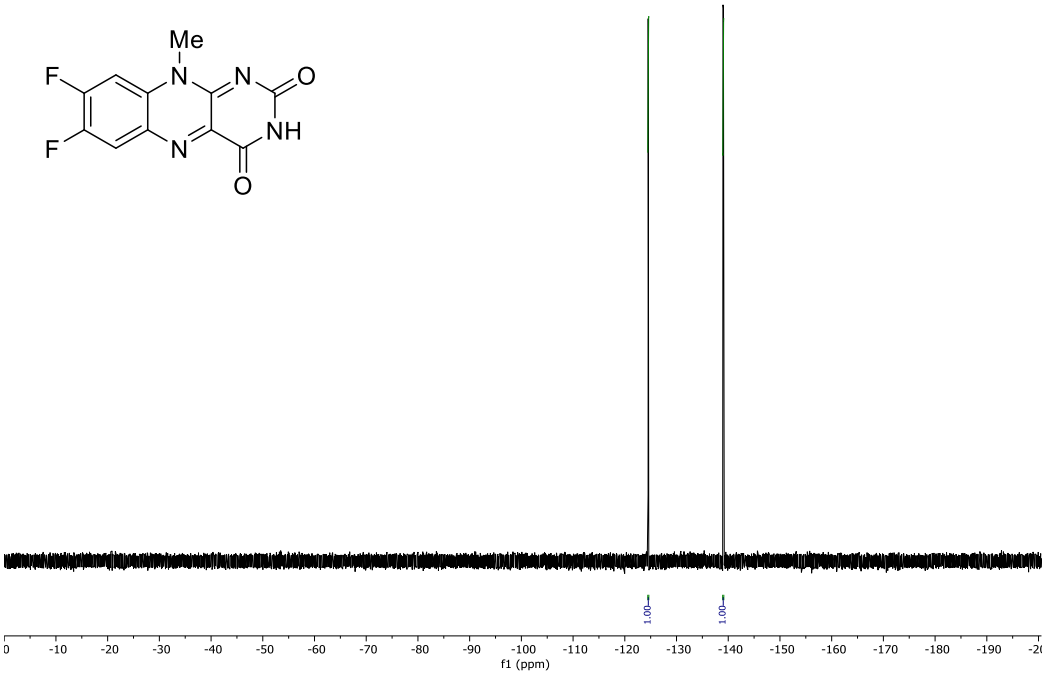

Spectrum 15 $^{19}F\{^{1}H\}$-NMR-spectrum (282 MHz, DMSO-d_6) of 7,8-difluoro-10-methylbenzo[*g*]pteridine-2,4(3*H*,10*H*)-dione (**8**).

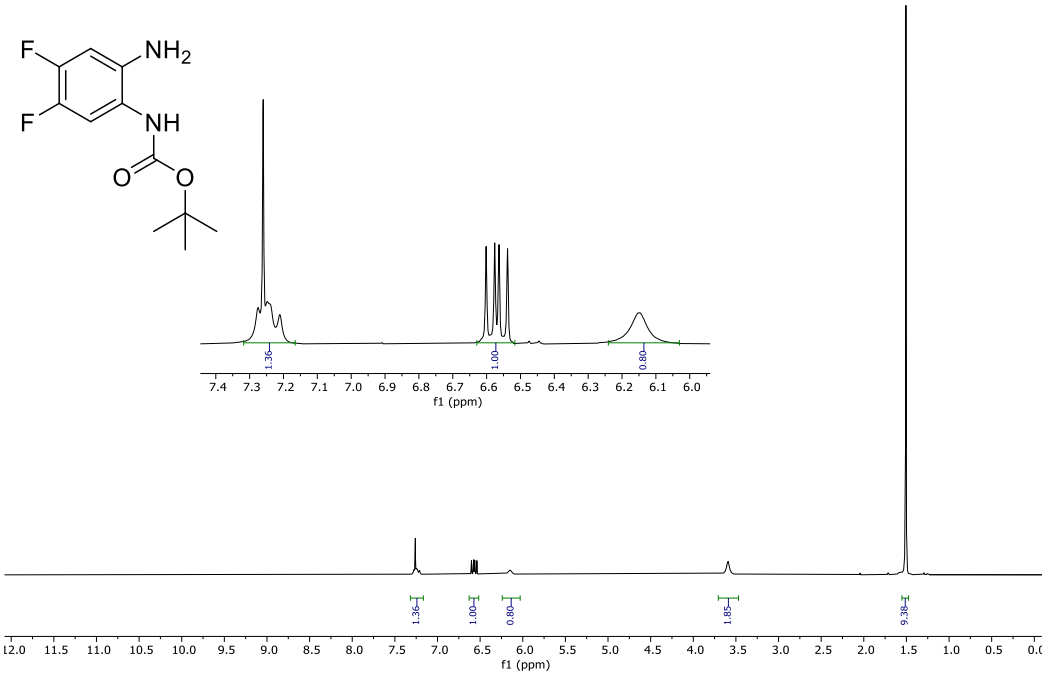

Spectrum 16 ^{1}H-NMR spectrum (300 MHz, $CDCl_3$)
of *tert*-butyl(2-amino-4,5-difluorophenyl)carbamate (**10**).

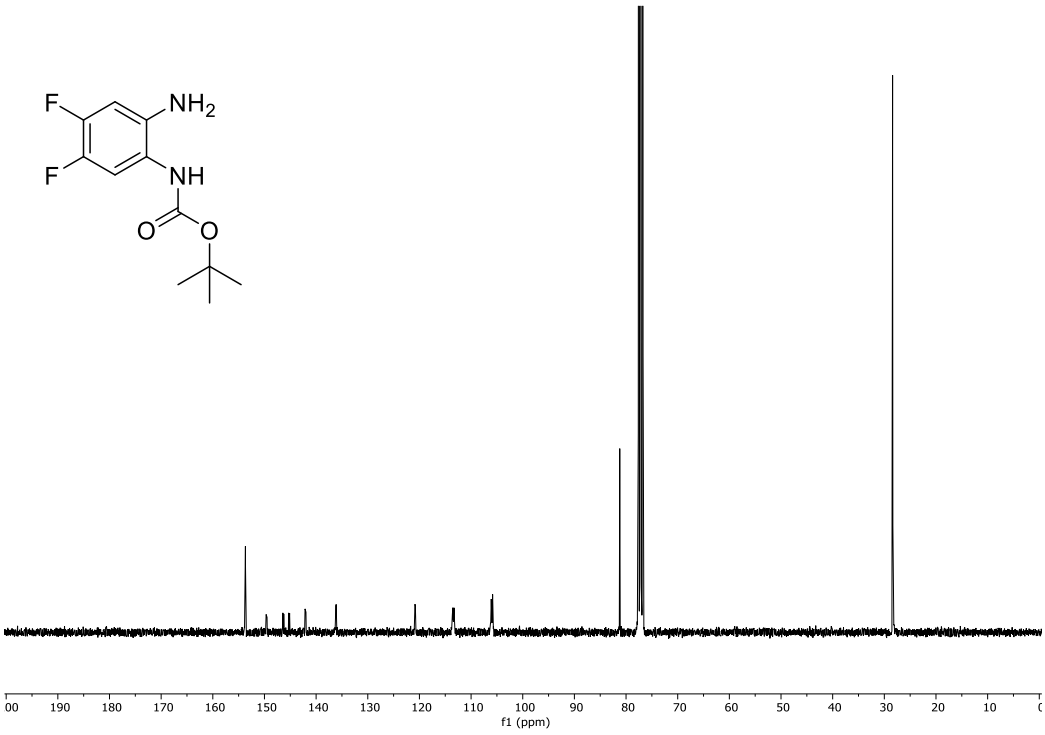

Spectrum 17 ^{13}C{^{1}H}-NMR spectrum (75 MHz, $CDCl_3$)
of *tert*-butyl(2-amino-4,5-difluorophenyl)carbamate (**10**).

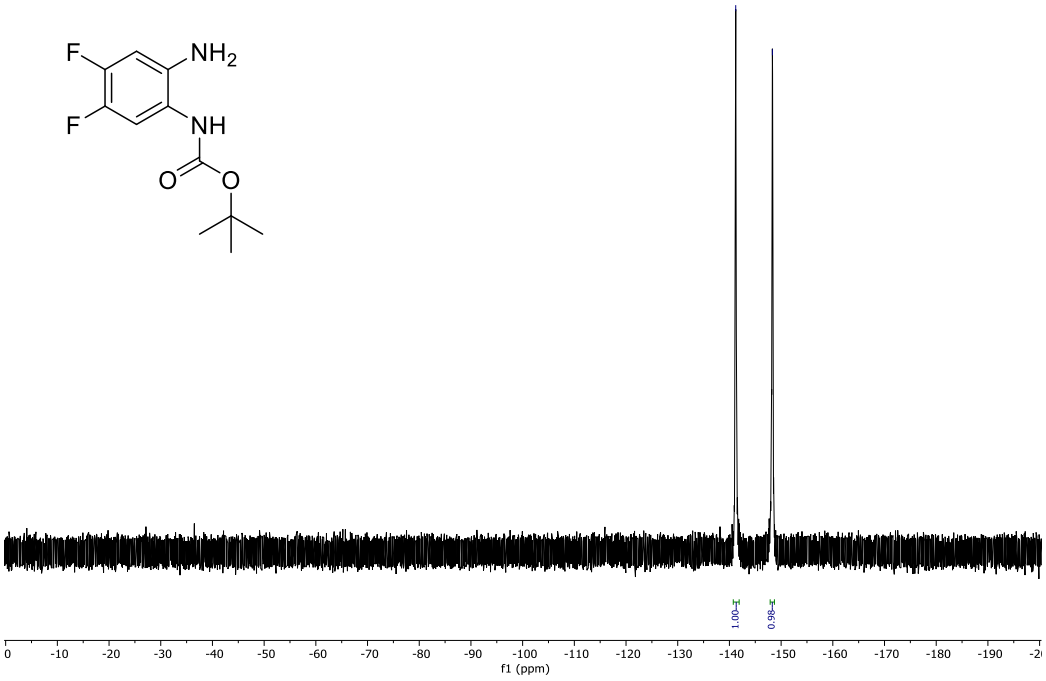

Spectrum 18 $^{19}F\{^{1}H\}$-NMR spectrum (282 MHz, $CDCl_3$)
of *tert*-butyl(2-amino-4,5-difluorophenyl)carbamate (**10**).

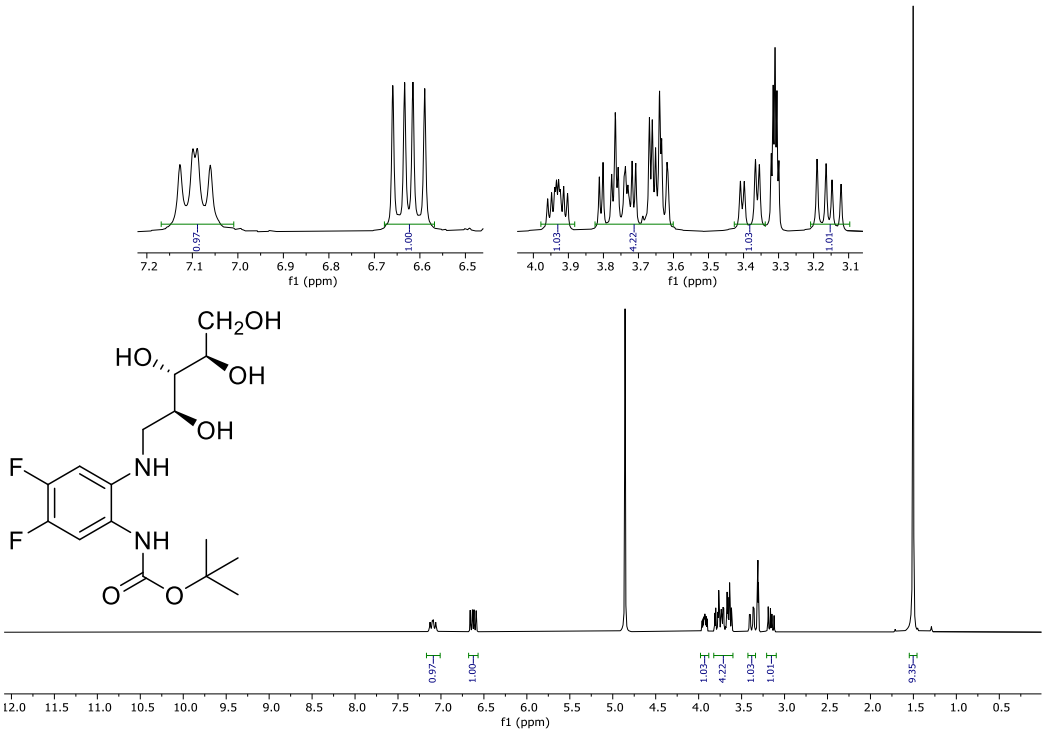

Spectrum 19 ^{1}H-NMR spectrum (300 MHz, MeOD) of *tert*-butyl(4,5-difluoro-2-(((2*S*,3*S*,4*R*)-2,3,4,5-tetrahyroxypentyl)amino)phenyl)carbamate (**11**).

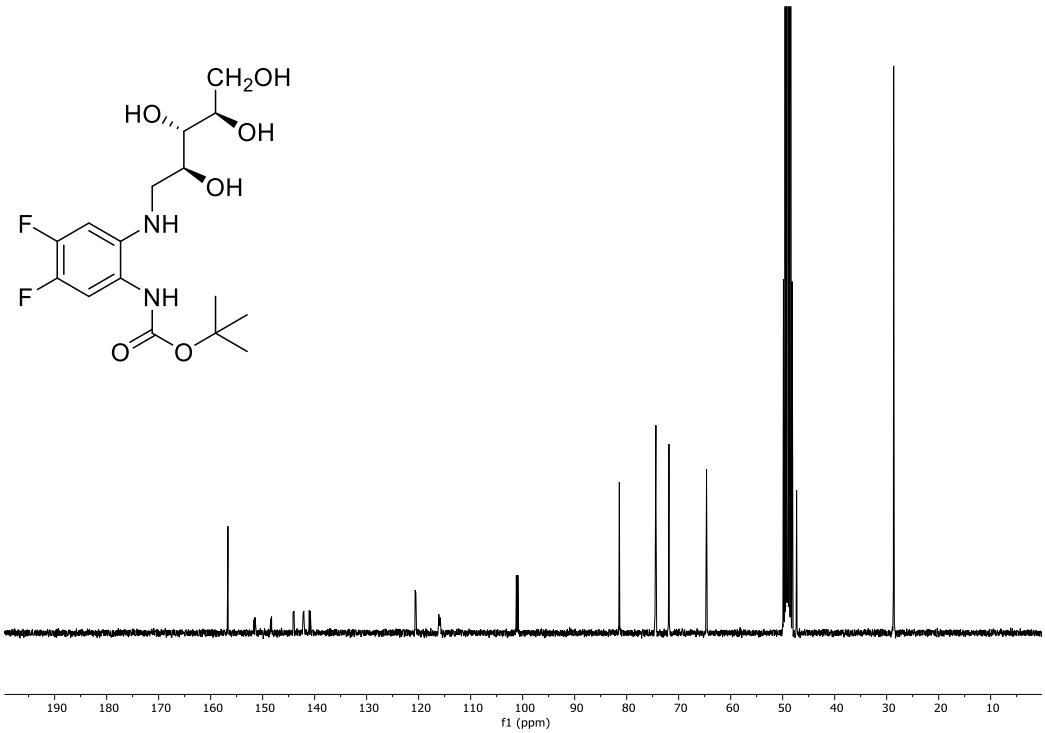

Spectrum 20 $^{13}C\{^{1}H\}$-NMR spectrum (75 MHz, MeOD) of *tert*-butyl(4,5-difluoro-2-(((2*S*,3*S*,4*R*)-2,3,4,5-tetrahydroxypentyl)amino)phenyl)carbamate (**11**).

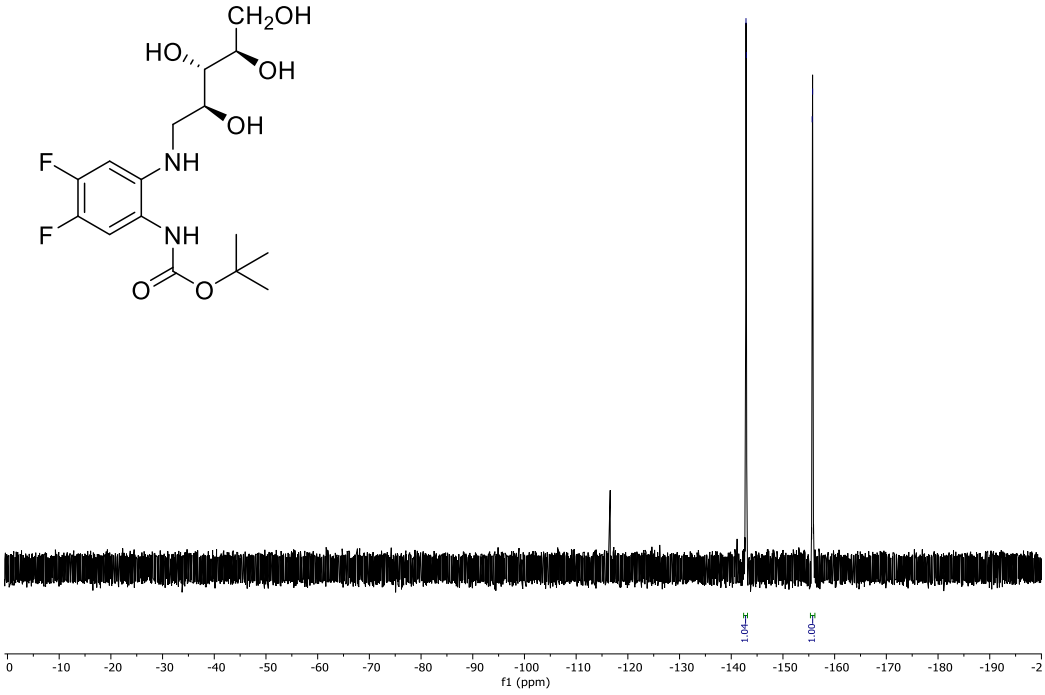

Spectrum 21 $^{19}F\{^{1}H\}$-NMR spectrum (282 MHz, MeOD) of *tert*-butyl(4,5-difluoro-2-(((2*S*,3*S*,4*R*)-2,3,4,5-tetrahydroxypentyl)amino)phenyl)carbamate (**11**).

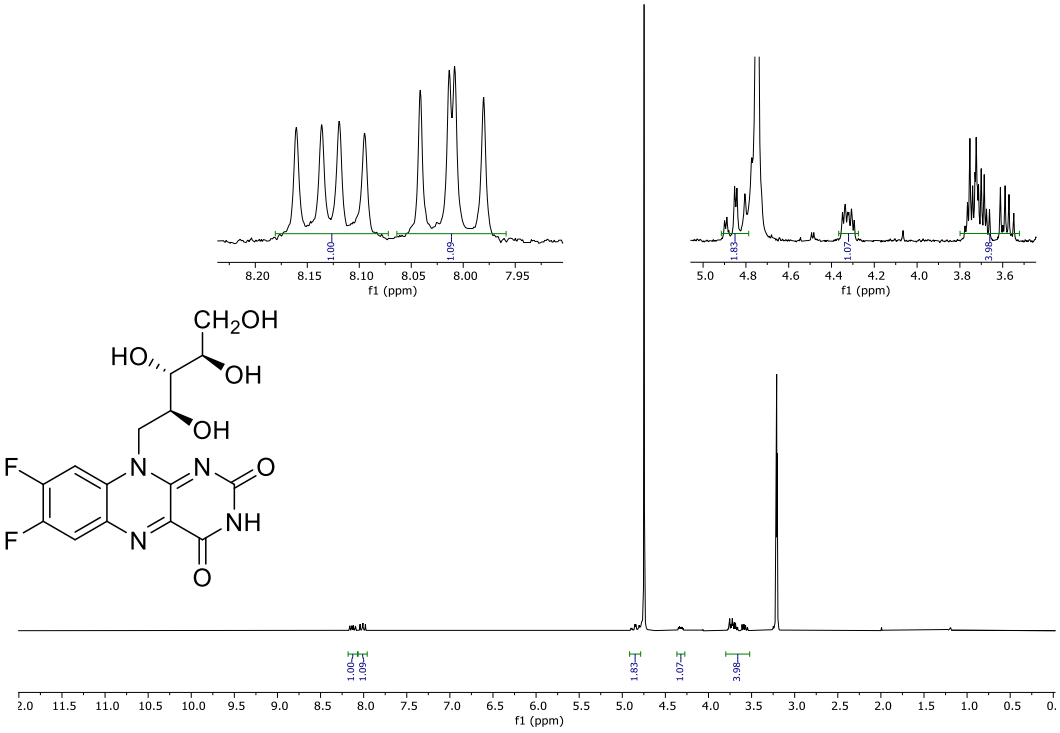

Spectrum 22 ^{1}H-NMR spectrum (300 MHz, MeOD) of 7,8-difluoro-10-((2*S*,3*S*,4*R*)-2,3,4,5-tetrahydroxypentyl)benzo[*g*]pteridine-2,4(3*H*,10*H*)-dione (**13**).

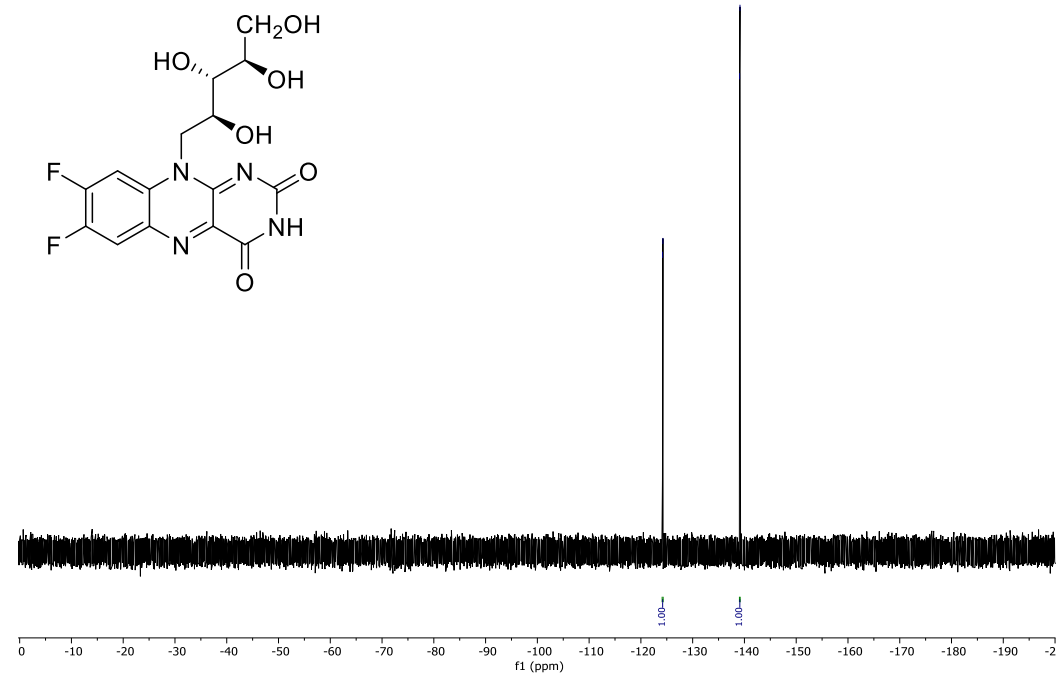

Spectrum 23 ^{19}F{^{1}H}-NMR spectrum (282 MHz, MeOD) of 7,8-difluoro-10-((2*S*,3*S*,4*R*)-2,3,4,5-tetrahydroxypentyl)benzo[*g*]pteridine-2,4(3*H*,10*H*)-dione (**13**).

ChemPhotoChem

Research Articles
doi.org/10.1002/cptc.202200040

Chemistry Europe
European Chemical Societies Publishing

www.chemphotochem.org

Special Collection

Computer-Aided Design of Fluorinated Flavin Derivatives by Modulation of Intersystem Crossing and Fluorescence

Mario Bracker,[a] Mira K. Kubitz,[b] Constantin Czekelius,[b] Christel M. Marian,[a] and Martin Kleinschmidt*[a]

This study aims at finding fluorinated flavin derivatives with modified intersystem crossing (ISC) and fluorescence properties. In total, photophysical properties of 8 derivatives were investigated computationally using combined density functional theory and multireference configuration interaction methods. On top of a screening procedure, the excited-state decay mechanisms of selected chromophores were investigated in detail. Kinetic schemes including fluorescence, ISC as well as internal conversion (IC) channels were set up to unravel the complex excited-state decay kinetics. We find two chromophores that exhibit promising properties with respect to fluorescence microscopy. Distinctive stabilization of the bright S_1 $\pi\pi^*$ state results in absorption in the green wavelength region and emission of (infra-)red light. The $^1(\pi_H\pi_L) \rightsquigarrow {}^3(\pi_{H-1}\pi_L)$ ISC channel of the flavin chromophore was found to be deactivated upon both modifications, but nonradiative deactivation of the fluorescence by IC appears to be a problem. Alternative modifications of the pteridine dione moiety were found to result in a marked stabilization of $n\pi^*$ states along with activation of El-Sayed allowed ISC channels. For the latter two compounds, we predict fluorescence to be quenched by ISC followed by efficient population of the long-lived T_1 state via IC.

Introduction

Diverse photoreactive proteins carry a flavin moiety.[1–7] Among photoreceptors, phototropins are plasma-membrane-associated proteins mediating primarily phototropic plant movement.[8–10] In phototropins, the optically active flavin mononucleotide (FMN) is incorporated into light, oxygen and voltage sensitive (LOV) domains. Upon characteristic blue-light absorption,[11–13] the photosensing LOV domain undergoes a photocycle: The lowest-lying triplet state of FMN is efficiently populated via intersystem crossing (ISC). Accompanied by another ISC, a metastable adduct between the cofactor and a nearby cysteine residue is formed transducing a structural signal to an effector domain.[13–15] Eventually, the adduct decomposes thermally on the timescale of seconds.[16] Various modified flavins (8-isopropyl,[17] 1- and 5-deaza,[18] 8-bromo and 8-trifluoromethyl,[19] roseoflavin[20,21] as well as methyl substitution patterns[17,22,23] in positions 7 and 8) have been incorporated into LOV domains. Riboflavin-5′-phosphate (FMN) can be divided into two parts: Lumiflavin (LF) and the ribophosphyl chain attached to the nitrogen atom in position 10 of the core ring (see Figure 1). The latter is involved in the signal transduction upon excitation of the LF moiety by blue-light absorption. The photophysics of FMN is dominated by the isoalloxazine core ring and the experimental absorption as well as emission spectra of FMN and LF are found to be very similar.[11,12] LF exhibits two methyl groups in positions 8 and 9 (see Figure 1), which have minor influence on the photophysics.[24]

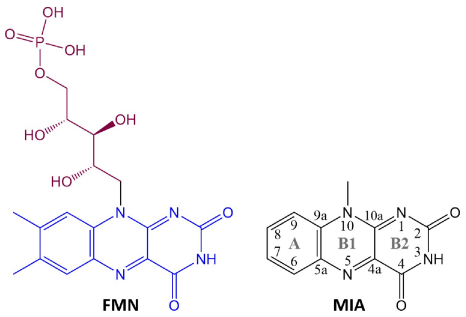

Figure 1. Chemical structures of flavin mononucleotide (FMN) and 10-methylisoalloxazine (MIA). The structure highlighted in blue colour is the lumiflavin (LF) chromophore and the ribophosphyl chain is illustrated in wine-red colour.

[a] M. Bracker, Prof. C. M. Marian, Dr. M. Kleinschmidt
Institute of Theoretical and Computational Chemistry, Heinrich-Heine-University Düsseldorf, D-40204 Düsseldorf, Germany
E-mail: Martin.Kleinschmidt@hhu.de
[b] M. K. Kubitz, Prof. C. Czekelius
Institute of Organic and Macromolecular Chemistry, Heinrich-Heine-University Düsseldorf, D-40204 Düsseldorf, Germany

Supporting information for this article is available on the WWW under https://doi.org/10.1002/cptc.202200040

An invited contribution to a Special Collection on Emissive Materials for Organic Light Emitting Diodes

Modulation of intersystem crossing

The ISC channels of naturally occurring flavins have been analyzed in several previous studies, either linked to the mechanism of photoreception[13,15,25] or describing the isolated chromophore.[24,26,27] In this study we focus on the core ring (MIA, see Figure 1). Starting from the equilibrium geometry of the S_1 $\pi_H\pi_L$ state of MIA, three triplet states have been found to be decisive for the efficiency of ISC: T_1, T_2 and T_3. The electronic structure of the T_1 state corresponds to the one of the bright S_1 state, the T_2 state exhibits nitrogen-centered [N(1+5)] $n_N\pi^*$ character and the T_3 $\pi_{H-1}\pi_L$ transition is an internal charge transfer (ICT) from the benzene (A) ring to the peridinone (B) rings of MIA (see Figure 1). The role of the latter two states for deactivation strongly depends on the polarity and proticity of the environment: Polar interactions cause a strong blueshift of the $n\pi^*$ states and a stabilization of the ICT state (see Figure 2, middle scheme). As a result, the fast El-Sayed allowed $^1(\pi_H\pi_L)\rightsquigarrow{}^3(n_N\pi_L)$ channel, accessible in vacuum and apolar media, is deactivated and ISC relies on spin–vibronic interactions instead.[24,27] $S_1\rightsquigarrow T_1$ and $S_1\rightsquigarrow T_3$ ISC are promoted by a Herzberg-Teller-like intensity borrowing mechanism:[28–30] Invoking vibrational spin–orbit coupling, the $\pi\pi^*$ states partially adopt $n\pi^*$ character thus increasing the ISC probability. Reiffers et al. determined ISC of MIA in aqueous medium from femtosecond transient absorption and nanosecond laser flash photolysis experiments ($k_{ISC} = \Phi_T/\tau_F$) to take place with a rate constant of about 1×10^8 s^{-1}.[26] With the aid of advanced quantum chemical methods, $^1(\pi_H\pi_L)\rightsquigarrow{}^3(\pi_{H-1}\pi_L)$ ISC was identified as the productive channel featuring a rate constant of 3×10^8 s^{-1}, approximately two orders of magnitude faster than the alternative $^1(\pi_H\pi_L)\rightsquigarrow{}^3(\pi_H\pi_L)$ channel.[24,27] $^3(\pi_{H-1}\pi_L)\rightsquigarrow{}^3(\pi_H\pi_L)$ internal conversion (IC) takes place at the femtosecond timescale ($>10^{13}$ s^{-1}, see Section S8 in the Electronic Supplementary Information (ESI)). The $^3(\pi_{H-1}\pi_L)$ population is thus rapidly transferred to the T_1 $^3(\pi_H\pi_L)$ state. The experimental triplet quantum yield of MIA amounts to $\Phi_T = 0.5\ (\pm0.1)$ in aqueous solution.[26] With a rate constant of approximately 5×10^7 s^{-1} and a quantum yield of $\Phi_F = 0.22\ (\pm0.01)$ fluorescence is nearly competitive to ISC in MIA.[26,27] This finding raises the question, whether and how the decay mechanism of MIA following photo excitation could be modified to either increase the fluorescence quantum yield or the triplet quantum yield of the chromophore.

In principle, there are two approaches to modulate the complex ISC mechanism of flavins: a) modify the chromophore itself[18,19,21,27,31,32] or b) adjust the polarity and proticity of the environment.[24,33] This study focuses on the modification of the MIA chromophore in aqueous solution. Activation of an El-Sayed favoured ISC channel is anticipated to result in high Φ_T and deactivation of the $^1(\pi_H\pi_L)\rightsquigarrow{}^3(\pi_{H-1}\pi_L)$ channel is taken as the best-case scenario for raising Φ_F (see Figure 2).

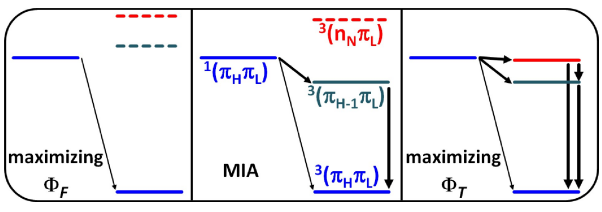

Figure 2. Schematic depiction of adiabatic energies associated with increased fluorescence quantum yield (left) or increased triplet quantum yield (right), respectively. The middle scheme illustrates the adiabatic energies of MIA in aqueous solution. Dashed states are thermodynamically inaccessible from the $^1(\pi_H\pi_L)$ state and the thickness of the arrows correlates with the magnitudes of the rate constants.

Modification of the flavin chromophore

To find potential chromophores suitable for each scenario depicted in Figure 2, we use a screening method that is motivated by our latest work on flavin derivatives fluorinated in the A-ring of MIA.[27] Fluorine is a very potent substituent when it comes to tailoring photophysical properties.[26,27,34–37] For one thing, it is the element with the highest electronegativity and therefore a strong impact on the electronic structure is expected. Secondly, the steric change when substituting hydrogen by fluorine is small.[38,39] A positive side effect is the stabilization with respect to photo-oxidation.[40,41] In the present study, fluorine is incorporated into the B-rings (Figure 3). In particular, the substitution pattern focuses on the carbonyl groups and the nitrogen atoms in positions 1 and 5 of the pteridine dione unit (see Figure 1 for atom labels). The studies address the influence of a single fluorine atom or geminal disubstitution by fluorine. Compounds $2CF_2$-MIA and $4CF_2$-MIA, in which the C=O moiety is replaced by a difluoromethylidene group, incorporate an electron-deficient enamine. In solution, acid-catalyzed tautomerization to the corresponding pteridi-

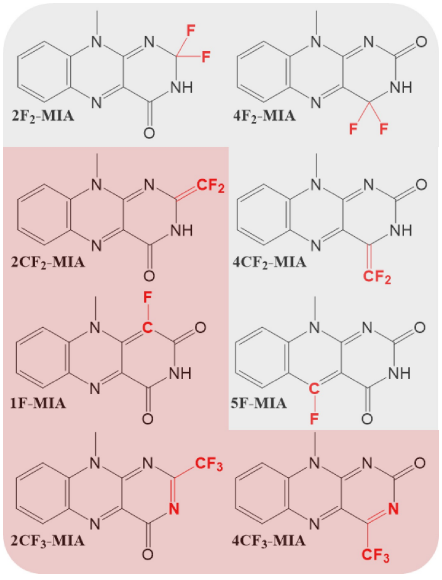

Figure 3. Chemical structures of flavin derivatives investigated in this work. Derivatives highlighted with red background are studied in detail with respect to excited state kinetics.

none may occur, which is prevented e.g. by N-alkylation rendering the depicted compounds suitable models for calculation.

Our previous in-depth study on the fluorination of carbon centers in the A-ring revealed that shifts of vertical electronic energies with respect to the parent compound at the ground-state geometry can be used to estimate adiabatic electronic energies of excited states with reasonable precision.[27] In the present study, we rely on this observation and, in a first step, characterize the derivatives at the ground state geometry. The most promising candidates are then investigated in further detail with respect to their excited state kinetics.

Methods and Computational Details

Ground state geometries were optimized at the density functional theory (DFT) level utilizing the Turbomole 7.3 program package.[42,43] The B3LYP functional[44,45] combined with the TZVP basis set[46] was employed. For excited singlet states, full linear response equations were solved[47] and for triplet states the Tamm–Dancoff approximation[48] was chosen to avoid triplet instabilities. Unless otherwise stated, a C_s symmetry constraint was applied for geometry optimization. Vibrational frequency analyses were carried out using numerical second derivatives with the SNF program.[49] Subsequent DFT/MRCI[50] single-point calculations were performed with the original parametrization established by Grimme and Waletzke.[51] DFT/MRCI is a semi-empirical multireference configuration interaction ansatz based on Kohn-Sham orbitals (BHLYP)[45,52] as a one-particle basis. For the construction of two-electron integrals, the TZVP auxiliary basis set[53] from the Turbomole library was applied for the resolution-of-identity approximation.[54] In the case of singlet states 12 roots were computed and for triplets 8 states were considered. DFT/MRCI computed line spectra were broadened in the cm^{-1} regime using a Gaussian function with a standard deviation of $\sigma = 1500\,cm^{-1}$ and then converted to nm. Environment effects of aqueous solution at ambient temperature were mimicked applying the implicit solvation model COSMO[55] with a relative permittivity of $\varepsilon_r = 80$ to the ground state optimizations as well as DFT/MRCI calculations. Solvation effects at the excited state geometries were included by introducing state-specific energy shifts as described in reference [56]. Wavefunction analysis based on Löwdin orthogonalization of the one-electron density matrix was carried out using the TheoDORE program.[57,58] We computed spin–orbit coupling matrix elements (SOCMEs) at the DFT/MRCI level of theory using the program package SPOCK[59,60] developed in our laboratory. The coupling is described by a spin–orbit mean-field (SOMF) approximation[61,62] of the Breit–Pauli spin–orbit operator. Non-adiabatic coupling matrix elements (NACMEs) were obtained with our newly developed program DELTA.[56] ISC and IC rate constants at ambient temperature were computed via the generating function approach as implemented in the program VIBES.[56,63,64] For all ISC channels, numerical derivatives of the SOCMEs were computed at the respective equilibrium geometries. Corresponding generating functions, G_{ISC} and G_{IC}, can be found in references [64] and [56] respectively.

$$k_{NR}^{a\rightsquigarrow b} = Z^{-1}\int_{-\infty}^{+\infty} G_{NR}\, e^{it\Delta E_{ab}}\, dt \qquad (1)$$

$Z = \sum_j e^{-E_{aj}/k_B T}$ is the canonical partition function for vibrational motion in the initial electronic state and ΔE_{ab} is the adiabatic separation of states a and b. Fluorescence rate constants are given by

$$k_F^{a\rightarrow b} = \frac{1}{3\pi\varepsilon_0 h^4 c^3}\Delta E_{ab}^3 |\vec{\mu}_{ab}|^2\,, \qquad (2)$$

where $\vec{\mu}_{ab}$ is the transition dipole moment and in this case ΔE_{ab} represents the vertical energy of electronic states a and b. Fluorescence spectra were computed with the program VIBES to include explicit vibrational broadening.

Results and Discussion

Screening of derivatives

Figure 4 illustrates the influence of each modification on the electronic energies of selected states at the ground state geometries in aqueous medium. The depicted shifts refer to the vertical excitation energies of the stem compound MIA. The respective data of MIA is summarized in Table 1. The character of the electronic states is determined by the leading configuration and the values in parentheses represent the squared coefficients of the contribution. The numbering of the n_N orbitals refers to the energetic order of the different linear

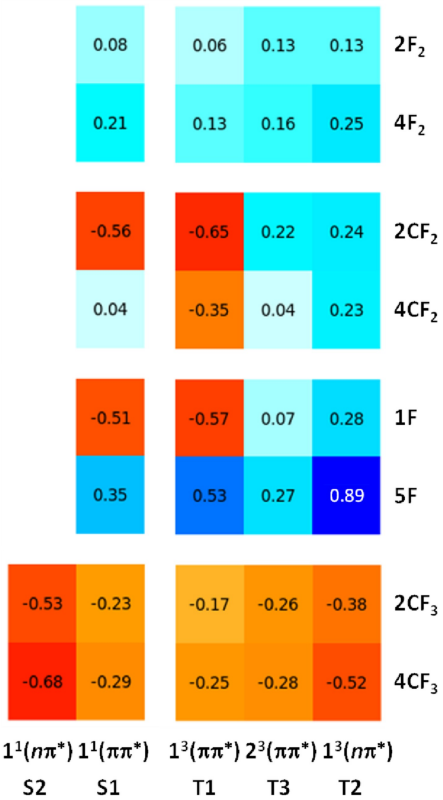

Figure 4. Illustration of the impact of modification on the electronic energies of the S1 as well as T1–T3 states in aqueous medium. For 2/4CF_3-MIA the $^1(n\pi^*)$state is included. The blue-/redshifts in eV are computed at the ground state geometries and refer to the vertical excitation energies of MIA.

Table 1. Excited states properties of MIA in aqueous solution.

State	Electronic structure ($\|c\|^2$)	$\Delta E_{vertical}$ / eV (*f*)
$^1(\pi_H\pi_L)$	$\pi_H \rightarrow \pi_L$(0.83)	2.96 (*0.275*)
$^1(n_N\pi_L)$	$n_{N2} \rightarrow \pi_L$(0.76)	3.47
$^3(\pi_H\pi_L)$	$\pi_H \rightarrow \pi_L$(0.88)	2.33
$^3(\pi_{H-1}\pi_L)$	$\pi_{H-1} \rightarrow \pi_L$(0.81)	2.86
$^3(n_N\pi_L)$	$n_{N2} \rightarrow \pi_L$(0.70) + $n_{N1} \rightarrow \pi_L$(0.14)	3.12

combinations. In the case of the deaza-compounds, only one n_N orbital remains and for $2CF_3$- as well as $4CF_3$-MIA a third n_N orbital is introduced. Corresponding oxygen-centered n_O orbitals are strongly stabilized in polar environment.[24,27] However, the n_{O2} orbital gains significance for the $n\pi^*$ states of the deaza-compounds. The notation of states without subscript (e.g. S1 instead of S_1) refers to the order of the electronic states at the ground-state equilibrium geometry.

For $2CF_3$- as well as $4CF_3$-MIA, the $^1(n_N\pi_L)$ state is added as the $n\pi^*$states are strongly stabilized. For the other molecules, the $^1(n_N\pi_L)$ state is blueshifted and therefore neglected. Molecular orbitals and tables summarizing excited state properties are presented here only for the most interesting derivatives, i.e., 1F-, $2CF_2$, $2CF_3$- as well as $4CF_3$-MIA. Corresponding data for the remaining fluorinated flavins is displayed in Section S1 in the ESI. Fragment-based analysis, absorption spectra, orbital energies, transition dipole moments and additional depictions of molecular orbitals are collected in Sections S2–6 in the ESI.

$2CF_2$-MIA and $4CF_2$-MIA. $2CF_2$-MIA and $4CF_2$-MIA differ from the stem chromophore MIA by an isolobal replacement of the oxygen atom in 2- or 4-position by difluoro-methylidene. Interestingly, these substitutions have vastly different effects on the energetic location of the first excited singlet state. While the S1 state undergoes a small blueshift of 0.04 eV in $4CF_2$-MIA, in the corresponding derivative modified in position 2 the $^1(\pi_H\pi_L)$ state is strongly redshifted by more than half an electronvolt (−0.56 eV). This remarkable difference is not reflected in the main character of the excitation, in both cases the S1 state is described as $\pi_H \rightarrow \pi_L$ transition by about 80 %. The molecular orbitals generally are destabilized upon introduction of CF_2. Whilst the effect is similar for the π_L orbitals, the energetic shift of the π_H orbital is far less pronounced for modification in position 4. To rationalize this finding, the π_H orbitals have to be inspected (compare Figures 5, and S1 in the ESI): In both cases we find a strong electron withdrawing effect diminishing the electron density on the benzene core and for modification in position 2 of the B2-ring, the nodal structure on the B1-ring is changed. The same applies to the T1 state, which is redshifted by −0.65 eV for $2CF_2$-MIA compared to −0.35 eV for modification in position 4. The blueshift of the $^3(n_N\pi_L)$ state is almost the same for both derivatives, whereas the destabilization of the $^3(\pi_{H-1}\pi_L)$ state strongly depends on the position of modification. The more pronounced blueshift of the latter excitation in $2CF_2$-MIA (0.22 eV compared to 0.04 eV) is explained by the remarkably high admixture of the $\pi_{H-2}\pi_L$ excitation to an extent that the main character changes (Table 2). As a consequence, the S1 and T1 states of $2CF_2$-MIA

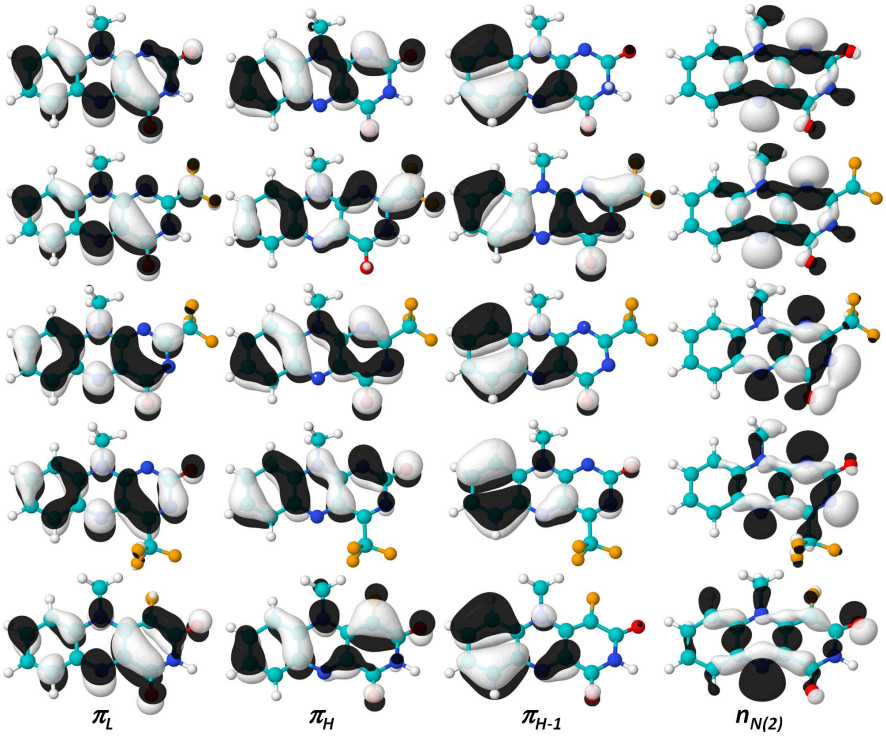

Figure 5. Frontier orbitals (isovalue = 0.03) of MIA, $2CF_2$-MIA, $2CF_3$-MIA, $4CF_3$-MIA, and 1F-MIA in aqueous solution (top to bottom).

Table 2. Excited states properties of $2CF_3$-MIA in aqueous solution.

State	Electronic structure ($\|c\|^2$)	$\Delta E_{vertical}$ / eV (*f*)
$^1(\pi_H\pi_L)$	$\pi_H \rightarrow \pi_L$(0.80)	2.40 *(0.271)*
$^3(\pi_H\pi_L)$	$\pi_H \rightarrow \pi_L$(0.85)	1.69
$^3(\pi_{H-2}\pi_L)$	$\pi_{H-2} \rightarrow \pi_L$(0.35) + $\pi_{H-1} \rightarrow \pi_L$(0.29) + $\pi_H \rightarrow \pi_{L+1}$(0.16)	3.08
$^3(n_N\pi_L)$	$n_{N2} \rightarrow \pi_L$(0.72) + $n_{N1} \rightarrow \pi_L$(0.10)	3.36

are separated energetically from higher lying states and depopulation of the S1 state via ISC is limited to the El-Sayed forbidden $^1(\pi_H\pi_L) \rightsquigarrow {}^3(\pi_H\pi_L)$ channel. In accordance with the mirror image rule, the fluorescence wavelength is predicted to be strongly redshifted by more than half an electronvolt resulting in emission of (infra-)red light. This prediction is confirmed by further studies in Section 3.2. In the case of $4CF_2$-MIA, the impact on the energetics of the $^1(\pi_H\pi_L) \rightsquigarrow {}^3(\pi_{H-1}\pi_L)$ ISC channel is found to be minimal and the $^3(n_N\pi_L)$ state remains inaccessible. Whilst the energetic position of the bright S1 absorption band barely changes, an increase of the transition dipole moment by about 20 % results in an oscillator strength of $f = 0.412$.

$2F_2$- and $4F_2$-MIA. Substitution of the oxygen atom in position 2 by two fluorine atoms results in a weak blueshift of the considered states. The effect ranges from 0.06 eV for the $^3(\pi_H\pi_L)$ state to 0.13 eV for the higher triplets and the S1 state is destabilized by 0.08 eV. The explanation for this uniform effect lies within the electron distribution of the π_L orbital (compare Figures 5 and S1 in the ESI): In the stem compound, MIA, it describes a π-system spanning the whole chromophore. The removal of the oxygen atom interrupts the π-system in position 2 and diminishes delocalisation. $4F_2$-MIA, in all aspects, is very similar to $2F_2$-MIA. Destabilization of the π_L orbital goes hand in hand with blueshifting the considered electronic states. The replacement of the oxygen atom attached to C(4) results in more pronounced shifts (0.13 eV–0.25 eV). Inspecting the π_L orbital of MIA, it is not surprising that the destabilization for $4F_2$-MIA turns out to be stronger: Electron density on the B2-ring is mainly localised in positions 4, 4(a) and 10(a). Contrary to the π_L orbital, the π_{H-1} orbital does not possess a significant amount of electron density in position 2 as well as 4 and consequently modification does not have a marked impact. The picture is similar for the σ-bonds described by the n_{N2} orbitals. In conclusion, the modifications investigated are not expected to have a strongly modulating effect on ISC. The absorption spectra resemble that of MIA aside from the general blueshift. The oscillator strength of the bright $^1(\pi_H\pi_L)$ absorption band is reduced by about 28 % upon replacement of the oxygen atom bound to C(2) by two fluorine atoms, whereas it does not decrease for modification in position 4 as the impairment of the transition dipole moment is much weaker and the increase in energy counteracts the effect. In agreement with the overall trend, the fluorescence wavelengths are predicted to be blueshifted by about 0.1 eV for $2F_2$-MIA and 0.2 eV for $4F_2$-MIA.

$2CF_3$- and $4CF_3$-MIA. $2CF_3$- and $4CF_3$-MIA are modified in positions 2/4 as well as 3. The carbon atoms in positions 2/4 are equipped with trifluoromethyl groups and the hydrogen atom in position 3 is removed, thus introducing an additional double bond in the B2 ring. For $2CF_3$- and $4CF_3$-MIA, all considered states are computed to be stabilized (Tables 3 and 4), regardless whether the state exhibits $\pi\pi^*$ or $n\pi^*$ character. The striking feature here is that the stabilization of $n\pi^*$ states is significantly stronger, which is a direct consequence of removing the hydrogen atom in position 3. As a result, a third nitrogen-centered n_N orbital is introduced and the nitrogen atom N(3) has a significant share in the energetically highest-lying n_{N3} orbital (Figure 5). The general redshift of all excitations is explained by a comparatively strong impact of the modification on the π_L orbital as it is stabilized to a higher extent than the other π orbitals. The principal difference between the π_L orbitals of MIA and those of $2CF_3$- and $4CF_3$-MIA is that the out-of-plane p orbital of the oxygen atom directly contributes to the π-system, whereas the trifluoromethyl group influences the π-system via hyperconjugation. Remarkably, for $4CF_3$-MIA all redshifts are computed to turn out even more pronounced. We attribute this effect to the clear quinoid structure of the π-system in the B-rings. As is to be expected, the stabilization of the considered states is reflected in the absorption spectra of $2/4CF_3$-MIA: The characteristic absorption bands are redshifted by >0.2 eV. Regarding the $^3(n_N\pi_L)$ state of $4CF_3$-MIA, the share of the oxygen lone pair is negligibly small. The enhanced stabilization of $n_N\pi^*$ states for $4CF_3$-MIA is predicted to have profound effects on the excited state kinetics of the chromophore. The $^1(n_N\pi_L)$ and $^1(\pi_H\pi_L)$ minima are estimated to be nearly isoenergetic, so that additional ISC channels are introduced. The El-Sayed allowed $^1(\pi_H\pi_L) \rightsquigarrow {}^3(n\pi^*)$ channel is computed to be activated for both derivatives.

1F- and 5F-MIA. 1F- and 5F-MIA are deaza-compounds in which the corresponding N(1) or N(5) atom was exchanged by a C–F group. Unlike the ground-state geometries of MIA and the modifications discussed previously, the S_0 equilibrium geometry of 1F-MIA is not planar. Steric interaction of the

Table 3. Excited states properties of $2CF_3$-MIA in aqueous solution.

	Electronic structure ($\|c\|^2$)	$\Delta E_{vertical}$ / eV (*f*)
$^1(\pi_H\pi_L)$	$\pi_H \rightarrow \pi_L$(0.81)	2.73 *(0.275)*
$^1(n_N\pi_L)$	$n_{N3} \rightarrow \pi_L$(0.75)	2.94
$^3(\pi_H\pi_L)$	$\pi_H \rightarrow \pi_L$(0.90)	2.17
$^3(\pi_{H-1}\pi_L)$	$\pi_{H-1} \rightarrow \pi_L$(0.84)	2.60
$^3(n_N\pi_L)$	$n_{N3} \rightarrow \pi_L$(0.70) + $n_{N2} \rightarrow \pi_L$(0.13)	2.74

Table 4. Excited states properties of $4CF_3$-MIA in aqueous solution.

	Electronic structure ($\|c\|^2$)	$\Delta E_{vertical}$ / eV (*f*)
$^1(\pi_H\pi_L)$	$\pi_H \rightarrow \pi_L$(0.81)	2.67 (*0.271*)
$^1(n_N\pi_L)$	$n_{N3} \rightarrow \pi_L$(0.81)	2.80
$^3(\pi_H\pi_L)$	$\pi_H \rightarrow \pi_L$(0.89)	2.09
$^3(\pi_{H-1}\pi_L)$	$\pi_{H-1} \rightarrow \pi_L$(0.82)	2.58
$^3(n_N\pi_L)$	$n_{N3} \rightarrow \pi_L$(0.78)	2.60

methyl group in 10-position and the fluorine atom gives rise to a shallow energy barrier of 0.05 eV (see Section S7 in the ESI).

5F-MIA is the derivative that experiences the strongest blueshifts. The effect ranges from 0.27 eV for the $^3(\pi_H\pi_L)$ state up to preeminent 0.89 eV for the $n\pi^*$ triplet. Comparison of the excitation energies of 1F-MIA and 5F-MIA (Tables 5 and S4 in the ESI) reveals that both chromophores behave fundamentally different. The importance of the position of modification is best demonstrated for the $\pi_H \rightarrow \pi_L$ transition: The electron density distribution in the π_H orbital of 5F-MIA (Figure S1 in the ESI) is almost unchanged with respect to MIA. The corresponding orbital of MIA (Figure 5) does not exhibit density on the N(5) atom at all and therefore modification in this position has no marked effect. By contrast, the same modification in position 1 leads to strong destabilization of the π_H orbital. For 1F-MIA, the largest contribution to the molecular orbital is centered on the C(1) atom and the orbital exhibits antibonding character for the C(1)–F bond (Figure 5). The resulting strong destabilization of the π_H orbital leads to a redshift of the S1 and T1 states (~0.5 eV). The blueshift of the $\pi_H\pi_L$ and $\pi_{H-1}\pi_L$ states of 5F-MIA is related to the destabilization of the π_L orbital. In analogy to the π_H orbital of 1F-MIA, the shift of the orbital energy is caused by the pronounced antibonding character of the introduced C–F bond (Figure S4 in the ESI). The stronger destabilization of the $^3(\pi_H\pi_L)$ state compared to the corresponding singlet is explained by the larger weight of the $\pi_H \rightarrow \pi_L$ transition in the triplet wavefunction (Table S4 in the ESI). The effect on the $n\pi^*$ triplet depends on the position of the modification as well. In either case, the energy of the remaing n_N orbital is lowered due to the removal of a nitrogen-centered lone pair. As a result, the n_O orbitals gain significance. While the $n_N\pi_L$ character clearly remains dominant in 1F-MIA, the lowest $n\pi^*$ excitation of 5F-MIA is of $n_{O2}\pi_L$ type.

Table 5. Excited states properties of 1F-MIA in aqueous solution.

	Electronic structure ($\lvert c\rvert^2$)	$\Delta E_{vertical}$ / eV (*f*)
$^1(\pi_H\pi_L)$	$\pi_H \rightarrow \pi_L$(0.82)	2.45 (*0.238*)
$^3(\pi_H\pi_L)$	$\pi_H \rightarrow \pi_L$(0.88)	1.76
$^3(\pi_{H-1}\pi_L)$	$\pi_{H-1} \rightarrow \pi_L$(0.73)	2.93
$^3(n_N\pi_L)$	$n_N \rightarrow \pi_L$(0.49) + $n_{O2} \rightarrow \pi_L$(0.11)	3.40

In spite of the fundamental changes in the electronic structure of the 5F-MIA chromophore, two ISC channels remain active because the blueshifts of the S1, T1, and $^3(\pi_{H-1}\pi_L)$ states are rather similar. Nonetheless, the substantial destabilization of the $n\pi^*$ states is expected to have an indirect impact on the El-Sayed forbidden channels as vibronic interaction between the $\pi\pi^*$ and $n\pi^*$ states is handicapped by their larger energy gap. In fact, a fluorescence quantum yield of $\Phi_F = 0.52$ has been observed for a closely related chromophore, 5-deazariboflavin,[31] which might be traced back to this effect. In the case of 1F-MIA, the strong stabilization of the $\pi_H\pi_L$ states is predicted to have profound impact on the ISC channels. Only the El-Sayed forbidden $^1(\pi_H\pi_L) \rightsquigarrow {}^3(\pi_H\pi_L)$ channel remains active and the $n\pi^*$ states are energetically separated from the $\pi_H\pi_L$ states hampering intensity borrowing via vibronic SOC. Previous experimental as well as quantum chemical studies on the related 1-deazariboflavin chromophore revealed a strong bathochromic shift of the S1 absorption maximum.[31]

Relaxation pathways

To get an estimate of the adiabatic energies of the derivatives in aqueous solution, we calculated approximated values by adding the computed blue-/redshifts at the ground-state geometries (see Figure 4) to the adiabatic energies of MIA in water. Deviations of the approximated adiabatic energies and those computed from optimized excited-state geometries of the derivatives are found to be below 0.10 eV. The resulting values for the $^1(\pi_H\pi_L) \rightsquigarrow T_{1-3}$ transitions are listed in Table 6 and enable clear assignment of the molecules to one of the scenarios sketched in Figure 2.

The screening reveals promising derivatives with respect to energetic schemes associated with increased Φ_F or Φ_T, respectively. The strong stabilization of $n\pi^*$ states for $2CF_3$- and $4CF_3$-MIA opens up the El-Sayed allowed $^1(\pi_H\pi_L) \rightsquigarrow {}^3(n_N\pi_L)$ channel. In the cases of $2CF_2$- and 1F-MIA, the S_1 and T_1 states are largely separated from the other excited states resulting in only one remaining El-Sayed-forbidden ISC channel. Therefore, we selected these four derivatives for a detailed examination of their excited state pathways. The application of the harmonic approximation with substantial adiabatic energy gaps of about

Table 6. Adiabatic excitation energies of the lowest triplet states of MIA and screened flavin derivatives with respect to the corresponding $^1(\pi_H\pi_L)$ minimum in aqueous solution. Values in bold print are computed from excited states geometries and the remaining entries are best estimates calculated from the adiabatic energies of MIA and the shifts for the screened derivatives at the ground state geometries (see Figure 4).

	$\Delta E_{adiabatic}$ / eV					
Derivative	$^3(\pi_H\pi_L)$		$^3(\pi_{H-1}\pi_L)$		$^3(n_N\pi_L)$	
MIA	—	**−0.56**	—	**−0.10**	—	**0.16**
$2F_2$-MIA	−0.58		−0.05		0.21	
$4F_2$-MIA	−0.62		−0.15		0.20	
$2CF_2$-MIA	−0.65	**−0.74**	0.68	—[a]	0.96	—[a]
$4CF_2$-MIA	−0.95		−0.10		0.35	
$2CF_3$-MIA	−0.50	**−0.49**	−0.13	**−0.11**	0.01	**0.00**
$4CF_3$-MIA	−0.52	**−0.56**	−0.09	**−0.05**	−0.07	**−0.16**
1F-MIA	−0.62	**−0.65**	0.48	—[a]	0.95	—[a]
5F-MIA	−0.38		−0.18		—[b]	

[a]Geometry of this state not optimized, as it is thermally inaccessible; [b]Energy not estimated due to change of electronic structure.

2 eV is not reliable for computing the nonradiative deactivation of the S_1 state to the ground state. Comparison with an experimentally determined rate constant for IC of MIA in aqueous solution at room temperature (2×10^7 s^{-1})[26] shows, however, that our computed value (5×10^7 s^{-1}) has the right order of magnitude. Information on the nonadiabatic coupling matrix elements $\langle GS|\nabla_R|S1\rangle$ and the most important coupling vibrational modes is provided in Section S8 in the ESI. Electric dipole transition moments are summarized in Table S9 in the ESI.

$2CF_2$- and 1F-MIA. Following green light absorption in the Franck–Condon region at 2.45 eV (**1F-MIA**) or 2.40 eV (**$2CF_2$-MIA**), respectively, relaxation of the geometry to the S_1 minimum mainly results in changes within the pteridine moiety (see Section S7 in the ESI). The S_1 and T_1 minimum geometries (**1F-MIA**) do not exhibit C_s symmetry. Like in the electronic ground state, steric interaction of the fluorine atom in position 1 and the methyl residue in position 10 causes the chromophore to lose planarity with a barrier of about 0.05 eV separating both minima. The S_1 and T_1 geometries are very similar, which can be traced back to the dominant $\pi_H \rightarrow \pi_L$ excitation contributing well above 80 %. In contrast, the geometries of the two $\pi_H \rightarrow \pi_L$ states of **$2CF_2$-MIA** differ markedly due to symmetry breaking of the T_1 state. TDDFT leads to very shallow double minima for symmetry-restrained optimizations of the $\pi_H \rightarrow \pi_L$ states (first-order saddle points). At the DFT/MRCI level of theory, however, the C_s symmetric structure of the S_1 state is lower in energy, which is not the case for the corresponding triplet.

The kinetic schemes in Figure 6 suggest that T_2 and T_3 are thermally not accessible from the S_1 minimum so that $S_1 \rightsquigarrow T_1$ remains as the only reasonable triplet population pathway. For flavins, typically the $S_1 \rightsquigarrow T_1$ ISC rate decreases exponentially with increasing energy difference: The transition is described by the weak coupling case as defined by Englman and Jortner.[65] The adiabatic $S_1 \rightsquigarrow T_1$ energy of **1F-MIA** in aqueous solution is computed to 0.65 eV compared to 0.55 eV for MIA. The efficiency of the vibronic spin–orbit coupling mainly depends on the energetic separation of the $\pi_H\pi_L$ states from the nitrogen-centered $n\pi^*$ states in each domain and the magnitude of the matrix elements $\langle {}^1(\pi_H\pi_L)|\hat{\mathcal{H}}_{SO}|{}^3(n_N\pi_L)\rangle$ as well as $\langle {}^3(\pi_H\pi_L)|\hat{\mathcal{H}}_{SO}|{}^1(n_N\pi_L)\rangle$. Herzberg-Teller-like intensity borrowing is most effective for small energy gaps and strong spin–orbit coupling. Despite the pronounced destabilization of the $n_N\pi_L$ states for **1F-MIA**, we compute the $S_1 \rightsquigarrow T_1$ ISC rate constant to be increased by one order of magnitude. The gain in efficiency can be traced back to stronger SOCMEs in terms of intensity borrowing (see Section S8 in the ESI). Despite the increased rate constant of the $S_1 \rightsquigarrow T_1$ channel, ISC in total is hampered because the productive ${}^1(\pi_H\pi_L) \rightsquigarrow {}^3(\pi_{H-1}\pi_L)$ channel of MIA is deactivated. Overall, the rate constant is decreased by about a factor of 5 to 2×10^7 s^{-1}. Due to the atypical deviation of the S_1 and T_1 geometries of **$2CF_2$-MIA**, the transition does no longer comply with the weak coupling case.[30] As a consequence, the adiabatic energy of 0.78 eV causes more efficient vibrational overlap. In the case of **$2CF_2$-MIA**, overall, ISC is computed to be slowed down to proceed at a rate constant of 3×10^7 s^{-1}.

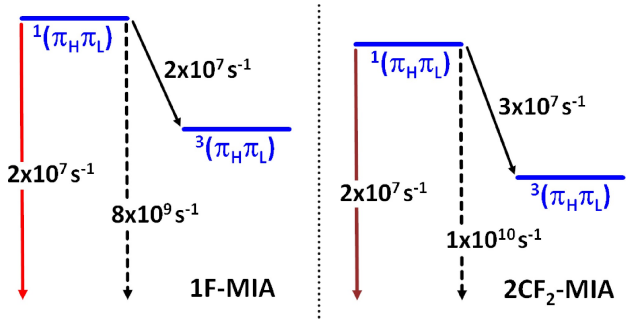

Figure 6. Adiabatic relaxation schemes of 1F- and $2CF_2$-MIA in aqueous medium. The solid vertical arrows originating from the ${}^1(\pi_H\pi_L)$ states refer to fluorescence, the dashed ones to IC.

As described by equation (2), the fluorescence rate constant depends on the transition dipole moment $\vec{\mu}_{S1S0}$ (**1F-MIA**: 4.73 D, **$2CF_2$-MIA**: 5.40 D) as well as the vertical $S_1 \rightarrow S_0$ transition energy (**1F-MIA**: 1.68 eV, **$2CF_2$-MIA**: 1.59 eV). The former enters the expression quadratically and the energy cubically. Hence, the characteristic redshift of the $\pi_H\pi_L$ states results in a decreased fluorescence rate constant as well and we obtain a value of 2×10^7 s^{-1} for both chromophores.

1F-MIA and **$2CF_2$-MIA** exhibit particularly interesting characteristics with respect to fluorescence microscopy. They can be addressed under milder conditions than the stem compound MIA or the related riboflavin which is the core chromophore of many blue-light receptors. Photoexcitation by green light is expected to cause fewer photochemical damages than blue-light irradiation. Furthermore, the wavelength window 650–900 nm is transparent in living tissue because hemoglobin, water and lipids do not absorb at those wavelengths and infrared light scatters much less in living tissue than visible light.[66,67] The unequalled redshift of the S_1 state of **$2CF_2$-MIA** results in an emission spectrum covering mainly near infrared wavelengths. The maximum of the emission spectrum (see Figure 7) is computed at 844 nm and half maximum is reached at 691 as well as 1211 nm. The emission spectrum of **1F-MIA** peaks at 765 nm and covers the wavelength region 640–1020 nm above half maximum.

The energy gap law typically makes nonradiative deactivation a serious competitor of infrared emission.[65,68] The rate constant for the $S_1 \rightsquigarrow S_0$ IC of MIA, computed in harmonic approximation, was found to be about twice as large as the experimental value. Hence, we expect the calculated IC rate constants for the $S_1 \rightsquigarrow S_0$ IC of **1F-MIA** and **$2CF_2$-MIA** to be overestimated as well, but to have roughly the right order of magnitude. Two factors enhance the probability of nonradiative deactivation of the S_1 state by IC to the S_0 state in relation to MIA: a better overlap of the vibrational wavefunctions of the accepting modes due to the smaller energy gap and the nonplanarity of the excited-state geometry resulting in larger NACMEs (see Section S8 in the ESI). While fluorescence and ISC appear to be competitive in both compounds (Figure 6), the computed IC rate constants of $\approx 8 \times 10^8$ s^{-1} (**1F-MIA**) and

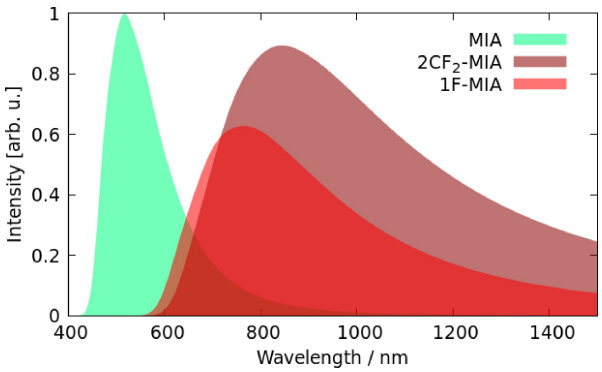

Figure 7. Emission spectra of **1F-MIA** and **2CF$_2$-MIA** as well as the stem compound **MIA** (normalized to intensity = 1) with explicit vibrational broadening. The vibrational overlaps are scaled by the squared transition dipole moments $\vec{\mu}^2_{S1S0}$. The maxima of the computed emission spectra are found at 1.47 eV (2CF$_2$-MIA), 1.62 eV (1F-MIA) and 2.40 eV (MIA).

$\approx 10^{10}$ s^{-1} (**2CF$_2$-MIA**) suggest that nonradiative deactivation is the dominating process. We therefore expect **1F-MIA** and **2CF$_2$-MIA** to emit fluorescence in the (infra-)red spectral range with comparatively small quantum yields. Unfluorinated 1-deaza-flavins have been investigated thorougly in the past.[18,31,69–71] 1-deazariboflavin does not show triplet quantum yield at all and fluorescence quantum yields have been reported to be well

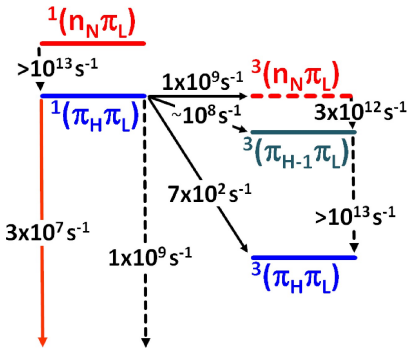

Figure 8. Adiabatic relaxation scheme of **2CF$_3$-MIA** in aqueous medium. The solid vertical arrow originating from the $^1(\pi_H\pi_L)$ state refers to fluorescence, the dashed one to IC.

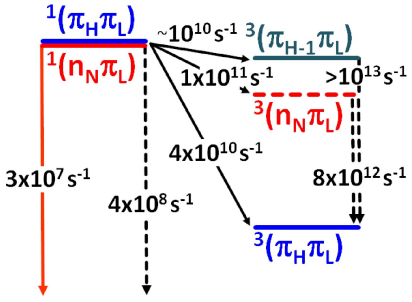

Figure 9. Adiabatic relaxation scheme of **4CF$_3$-MIA** in aqueous medium. The solid vertical arrow on the left side refers to fluorescence of the $^1(\pi_H\pi_L)$ state, the dashed one to IC.

below 1% in aqueous solution and acetonitrile.[13,71] However, the reason for the lack of fluorescence remained unclear and ultrafast spin-allowed nonradiative processes were contemplated to quench spin-allowed radiation. In the case of 1-deaza-FMN incorporated into the LOV domain of the YtvA protein from *Bacillus subtilis*, Silva-Junior et al. proposed a mechanism of internal conversion through a biradicaloid conical intersection of S_1 and S_0.[18] Similar photochemical reactivity of **1F-MIA** or **2CF$_2$-MIA** in the S_1 state cannot be ruled out within this study.

2CF$_3$- and 4CF$_3$-MIA. In the cases of **2CF$_3$-** and **4CF$_3$-MIA**, the $^3(\pi_{H-1}\pi_L)$ state and first singlet and triplet $n\pi^*$ states are energetically accessible after $^1(\pi_H\pi_L)$ absorption and hence are added to the kinetic schemes (Figures 8 and 9). For all states, C_s symmetric geometries are used. Complications arose while searching the minima of the $^1(\pi_H\pi_L)$ and $^3(\pi_{H-1}\pi_L)$ potentials: TDDFT optimization favours C_1-symmetric structures, whereas DFT/MRCI scans along the concerned out-of-plane modes reveal flat potential energy surfaces. Artificial symmetry breaking deformations at the TDDFT level have been observed for various ketones[56,72,73] and have been reported for the flavin chromophore[24,27] as well. In such occasions we replace the imaginary frequency by a real value corresponding to the outer branches of the TDDFT potential energy profile. In case of the S_1 state we utilize the T_1 equilibrium geometry as a proxy: Both states are characterized by the $\pi_H \rightarrow \pi_L$ transition contributing well above 80% and the DFT/MRCI energy for the S_1 state is found to be slightly lower at the T_1 TDDFT minimum.

Following excitation to the Franck–Condon region of the bright $^1(\pi_H\pi_L)$ state (**2CF$_3$-MIA**: 2.73 eV, **4CF$_3$-MIA**: 2.67 eV), relaxation to the equilibrium geometry goes hand in hand with substantial geometrical changes within the pteridine moiety. In the cases of **2CF$_3$-** and **4CF$_3$-MIA**, the C(4)–C(4a) and C(4a)–C(10a) bonds are shortened and the C(4a)–N(5) as well as C(4)–O bonds are elongated considerably (see Section S7 in the ESI). The excited state decay kinetics of both derivatives are strongly influenced by the $n\pi^*$ states.

In the case of **2CF$_3$-MIA**, we compute the $^1(\pi_H\pi_L)$ and $n_N\pi_L$ triplet states to be almost isoenergetic. According to the calculations, the El-Sayed allowed ISC proceeds at a rate constant of 1×10^9 s^{-1}. The direct electronic coupling is increased to 24.9 cm^{-1} compared to 8.8 cm^{-1} for MIA. The enhancement of the spin–orbit interaction can be traced back to the coupling of the out-of plane p orbital at the N(3) center (π_H) with the lone pair that results from removing the hydrogen atom (n_{N3}). In addition to the activation of the $^1(\pi_H\pi_L) \rightsquigarrow {}^3(n_N\pi_L)$ channel, we find $^1(\pi_H\pi_L) \rightsquigarrow {}^3(\pi_{H-1}\pi_L)$ ISC to be efficiently promoted by vibronic interactions. The rate constant of 10^8 s^{-1} is an estimate oriented towards the El-Sayed allowed process, because the $\pi_{H-1}\pi_L$ and $n_N\pi_L$ triplets are almost degenerate at the S_1 geometry resulting in oversized numerical derivatives. Unsurprisingly, the $S_1 \rightsquigarrow T_1$ channel can be neglected as relaxation pathway: The sequential transitions via the T_2 and T_3 states are found to be drastically more efficient. Internal conversion from the $n\pi^*$ triplet to the $^3(\pi_{H-1}\pi_L)$ state is computed to take place on the timescale of 10^{12} s^{-1}. Subsequent IC to the T_1 state is found to be even faster occuring on

the femtosecond timescale. The alternative direct IC channel, $^3(n_N\pi_L)\rightsquigarrow^3(\pi_H\pi_L)$, is computed to be slower by almost two orders of magnitude (6×10^{10} s^{-1}). The primary reason for this finding lies in the size of the electronic coupling: The magnitude of NACMEs is antiproportional to the vertical energy difference of the interacting states[56] at the initial geometry and the energy gap for the ultrafast $^3(\pi_{H-1}\pi_L)\rightsquigarrow^3(\pi_H\pi_L)$ IC amounts to 0.11 eV, whereas is it about four times as big for the slower channels [$^3(n_N\pi_L)\rightsquigarrow^3(\pi_H\pi_L)$: 0.44 eV, $^3(n_N\pi_L)\rightsquigarrow^3(\pi_{H-1}\pi_L)$: 0.38 eV]. Nonradiative transition of the initially excited S_1 state by IC to the electronic ground state is estimated to proceed with a rate constant of $\approx 1 \times 10^9$ s^{-1} and might therefore be competitive deactivation channel. The $^1(n_N\pi_L)$ state lies adiabatically 0.16 eV above the $^1(\pi_H\pi_L)$ minimum and does not play an important role in the triplet population of **2CF$_3$-MIA**.

In contrast, we compute the first $n\pi^*$ and $\pi\pi^*$ singlets to be adiabatically almost isoenergetic for **4CF$_3$-MIA** [E($\pi\pi^*\rightarrow n\pi^*$) = 0.01 eV] in polar environment. Hence, two El-Sayed allowed ISC channels have to be taken into account. $^1(\pi_H\pi_L)\rightsquigarrow^1(n_N\pi_L)$ internal conversion and vice versa is computed to $6-7 \times 10^{11}$ s^{-1}. The reason for the surprisingly slow equilibration is a moderate change in geometry combined with the vanishingly small adiabatic energy difference resulting in small overlap of the nuclear wavefunctions. The transition between the equilibrium geometries causes a substantial change of the C(4)–O coordinate as the $\pi_H \rightarrow \pi_L$ excitation is accompanied by an elongation of the bond by 4.0 pm. Figure 9 depicts the fastest ISC channels starting from either S_1 or S_2. The computed rate constant for the $^1(n_N\pi_L)\rightsquigarrow^3(\pi_H\pi_L)$ ransition amounts to 4×10^{10} s^{-1}. The rate constant increases to 1×10^{11} s^{-1} for the $^1(\pi_H\pi_L)\rightsquigarrow^3(n_N\pi_L)$ channel. Consistently, the direct spin-orbit coupling for the faster channel is stronger: The matrix elements amount to 31.2 cm^{-1} and 12.8 cm^{-1}, respectively. The geometrical changes of both ISC channels are closely related due to the similarity of the $^1(n_N\pi_L)$ and $^3(n_N\pi_L)$ (as well as $\pi_H\pi_L$) geometries (see Section S7 in the ESI). As is the case for **2CF$_3$-MIA**, the depicted rate constant for $^1(\pi_H\pi_L)\rightsquigarrow^3(\pi_{H-1}\pi_L)$ ISC is an estimate oriented towards the El-Sayed allowed process. Within the triplet domain, we find the $n_N\pi_L\rightsquigarrow\pi_H\pi_L$ transition to occur with a rate constant of 8×10^{12} s^{-1}. Interestingly, the direct transition from the $\pi_{H-1}\pi_L$ triplet to the T_1 state is computed to be preferred over the cascade via the $n\pi^*$ triplet: The rate determining step, $^3(\pi_{H-1}\pi_L)\rightsquigarrow^3(n_N\pi_L)$ IC, turns out to take place with a rate constant of 3×10^{11} s^{-1}. The vertical energy differences of the interacting triplet states amount to 0.2 eV for the productive channels [$^3(n_N\pi_L)\rightsquigarrow^3(\pi_H\pi_L)$: 0.20 eV, $^3(\pi_{H-1}\pi_L)\rightsquigarrow$ $^3(\pi_H\pi_L)$: 0.23 eV], whereas it is about twice as large (0.42 eV) for the slower IC channel.

As expected, the timescale of fluorescence of the bright $^1(\pi_H\pi_L)$ state (10^7 s^{-1}) does not change for the investigated modifications and the radiative rate constant of the $^1(n_N\pi_L)$ state of **4CF$_3$-MIA** is substantially slower (2×10^4 s^{-1}). Therefore, radiative depopulation cannot compete against the El-Sayed allowed ISC channels. The nonadiabatic coupling at the $^1(\pi_H\pi_L)$ geometries as well as the $^1(n_N\pi_L)$ minimum of **4CF$_3$-MIA** is found to be similar in size to MIA: The couplings of the five most efficient promoting modes vary between 0.05 a_0^{-1} and 0.02 a_0^{-1} (see Section S8 in the ESI). The computed value for the $S_1\rightsquigarrow S_0$ IC rate constant of 4×10^8 s^{-1} is considered an upper estimate showing that IC cannot compete with the much faster ISC in this compound. In summary, we expect the triplet quantum yield to be significantly increased for both derivatives in comparison to MIA.

Summary and Conclusions

In this work, we have investigated various fluorinated flavin derivatives with respect to increasing triplet or fluorescence quantum yield, respectively. Based on shifts of electronic energies of selected states at the ground state geometries, we identified promising chromophores for detailed characterization of excited-state decay mechanisms. We find two derivatives with promising properties concerning fluorescence microscopy: In the case of **1F-MIA** and **2CF$_2$-MIA**, the $\pi_H\pi_L$ transitions are strongly stabilized and separated energetically from higher-lying states. We predict both compounds to absorb in the green wavelength region, redshifted by more than half an electronvolt compared to MIA. Particularly interesting for *in-vivo* fluorescence microscopy, the stabilization of the bright $\pi_H\pi_L$ singlet state is computed to result in emission of (infra-) red light. Using advanced quantum chemical methods, we find fluorescence and ISC to proceed on the same timescale (10^7 s^{-1}) for both compounds. Estimates of the $S_1\rightarrow S_0$ IC rate constants unfortunately suggest that nonradiative deactivation outcompetes the two former processes in **1F-MIA** and **2CF$_2$-MIA**. We therefore expect the photoluminescence quantum yields of these compounds to be low.

Aiming at increased triplet quantum yields, we detected two other promising derivatives: **2CF$_3$-MIA** and **4CF$_3$-MIA**. Removal of the hydrogen atom in position 3 is found to result in a marked stabilization of the $n\pi^*$ states. As a consequence, even in polar environments, El-Sayed allowed ISC channels become accessible and our computations predict fluorescence to be efficiently quenched by those. We have set up kinetic schemes including fluorescence as well as ISC and IC channels of the excited states. In the case of **2CF$_3$-MIA**, we compute $^1(\pi_H\pi_L)\rightsquigarrow^3(n_N\pi_L)$ ISC to take place with a rate constant of 1×10^9 s^{-1} in aqueous solution, surpassing fluorescence by almost two orders of magnitude (3×10^7 s^{-1}). For the derivative modified in position 4 we have found the $^1(n_N\pi_L)$ state to exhibit a markedly higher dipole moment resulting in a less distinct destablization by polar environment and ultimately further accessible El-Sayed allowed ISC channels. We compute ISC of **4CF$_3$-MIA** (1×10^{11} s^{-1}) to proceed considerably faster than for MIA or even **2CF$_3$-MIA**, which can be traced back to stronger electronic coupling (direct and vibronic SOC) as well as more efficient vibrational overlap for the $^1(\pi_H\pi_L)\rightsquigarrow^3(n_N\pi_L)$ channel. Subsequent to ISC, we compute the long-lived T_1 state to be populated on the picosecond timescale for both derivatives.

Supporting Information

Electronic Supplementary Information (ESI) available: Assessment of the screening protocol, excited-state properties of less promising derivatives, frontier molecular orbitals and their energies, fragment-based wavefunction analysis, transition dipole moments, computed absorption spectra, molecular geometries, spin-orbit and nonadiabatic couplng matrix elements, harmonic vibrational frequencies, selected vibronic coupling modes.

Acknowledgment

We cordially thank Peter Gilch for helpful discussion. This research was funded by the Deutsche Forschungsgemeinschaft (DFG, German Research Foundation) – 396890929/GRK 2482. Open Access funding enabled and organized by Projekt DEAL.

Conflict of Interest

The authors declare no conflict of interest.

Data Availability Statement

The data that support the findings of this study are available from the corresponding author upon reasonable request.

Keywords: ab initio calculations · computational photochemistry · excited states · fluorine · quantum chemistry

[1] L. O. Björn. Photobiology: The Science of Light and Life. Springer, New York, **2015**.
[2] A. Sancar, *Chem. Rev.* **2022**, *103*, 2203–2237.
[3] R. Banerjee, A. Batschauer, *Planta* **2005**, *220*, 498–502.
[4] A. Losi, W. Gärtner, *Annu. Rev. Plant Biol.* **2012**, *63*, 49–72.
[5] J. M. Christie, L. Blackwood, J. Petersen, S. Sullivan, *Plant Cell Physiol* **2014**, *56*, 401–413.
[6] Q. Mei, V. Dvornyk, *PLoS One* **2015**, *10*, e0135940.
[7] P. Parihar, R. Singh, S. Singh, D. K. Tripathi, D. K. Chauhan, V. P. Singh, S. M. Prasad, *J. Photochem. Photobiol. B* **2016**, *162*, 223–231.
[8] W. R. Briggs, C. F. Beck, A. R. Cashmore, J. M. Christie, J. Hughes, J. A. Jarillo, T. Kagawa, H. Kanegae, E. Liscum, A. Nagatani, K. Okada, M. Salomon, W. Rüdiger, T. Sakai, M. Takano, M. Wada, J. C. Watson, *Plant Cell* **2001**, *13*, 993–997.
[9] W. Holzer, A. Penzkofer, P. Hegemann, *Chem. Phys.* **2005**, *308*, 79–91.
[10] J. M. Christie, *Annu. Rev. Plant Biol.* **2007**, *58*, 21–45.
[11] A. Bowd, P. Byrom, J. B. Hudson, J. H. Turnbull, *Photochem. Photobiol.* **1968**, *8*, 1–10.
[12] M. Sun, T. A. Moore, P.-S. Song, *J. Am. Chem. Soc.* **1972**, *94*, 1730–1740.
[13] S. Salzmann, M. R. Silva-Junior, W. Thiel, C. M. Marian, *J. Phys. Chem. B* **2009**, *113*, 15610–156189.
[14] C. Neiß, P. Saalfrank, *Photochem. Photobiol.* **2003**, *77*, 101–109.
[15] S. Nakagawa, O. Weingart, C. M. Marian, *J. Phys. Chem. B* **2017**, *121*, 9583–9596.
[16] B. D. Zoltowski, B. Vaccaro, B. R. Crane, *Nat. Chem. Biol.* **2009**, *5*, 827–834.
[17] M. Mansurova, P. Scheercousse, J. Simon, M. Kluth, W. Gärtner, *Chem. Bio Chem.* **2011**, *12*, 641–646.
[18] M. R. Silva-Junior, M. Mansurova, W. Gärtner, W. Thiel, *Chem. Bio Chem.* **2013**, *14*, 1648–1661.
[19] M. Mansurova, J. Simon, S. Salzmann, C. M. Marian, W. Gärtner, *Chem. Bio Chem.* **2013**, *14*, 645–654.
[20] A. Tyagi, A. Penzkofer, T. Mathes, P. Hegemann, *J. Photochem. Photobiol. B* **2010**, *101*, 76–88.
[21] B. Karasulu, W. Thiel, *J. Phys. Chem. B* **2015**, *119*, 928–943.
[22] S. Richert, J. Chen, N. Pompe, V. Radtke, B. Illarionov, M. Fischer, A. Bacher, S. Weber, *J. Chem. Phys.* **2019**, *151*, 235102.
[23] A. Brosi, B. Illarionov, T. Mathes, M. Fischer, M. Joshi, A. Bacher, P. Hegemann, R. Bittl, S. Weber, E. Schleicher, *J. Am. Chem. Soc.* **2010**, 132, 8935–8944.
[24] S. Salzmann, J. Tatchen, C. M. Marian, *J. Photochem. Photobiol. A* **2008**, *198*, 221–231.
[25] K. Zenichowski, M. Gothe, P. Saalfrank, *J. Photochem. Photobiol.* **2007**, *190*, 290–300.
[26] A. Reiffers, C. Torres Ziegenbein, A. Engelhardt, R. Kühnemuth, P. Gilch, C. Czekelius, *Photochem. Photobiol.* **2018**, *94*, 667–676.
[27] M. Bracker, F. Dinkelbach, O. Weingart, M. Kleinschmidt, *Phys. Chem. Chem. Phys.* **2019**, *21*, 9912–9923.
[28] J. Tatchen, N. Gilka, C. M. Marian, *Phys. Chem. Chem. Phys.* **2007**, *9*, 5209–5221.
[29] T. J. Penfold, E. Gindensperger, C. Daniel, C. M. Marian, *Chem. Rev.* **2018**, *118*, 6975–7025.
[30] C. M. Marian, *Annu. Rev. Phys. Chem.* **2021**, *72*, 617–640.
[31] S. Salzmann, V. Martinez-Junza, B. Zorn, S. E. Braslavsky, M. Mansurova, C. M. Marian, W. Gärtner, *J. Phys. Chem. A* **2009**, *113*, 9365–9375.
[32] C. M. Marian, S. Nakagawa, V. Rai-Constapel, B. Karasulu, W. Thiel, *J. Phys. Chem. B* **2014**, *118*, 1743–1753.
[33] E. Sikorska, I. V. Khmelinskii, D. R. Worrall, J. Koput, M. Sikorski, *J. Fluoresc.* **2004**, *14*, 57–64.
[34] T. Mondal, S. Mahapatra, *J. Chem. Phys.* **2010**, *133*, 084304.
[35] T. Mondal, S. Mahapatra, *J. Chem. Phys.* **2010**, *133*, 084305.
[36] M. A. H. Alamiry, A. C. Benniston, J. Hagon, T. P. L. Winstanley, H. Lemmetyinen, N. V. Tkachenko, *RSC Adv.* **2012**, *2*, 4944–4950.
[37] X. Zhang, J. Wu, D. Wei, Y. Cai, X. Sun, *Dyes Pigm.* **2021**, *187*, 109109.
[38] A. Bondi, *J. Phys. Chem.* **1964**, *68*, 441–451.
[39] J. C. Biffinger, H. W. Kim, S. G. DiMagno, *Chem. Bio Chem.* **2004**, *5*, 622–627.
[40] F. Babudri, G. M. Farinola, F. Naso, R. Ragni, *Chem. Commun.* **2007**, 1003–1022.
[41] A. Calzolari, B. Vercelli, A. Ruini, T. Virgili, M. Pasini, *J. Phys. Chem. C* **2013**, *117*, 26760–26767.
[42] M. von Arnim, R. Ahlrichs, *J. Comput. Chem.* **1999**, *19*, 1746–1757.
[43] TURBOMOLE V7.3 2018, development of University of Karlsruhe and Forschungszentrum Karlsruhe GmbH, 1989–2007, TURBOMOLE GmbH, since 2007; available from http://www.turbomole.com.
[44] A. D. Becke, *J. Chem. Phys.* **1993**, *98*, 5648–5652.
[45] C. Lee, W. Yang, R. G. Parr, *Phys. Rev. B* **1988**, *37*, 785–789.
[46] A. Schäfer, C. Huber, R. Ahlrichs, *J. Chem. Phys.* **1994**, *100*, 5829–5835.
[47] F. Furche, R. Ahlrichs, *J. Chem. Phys.* **2002**, *117*, 7433–7447.
[48] S. Hirata, M. Head-Gordon, *Chem. Phys. Lett.* **1999**, *314*, 291–299.
[49] T. Weymuth, M. P. Haag, K. Kiewisch, S. Luber, S. Schenk, C. R. Jacob, C. Herrmann, J. Neugebauer, M. Reiher, *J. Comput. Chem.* **2012**, *33*, 2186–2198.
[50] C. M. Marian, A. Heil, M. Kleinschmidt, *Wiley Interdiscip. Rev. Comput. Mol. Sci.* **2018**, *9*, e1394.
[51] S. Grimme, M. Waletzke, *J. Chem. Phys.* **1999**, *111*, 5645–5655.
[52] A. D. Becke, *J. Chem. Phys.* **1993**, *98*, 1372–1377.
[53] F. Weigend, M. Häser, H. Patzelt, R. Ahlrichs, *Chem. Phys. Lett.* **1998**, *294*, 143–152.
[54] O. Vahtras, J. Almöf, M. W. Feyereisen, *Chem. Phys. Lett.* **1993**, *213*, 514–518.
[55] A. Klamt, G. Schürmann, *J. Chem. Soc., Perkin Trans. 2* **1993**, 799–805 .
[56] M. Bracker, C. M. Marian, M. Kleinschmidt, *J. Chem. Phys.* **2021**, *155*, 014102.
[57] F. Plasser, H. Lischka, *J. Chem. Theory Comput.* **2012**, *8*, 2777–2789.
[58] F. Plasser, *J. Chem. Phys.* **2020**, *152*, 084108.
[59] M. Kleinschmidt, J. Tatchen, C. M. Marian, *J. Comp. Chem.* **2002**, *23*, 824–833.
[60] M. Kleinschmidt, C. M. Marian, *Chem. Phys.* **2005**, *311*, 71–79.
[61] AMFI is an atomic spin–orbit integral program, B. Schimmelpfennig, University of Stockholm, **1996**.
[62] B. A. Heß, C. M. Marian, U. Wahlgren, O. Gropen, *Chem. Phys. Lett.* **1996**, *251*, 365–371.
[63] M. Etinski, J. Tatchen, C. M. Marian, *J. Chem. Phys.* **2011**, *134*, 154105.
[64] M. Etinski, J. Tatchen, C. M. Marian, *J. Chem. Phys.* **2014**, *140*, 114104.

[65] R. Englman, J. Jortner, *Mol. Phys.* **1970**, *18*, 145–164.
[66] R. Weissleder, V. Ntziachristos, *Nat. Med.* **2003**, *9*, 123–128.
[67] V. Marx, *Nat. Methods* **2014**, *11*, 717–720.
[68] Yu-Chen Wei, Sheng Fu Wang, Yun Hu, Liang-Sheng Liao, Deng-Gao Chen, Kai-Hsin Chang, Chi-Wei Wang, Shih-Hung Liu, Wei-Hsiang Chan, Jia-Ling Liao, Wen-Yi Hung, Tsai-Hui Wang, Po-Ting Chen, Hsiu-Fu Hsu, Yun Chi, Pi-Tai Chou, *Nat. Photonics* **2020**, *14*, 570–577.
[69] R. Spencer, J. Fisher, C. Walsh, **1977**, *16*, 3586–3594.
[70] S. Ghisla, V. Massey, *Biochem. J.* **1986**, *239*, 1–12.
[71] C. Slavov, M. Mansurova, A. R. Holzwarth, W. Gärtner, *Photochem. Photobiol.* **2010**, *86*, 31–38.
[72] K. Tomi'c, J. Tatchen, C. M. Marian, *J. Phys. Chem. A* **2005**, *109*, 8410–8418.
[73] J. Tatchen, C. M. Marian, *Phys. Chem. Chem. Phys.* **2006**, *8*, 2133–2144.

Manuscript received: February 10, 2022
Revised manuscript received: March 21, 2022
Version of record online: April 27, 2022